From Catalysis to Anion Recognition

A THESIS
SUBMITTED TO THE FACULTY OF THE GRADUATE SCHOOL
OF THE UNIVERSITY OF MINNESOTA
BY

Evgeny V. Beletskiy

IN PARTIAL FULFILLMENT OF THE REQUIREMENTS
FOR THE DEGREE OF
DOCTOR OF PHILOSOPHY

Dr. Steven R. Kass, Advisor

January, 2014

Acknowledgments

Thank you to all the members of the Chemistry Department for creating an outstanding academic environment and providing me an opportunity to learn so much more in the field of Chemistry. Thanks to the faculty for excellent teaching and organizing various problem-solving meetings, literature discussions and contests. Thanks to the staff for their friendly assistance.

Special thanks to my advisor, Prof. Steven Kass, for his guidance, encouragement and kind support. His enthusiasm and desire to learn more motivated me in my studies and I can not imagine a better advisor for the graduate research. I would also like to thank my labmates, especially Elisey Yagodkin and Masoud Samet, for useful discussions and a safe and productive atmosphere in the lab.

Last but not least, thanks to Natalie Olson and all my family and friends for their endless love, kindness and support.

Abstract

Part 1. A novel approach to enantioselective hydroacylation. A known methodology for hydroacylation of monosubstituted alkenes utilizing 2-amino-3-picoline as a temporary directing group was studied in order to broaden its scope and enable access to chiral products. This transformation was expanded to include intramolecular process of prochiral 1,1-disubstituted alkenes, which leads to the formation of six and seven-membered cyclic β-substituted ketones. Various approaches to induce enantioselectivity were investigated and promising results were obtained with a chiral derivative of 2-amino-3-picoline.

Part 2. Three hydrogen bond donor catalysts. Inspired by Nature's three pronged oxy anion holes, the first study on the effect of a third hydrogen bond on catalysis was carried out. Model compounds based on a 1,3,5-triarylbenzene core containing two or three hydrogen bond donors were designed and synthesized. Kinetic studies of various reactions showed that the catalysts that can provide three hydrogen bonds often lead to much faster rates and give higher selectivities compared to their two hydrogen bond donor analogs.

Part 3. Functionalized 1,3,5-triarylbenzenes as anion receptors. Anion binding affinities of structural analogs of the catalysts in Part 2 were studied. A neutral tris-thiourea derivative was discovered to be a selective dihydrogen phosphate receptor in aqueous solutions. Model compounds with one and two thiourea arms were synthesized. UV-VIS, IR and NMR spectra along with binding constant determinations elucidated the mode of interaction of various anions to these thiourea compounds. Fluorescent and bifunctional receptors were also studied to further increase the selectivity for dihydrogen phosphate.

Table of Contents

List of Tables

Chapter 1

Chapter 2

Chapter 4

Chapter 5

Chapter 7

List of Figures

Chapter 3

Chapter 4

Chapter 5

Chapter 6

Chapter 7

Chapter 8

Chapter 9

Chapter 10

List of Schemes

Chapter 1

Chapter 2

Chapter 3

Chapter 4

Chapter 5

Chapter 6

Chapter 7

Chapter 8

Chapter 9

Chapter 10

Part 1: A novel approach to enantioselective hydroacylation

Chapter 1: Introduction*

Transition metal catalyzed activation of aromatic and vinylic sp^2 C–H bonds has been extensively studied and a number of useful methods such as alkylations with alkenes and arylations with aryl bromides or iodides are now available.[1] This introductory Chapter will discuss reactions where the substrate is an aldehyde (**1**, Scheme 1). These reactions are termed hydroacylation and currently have very limited application. Nevertheless, they open an easy way to access various ketone products without by-products and possess strong potential.

Scheme 1. C–H activation of aldehydes.

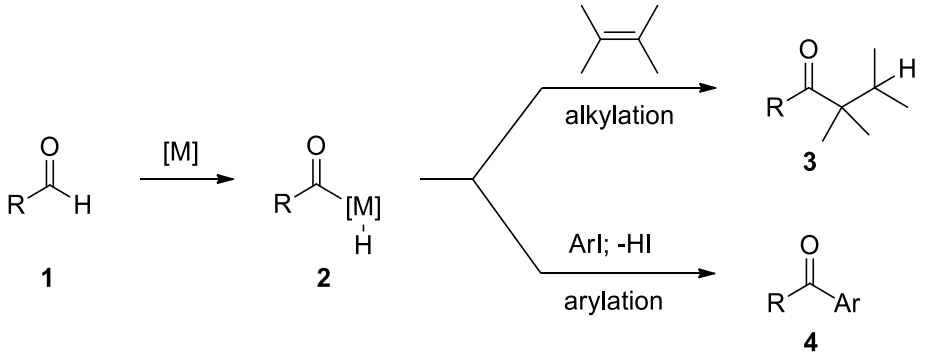

* Chapter 1 is an edited and slightly revised version of the November 2009 Written Preliminary Exam.

Hydroacylation of alkenes or alkynes as well as cross-coupling with aryl halides will be a powerful method for construction of unsymmetrical ketones (such as **3** and **4**) when a general and reliable procedure is developed. The advantage of this protocol over alternatives such as the reaction of the aldehyde with a corresponding alkyl or aryl Grignard reagent followed by oxidation is the higher functional group tolerance. Indeed, substrates bearing groups prone to reduction (nitro-group, etc.) or oxidation (alcohols, etc.) as well as electrophilic (ketones, esters, etc.) and acidic groups (aliphatic ketones, nitriles, etc.) can not be used in the latter method. However, transition metal catalyzed reactions are expected to be tolerant to all these groups and will enable the synthesis of a broader range of functionalized ketones. Even more attractive is the enantioselective hydroacylation of 1,1-disubstituted alkenes shown in Scheme 2 which would lead to ketones (**5**) with a chiral center in the β-position. These compounds are not directly available by other methods.

Scheme 2. A general enantioselective hydroacylation.

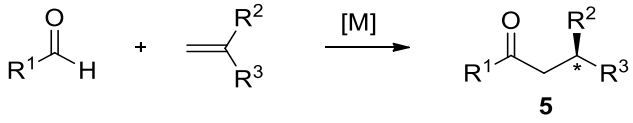

5

In the following section, a brief review of reported transition metal catalyzed reactions of aldehydes is given involving cleavage of the C(=O)–H bond beginning with the most studied reaction of this type, hydroacylation.

Cyclization of 4-pentenals

Discovery of hydroacylation has its origin in Tsuji's findings that aldehydes decarbonylate in the presence of Wilkinson's catalyst.[2] Although not isolated, the intermediate was believed to be an acylrhodium(III) hydride (such as **2**, Scheme 1).

The first intramolecular hydroacylation reaction was observed by Sakai *et al.* in 1972 as a stoichiometric reaction of 4-pentenals (**6**) with Wilkinson's catalyst, $Rh(PPh_3)_3Cl$, to give cyclopentanones (**7**) as shown in Scheme 3.[3] Cyclopropanes (**8**) were observed in all cases as a byproduct resulting from decarbonylation.

Scheme 3. The first reported hydroacylation reaction.

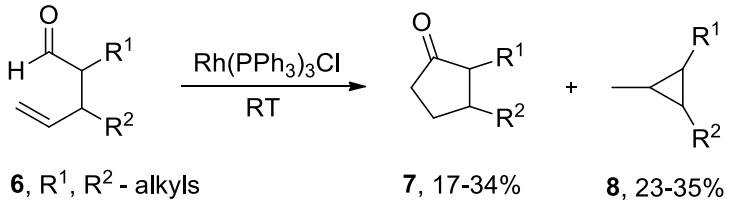

6, R^1, R^2 - alkyls **7**, 17-34% **8**, 23-35%

A few years later, a cyclization of 4-pentanals was performed catalytically by Miller *et al.*[4] The key in obtaining the high yields was the introduction of ethylene to the reaction mixture (Scheme 4): Only 32% conversion was observed for the unsubstituted 4-pentenal when using 10 mol% of Wilkinson' catalyst without ethylene, however, it was doubled (65%) when the chloroform solvent was saturated with ethylene prior to carrying out this reaction.

Scheme 4. Effect of ethylene as an additive on the hydroacylation reaction.

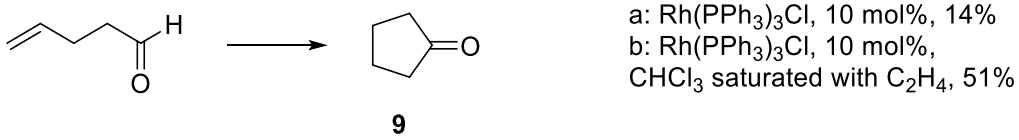

9

At that time, the formation of the intermediate acylrhodium(III) hydride species as a result of oxidative addition of an aldehyde C–H bond to rhodium(I) was partially confirmed by Suggs.[5] 8-Formylquinoline (**10**) was reported to react with Wilkinson's catalyst, forming the stable acylrhodium hydride chelate **11**, which was fully characterized.

Scheme 5. Formation of a stable rhodium hydride.

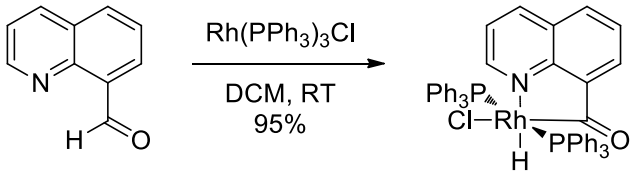

10 **11**

Following Miller's work, Larock *et al.* studied cyclization reactions of various 4-pentenals with Wilkinson-type catalysts.[6] Ethylene proved to be the best alkene additive and other additives such as cyclooctene, acetylene, vinyl bromide produced lower yields. Poor to moderate catalyst turnovers (1-10) were observed and were terminated by the formation of inactive carbonyl rhodium species resulting from aldehyde decarbonylation. Increased product yields with ethylene were ascribed to the formation of a saturated rhodium species **12** (Scheme 6), for which decarbonylation could not occur because it

requires at least one vacant coordination site.[7] At the same time, hydroacylation of ethylene does not occur due to the fact that its migratory insertion into a Rh–H bond is accompanied by an internal alkene chelation which places the newly formed ethyl group *trans* to the acyl group in **13** and precludes their reductive elimination. Due to these reasons ethylene, increases the turnover of the catalyst, but does not react itself.

Scheme 6. Proposed mechanism that is consistent with the role of ethylene as an additive.

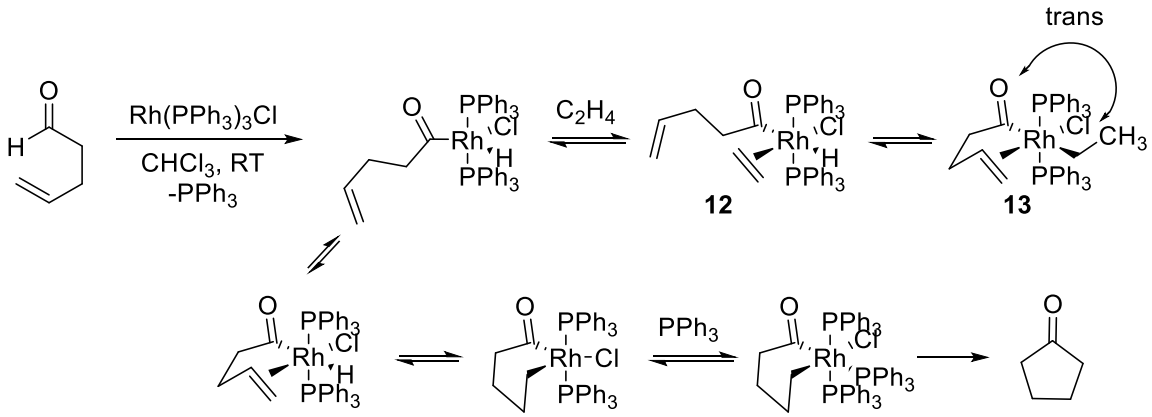

Milstein *et al.* directly confirmed the *cis* relationship of the hydride and the acyl groups in the intermediate **2** by isolation of the corresponding intermediate **14** in the reaction of 4-pentenal (**6**) with a Wilkinson-type catalyst, $Rh(PMe_3)_3Cl$, as shown in scheme 7.[8] Its structure was confirmed by P–P and H–P NMR coupling constants. This compound is stable at room temperature but decomposed at 50 °C via decarbonylation and an intramolecular hydroacylation. In order to determine which of the three PMe_3 ligands dissociated from **14** prior to the alkene coordination, **14** was introduced to an excess of *d*-labeled PMe_3. This experiment showed that only the phosphine *trans* to the hydride

undergoes exchange. Based on these results the following mechanistic sequence was proposed for the hydroacylation reaction: fast oxidative addition of an aldehyde to the Rh catalyst to form **14**, followed by slow and reversible dissociation of the phosphine to form the square pyramidal complex **15** (and not a bipyramidal structure in which rapid Berry pseudorotations would lead to scrambling of the phosphine ligands). Finally, intramolecular insertion of the alkene into the Rh–H bond followed by reductive elimination leads to cyclopentanone (**9**).

Scheme 7. A synthesis of a stable rohdium hydride and its reactions.

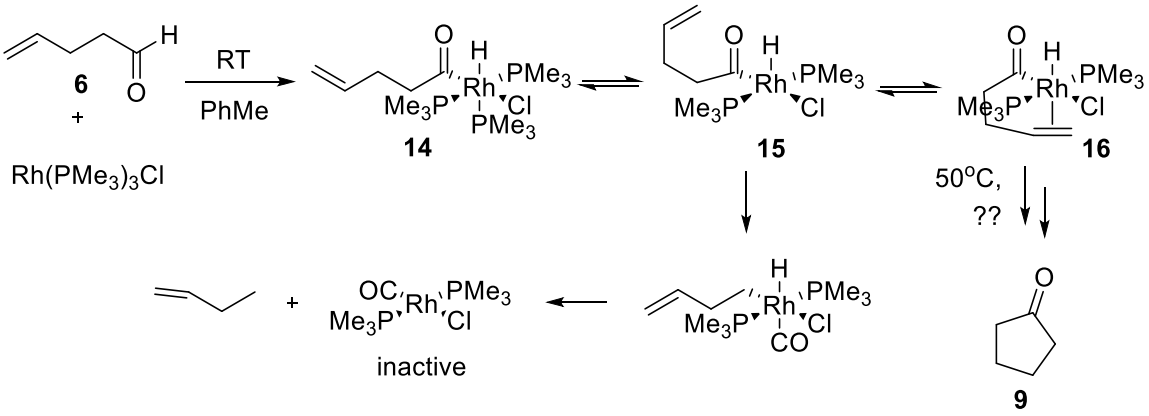

Although the structure of the intermediate **14** and the most labile ligand were clearly established, experimental evidence for the last steps in the mechanism was not provided. Indeed, the insertion of an alkene into the *trans* related Rh–H bond in **16** is unreasonable. It is more likely that the reaction proceeds via very slow dissociation of the *cis* phosphine. Exchange of this ligand was not observed probably due to rapid Rh–H insertion in the intermediate leading to **9**.

Better results, in terms of catalyst turnover, were achieved by Bosnich *et al.* when using cationic rhodium complexes bearing one diphosphine ligand (i.e., dppe = bis(diphenylphosphino)ethane, Scheme 8).[9] It was argued[10] that in this case the improvements compared to Wilkinson's catalyst are due to: first, no coordination of the solvent and counteranion to provide two vacant sites on the rhodium center and enable easy coordination of the alkene. Second, cationic diphosphine carbonyl complexes $[Rh(dppe)CO]^+$ are expected to be less stable then the corresponding *trans* complexes derived from Wilkinson's catalyst, therefore precluding decarbonylation in the former case. Indeed, it was shown that that up to 200-300 rapid turnovers (i.e., this is *ca.* 1000 fold faster than with Wilkinson's catalyst) could be achieved with this catalytic system before the catalyst is poisoned with CO. It is worth mentioning that the catalyst was obtained by premixing $[Rh(nbd)_2]BF_4$ with the ligand followed by hydrogenation to remove norbornodiene (i.e., nbd).

Scheme 8. Cyclization of 4-pentenal in the presence of a cationic rhodium complex.

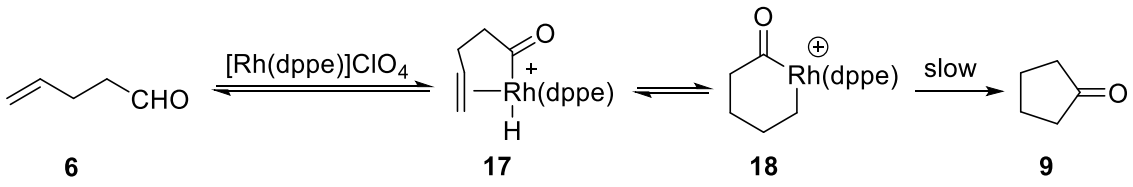

Further studies by Bosnich *et al.* showed that the hydroacylation reaction with $[Rh(dppe)]^+$ is a very complex process with many unproductive equilibriums taking place such as the addition of the Rh–H bond into the carbon-carbon double bond in the "wrong"

way to afford a five-membered metallocycle (not shown).[11] The reaction of d_1-aldehyde **6** with the deuterium at the aldehyde position produced up to 30% of α-*d*-cyclopentanone along with the expected β-*d* product, and a non-labeled aldehyde **6** was also observed in the NMR spectrum of the reaction mixture. This means that the C–H activation step (**6** to **17**) and the insertion of the C=C bond into Rh–H (**17** to **18** or the five-membered metallocycle) are reversible and fast relative to the reductive elimination (**18** to **9**). At the same time, complete equilibrium of these steps is never achieved during the reaction, since deuterium is not evenly distributed in the product. The turnover-limiting step of the reaction is the reductive elimination (i.e., the final step, **18** to **9**). As for all the other cases discussed, decarbonylation competes with reductive elimination (limiting step), however, chelation in **17** prevents the decarbonylation because a smaller unstable ring would form. It was also shown that racemic 2-phenyl-4-pentenal (**19**) reacts with an S-BINAP derived catalyst (not shown) to give 51% of the corresponding cyclopentanone product and 42% of an unexpected product, 4-phenyl-4-pentenal (**20**) (scheme 9). The latter species slowly produces the former at prolonged reaction times. Formation of **20** was ascribed to reversible CO migration, which additionally complicates the mechanism of the hydroacylation reaction.

Scheme 9. Reversibility of CO migration.

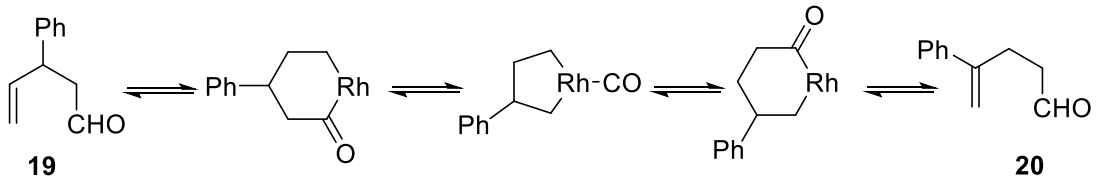

Further development of this catalytic system was focused on asymmetric cyclizations of 4-pentenals utilizing chiral bidentate phosphine ligands (Scheme 10). The first synthetic efforts were reported by James and Young, when the kinetic resolution of racemic 2-methyl-2-phenyl-4-pentenal was accomplished by heating (150 ºC) with $[Rh(ChiraPhos)_2]Cl$.[12] Sakai *et al.* were the first to obtain enantioenriched pentanones (3 examples with *ee*'s > 70% for [Rh(DIMPC)]Cl).[13] The highest *ee*'s were obtained by

Scheme 10. Enantioselective cyclization of 4-pentenals.

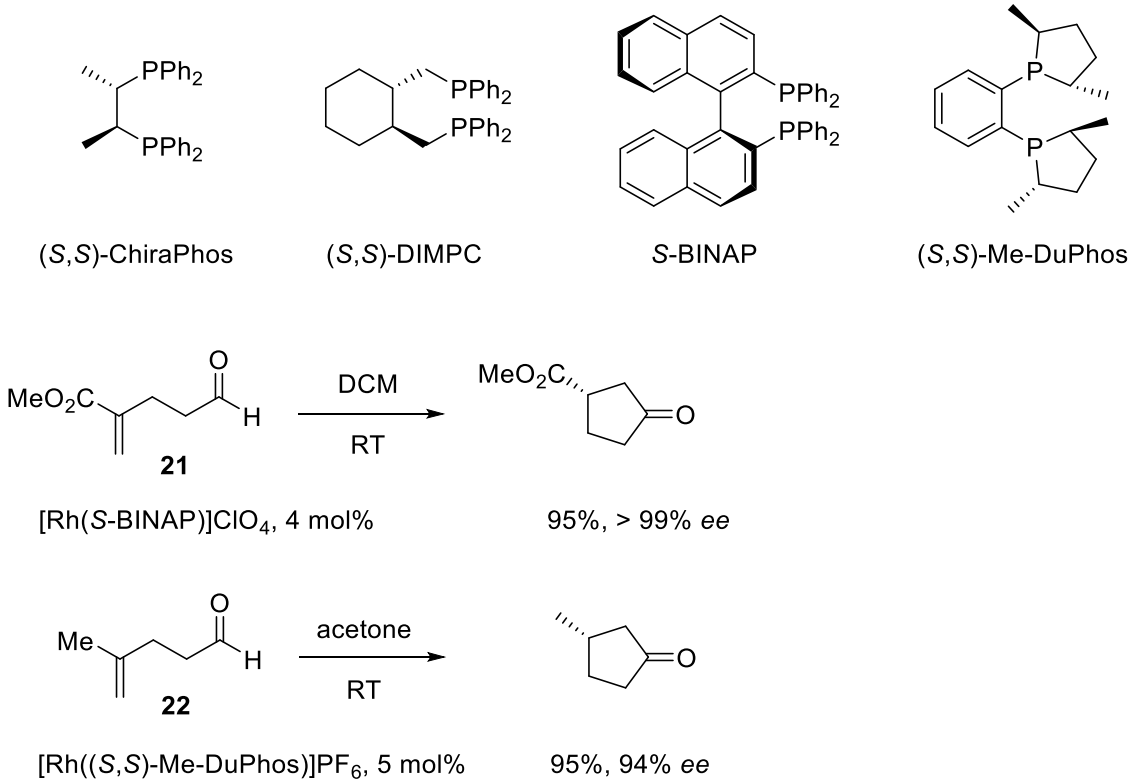

Bosnich *et al.* when cationic $[Rh(L)]^+$ with L = BINAP (10 examples with *ee*'s of 90-99% for substrates with bulky substituents in the 4-position of 4-pentenal and > 99% *ee* was

found for aldehydes such as **21** with an ester group in the 4-position)[14] or Me-DuPhos (> 93% *ee* for all examples, even for **22** which possesses a relatively small substituent at the 4-position)[15] were used as catalysts.

An interesting hydroacylation reaction that forms a seven-membered ring (Scheme 11) was reported by Sato *et al.*[16] Generally, formation of six and larger membered rings are unsuccessful. However, it is most likely that this substrate (4,6-pentadienal **23**) first cyclizes as a regular 4-pentenal and forms the allylic rhodium species **24**, which then rearranges to the cycloheptenone product.

Scheme 11. Formation of a cycloheptenone.

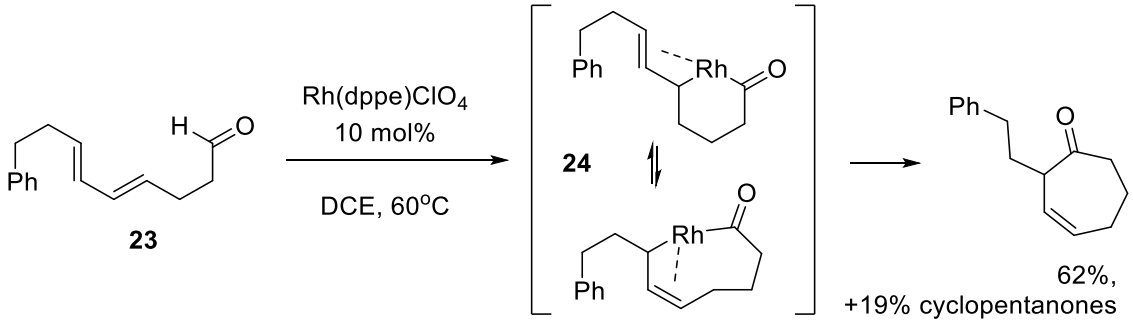

Other transition metal catalyzed hydroacylation reactions

As mentioned, the major problem in hydroacylation reactions is the reductive decarbonylation that irreversibly leads to undesired products and catalyst poisoning. Bosnich *et al.* showed that the rate-limiting step of hydroacylation with cationic catalysts is the final reductive elimination step and decarbonylation occurs from earlier

intermediates. This means that the slower the final step, the greater is the extent of decarbonylation and the fewer turnovers the catalyst achieves. In hydroacylation reactions where larger than a five-membered ring is formed, the concentration of the metallocycle intermediate such as **18** would be smaller than for 4-pentenal (**6**) thus making the desired reaction slower overall. Also in this case, the decarbonylation might occur from a **17**-type intermediate due to a larger chelation ring. Both reasons lead to an increase in the percentage of decarbonylation and a decrease in the overall reaction efficiency. This is even more of a problem for intermolecular hydroacylation reactions. That is why all the hydroacylation reactions that do not involve 4-pentenals (**6**) either employ a stabilizing directing group or other special substrates. This is briefly summarized below.

Hydroacylation with imines

One of the possible strategies to overcome the decarbonylation problem would be to perform the reaction with imines since in this case formation of isonitrile complexes would be less favorable. In 1997, Jun *et al.* reported intermolecular hydroacylation reactions with a co-catalyst, 2-amino-3-picoline (**25**, Scheme 12). Aromatic or aliphatic aldehydes added

Scheme 12. An aminopyridine- directed hydroacylation reaction.

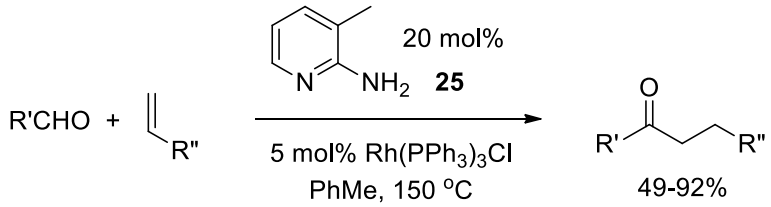

regioselectively to monosubstituted alkenes in the presence of Wilkinson's catalyst.[17] Table 1 shows the results for the hydroacylation of 1-pentene with *p*-methoxybenzaldehyde in the presence of different amounts of **25** as an additive. The higher the loadings of this co-catalyst, the smaller the amount of the decarbonylation product (i.e., anisole) that is formed and the higher the yield.

Table 1. Influence of the aldehyde to **25** ratio on the ketone yield.

Entry	1	2	3	4	5	6
Aminopicoline, mol%	0	10	20	50	70	100
Product : Anisole	0:100 (46%)	58:42	85:15	85:15	90:10	93:7
Isolated yield, %	0	14	57	70	80	83

Using Wilkinson-type catalysts showed the influence of the phosphine ligand nature on the reaction (the catalysts were formed *in situ* by reaction of bis(cyclooctene)rhodium(I) chloride dimer $[Rh(C_8H_{14})_2Cl]_2$ with an excess of phosphine). Table 2 shows the results for this reaction when 1-pentene and benzaldehyde are used as substrates. *Para* substitution of the phenyl groups in PPh_3 (bulkier phosphines) increases the yield of the desired ketone.

Table 2. Influence of the ligand in Wilkinson type catalyst on ketone yield.

Ligand	PPh_3	$P(C_6H_4Me\text{-}p)_3$	$P(C_6H_4OMe\text{-}p)_3$	$P(C_6H_{12}\text{-}c)_3$	PMe_3
Yield, %	48	61	56	38	0

In contrast, an increase in the basicity of the phosphine (i.e., trialkyl derivatives) leads to a decreased yield. The rhodium species $Rh(CO)(PPh_3)_2Cl$ resulting from the decarbonylation of the aldehyde was reported to catalyze the hydroacylation under these reaction conditions, however the yield was only 16% with a 10 mol% catalyst loading. The proposed mechanism is shown in Scheme 13. An intermediate imine **26** is formed and the C–H insertion is promoted by formation of the stable five-membered metallocycle **27**. Insertion of an alkene into these rhodium hydride species followed by reductive elimination results in the formation of an imine, which upon hydrolysis gives the ketone product and regenerates the co-catalyst **25**.

Scheme 13. Proposed catalytic cycle for the reaction in Scheme 12.

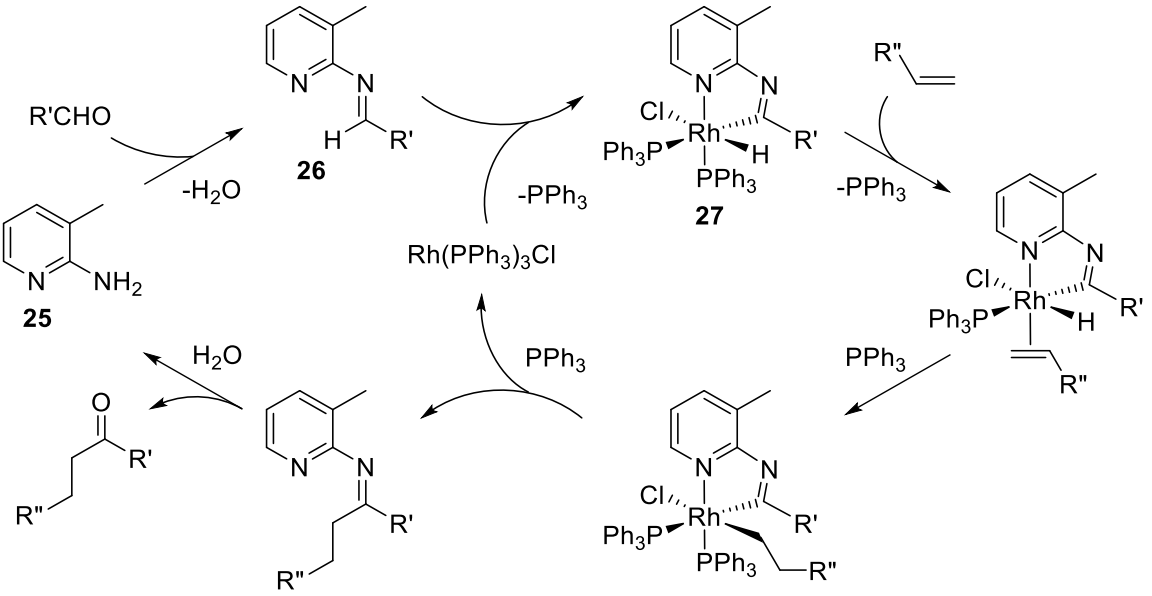

Later an improved catalytic system was reported by Jun *et al.* (Scheme 14).[18] It was found that addition of aniline and benzoic acid to the reaction mixture significantly

improved this procedure: Only a 9% GC yield of 1-phenyl-1-hexanone was achieved in the absence of additives at 130 °C, but the addition of benzoic acid increased the yield to to 28% and the addition of both benzoic acid and aniline led to a 98% yield.

Scheme 14. Improved catalytic system with aniline/benzoic acid additives.

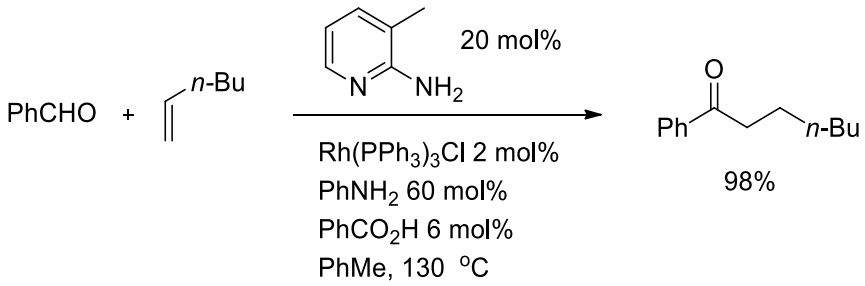

Under the reaction conditions, the aldehyde rapidly reacts with aniline forming the imine **28** which, when protonated by benzoic acid is more electrophilic than the starting aldehyde (Scheme 15). Therefore the 2-amino-3-picoline derived aldimine **29** is produced faster than in the catalytic system without these additives. It was proposed that the formation of the

Scheme 15. Jun *et al.* explanation of the role of aniline/benzoic acid additives.

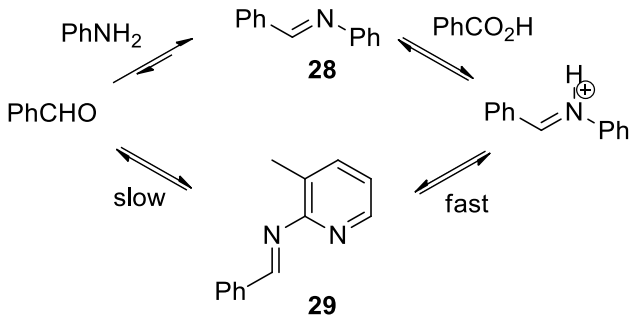

key imine **29** is the rate determining step of the hydroacylation reaction. This explains the role of aniline and benzoic acid on the reaction rate enhancement.

This methodology (using a chelation auxiliary) also proved to be effective for the hydroacylation of alkynes.[19] Branched α,β-enones such as **30** were formed with high selectivity and in high yields from 1-alkynes and aromatic or aliphatic aldehydes in the presence of Wilkinson's catalyst and 2-amino-3-picoline (**25**) (Scheme 16). Interestingly, a significantly lower reaction temperature is required for this process compared to alkene hydroacylation (80 versus 130 °C) and no aniline additive is needed. This suggests that the formation of the imine **26** is not the limiting step of the reaction at least in case of alkenes, which is contradictory to the proposal by Jun *et al*.

Scheme 16. Jun *et al.* methodology in the hydroacylation of alkynes.

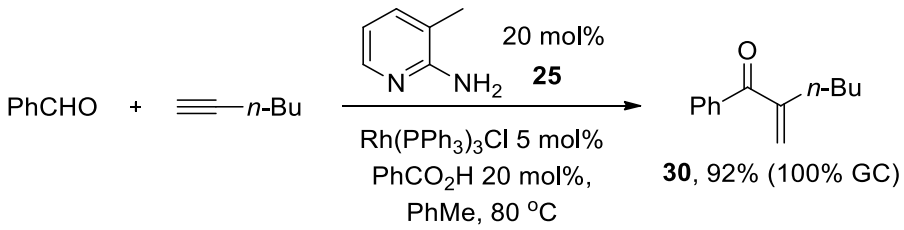

Hydroacylation with aldehydes containing embedded coordinating groups

Another way to prevent decarbonylation is to use substrates with embedded groups that can coordinate to rhodium in intermediates like **2** and form a stable five-membered metallocycle. Decarbonylation of these species is very slow because it leads to four-

membered chelates. Early examples of this approach are the reactions of salicylaldehyde derivatives such as **31** with alkynes reported by Miura *et al.* (Scheme 17).[20] The catalyst used for this transformation contained a bidentate dppf ligand (i.e., bis(diphenyl-phosphino)ferrocene). Addition of sodium carbonate to the reaction mixture enhanced the rate due to deprotonation of the phenolic OH-group and a stronger interaction with rhodium in the chelate, but caused product decomposition at prolonged times. High yields were achieved for all of the examples shown in this report, but little or no regioselectivity was observed for terminal alkynes (other nonsymmetrical alkynes were not reported).

Scheme 17. Hydroxy-group directed hydroacylation of alkynes.

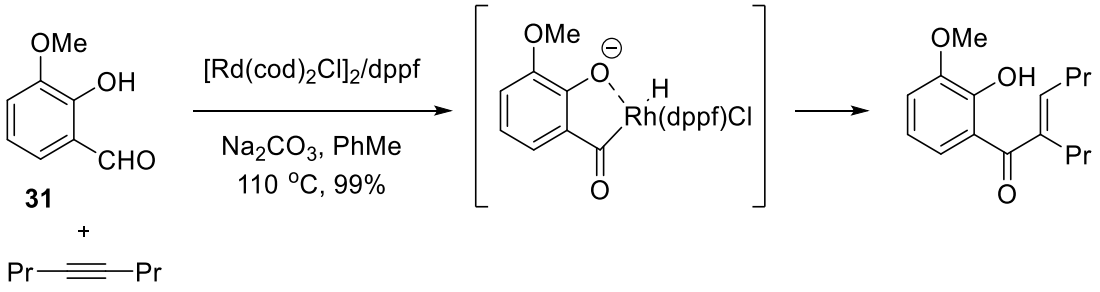

Intermolecular hydroacylations of alkenes with salicylaldehydes were investigated by Tanaka *et al.* Good results were achieved for 1,4- and 1,5-dienes.[21] Symmetrical 1,5-hexadienes gave a mixture of 1- and 2-acylated products in a 1:4 ratio. Asymmetrical dienes such as **32** (Scheme 18**)** produced a mixture resulting from attacks at different C=C bonds, but generally addition at C-2 of the 1,5-hexadiene system to give **33** and **34** was favored (an explanation is given below). Dienes with larger chains in between the alkene bonds did not react well (i.e., only a 4% yield was obtained for 1,6-heptadiene).

Scheme 18. Hydroxy-group directed hydroacylation of 1,5-dienes.

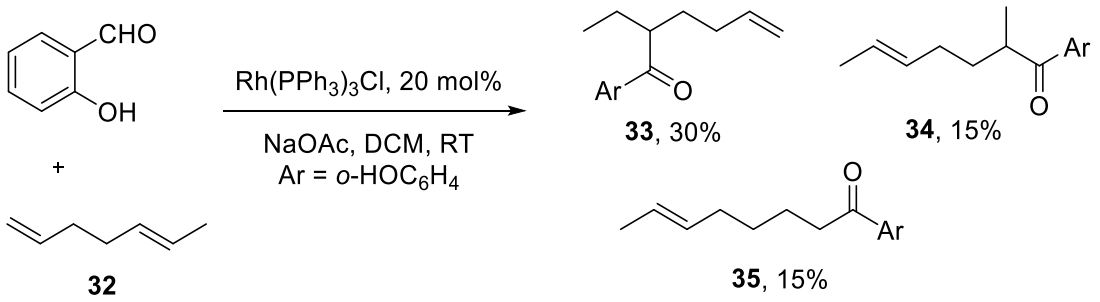

For simple alkenes such as 1-hexene, lower yields were observed in this reaction except for norbornenes (**36**) which are strained and reactive substrates.[22] For norbornene, the reaction with salicylaldehyde in the presence of Wilkinson's catalyst required an elevated temperature of 80 °C (Scheme 19). However, addition of $AgClO_4$ produced a cationic rhodium complex that allowed the reaction to proceed at room temperature but the diphosphine ligand dppf derived catalyst produced a significantly lower yield (39% *vs.* 90%).

Scheme 19. Hydroxy-group directed hydroacylation of norbornene.

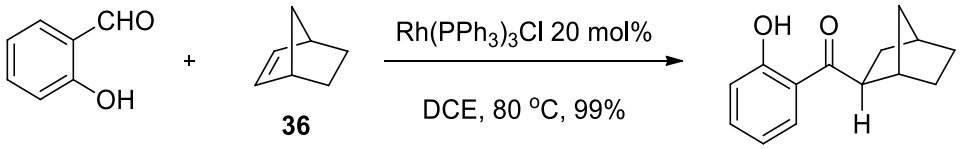

These results indicate that two chelating C=C bonds in a hydrocarbon molecule are required for the reaction to go smoothly. Deuterium labeling of the aldehyde group (similar to Bosnich *et al.* studies for Scheme 8) showed rapid reversible chelation of both aldehyde

and diene to the rhodium center with reductive elimination being the turnover-limiting step. Based on this, the mechanism shown in Scheme 20 was proposed.[23] Chelation of the diene achieved the saturation of the rhodium center and precluded decarbonylation. Favoring of the C-2 hydroacylation could be ascribed to faster reductive elimination due to stronger steric repulsion in **37**. The population of **37** is somewhat increased due to a tighter and more stable chelation ring compared to **38** which also favors the C-2 pathway.

Scheme 20. A proposed mechanism for the hydroacylation of 1,5-dienes with salicylic aldehyde.

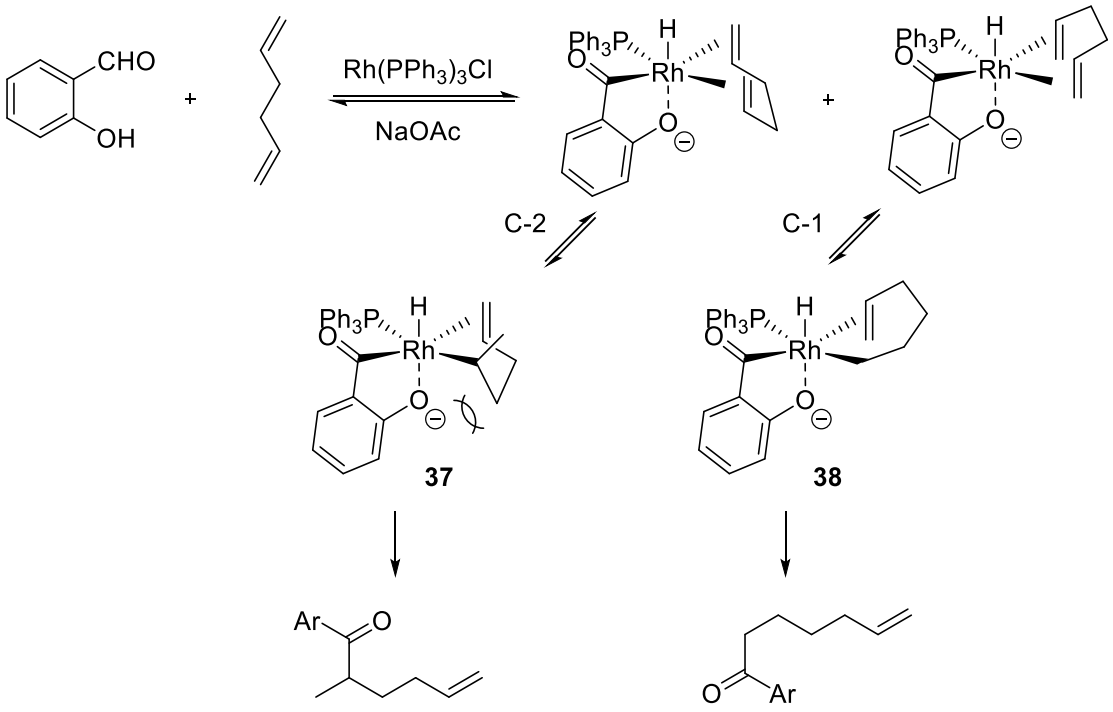

Tanaka *et al.* showed that the addition of MeCN to this reaction mixture enabled hydroacylation of simple monosubstituted alkenes such as **39** with salicylaldehyde

(Scheme 21).[24] However, a high catalyst loading of 40 mol% was required, so only about 2 turnovers were achieved. In this case, only the linear ketone isomer was observed.

Scheme 21. Hydroacylation with salicylaldehyde in the presence of acetonitrile.

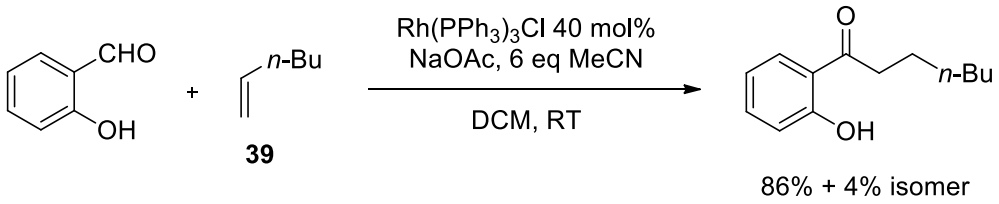

The same approach of stabilizing the key acyl-metal intermediate by chelation was used by Bendorf *et al.* to prepare seven and eight-membered heterocycles (**42**, Scheme 22).[25] In

Scheme 22. First report on sulfur directed hydroacylation.

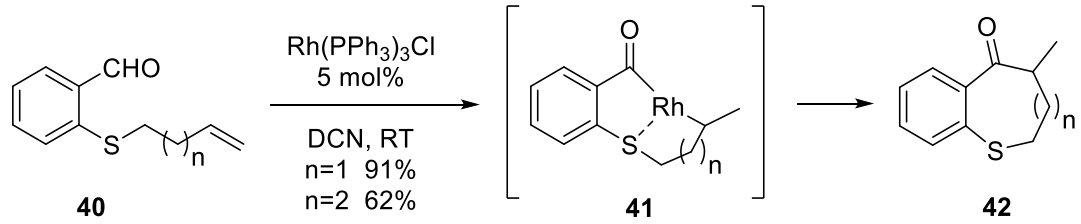

this work, oxygen was substituted for sulfur in the salicylaldehyde framework, which allowed for intermolecular hydroacylation of an alkenyl substituent tethered via sulfur in **40**. The reaction proceeds via a [3.3.0] (n=1) or [4.3.0] (n=2) metallobicycle **41**, which explains the unusual ease in the formation of medium rings in this process.

Following Bendorf's report, Willis *et al.* showed that readily-available β-S-substituted aldehydes (**43**, n=1, Scheme 23) are also useful substrates for intermolecular hydroacylation of various unsaturated compounds. In the first report, the catalyst $Rh(dppe)ClO_4$ was generated *in situ* by hydrogenation of $Rh(dppe)(nbd)ClO_4$ and satisfactory results were only achieved with electron deficient alkenes such as methyl acrylate (**44**).[26]

Scheme 23. Sulfur directed intermolecular hydroacylation of electron deficient alkenes.

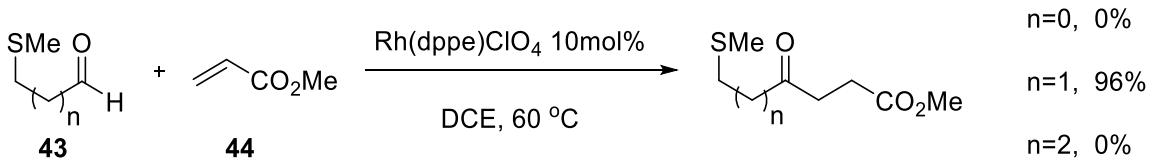

Only decarbonylation products were observed in reaction of **44** with α- and γ-S-substituted aldehydes (**43**, n=0 and 2) showing the unique role of five-membered metallocycle intermediates in the reaction.

A second generation catalyst reported by Willis *et al.* could be easily generated by premixing commercial reagents and is also suitable for hydroacylation of less reactive unfunctionalized alkenes and alkynes (Scheme 24).[27] The ligand used was the tridentate P–O–P DPEphos (**45**). It's role is to saturate the rhodium center, prevent decarbonylation, and increase the life-time of the catalyst. At the same time coordination of **45**'s oxygen is weak enough to dissociate (with bending of the skeleton) and allow alkene coordination.[28]

Scheme 24. Improved catalytic system for sulfur directed hydroacylation of alkenes.

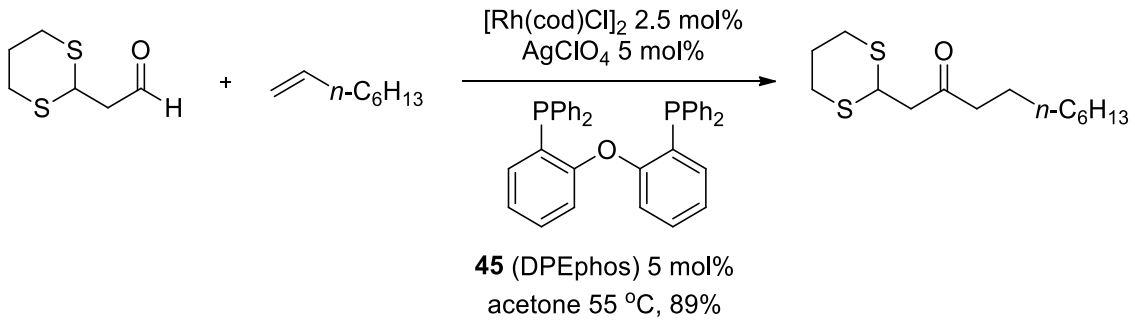

Only monosubstituted alkenes can be used for hydroacylation in this methodology and reactions with potentially prochiral 1,1- or 1,2-disubstituted alkenes are generally unsuccessful. An enantioselective version was reported for intermolecular hydroacylation of allenes.[29] Racemic disubstituted allenes (such as **46**, Scheme 25) when hydroacylated in the presence of Rh(Me-DuPhos)$^+$ provide 2,3-unsaturated ketones such as **47** with 90–96% *ee*.

Scheme 25. Enantioselective intermolecular hydroacylation.

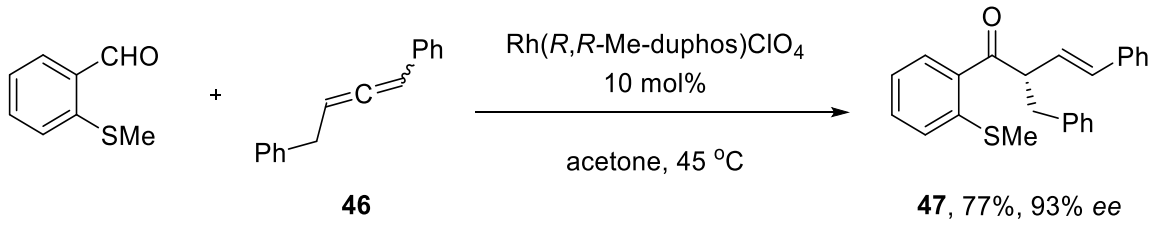

Hydroacylation reactions with unfunctionalized aldehydes

Tanaka *et al.* reported that intermolecular hydroacylation of α,β-unsaturated amides (such as **48**, Scheme 26) with aldehydes containing no embedded chelating groups is possible in the presence of cationic $Rh(dppb)^+$, which was generated by hydrogenation of its norbornodiene adduct.[30] This success was ascribed to the effective chelate-binding of amides to the rhodium center in intermediate **49** leading to its saturation and the prevention of decarbonylation. Coordination of the amide oxygen to the metal center also provides exclusive regioselectivity of the addition to the C=C bond leading to 1,4-dicarbonyl compounds (**50**).

Scheme 26. Intermolecular hydroacylation of α,β-unsaturated amides.

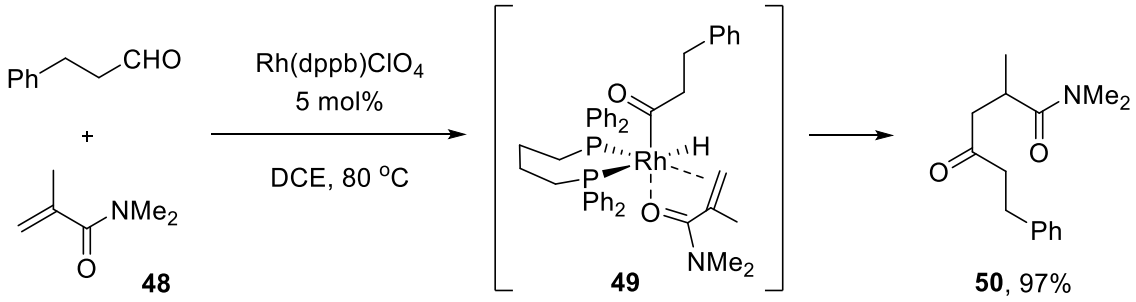

Recently, an enantioselective version of this reaction was developed (Scheme 27).[31] In the presence of a cationic rhodium complex and a bidentate ligand QuinoxP (**52**), 2-substituted acrylamides underwent hydroacylation with aliphatic aldehydes to give chiral 1,4-diketones such as **51** with 97–98% *ee*. However the conditions did not work as well for aromatic aldehydes.

Scheme 27. Enantioselective intermolecular hydroacylation.

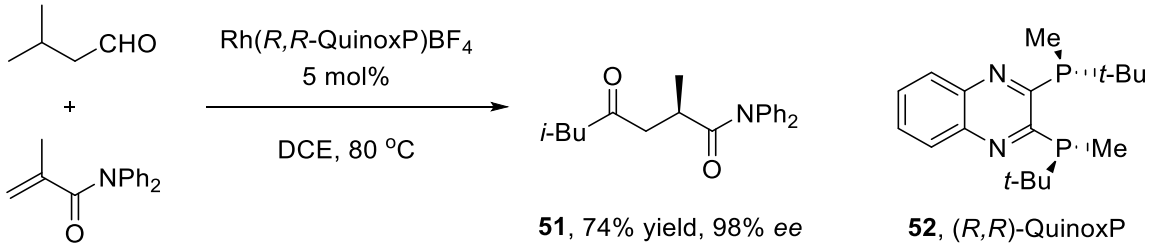

51, 74% yield, 98% *ee*

52, (*R,R*)-QuinoxP

The turn-over number of intermolecular hydroacylation reactions could be greatly increased not only by choosing the appropriate alkene substrate as in Tanaka's work, but also by using the appropriate catalytic system as shown by Brookhart *et al.* They found that cyclopentadienyl complexes of cobalt(I)[32] and rhodium(I)[33] can catalyze the alkylation of aromatic aldehydes with alkenes. Only vinyl silanes were reactive with cobalt complexes, however, the scope was broader for rhodium complexes and included non-conjugated monosubstituted alkenes and strained cyclic alkenes. NMR studies were consistent with the reaction mechanism shown in Scheme 28. The resting state of the catalyst is the carbonyl species **56**, which was observed as the main compound in the early stages of the stoichiometric reaction. All equilibria are fast, with the turn-over limiting step being the reductive elimination from **57**. It was postulated that the major pathway to the product is from acyl-aryl species **57** and not acyl-alkyl **55** due to higher rates for sp^2-sp^2 reductive eliminations compared to sp^2-sp^3 to processes.

Scheme 28. Intermolecular hydroacylation with a cyclopentadienyl-rhodium complex.

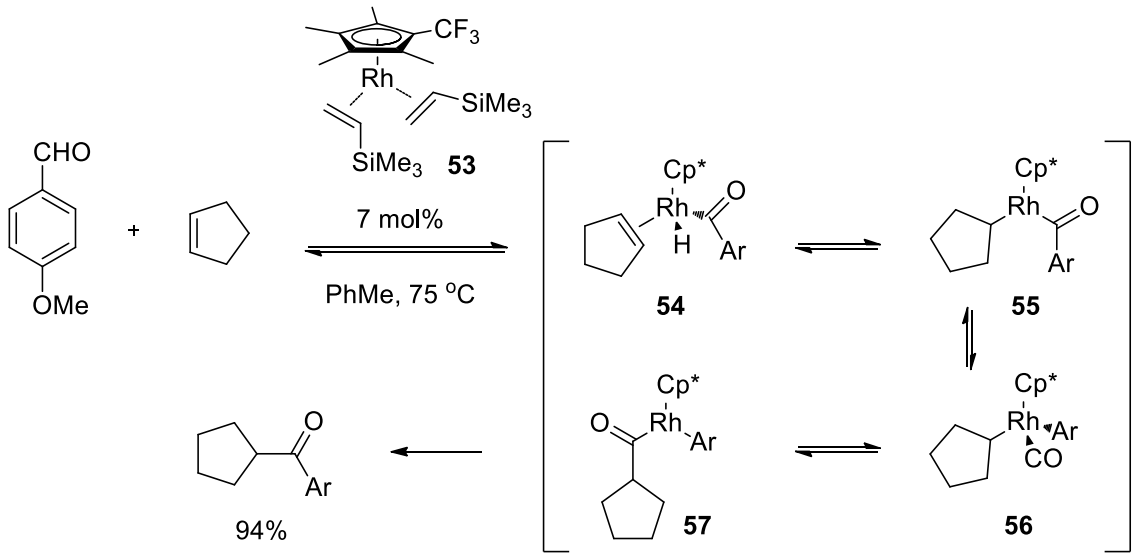

The best results were obtained when rhodium(I) compound **53** (bearing a CF_3 group on the cyclopentadienyl ring) was used as the catalyst. This was ascribed to an increased rate of reductive elimination on a more electron deficient metal center. The relative rate of the reductive elimination of **56** (i.e., decarbonylation), however, is significantly lower than that for other rhodium compounds; the reason for this is not well understood. This allows high turn-over numbers for intermolecular hydroacylation reactions, but this transformation is limited to aromatic aldehydes.

Hydroacylation reactions not involving C–H activation

In all of the hydroacylation examples described above, the aldehyde C–H bond was broken by rhodium insertion leading to the formation of **2**. One could also envision a

mechanism in which this bond is broken in the last stages by a β-hydride elimination process. This pathway was realized by using a ruthenium hydride catalyst (**58**) as shown by Ryu *et al.* (Scheme 29). Aromatic and aliphatic aldehydes were found to react with enones to give 1,3-diketones **60**.[34] Deuterium labeling showed rapid and reversible addition of Ru–H to the enone's C=C bond at both positions but the more nucleophilic ruthenium enolate **59** leads to the final product (i.e., **60**). Reactions with dienes proceed by an analogous mechanism via an allyl ruthenium species and give β,γ-unsaturated ketones.[35]

Scheme 29. Ruthenium-hydride catalyzed hydroacylation.

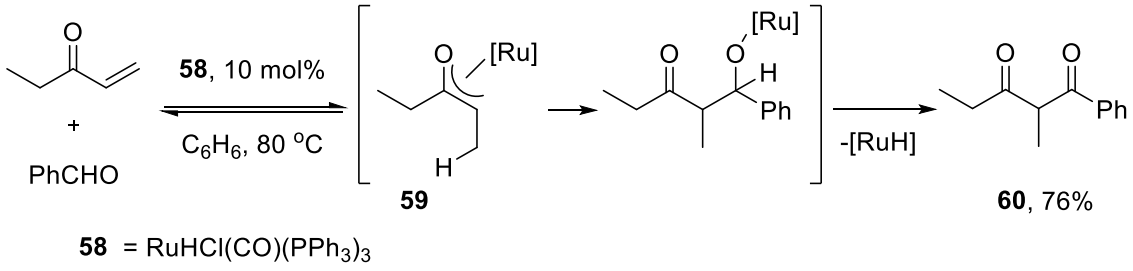

Cascade reactions

As described above, the turn-over limiting step for hydroacylations is typically the reductive elimination from the final intermediate (e.g., **18**) and all of the reactions leading to this intermediate are fast and reversible. Therefore under certain conditions, one might expect this intermediate to participate in further reactions such as migratory insertion of another C=C bond.

In Bosnich's first report on cyclizations of 4-pentenals to pentanones in the presence of cationic rhodium complexes, it was shown that 2-vinylbenzaldehyde (**61**) produced only 30% of the desired 2-indanone **62** along with an unidentified byproduct. Morehead *et al.* later determined the structure of this byproduct to be a dimer **63** (Scheme 30).[36] It was proposed that **63** arises from migratory insertion of the C=C bond of **61** into the C–Rh bond of the five-membered metallocycle intermediate **65**, which cannot undergo reductive elimination as its six-membered isomer **64**. This mechanism is consistent with the facts in that the yield of indanone **62** could be dramatically improved by slow addition of **61** to the catalyst, and 3-substituted indanones can be obtained in good yields.

Scheme 30. Competitive cyclization and dimerization of 2-vinylbenzaldehyde.

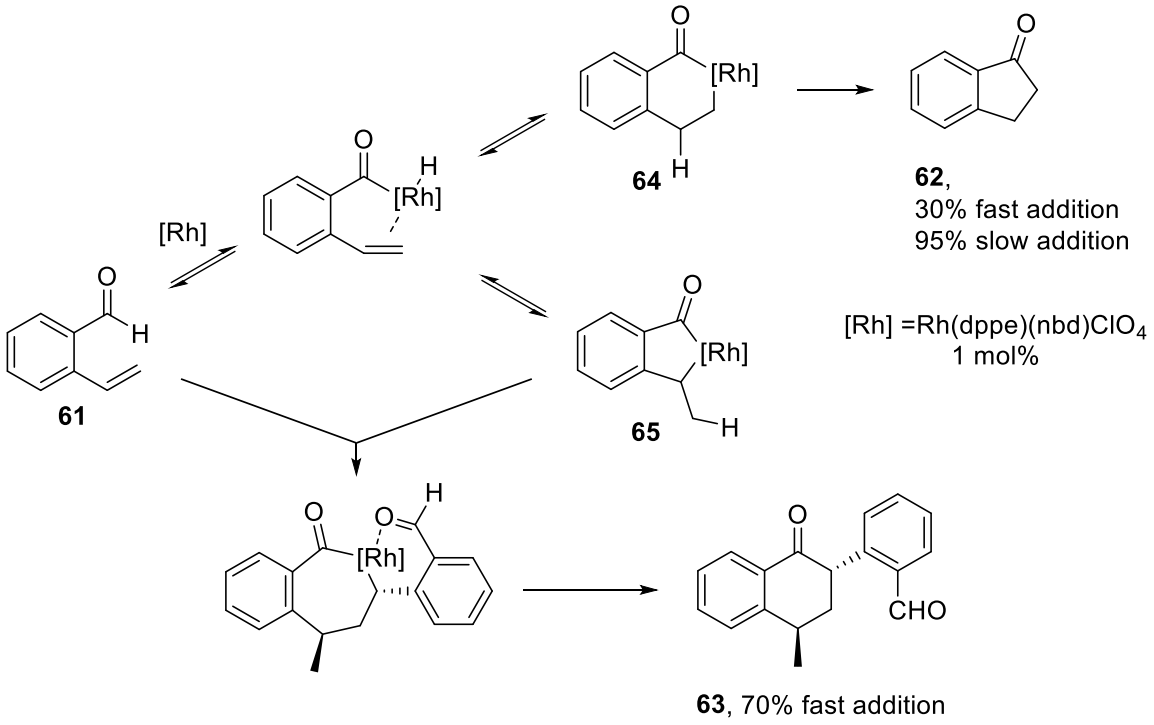

Fu *et al.* reported a tandem [4+2] annulation of 4-alkynals with alkynes to generate cyclohexenones (**66**) proceeding via an analogous mechanism as shown in Scheme 31.[37]

Scheme 31. Cascade of two consecutive insertions of alkynes.

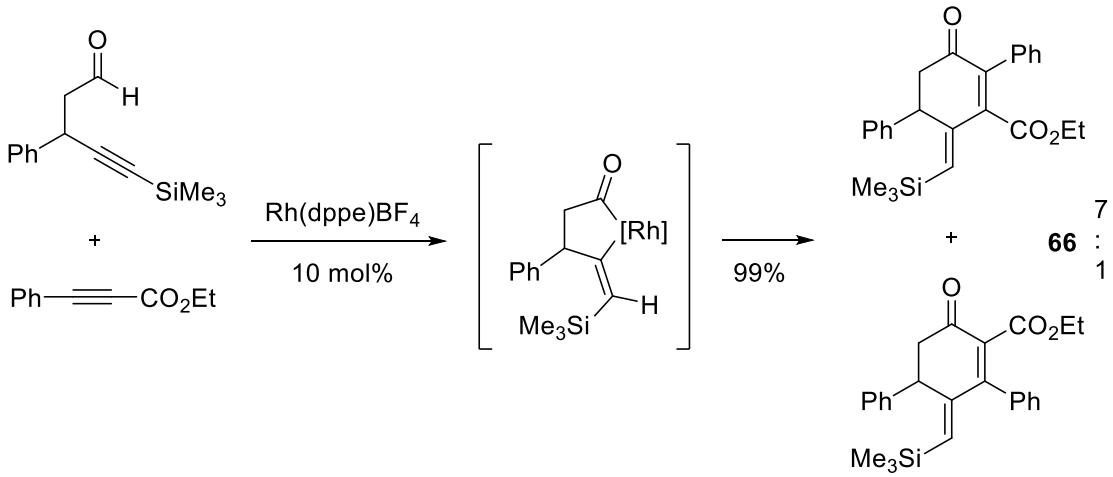

Later the same reaction was performed with carbonyl compounds instead of alkynes[38] and the est results were achieved with isotin derivatives **67** (Scheme 32). A new chiral center was generated in this reaction and *ee*'s of 90-99% were achieved for **68** using the ferrocene derived bidentate phosphine ligand **69**.

Scheme 32. Cascade of C≡C and then C=O insertions.

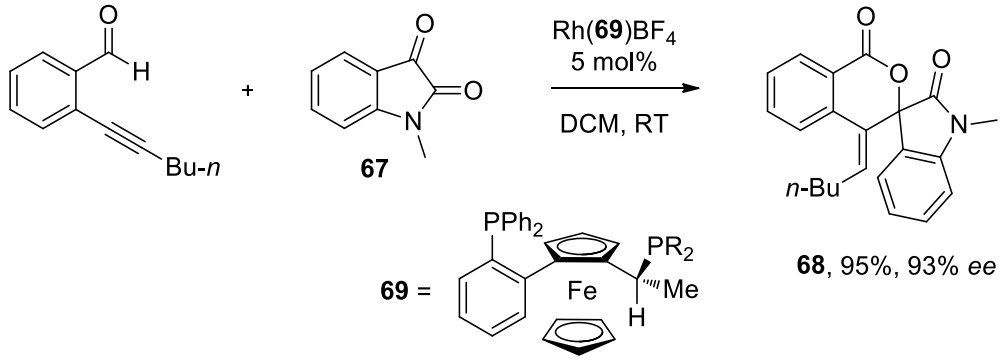

Cross-coupling reactions of aldehydes with haloarenes

One can envision using the intermediate of hydroacylation reactions (i.e., **2**) in cross-coupling reactions with haloarenes because the oxidative addition of Ar–I to Rh followed by a reductive elimination could lead to a ketone. This approach was shown in many analogous C–H activation reactions, for example the one in which phenols (such as **70**, Scheme 33) were coupled with aryl halides (such as **71**) in the presence of Wilkinson's catalyst and phosphinite **72**.[39] In this reaction, the phenoxy-group in **72** is first exchanged with the phenol (i.e., **70**) and the newly formed phosphinite group directs C–H activation to the *ortho*-position of **70**. Cross-coupling of the rhodium-hydride intermediate with aryl iodide leads to *ortho*-arylated phenol **73**.

Scheme 33. Ortho-arylation of phenols.

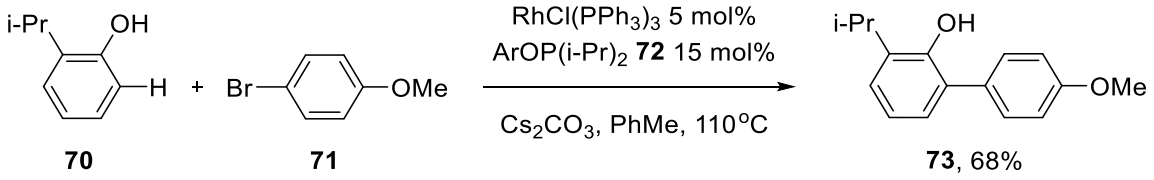

70 **71** **73**, 68%

However, there are only a few reports on arylation of aldehydes. Using rhodium based catalysts in these reactions was never reported. Palladium (II) chloride was shown to catalyze the reaction of salicyl aldehydes (chelation assistance, Scheme 34), however very active iodonium salts **74** were required as the second partner of this cross-coupling reaction.[40]

Scheme 34. Cross-coupling of salicyl aldehyde with iodonium salt.

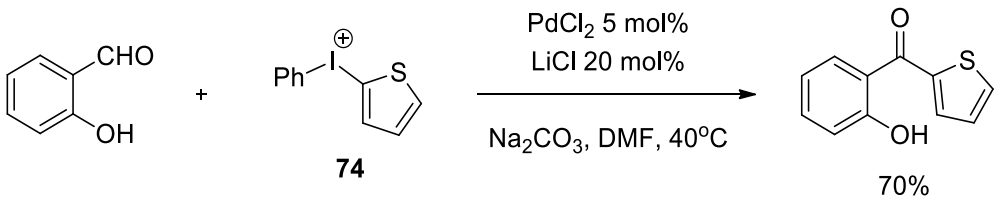

An elegant chelation assisted cross-coupling reaction between 8-formylquiniline (**10**) and aryl iodides was reported by Chang *et al.* (Scheme 35).[41] A cooperative catalysis with ruthenium(0) and palladium(0) was employed in this reaction. First a ruthenium carbonyl inserts into the C–H bond (as in a regular hydroacylation of an alkene) to form **75**. Transmetallation of **75** with palladium gives **76**, which eventually leads to ketone **77** after the reductive elimination step.

Scheme 35. Cooperative catalysis in the cross-coupling of an aldehyde and an aryl iodide.

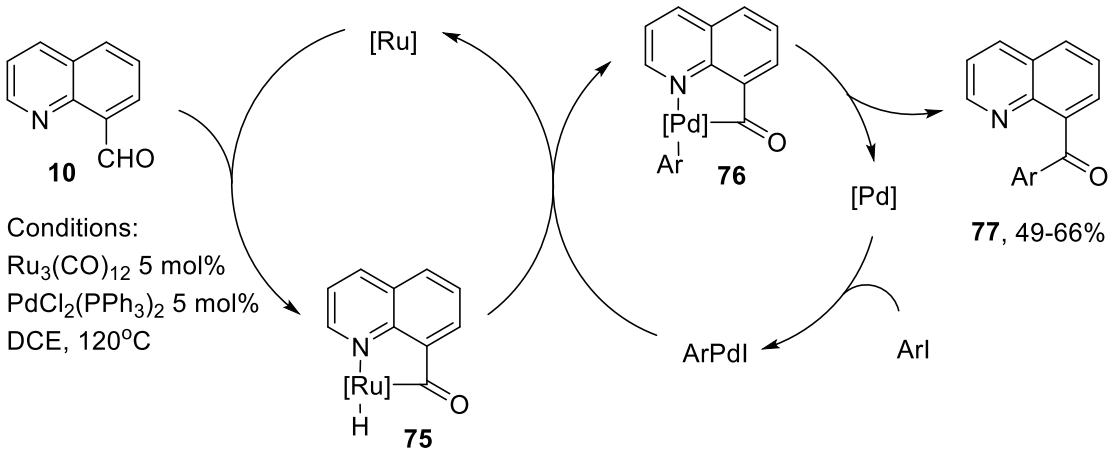

Conclusion

A review of the current literature shows that the most studied application of C–H activation in aldehydes is their alkylation with alkenes. However, most of the reported methodologies are limited to specific aldehydes such as 4-pentenals, and aldehydes containing an embedded chelating group, or specific alkenes such as α,β-unsaturated amides. The methodology reported by Jun uses temporary chelating groups and therefore is the most promising in terms of the scope of the reaction. However, harsh conditions are currently used and this process is not applicable with prochiral disubstituted alkenes.

Arylation of aldehydes with aryl halides is less studied. Embedded directing groups are required in all coupling reactions reported but Jun's iminium catalysis has not been studied for this transformation.

Chapter 2: A cooperative catalysis approach to intramolecular hydroacylation*

Introduction

Medium rings are traditionally challenging to prepare in synthetic organic chemistry. Although numerous strategies have been described for their preparation, metal-catalyzed hydroacylation is a potentially efficient method for the construction of medium ring ketones from simple alkenes and aldehydes.[1] Existing metal-mediated intramolecular alkene hydroacylation methods are typically limited to reactions in which cyclopentanones are generated.[2] Larger rings can only be directly accessed in cases where judiciously placed heteroatoms[3] are embedded into the starting materials (Scheme 1).[4,5] Alternatively, other strategies have employed more complex substrates that provide a proximal alkene.[6] Embedding a proximal chelating-group into the substrate has been successfully applied in intermolecular hydroacylation as well.[7] The requirement for proximal heteroatoms or alkenes to the aldehyde is often attributed to competitive aldehyde decarbonylation,[8] a process that is slowed by stabilizing the acyl metal intermediate via chelate formation. These substrate limitations are severely limiting to the broad applicability of hydroacylation.

* Reproduced from: Beletskiy, E. V.; Sudheer, C.; Douglas, C. J. *J. Org. Chem.* **2012**, *77*, 5884–5893.

An alternative to substrate embedded chelating groups is co-operative catalysis. Over thirty years ago, Suggs suppressed decarbonylation by forming 3-methyl-2-aminopyridyl aldimines, which functioned as surrogates for aldehydes in intermolecular hydroacylation.[9] Jun expanded upon this work, describing that 2-aminopicoline-based aldimines can form in catalytic amounts under intermolecular hydroacylation conditions, again suppressing decarbonylation via transiently formed chelating groups in a process termed cooperative catalysis.[10,11] Suggs and Jun's work is largely limited to mono-substituted alkenes. Recently, Breit and co-workers descried a bifunctional co-catalyst, 6-((diphenylphosphino)methyl)-2-aminopicoline, which improved co-catalyst efficiency relative to 2-aminopicoline in intermolecular hydroacylation reactions of mono-substituted alkenes.[10b] Briet also described increased efficiency in intramolecular hydroacylation reactions of 2-vinylbenzaldehydes to form the five-membered ring of 1-indanones. Briet's co-catalyst is prepared via a 5-step sequence (27% overall yield) from the pivalamide of 6-methyl-2-aminopyridine. A general metal-catalyzed intramolecular hydroacylation approach for the synthesis of six- and larger-membered rings, remains elusive. Moreover, hydroacylation of 1,1-disubstituted alkenes to form ketones bearing stereocenters has only been reported for the limited substrate classes discussed above.

We were inspired by the above work to develop a general strategy that would allow traditionally challenging, direct intramolecular hydroacylation of disubstituted alkenes (Scheme 1). The aminopyridine co-catalyst is a potential platform for asymmetric catalysis. This work could greatly expand the types of intramolecular hydroacylation reactions beyond those currently possible. A potential challenge in this strategy is that aldimine

formation and hydroacylation must be faster than aldehyde decarbonylation. Therefore, one of our goals was to enhance aldimine formation. Moreover, we were aware that competitive isomerization of the alkene to a more substituted olefin may require suppression. Our results to these ends are reported herein.

Scheme 1. Medium rings via hydroacylation.

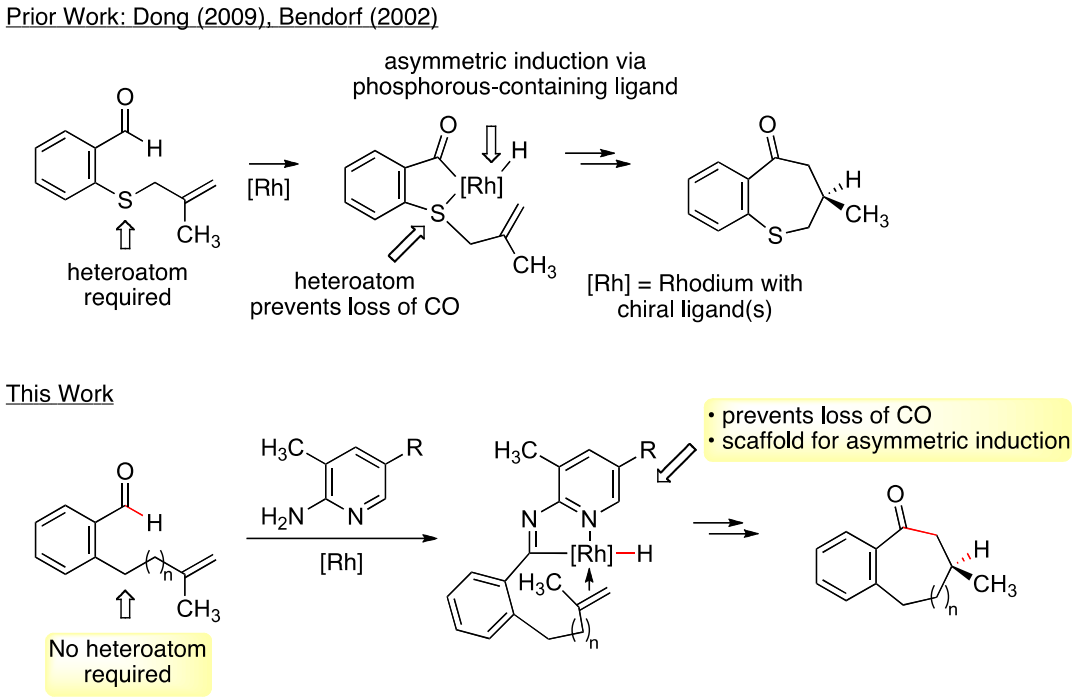

Results and discussion

We envisioned several strategies to accelerate hydroacylation and suppress the decomposition pathways outlined above. We chose to utilize one of Jun's strategies that

was successful in intermolecular hydroacylation reactions; adding $PhNH_2$ and BzOH to presumably convert free aldehyde to the aniline-derived aldimine, providing in situ protection of the aldehyde from decarbonylation.[10d] Our initial attempts to convert aldehyde **1a** to cycloheptanone **2a** using the temporary chelating imine strategy with 2-amino-3-picoline **3** (Table 1, entries 1-7),[12] required an excess of **3** (120 mol %) to achieve acceptable yield of **2a**. In attempts with BF_4 as the rhodium counter ion, acceptable yields could be obtained once the ratio of $Rh:PPh_3$ was 1:3 (Table 1, entries 1-3). Without phosphine in the reaction mixture (Table 1, entry 1) no **2a** was detected. As phosphine was added, the hydroacylation became more efficient at 1:2 (42%, entry 2) and plateaued at 1:3 (72%, entry 3). The amount of phosphine present also impacted reactions in which Cl was the rhodium counter ion. Without phosphine, $[RhCl(coe)_2]_2$ did not provide a detectable amount of ketone **2a** (entry 4). Addition of 5 mol % of PPh_3 to give a $Rh:PPh_3$ mole ratio of 1:1 led to an acceptable 77% yield of **2a** (entry 5). Increasing the $Rh:PPh_3$ ratio to 1:3 with Wilkinson's catalyst decreased the yield of **2a** to 60% (entry 6). The optimal phosphine to rhodium ratio may have changed with the counter ion due to coordination of Cl, but not BF_4, to rhodium under the reaction conditions.

Taking our best conditions that used a stoichiometric amount of **3** (entry 5) and attempting to use amine **3** as a co-catalyst at 25 mol % (entry 7) led to incomplete conversion and a decrease in the yield of **2a** from 77% to 45%. We hypothesized that aldimine formation of 2-amino-3-picoline **3** with **1a** or its *N*-phenyl imine congener was sluggish due to the poor nucleophilicity of the amino group in **3** due to the amine's conjugation with an electron-deficient aromatic system.

Table 1. Initial optimization of hydroacylation.[a]

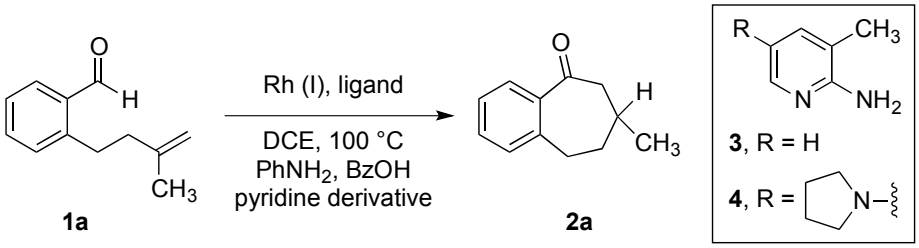

Entry	Rh(I) cat.	cat. (mol %)	ligand	ligand (mol %)	2-aminopyridine (mol %)	yield **2a**[b]
1	$Rh(BF_4)(cod)_2$	5%	None	-	**3** (120%)	ND
2	$Rh(BF_4)(cod)_2$	5%	PPh_3	10%	**3** (120%)	42%
3[c]	$Rh(BF_4)(cod)_2$	5%	PPh_3	15%	**3** (120%)	72%
4	$[RhCl(coe)_2]_2$	2.5%	None	-	**3** (120%)	ND
5	$[RhCl(coe)_2]_2$	2.5%	PPh_3	5%	**3** (120%)	77%
6	$RhCl(PPh_3)_3$	5%	None	-	**3** (120%)	60%
7	$[RhCl(coe)_2]_2$	2.5%	PPh_3	5%	**3** (25%)	45%
8	$[RhCl(coe)_2]_2$	2.5%	PPh_3	5%	**4** (25%)	76%
9[c]	$[RhCl(coe)_2]_2$	2.5%	PPh_3	5%	**3** (10%)	81%
10	$[RhCl(coe)_2]_2$	2.5%	P(*o*-Tol)$_3$	5%	**3** (25%)	ND
11	$[RhCl(coe)_2]_2$	2.5%	PPh_2Me	5%	**3** (25%)	68%
12	$[RhCl(coe)_2]_2$	2.5%	$PPhMe_2$	5%	**3** (25%)	37%
13	$[RhCl(coe)_2]_2$	2.5%	$PPhCy_2$	5%	**3** (25%)	29%
14	$[RhCl(coe)_2]_2$	2.5%	P(*t*-Bu)$_3$	5%	**3** (25%)	ND
15	$[RhCl(coe)_2]_2$	2.5%	$P(C_6F_5)_3$	5%	**3** (25%)	ND

[a] Conditions: Rh(I) cat, ligand, $PhNH_2$ (1.2 equiv), BzOH (10 mol %), DCE, 100 °C [b] Yields by ^1H NMR spectroscopy of the crude reaction mixture with 4-methoxyacetophenone as an internal standard; ND = **2a** not detected. [c] Entries 3 and 9–15 used $PhCF_3$ as solvent. DCE = 1,2-dichloroethane, cod = 1,5-cyclooctadiene, coe = cyclooctene.

To reduce the loading of the 2-amino-pyridine derivative to catalytic levels, we turned to exploring more reactive co-catalysts in the reaction. Commercially available 2-aminotriazol, 1-aminobenzotriazol and 2-aminobenzimidazole gave only traces of product **2a** as replacements for **3** in attempted hydroacylation reactions. However, amine **4** proved to be significantly more efficient as a co-catalyst (Table 1, entry 8 vs. 7). We attribute this observation to the higher nucleophilicity of the amine in **4** compared to **3** and thus higher rate of imine equilibration. Co-catalyst **4** can be prepared from **3** in two steps (46% yield overall) via a straightforward iodination/amination sequence. See the experimental section for details.

We examined the influence of solvent on reaction by measuring the yield of **2a** at lower temperatures to accentuate solvent effects in the conversion range 0-20% (not shown). We found that reaction rate qualitatively increases in the order of DCE < THF < PhMe < $PhCF_3$. We could not explain these observations because they do not track well with trends in solvent polarity or Lewis basicity. It is well known, however, that $PhCF_3$ can be a useful alternative in organic reactions that are typically conducted in chlorinated solvents.[13] In our hydroacylation reactions, it is superior to DCE as well as toluene. Changing solvent from DCE to $PhCF_3$ allowed for the reduction of the co-catalyst loading to 10 mol % while improving the yield of **2a** to 81% (entry 9).

We examined different phosphine ligands to examine the impact of phosphine basicity and sterics on the hydroacylation reaction (Table 1, entries 9–15). Coincidentally, the ligand we initially chose, triphenylphosphine, appeared to be the best ligand of those examined (entry 9). Increasing the steric bulk of the ligand (tri-ortho-tolyl phosphine, Table

1, entry 10) suppressed the formation of **2a** to below our detection limit. Mixed alkyl/aryl phosphine ligands (methyldiphenylphosphine and dimethylphenylphosphine; entries 11, 12) decreased the efficiency of the catalytic system, providing **2a** in 68% and 37% yield respectively when 25 mol % of **3** was employed. Bulky alkyl phosphine ligands (cyclohexyldiphenyl phosphine and tri-*tert*-butylphosphine; entries 13 and 14) proved to be largely ineffective, with only a 29% yield of **2a** (entry 13). The steric effect might be attributed to the requirement of an extra coordination site for the catalytic directing group in these hydroacylation reactions. This is in contrast to typical cyclopentanone-forming hydroacylation reactions without 2-aminopyridine co-catalysts where the alkene serves the dual purpose of forming a metal chelate to prevent carbon monoxide loss while still undergoing migratory insertion. Therefore, the reaction exhibits high sensitivity to the steric bulk of the ligand compared to the side reactions. A less basic wide cone-angle phosphine, tris(pentafluorophenyl)-phosphine was also completely ineffective in hydroacylation (entry 15).

With the identification of several acceptable conditions (Table 1, entries 8 and 9), we turned to examine the substrate scope (Table 2). Variation of the substituent on the aryl ring (entries 1-4) did not require changes in reaction conditions from those used to obtain acceptable yields of **2a** (Table 1, entry 9). Substrates containing both electron donating (R^1 = CH_3 or OCH_3, entries 1 and 3) and electron withdrawing groups (R^1 = CF_3 or F, entries 2 and 4) para to the aldehyde underwent hydroacylation in acceptable yields (76–85%) using 10 mol % of co-catalyst **3**. We examined substitution of the alkene portion of the substrate. Replacing the alkene methyl group with an ethyl substituent (**1f**, R^2 = Et, entry

5), the corresponding hydroacylation product **2f** was obtained in 86% yield using 10 mol % co-catalyst **3**. Changing R^2 from an alkyl to an aryl group, however, made the hydroacylation more challenging. Phenyl-substituted alkene **1g** required a higher loading (25 mol %) of the more nucleophilic co-catalyst **4** to provide an acceptable 77% yield of cycloheptanone **2g**.[14-16]

Table 2. Scope of intramolecular hydroacylation.

Entry[a]	substrate **1**			**3** or **4** (mol %)	product **2**	yield[b]
	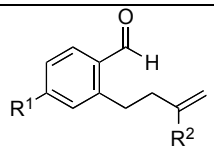				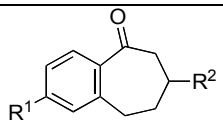	
		R^1	R^2			
1	**1b**	Me	Me	**3** (10%)	**2b**	84%[c]
2	**1c**	CF_3	Me	**3** (10%)	**2c**	76%
3	**1d**	OMe	Me	**3** (10%)	**2d**	85%
4	**1e**	F	Me	**3** (10%)	**2e**	80%[c]
5	**1f**	H	Et	**3** (10%)	**2f**	86%
6	**1g**	H	Ph	**4** (25%)	**2g**	77%
7	**1h**	H	CH_2OTBS	**4** (10%)	**2h**	78%
8[d]	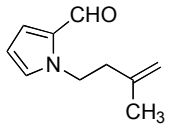 **1i**			**4** (25%)	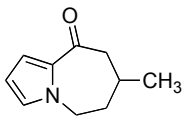 **2i**	63%

Table 2 (continued). Scope of intramolecular hydroacylation.

9[d]	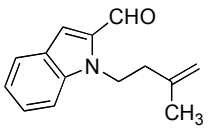 **1j**	**4** (25%)	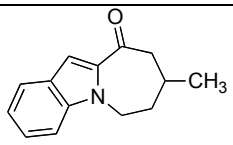 **2j**	66%
10	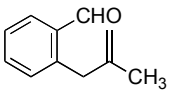 **1k**	**4** (90%)	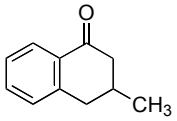 **2k**	65%[e]
11	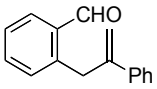 **1l**	**4** (25%) **4** (100%)	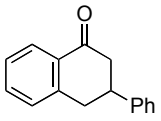 **2l**	48% 58%
12[d]	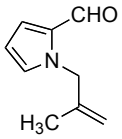 **1m**	**4** (25%)	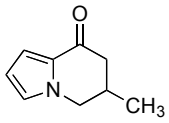 **2m**	67%
13[d]	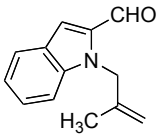 **1n**	**4** (100%)	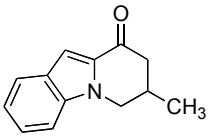 **2n**	69%

[a] Conditions: $[RhCl(coe)_2]_2$ (2.5 mol %), PPh_3 (5 mol %), $PhNH_2$ (1.2 equiv), BzOH (10 mol %), $PhCF_3$, 100 °C. [b] Isolated yield after silica gel chromatography. Except where noted, regioisomeric hydroacylation products were not observed, indicating regioselectivity was (<10:1) [c] Contaminated with a minor <5% of the corresponding indanone, pure sample could be obtained by preparative TLC. [d] Conditions: $[RhCl(coe)_2]_2$ (5 mol %), PPh_3 (10 mol %), $PhNH_2$ (1.2 equiv), BzOH (10 mol %). [e] yield by ^1H NMR spectroscopy of the crude reaction mixture with 4-methoxyacetophenone as an internal standard. An attempt with 25% **4** gave 30% yield of **2k** after a challenging purification by chromatography.

Allylic oxygenation on the alkene also appeared rendered the alkene less reactive (**1h**, entry 7), requiring co-catalyst **4** (10 mol %) to provide **2h** in 78% yield (entry 6). Since **1h** was not completely consumed when **3** was the co-catalyst, the more reactive co-catalyst **4** was used. These results show the impact of alkene substitution beyond simple alkyl groups. A more reactive catalyst system is required when additional functional groups are proximal to the alkene.

We also examined substrates in which the alkene and aldehyde are linked via heterocycles rather than a benzene ring. Note that in pyrrole **1i** and indole **1j** (entries 8 and 9), the nitrogen is not a suitable donor for chelation stabilization of the rhodium hydride intermediate. These substrates reacted sluggishly under hydroacylation conditions and required 25 mol % of co-catalyst **4**, 5 mol % of $[RhCl(coe)_2]_2$, and 10 mol % PPh_3 to provide 63% and 66% yield of dihydro-pyrroloazepineone **2i** and dihydro-azepinoindolone **2j** respectively. We attribute the lower reactivity of these substrates to increased conjugation to the carbonyl, which may lower its electrophilicity and slow imine formation and/or subsequent hydroacylation steps.

We note that the high preference for 7-endo cyclization is completely reversed from the 6-exo selectivity recently reported *N*-heterocyclic carbene (NHC) catalyzed intramolecular hydroacylation with **1g** reported by Grimme, Glorius, and co-workers, which proceeds by a completely different mechanism.[17] The regioselectivity in NHC compared to Rh-catalyzed reactions provides chemists with a powerful means of complementary control in hydroacylation reactions. Six membered rings are also traditionally challenging to form via metal-catalyzed intramolecular hydroacylation. As we expanded our study to target six-

membered ring products, we were somewhat surprised that these substrates (**1k**–**1n**, Table 2, entries 10–13) reacted much more slowly than their longer-tether counterparts. Typically, six-membered ring formation is more facile than seven-membered ring construction.[18] In our case, however, higher loadings of aminopyridine **4** were required to achieve yields ranging from 48–69% and in some cases, a full equivalent of **4** was required (entries 11 and 13). The poorer behavior of **1k**–**1n** compared to congeners targeting seven-membered rings might be explained by slower migratory insertion in these substrates compared their higher homologs. We speculate that the more proximal alkene might lead to a stable alkene complex after C-H activation, perhaps raising the barrier to migratory insertion. Alternatively, reductive elimination may slower from the presumptive 7-membered metallacycle in the formation of **2k**–**2n** compared to their congeners that should proceed via 8-membered metallacycle, which may undergo more rapid reductive elimination. Typically, reductive elimination is rate-limiting in intramolecular hydroacylation reactions.[19]

Interestingly, substrate **1o**, containing a mono-substituted alkene, also required higher loadings of co-catalyst for successful hydroacylation to form 1-benzosuberone (**2o**, Scheme 2). We found that without co-catalyst **3**, isomerization from the terminal to the internal alkene (**1o** → **1p**) occurred to form a mixture of trans/cis **1p**. Thus higher loadings of co-catalyst are required to suppress this side reaction. With low loadings of co-catalyst **3**, the isomerization is prevailing and no **2o** is observed. Instead, indanone **2p** is formed as the major product under these reaction conditions, presumably by cyclization of **1p**. A small amount of 2-methyl dihydronaphthalenone was also observed in this attempt. We

also note that under many of our optimization reactions in Table 1, a minor amount of 2-isopropyl-2,3-dihydroindenone (tentatively assigned) was observed in the crude product mixtures.

Scheme 2. Mono-substituted alkene hydroacylation.

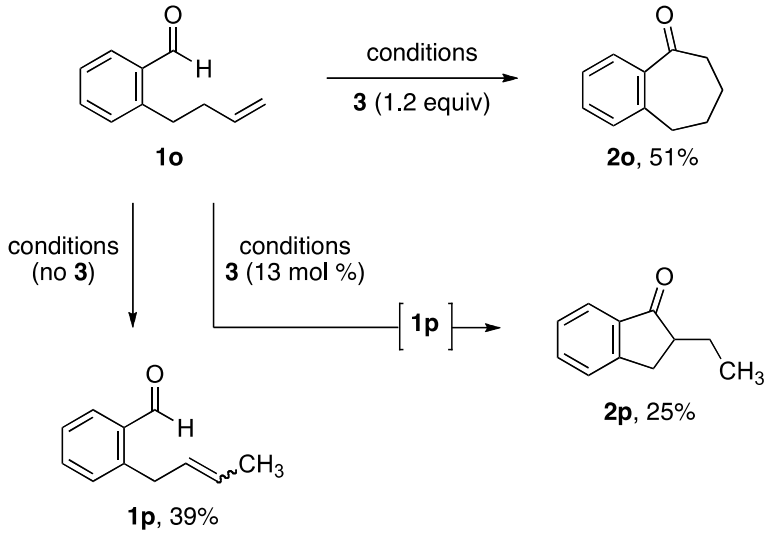

Conditions: $[RhCl(coe)_2]_2$ (2.5 mol %), PPh_3 (5 mol %), BzOH (10 mol %), $PhNH_2$ (1.2 equiv), $PhCF_3$, 100 °C.

Given recent advances in asymmetric hydroacylation, we performed a preliminary investigation on asymmetric hydroacylation, using the conversion **1a** to **2a** as our test reaction. No reaction was observed when bidentate ligands (BINAP, DUPHOS, dppe, or dppp) were used as additives to various rhodium species (results not shown). Product **2a** was observed when chiral monodentate ligands (entries 2-4, Table 3) were used as additives, although, yields were low in all cases examined. Given the high sensitivity of the efficiency of hydroacylation to the structure of the phosphorous-containing ligand

(Table 3 and Table 2, entries 9–15), we curtailed our investigation of these types of ligands and sought new ways to induce asymmetry in the reaction.

Table 3. Effects of Chiral Ligands.[a]

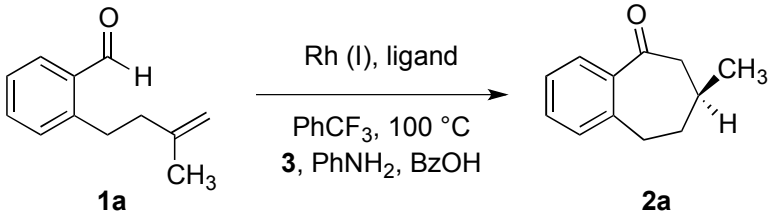

Entry	Ligand	yield[b]	ee[c]
1	(+)-MONOPHOS	ND	--
2[d]	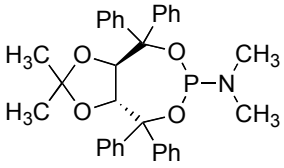	30%	23%
3	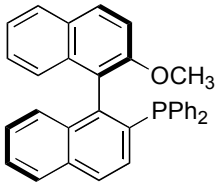	10%	24%
4	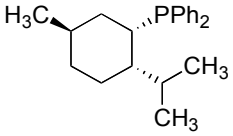	3%	18%

[a] Conditions: $[RhCl(coe)_2]_2$ (2.5 mol %), ligand (5 mol %), $PhNH_2$ (1.2 equiv), BzOH (10 mol %), $PhCF_3$, 100 °C. [b] yield after silica gel chromatography; ND = **2a** not detected [c] determined by HPLC (Chiralcel OD-H, *n*-hexane:IPA (9:1), λ = 220 nm) [d] **1a**, $PhNH_2$, BzOH in $PhCF_3$ were premixed before adding $[RhCl(coe)_2]_2$, ligand, and **3**.

Since our optimization studies had conclusively shown that co-catalysts **3** and **4** were also necessary for hydroacylation, we hypothesized that incorporating chirality into the 2-amino-3-picoline structure would provide an entry to asymmetric hydroacylation. We decided to use analogs of **4** with chiral 5-amino group, due to ease of preparation of these compounds and expected high reactivity from the electron-donating group.[20]

Our initial studies with **5** (Scheme 3), which was derived from a chiral oxazolidinone, showed that it is less reactive than **4** and even **3**. However, the reaction could still be successfully accomplished with 25 mol % loading of co-catalyst **5**. Promising enantioselectivity was observed in this case (**2a**, 82 % yield, 31% ee). Although not yet

Scheme 3. Enantioselective hydroacylation.

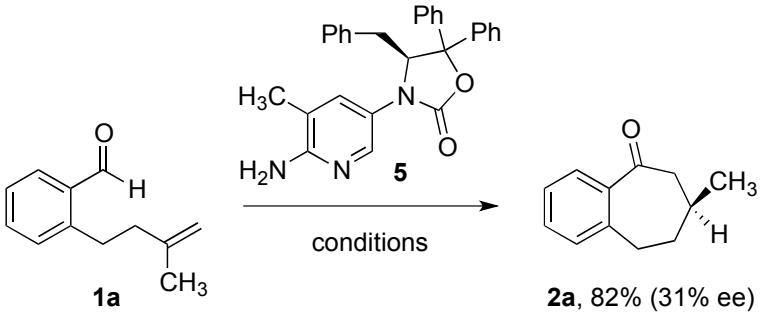

Conditions: $[RhCl(coe)_2]_2$ (2.5 mol %), PPh_3 (5 mol %), $PhNH_2$ (1.2 equiv), BzOH (10 mol %), $PhCF_3$, 80 °C.

synthetically useful, this showcases a new strategy for inducing asymmetry in hydroacylation reactions. Our approach is a significant departure from prior work based on chiral phosphorous-containing ligands in hydroacylation chemistry. Given the high degree of recent interest in asymmetric hydroacylation, these results should inspire

additional work, which we envision will achieve high levels of enantioinduction in the fullness of time.

Conclusion

In conclusion, we have reported the first effective method for metal-catalyzed synthesis of six- and seven-membered ring ketones via hydroacylation that is free of the requirement of chelating groups embedded into the substrate. The development of electron rich 2-amino-3-picolines **4** and **5** enables the incorporation of a temporary chelate scaffold on the aldehyde that prevents decomposition via aldehyde decarbonylation and alkene isomerization pathways. For challenging substrates, **4** may also be used in stoichiometric amounts. The regiochemistry of the hydroacylation is complementary to NHC-catalyzed hydroacylation reactions,[17] which should prove useful in synthesis planning. Chiral 2-aminopyridines such as **5** represent a new strategy for asymmetric catalysis in hydroacylation. Future work will be directed at improvement of the asymmetric induction in hydroacylation and applications in target-directed synthesis.

Experimental details

Trifluorotoluene ($PhCF_3$) was distilled over phosphorous pentoxide, degassed by four freeze-pump-thaw cycles in a Straus flask and then stored in a nitrogen-filled glove box. All rhodium complexes were purchased and used as received, except $[RhCl(coe)_2]_2$ which

was prepared by a known procedure.[21] The preparations of aldehydes **1a**,[22] **1k**,[23] **1g**,[21] and **1o**[21] have been previously reported, new procedures for the preparations of **1k** and **1g** are reported below. Aldehyde **1o** was prepared in analogy to **1b**. All rhodium-catalyzed processes were carried out in a N_2 filled glove box in 1 dram vials with polytetrafluoroethylene-lined caps and heating was applied by aluminum block heaters. HRMS measurements using electrospray ionization (ESI) were performed with a time of flight (TOF) mass analyzer and HRMS measurements using chemical ionization (CI) were performed with a magnetic sector mass analyzer.

General Procedure for the Synthesis of Aldehydes 1b-1e:[24]

N,N,N-Trimethylethyldiamine (0.41 mL, 3.2 mmol) in THF (8 mL) was added to a flame-dried flask under nitrogen, the solution was cooled to –78 °C, and *n*-BuLi (2.5 M in hexanes, 1.35 mL, 3.10 mmol) was added dropwise. The reaction was allowed to stir for 30 min at –78 °C, followed by slow addition of 2-methylbenzaldehyde derivative (3.0 mmol). The solution was warmed to –16 °C for 20 min, and re-cooled to –55 °C for the dropwise addition of *t*-BuLi (1.7 M in pentane, 5.3 mL, 9.0 mmol). The resulting deep red solution was stirred at –55 °C for 2.5 h, and re-cooled to –78 °C. Isobutenyl chloride (1.75 mL, 18 mmol) was added rapidly, and the pale yellow solution was allowed to warm to room temperature and stirred for 30 min. The solution was poured onto cold 1.0 M HCl (15 mL), stirred for 10 min, and the layers were separated. The aqueous layer was extracted with Et_2O (3 × 15mL), and the combined organics were washed with brine, dried over Na_2SO_4, and concentrated in vacuo. Silica gel chromatography (EtOAc:Hex) afforded compounds **1b-1e** in reported yields.

4-Methyl-2-(3-methylbut-3-en-1-yl)benzaldehyde (1b): See general procedure for the synthesis of aldehydes **1b-1e**. Reaction carried out with 308 mg (2.3 mmol) of 2,4-dimethylbenzaldehyde. The crude product mixture was purified by silica gel column chromatography (1:6 EtOAc:Hex) to afford 360 mg (83% yield) of **1b** as a colorless oil: R_f 0.60 (1:4 EtOAc:Hex). ^{1}H NMR (300 MHz, $CDCl_3$) δ 10.20 (s, 1H), 7.72 (d, *J* = 8.1 Hz, 1H), 7.17 (d, *J* = 7.8 Hz, 1H), 7.09 (s, 1H), 4.77–4.72 (m, 2H), 3.15–3.10 (m, 2H), 2.39 (s, 3H), 2.31–2.26 (m, 2H), 1.81 (s, 3H); ^{13}C NMR (75 MHz, $CDCl_3$) δ 191.9, 144.96, 144.92, 144.7, 132.3, 131.6, 131.3, 127.3, 110.5, 40.1, 31.1, 22.5, 21.7; IR (film) 3047, 2973, 2919, 1691, 1607, 1451, 1300 cm^{-1}; HRMS (CI) calcd for $[C_{13}H_{16}O + NH_4]^+$, *m/z* 206.1539, found 206.1544.

2-(3-Methylbut-3-en-1-yl)-4-(trifluoromethyl)benzaldehyde (1c): See general procedure for the synthesis of aldehydes **1b-1e**. Reaction carried out with 2-methyl-4-trifluoromethylbenzaldehyde (188 mg, 1.0 mmol). The crude mixture was purified by silica gel column chromatography (1:6 EtOAc:Hex) to afford 203 mg (84% yield) of **1c** as a colorless oil: R_f 0.50 (1:4 EtOAc:Hex). ^{1}H NMR (300 MHz, $CDCl_3$) δ 10.34 (s, 1H), 7.96 (d, *J* = 8.1 Hz, 1H), 7.63 (d, *J* = 8.1 Hz, 1H), 7.55 (s, 1H), 4.79–4.71 (m, 2H), 3.26–3.20 (m, 2H), 2.33 (t, *J* = 8.1 Hz, 2H), 1.81 (s, 3H); ^{13}C NMR (75 MHz, $CDCl_3$) δ 191.1, 145.6, 144.1, 136.0, 134.8 (q, *J* = 32.3 Hz), 131.9, 127.8 (q, *J* = 3.2 Hz), 123.5 (q, *J* = 272.9 Hz), 123.4 (q, *J* = 3.7 Hz), 111.2, 39.9, 30.9, 22.4; IR (film) 3056, 2983, 2939, 1706, 1498, 1422, 1330, 1266, 1173,1132 cm^{-1}; HRMS (CI) calcd for $[C_{13}H_{13}F_3O + H]^+$, *m/z* 243.0991, found 243.1015.

4-Methoxy-2-(3-methylbut-3-en-1-yl)benzaldehyde (1d): See general procedure for

the synthesis of aldehydes **1b-1e**. Reaction carried out with 4-methoxy-2-methylbenzaldehyde (345 mg, 2.3 mmol). The crude mixture was purified by silica gel column chromatography (1:4 EtOAc:Hex) to afford 388 mg (83% yield) of **1d** as a colorless oil: R_f 0.40 (1:4 EtOAc:Hex). ^{1}H NMR (300 MHz, $CDCl_3$) δ 10.10 (s, 1H), 7.78 (d, *J* = 8.7 Hz, 1H), 6.85 (dd, *J* = 2.7, 8.7 Hz, 1H), 6.76 (d, *J* = 2.4 Hz, 1H), 4.74 (d, *J* = 11.4 Hz, 2H), 3.87 (s, 3H), 3.17–3.11 (m, 2H), 2.32–2.27 (m, 2H), 1.79 (s, 3H); ^{13}C NMR (75 MHz, $CDCl_3$) δ 190.7, 163.7, 147.6, 144.9, 134.8, 127.3, 116.1, 111.6, 110.6, 55.4, 39.8, 31.3, 22.5; IR (film) 3056, 2934, 2841, 1687, 1601, 1567, 1496, 1461 cm^{-1}; HRMS (CI) calcd for $[C_{13}H_{16}O_2 + H]^+$, *m/z* 205.1223, found 205.1235.

4-Fluoro-2-(3-methylbut-3-en-1-yl)benzaldehyde (1e): See general procedure for the synthesis of aldehydes **1b-1e**. Reaction carried out with 2-methoxy-4-methylbenzaldehyde (303 mg, 2.2 mmol). The crude mixture was purified by silica gel column chromatography (1:6 EtOAc:Hex) to afford 340 mg (80% yield) of **1e** as a colorless oil: R_f 0.60 (1:4 EtOAc:Hex). ^{1}H NMR (300 MHz, $CDCl_3$) δ 10.18 (s, 1H), 7.87–7.81 (m, 1H), 7.07–6.94 (m, 2H), 4.77–4.69 (m, 2H), 3.19–3.14 (m, 2H), 2.32–2.27 (m, 2H), 1.80 (s, 3H); ^{13}C NMR (75 MHz, $CDCl_3$) δ 190.5, 165.7 (d, *J* = 256.6 Hz), 148.4 (d, *J* = 9.1 Hz), 144.3, 134.7 (d, *J* = 10.0 Hz), 130.3 (d, *J* = 2.6 Hz), 117.6 (d, *J* = 21.7 Hz), 113.8 (d, *J* = 21.7 Hz), 111.0, 39.5, 30.8, 22.4; IR (film) 3054, 2984, 2937, 1695, 1606, 1583, 1491, 1266 cm^{-1}; HRMS (CI) calcd for $[C_{12}H_{13}FO + NH_4]^+$, *m/z* 210.1289, found 210.1292.

2-(3-Methylenepentyl)benzaldehyde (1f): *N,N,N*-Trimethylethyldiamine (0.40 mL, 3.15 mmol) in THF (8 mL) was added to a flame-dried flask under nitrogen, the solution was cooled to –78 °C, and *n*-BuLi (2.5 M in hexanes, 1.24 mL, 3.10 mmol) was added

dropwise. The reaction was allowed to stir for 30 min at –78 °C, followed by slow addition of 2-methylbenzaldehyde (0.35 mL, 3.0 mmol). The solution was warmed to –15 °C for 20 min, and re-cooled to –55 °C for the dropwise addition of *t*-BuLi (1.7 M in pentane, 3.5 mL, 6.0 mmol). The resulting deep red solution was stirred at –55 °C for 4 h. 2-Methylenebutyl-4-methylbenzenesulfonate[20] (2.16 g, 9 mmol) in THF (2 mL) was added rapidly, and the pale yellow solution was allowed to warm to room temperature and stirred for 30 min. The solution was poured onto cold 1.0 M HCl (15 mL), and stirred for 10 min. PhMe (50 mL) was added, the layers were separated and the organic extracts were concentrated in vacuo. Silica gel chromatography (1:30 EtOAc:Hex) afforded compound **1f** (322 mg, 1.71 mmol, 57%) as a colorless oil: R_f 0.60 (1:4 EtOAc:Hex). ^{1}H NMR (300 MHz, $CDCl_3$) δ 10.27 (s, 1H), 7.83 (dd, *J* = 1.5, 8.9 Hz, 1H), 7.53 (dt, *J* = 1.5, 7.5 Hz, 1H), 7.37 (dt, *J* = 0.9, 7.5 Hz, 1H), 7.28 (dd, *J* = 0.6, 7.5 Hz, 1H), 4.78–4.76 (m, 2H), 3.20–3.14 (m, 2H), 2.32–2.29 (m, 2H), 2.10 (dq, *J* = 0.3, 7.2 Hz, 2H), 1.05 (t, *J* = 7.2 Hz, 3H); ^{13}C NMR (75 MHz, $CDCl_3$) δ 192.3, 150.5, 145.1, 133.8, 131.8, 131.0, 126.5, 110.1, 108.5, 38.7, 31.3, 28.8, 12.3; IR (film) 2964, 2728, 1693, 1599 cm^{-1}; HRMS (ESI) calcd for $[C_{13}H_{16}O + Na]^+$ 211.1093, found 211.1098.

2-(3-Phenylbut-3-en-1-yl)benzaldehyde (1g): *N,N,N*-Trimethylethyldiamine (0.40 mL, 3.15 mmol) in THF (8 mL) was added to a flame-dried flask under nitrogen, the solution was cooled to –78 °C, and *n*-BuLi (2.5 M in hexanes, 1.24 mL, 3.10 mmol) was added dropwise. The reaction was allowed to stir for 30 min at –78 °C, followed by slow addition of 2-methylbenzaldehyde (0.35 mL, 3.0 mmol). The solution was warmed to –15 °C for 20 min, and re-cooled to –55 °C for the dropwise addition of *t*-BuLi (1.7 M in

pentane, 3.5 mL, 6.0 mmol). The resulting deep red solution was stirred at –55 °C for 3 h and cooled to –78 °C. 3-Bromo-2-phenylpropene[25] (1.76 g, 9 mmol) in THF (2 mL) was added rapidly, and the pale yellow solution was allowed to warm to room temperature and stirred for 30 min. The solution was poured onto cold 1.0 M HCl (15 mL), and stirred for 10 min. PhMe (50 mL) was added, the layers were separated and the organic layer was concentrated in vacuo. Silica gel chromatography (1:30 EtOAc:Hex) afforded compound **1g** (306 mg, 1.30 mmol, 43%) as a colorless oil: R_f 0.55 (1:4 EtOAc:Hex). The characterization data are consistent with those previously reported.[21]

2-(3-(((*tert*-Butyldimethylsilyl)oxy)methyl)but-3-en-1-yl)benzaldehyde (1h): *N,N,N*-Trimethylethyldiamine (0.14 mL, 1.1 mmol) in THF (5 mL) was added to a flame-dried flask under nitrogen, the solution was cooled to –78 °C, and *n*-BuLi (2.5 M in hexanes, 0.44 mL, 1.10 mmol) was added dropwise. The reaction was allowed to stir for 30 min at –78 °C, followed by slow addition of 2-methylbenzaldehyde (0.12 mL, 1.0 mmol). The solution was warmed to –15 °C for 20 min, and re-cooled to –55 °C for the dropwise addition of *t*-BuLi (1.7 M in pentane, 0.88 mL, 1.5 mmol). The resulting deep red solution was stirred at –55 °C for 3 h and cooled to –78 °C. ((2-(bromomethyl)allyl)oxy)(*tert*-butyl)dimethylsilane[26] (619 mg, 2.34 mmol) in THF (1 mL) was added rapidly, and the pale yellow solution was stirred for 5 min and quenched with 1.0 M HCl (3 mL). The reaction mixture was allowed to warm to room temperature, PhMe (10 mL) was added, the layers were separated and the organic extracts were concentrated in vacuo. Silica gel chromatography (1:50 EtOAc:Hex) afforded compound **1h** (74 mg, 0.24 mmol, 24%) as a colorless oil: R_f 0.50 (1:4 EtOAc:Hex). ^{1}H NMR (300 MHz, $CDCl_3$)

δ 10.20 (s, 1H), 7.76 (dd, *J* = 1.3, 7.5 Hz, 1H), 7.43 (dt, *J* = 1.5, 7.5 Hz, 1H), 7.32 (dt, *J* = 1.5, 7.5 Hz, 1H), 7.21 (dd, *J* = 1.5, 7.5 Hz, 1H), 5.01 (d, *J* = 1.8 Hz, 1H), 4.80 (dd, *J* = 1.2, 2.7 Hz, 1H), 4.04 (s, 2H), 3.11 (m, 2H), 2.24 (t, *J* = 8.1 Hz, 2H), 0.83 (s, 9H), 0.01 (s, 3H); ^{13}C NMR (75 MHz, $CDCl_3$) δ 192.3, 147.6, 144.8, 133.8, 133.7, 131.9, 131.0, 126.6, 109.5, 65.9, 35.0, 31.3, 25.9, 18.4, –5.4; IR (film) 2953, 2928, 2855, 2730, 1697, 1600, 1249, 1114, 1086 cm^{-1}; HRMS (ESI) calcd for $[C_{18}H_{28}O_2Si + Na]^+$ 327.1756, found 327.1754.

2-(2-Methyallyl)benzaldehyde (1k): In a round bottom flask equipped with a reflux condenser and magnetic stir bar under nitrogen was placed Mg (150 mg, 6.25 mmol) and a small crystal of I_2. The flask was flame-dried under high vacuum. THF (3 mL) and 2-(2-bromophenyl)-1,3-dioxolane[27] (1.15 g, 5 mmol) were added and the mixture was maintained at reflux for 2 h. The resulting solution was allowed to cool to room temperature, then added dropwise to a stirred solution of isobutenyl chloride (0.74 mL, 7.5 mmol) and suspension of CuI (95 mg, 0.5 mmol) in THF (5 mL) at 0 °C. The reaction mixture was stirred for 2 h at 0 °C and then allowed to warm to room temperature overnight. CH_2Cl_2 (10 mL) was added and the mixture was washed with a saturated aqueous NH_4Cl solution. The organic phase was separated and concentrated in vacuo. TsOH (20 mg, 0.1 mmol), water (10 mL) and acetone (10 mL) were added and the resulting solution was heated at reflux for 2 h. The reaction mixture was extracted with CH_2Cl_2 (40 mL). The organic phase was separated, dried over Na_2SO_4 and concentrated in vacuo. Silica gel chromatography (1:20 EtOAc:Hex) afforded compound **1k** (345 mg, 2.16 mmol, 43%) as a colorless oil: R_f 0.65 (1:4 EtOAc:Hex). The characterization data are consistent with those previously reported.[21]

2-(2-Phenylallyl)benzaldehyde (1l): In a round bottom flask equipped with a reflux condenser and magnetic stir bar under nitrogen was placed Mg (150 mg, 6.25 mmol) and a small crystal of I_2. The flask was flame-dried under high vacuum. THF (3 mL) and 2-(2-bromophenyl)-1,3-dioxolane[25] (1.15 g, 5 mmol) were added and the mixture was maintained at reflux for 2 h. The resulting solution was added dropwise to a stirred solution of 3-bromo-2-phenylpropene (1.48 g, 7.5 mmol) and suspension of CuI (95 mg, 0.5 mmol) in THF (5 mL) at 0 °C. The reaction mixture was stirred for 2 h at 0 °C and then allowed to warm to room temperature overnight. CH_2Cl_2 (10 mL) was added and the mixture was washed with a saturated aqueous NH_4Cl solution. The organic phase was separated and concentrated in vacuo. TsOH (20 mg, 0.1 mmol), water (10 mL) and acetone (10 mL) were added and the resulting solution was heated at reflux for 2 h. The reaction mixture was extracted with CH_2Cl_2 (40 mL). The organic phase was separated, dried over Na_2SO_4 and concentrated in vacuo. Silica gel chromatography (1:20 EtOAc:Hex) afforded compound **1l** (445 mg, 2.00 mmol, 40%) as a colorless oil: R_f 0.60 (1:4 EtOAc:Hex). ^{1}H NMR (300 MHz, $CDCl_3$) δ 10.22 (s, 1H), 7.86 (dd, J = 1.5, 7.5 Hz, 1H), 7.51–7.22 (m, 8H), 5.45 (t, J = 0.9 Hz, 1H), 4.71 (dd, J = 1.5, 2.4 Hz, 1H), 4.23 (s, 1H); ^{13}C NMR (75 MHz, $CDCl_3$) δ 192.2, 147.4, 141.7, 140.8, 134.1, 133.8, 131.5, 131.4, 128.3, 127.7, 127.0, 125.9, 114.8, 37.6; IR (film) 3055, 3029, 2855, 2753, 1696, 1599, 1210 cm^{-1}; HRMS (ESI) calcd for $[C_{16}H_{14}O + Na]^+$ 245.0942, found 245.0951.

General Procedure for the Synthesis of Pyrrole- and Indole-Containing Aldehydes (1i, **1j**, **1m**, **1n)**. Aldehyde (5 mmol), 18-crown-6 (5 mmol), and powdered KOH (10 mmol) were refluxed in benzene (5 mL) for 2 h. 4-Iodo-2-methyl-1-butene or isobutenyl chloride

(15.0 mmol) was added as a solution in benzene (2.5 mL) and reflux was maintained for an additional 6 h. The solution was washed with water, and the layers were separated. The aqueous layer was extracted with Et_2O (3 □ 15 mL), and the combined organic phases were washed with brine, dried over Na_2SO_4, and concentrated in vacuo. Silica gel chromatography (EtOAc:Hex) afforded **1i, 1j, 1m,** or **1n** as yellow oils in the reported yields.

1-(3-Methylbut-3-en-1-yl)-1*H*-pyrrole-2-carbaldehyde (1i): See general procedure for the synthesis of pyrroles and indoles **1i**, **1j**, **1m**, **1n.** Reaction carried out with 1*H*-pyrrole-2-carbaldehyde (475 mg, 5.0 mmol). The crude product mixture was purified by silica gel column chromatography (1:3 EtOAc:Hex) to afford 407 mg (50% yield) of **1i** as a yellow oil. R_f 0.35 (1:3 EtOAc:Hex). ^{1}H NMR (300 MHz, $CDCl_3$) δ 9.53 (s, 1H), 6.92 (d, *J* = 3.6 Hz, 2H), 6.19 (t, *J* = 3.6 Hz, 1H), 4.77–4.76 (m, 1H), 4.64–4.63 (m, 1H), 4.41 (t, *J* = 7.2 Hz, 1H), 2.44 (t, *J* = 7.3 Hz, 1H), 1.74 (s, 3H); ^{13}C NMR (75 MHz, $CDCl_3$) δ 179.0, 141.7, 131.2, 131.0, 124.7, 112.4, 109.3, 47.5, 39.2, 22.2; IR (film) 3052, 2983, 2810, 1671, 1613, 1466, 1264 cm^{-1}; HRMS (CI) calcd for $[C_{10}H_{13}NO + H]^+$, *m/z* 164.1070, found 164.1086.

1-(3-Methylbut-3-en-1-yl)-1*H*-indole-2-carbaldehyde (1j): See the general procedure for the synthesis of pyrroles and indoles **1i**, **1j**, **1m**, **1n**. Reaction carried out with 1*H*-indole-2-carbaldehyde (290 mg, 2.0 mmol). The crude product mixture was purified by silica gel column chromatography (1:3 EtOAc:Hex) to afford 225 mg (53% yield) of **1j** as a yellow oil. R_f 0.50 (1:3 EtOAc:Hex). ^{1}H NMR (300 MHz, $CDCl_3$) δ 9.89 (s, 1H), 7.74 (dt, *J* = 8.1, 0.9 Hz, 1H), 7.44–7.42 (m, 3H), 7.23–7.16 (m, 1H), 4.79 (q, *J* = 1.5 Hz, 1H),

4.71–4.70 (m, 1H), 4.67 (t, J = 2.1 Hz, 1H), 4.64 (s, 1H), 2.46 (t, J = 7.8 Hz), 1.84 (s, 3H). ^{13}C NMR (75 MHz, $CDCl_3$) δ 182.5, 142.4, 140.1, 135.2, 126.8, 126.4, 123.4, 120.9, 117.9, 112.3, 110.5, 43.6, 38.3, 22.6; IR (film) 3075, 2968, 2806, 1664, 1526, 1322, 1266, 1216 cm^{-1}; HRMS (CI) calcd for $[C_{14}H_{15}NO + H]^+$, *m/z* 214.1226, found 214.1236.

1-(2-Methylallyl)-1*H*-pyrrole-2-carbaldehyde (1m): See general procedure for the synthesis of pyrroles and indoles **1i**, **1j**, **1m**, **1n.** Started with 380 mg (4.0 mmol) of 1H-pyrrole-2-carboxaldehyde. The crude mixture was purified by silica gel column chromatography (1:3 EtOAc:Hex) to afford 423 mg (71% yield) of **1m** as yellow oil. R_f 0.35 (1:3 EtOAc:Hex). ^{1}H NMR (300 MHz, $CDCl_3$) δ 9.54 (s, 1H), 6.95–6.93 (m, 2H), 6.26 (t, J = 3.2 Hz, 1H), 4.90 (s, 2H), 4.84 (s, 1H), 4.48 (s, 1H), 1.71 (s, 3H); ^{13}C NMR (75 MHz, $CDCl_3$) δ 179.4, 142.0, 131.5, 124.4, 111.6, 109.8, 53.8, 19.9; IR (film) 3056, 2983, 2924, 1665, 1529, 1479, 1371, 1267 cm^{-1}; HRMS (CI) calcd for $[C_9H_{11}NO + H]^+$, *m/z* 150.0913, found 150.0926.

1-(2-Methylallyl)-1*H*-indole-2-carbaldehyde (1n): See general procedure for the synthesis of pyrroles and indoles **1i**, **1j**, **1m**, **1n.** Started with 290 mg (2.0 mmol) of 1*H*-indole-2-carbaldehyde. The crude mixture was purified by silica gel column chromatography (1:3 EtOAc:Hex) to afford 258 mg (65% yield) of **1n** as yellow oil. R_f 0.50 (1:3 EtOAc:Hex). ^{1}H NMR (300 MHz, $CDCl_3$) δ 9.89 (s, 1H), 7.76 (d, J = 8.1 Hz, 1H), 7.44–7.41 (m, 1H), 7.39 (s, 1H), 7.29 (s, 1H), 7.22–7.17 (m, 1H), 5.17 (s, 2H), 4.82 (s, 1H), 4.41 (s, 1H), 1.73 (s, 3H); ^{13}C NMR (75 MHz, $CDCl_3$) δ 182.5, 141.2, 140.6, 135.3, 126.9, 126.3, 123.3, 121.0, 117.9, 111.0, 110.8, 49.9, 19.9; IR (film) 3054, 2984, 2818, 1671, 1614, 1464, 1266 cm^{-1}; HRMS (CI) calcd for $[C_{13}H_{13}NO + H]^+$, *m/z* 200.1070, found

200.1089.

2-(But-2-en-1-yl)benzaldehyde (mix of *E* and *Z*) **(1p)**: 2-(But-3-en-1-yl)benzaldehyde **1o** (38.6 mg, 0.24 mmol), aniline (32 mg, 0.34 mmol), benzoic acid (2.9 mg, 0.024 mmol), and triphenylphosphine (3.1 mg, 0.012 mmol) were added to a 1 dram vial with a magnetic stir bar in the nitrogen atmosphere of the glove box. $PhCF_3$ (0.50 mL) and chlorobis(cyclooctene)rhodium (I) dimer (4.3 mg, 0.006 mmol) were added. The resulting solution was stirred for 16 h at 100 °C and the reaction vial was removed from glovebox. Aqueous HCl (1.0 mL, 1M) was added, and the mixture was vigorously stirred for 10 min. The organic phase was separated and concentrated in vacuo. Column chromatography on silica gel (30:1 Hex:EtOAc) afforded **1p** as a colorless oil, which could not be separated from minor impurities (15 mg, 0.09 mmol, 39%). R_f 0.58 (4:1 Hex:EtOAc). Peaks corresponding to *E*-**1p**: ^{1}H NMR (300 MHz, $CDCl_3$) δ 10.28 (s, 1H), 7.86–7.82 (m, 1H), 7.55–7.49 (m, 1H), 7.40–7.34 (m, 1H), 7.30–7.28 (m, 1H), 5.67–5.59, 5.49–5.39, 3.74 (d, J = 6.3 Hz, 2H), 1.74–1.65 (m, 3H).[28]

7-Methyl-6,7,8,9-tetrahydro-5*H*-benzo[7]annulen-5-one (2a): Aldehyde **1a** (51.3 mg, 0.29 mmol), amine **3** (3.5 mg, 0.030 mmol, 10 mol %), aniline (33 mg, 0.36 mmol), benzoic acid (4.4 mg, 0.036 mmol), and triphenylphosphine (3.9 mg, 0.015 mmol) were added to a 1 dram vial with a magnetic stir bar, and brought into a nitrogen atmosphere glove box. $PhCF_3$ (0.60 mL) and chlorobis(cyclooctene)rhodium (I) dimer (5.4 mg, 0.0075 mmol) were added. The resulting solution was stirred for 15 h at 100 °C, and the reaction vial was removed from the glove box. CH_2Cl_2 (1 mL) and 1 M aqueous HCl (0.6 mL) were added, and the mixture was vigorously stirred for 10 min. The organic layer was

concentrated with silica gel in vacuo. Silica gel chromatography with CH_2Cl_2:Hex (2:1) provided **2a** as a colorless oil (41.7 mg, 0.24 mmol, 81%). R_f 0.43 (2:1 CH_2Cl_2:Hex). ^{1}H NMR (500 MHz, $CDCl_3$) δ 7.72 (dd, *J* = 7.5 Hz, 1.5 Hz, 1H), 7.41–7.38 (m, 1H), 7.30–7.26 (m, 1H), 7.20 (d, *J* = 7.5 Hz, 1H), 3.04–2.99 (m, 1H), 2.90–2.75 (m, 1H), 2.77 (dd, *J* = 15 Hz, 4.5 Hz, 1H), 2.60 (dd, *J* = 15 Hz, 9.0 Hz, 1H), 2.10-2.00 (m, 2H), 1.55-1.51 (m, 1H), 1.06 (d, *J* = 6.6 Hz, 3H); ^{13}C NMR (125 MHz, $CDCl_3$) δ 204.5, 142.4, 138.8, 131.9, 129.7, 128.4, 126.5, 49.0, 34.3, 32.1, 28.6, 21.7; IR (neat film NaCl) 2954, 2926, 2870, 1679, 1599, 1299, 1292, 1279 cm^{-1}; HRMS (ESI) calcd for $[C_{12}H_{14}O + Na]^+$ 197.0942, found 197.0934. The structure was also confirmed by COSY, HMQC and HMBC.

(–)-7-Methyl-6,7,8,9-tetrahydro-5*H*-benzo[7]annulen-5-one, (–)-2a: Aldehyde (34.0 mg, 0.20 mmol), amine **5** (22 mg, 0.05 mmol, 25 mol %), aniline (22 mg, 0.24 mmol), benzoic acid (2.4 mg, 0.02 mmol), and triphenylphosphine (5.2 mg, 0.02 mmol) were added to a 1 dram vial with a magnetic stir bar in the nitrogen atmosphere of the glove box. $PhCF_3$ (0.2 mL) and chlorobis(cyclooctene)rhodium (I) dimer (7.2 mg, 0.01 mmol) were added. The resulting solution was stirred for 15 h at 80 °C and reaction vial was removed from glovebox. Aqueous HCl (1.0 mL, 1M) and CH_2Cl_2 (1 mL) were added, and the mixture was vigorously stirred for 10 min. The organic phase was separated and concentrated in vacuo. Column chromatography on silica gel (1:2 Hex:CH_2Cl_2) afforded (–)-**2a** as a colorless oil (27.9 mg, 0.16 mmol, 82%). R_f, ^{1}H NMR, ^{13}C NMR, IR, and HRMS data as reported above for (±)-**2a**. HPLC analysis: *ee* 31% (Chiracel OD, 1:19 isopropanol:hexanes, 1.0 mL/min, 254 nm, t_{R1} = 5.5 min, t_{R2} = 5.9 min). $[\alpha]^{25}_D$ = –15 (c = 0.80, $CHCl_3$).

General Procedure for Preparation of Ketones 2b-2e:

Aldehyde (0.30 mmol), amine **3** (3.5 mg, 0.030 mmol, 10 mol %), aniline (33 mg, 0.36 mmol), benzoic acid (4.4 mg, 0.036 mmol), and triphenylphosphine (3.9 mg, 0.015 mmol) were added to a 1 dram vial with a magnetic stir bar, and brought into a nitrogen atmosphere glove box. $PhCF_3$ (0.30 mL) and chlorobis(cyclooctene)rhodium (I) dimer (5.4 mg, 0.0075 mmol) were added. The resulting solution was stirred for 15 h at 100 °C, and the reaction vial was removed from the glove box. Et_2O (1 mL) and 1 M aqueous HCl (0.5 mL) were added, and the mixture was vigorously stirred for 10 min. To the mixture was added H_2O (5 mL). The aqueous layer was extracted with Et_2O (3 × 10 mL). Combined organic layers were washed with brine (10 mL), dried over anhydrous Na_2SO_4 and concentrated in vacuo. Silica gel chromatography (EtOAc:Hex) gave the ketones **2** in the reported yields.

2,7-Dimethyl-6,7,8,9-tetrahydro-5*H*-benzo[7]annulen-5-one (2b): See general procedure for the hydroacylation of aldehydes **1b-1e.** Reaction was carried out with 56 mg (0.3 mmol) of aldehyde **1b**. The crude mixture was purified by silica gel flash column chromatography (1:9 EtOAc:Hex) to afford 47 mg (84% yield) of inseparable mixture of ketone **2b** and a very minor amount of the corresponding indanone derivative as colorless oil. Pure compound for NMR was obtained by preparative thin layer chromatography (Hex:C_6H_6:$CHCl_3$ 11:2:2, 6 elutions). R_f 0.50 (1:4 EtOAc:Hex). ^{1}H NMR (300 MHz, $CDCl_3$) δ 7.66 (d, J = 8.1 Hz, 1H), 7.09 (d, J = 7.8 Hz, 1H), 7.01 (s, 1H), 2.98–2.93 (m, 1H), 2.85 (dd, J = 6.1, 3.5 Hz, 1H), 2.78 (d, J = 3.9 Hz), 2.73 (d, J = 3.9 Hz, 1H), 2.58 (dd, J = 14.5, 9.2 Hz, 1H), 2.35 (s, 3H), 2.14–1.94 (m, 1H), 1.57–1.45 (m, 1H), 1.05 (d, J = 6.6 Hz, 3H); ^{13}C NMR (75 MHz, $CDCl_3$) δ 204.1, 142.7, 142.5, 136.1, 130.5, 128.7, 127.2,

49.0, 34.4, 32.1, 28.4, 21.8, 21.4; IR (neat film NaCl) 2956, 2927, 1702, 1671, 1608, 1459, 1234 cm^{-1}; HRMS (CI) calcd for $[C_{13}H_{16}O + NH_4]^+$, *m/z* 206.1539, found 206.1538.

7-Methyl-2-(trifluoromethyl)-6,7,8,9-tetrahydro-5*H*-benzo[7]annulen-5-one (2c): See general procedure for the hydroacylation of aldehydes **1b-1e.** Reaction was carried out with 63 mg (0.26 mmol) of aldehyde **1c**. The crude mixture was purified by silica gel flash column chromatography (1:9 EtOAc:Hex) to afford 48 mg (76% yield) of ketone **2c** as a colorless oil. R_f 0.40 (1:4 EtOAc:Hex). ^{1}H NMR (300 MHz, $CDCl_3$) δ 7.78 (d, *J* = 7.8 Hz, 1H), 7.53 (d, *J* = 8.1 Hz, 1H), 7.47 (s, 1H), 3.11–2.90 (m, 2H), 2.80 (dd, *J* = 14.8, 4.5 Hz, 1H), 2.60 (dd, *J* = 14.7, 9.3 Hz, 1H), 2.16–1.99 (m, 2H), 1.64–1.50 (m, 1H), 1.08 (d, *J* = 6.6 Hz, 3H); ^{13}C NMR (75 MHz, $CDCl_3$) δ 203.6, 142.7, 141.7, 133.1 (q, *J* = 32.2 Hz), 128.9, 126.6 (q, *J* = 3.4 Hz), 123.7 (q, *J* = 272.6 Hz), 123.3 (q, *J* = 3.4 Hz), 48.8, 34.1, 32.1, 28.7, 21.6; IR (neat film NaCl) 3032, 2957, 2929, 2872, 1686, 1577, 1330, 1168 cm^{-1}; HRMS (CI) calcd for $[C_{13}H_{13}F_3O + H]^+$, *m/z* 243.0991, found 243.1008.

2-Methoxy-7-methyl-6,7,8,9-tetrahydro-5*H*-benzo[7]annulen-5-one (2d): See general procedure for the hydroacylation of aldehydes **1b-1e.** Reaction was carried out with 67 mg (0.33 mmol) of aldehyde **1d**. The crude mixture was purified by silica gel flash column chromatography (1:5 EtOAc:Hex) to afford 57 mg (85% yield) of ketone **2d** as colorless oil. R_f 0.30 (1:4 EtOAc:Hex). ^{1}H NMR (300 MHz, $CDCl_3$) δ 7.77 (d, *J* = 8.7 Hz, 1H), 6.79 (dd, *J* = 8.7, 2.4 Hz, 1H), 6.69 (d, *J* = 2.4 Hz, 1H), 3.83 (s, 3H), 3.05–2.95 (m, 1H), 2.88–2.81 (m, 1H), 2.71 (d, *J* = 3.9 Hz, 1H), 2.58 (dd, *J* = 14.7, 8.9 Hz, 1H), 2.13–1.95 (m, 2H), 1.56–1.44 (m, 1H), 1.04 (d, *J* = 6.6 Hz, 3H); ^{13}C NMR (75 MHz, $CDCl_3$) δ 202.6, 162.4, 145.3, 131.5, 131.1, 114.9, 111.6, 55.3, 48.9, 34.2, 32.5, 28.2, 21.8; IR (neat

film NaCl) 3055, 2961, 1712, 1600, 1362, 1266, 1221 cm^{-1}; HRMS (CI) calcd for $[C_{13}H_{16}O_2 + H]^+$, *m/z* 205.1223, found 205.1219.

2-Fluoro-7-methyl-6,7,8,9-tetrahydro-5*H*-benzo[7]annulen-5-one (2e): See general procedure for the hydroacylation of aldehydes **1b-1e.** Reaction was carried out with 67 mg (0.35 mmol) of aldehyde **1e**. The crude mixture was purified by silica gel flash column chromatography (1:9 EtOAc:Hex) to afford 54 mg (80% yield) of inseparable mixture of ketone **2e** and a minor amount of the corresponding indanone derivative as colorless oil. Pure compound for NMR was obtained by preparative thin layer chromatography (Hex:C_6H_6:$CHCl_3$ 11:2:2, 6 elutions). R_f 0.50 (1:4 EtOAc:Hex). ^1H NMR (300 MHz, $CDCl_3$) δ 7.77 (dd, *J* = 8.7, 6.0 Hz, 1H), 7.0–6.88 (m, 2H), 3.06–3.0 (m, 1H), 2.90–2.79 (m, 2H), 2.75 (d, *J* = 4.2 Hz, 1H), 2.58 (dd, *J* = 14.7, 9.0 Hz, 1H), 2.13–1.97 (m, 1H), 1.58–1.47 (m, 1H), 1.06 (d, *J* = 6.6 Hz, 3H); ^{13}C NMR (75 MHz, $CDCl_3$) δ 202.7, 164.6 (d, *J* = 252.8 Hz), 145.7 (d, *J* = 8.1 Hz), 135.0, 131.3 (d, *J* = 9.7 Hz), 116.4 (d, *J* = 21.3 Hz), 113.5 (d, *J* = 21.3 Hz), 48.8, 34.1, 32.1, 28.3, 21.7; IR (neat film NaCl) 3061, 2957, 2928, 2870, 1708, 1677, 1606, 1582, 1459, 1247 cm^{-1}; HRMS (CI) calcd for $[C_{12}H_{13}FO + NH_4]^+$, *m/z* 210.1289, found 210.1280.

7-Ethyl-6,7,8,9-tetrahydro-5*H*-benzo[7]annulen-5-one (2f): Aldehyde **1f** (39.4 mg, 0.21 mmol), amine **3** (0.021 mmol, 10 mol %), aniline (0.45 mmol), benzoic acid (2.4 mg, 0.02 mmol), and triphenylphosphine (2.6 mg, 0.01 mmol) were added to a 1 dram vial with a magnetic stir bar, and brought into a nitrogen atmosphere glove box. $PhCF_3$ (0.18 mL) and chlorobis(cyclooctene)rhodium (I) dimer (3.6 mg, 0.005 mmol) were added. The resulting solution was stirred for 15 h at 100 °C and the reaction vial was removed from

the glove box. CH_2Cl_2 (1 mL) and 1 M aqueous HCl (0.6 mL) were added, and the mixture was vigorously stirred for 10 min. The organic layer was concentrated with silica gel in vacuo. Silica gel chromatography with CH_2Cl_2:Hex (2:1) provided **2f** as a colorless oil (33.7 mg, 0.18 mmol, 86%). R_f 0.39 (2:1 CH_2Cl_2:Hex). ^{1}H NMR (300 MHz, $CDCl_3$) δ 7.73 (d, *J* = 7.8 Hz, 1H), 7.42–7.25 (m, 2H), 7.20 (d, *J* = 7.5 Hz, 1H), 3.06–2.76 (m, 3H), 2.63–2.55 (m, 1H), 2.07–1.97 (m, 1H), 1.85–1.76 (m, 1H), 1.60–1.49 (m, 1H), 1.45–1.35 (m, 2H), 0.92 (t, *J* = 7.5 Hz); ^{13}C NMR (75 MHz, $CDCl_3$) δ 204.5, 142.4, 138.6, 131.9, 129.7, 128.4, 126.4, 46.8, 34.9, 32.0, 31.9, 28.7, 11.6; IR (neat film NaCl) 2960, 2929, 1677, 1599, 1460, 1449, 1290, 1254, 1245 cm^{-1}; HRMS (ESI) calcd for $[C_{13}H_{16}O + Na]^+$ 211.1093, found 211.1100.

7-Phenyl-6,7,8,9-tetrahydro-5*H*-benzo[7]annulen-5-one (2g): Aldehyde **1g** (31.9 mg, 0.135 mmol), amine **4** (6 mg, 0.015 mmol, 25 mol %), aniline (0.15 mmol), benzoic acid (1.7 mg, 0.014 mmol), and triphenylphosphine (1.8 mg, 0.0068 mmol) were added to a 1 dram vial with a magnetic stir bar, and brought into a nitrogen atmosphere glove box. $PhCF_3$ (0.15 mL) and chlorobis(cyclooctene)rhodium (I) dimer (2.4 mg, 0.0034 mmol) were added. The resulting solution was stirred for 15 h at 100 °C and the reaction vial was removed from the glove box. CH_2Cl_2 (1 mL) and 1 M aqueous HCl (0.6 mL) were added, and the mixture was vigorously stirred for 10 min. The organic layer was concentrated with silica gel in vacuo. Silica gel chromatography with CH_2Cl_2:Hex (2:1) provided **2g** as a colorless oil (24.7 mg, 0.10 mmol, 77%). R_f 0.29 (2:1 CH_2Cl_2:Hex). The characterization data are not consistent with those previously reported.[14] ^{1}H NMR (500 MHz, acetone-d^6) δ 7.68 (d, *J* = 7.0 Hz, 1H), 7.51 (t, *J* = 7.5 Hz, 1H), 7.39-7.29 (m, 6H), 7.23-7.19 (m, 1H),

3.29-3.22 (m, 2H), 3.15-3.08 (m, 1H), 3.00 (dt, J = 15 Hz, 4.5 Hz, 1H), 2.85 (dd, J = 16 Hz, 2.5 Hz, 1H), 2.23-2.16 (m, 1H), 2.06-1.99 (m, 1H); ^{13}C NMR (75 MHz, acetone-d^6) δ 203.7, 147.0, 142.2, 139.6, 133.2, 130.8, 129.5, 129.3, 128.0, 127.6, 127.3, 48.6, 40.3, 35.8, 32.8; IR (neat film, NaCl) 2935, 1667, 1599, 1449, 1289. HRMS (ESI) calcd for $[C_{17}H_{16}O + Na]^+$ 259.1099, found 259.1101. The structure was also confirmed by COSY, ^{1}H NMR decoupling experiments, HMQC and HMBC.[29]

7-(((tert-Butyldimethylsilyl)oxy)methyl)-6,7,8,9-tetrahydro-5*H*-benzo[7]annulen-5-one (2h): Aldehyde (25.9 mg, 0.085 mmol), amine **4** (1.5 mg, 0.0085 mmol, 10 mol %), aniline (0.11 mmol), benzoic acid (1.0 mg, 0.009 mmol), and triphenylphosphine (1.1 mg, 0.0043 mmol) were added to a 1 dram vial with a magnetic stir bar, and brought into a nitrogen atmosphere glove box. $PhCF_3$ (0.17 mL) and chlorobis(cyclooctene)rhodium (I) dimer (1.5 mg, 0.0021 mmol) were added. The resulting solution was stirred for 15 h at 100 °C and the reaction vial was removed from the glove box. CH_2Cl_2 (1 mL) and 1 M aqueous HCl (0.4 mL) were added, and the mixture was vigorously stirred for 10 min. The organic layer concentrated with silica gel in vacuo. Silica gel chromatography with CH_2Cl_2:Hex (2:1) provided **2h** as a colorless oil (16.7 mg, 0.055 mmol, 78%). R_f 0.24 (2:1 CH_2Cl_2:Hex). ^{1}H NMR (300 MHz, $CDCl_3$) δ 7.70 (d, J = 7.8 Hz, 1H), 7.37–7.34 (m, 1H), 7.25 (t, J = 7.5 Hz, 1H), 7.16 (d, J = 7.5 Hz, 1H), 3.52–3.44 (m, 2H), 3.05–2.95 (m, 1H), 2.89–2.75 (m, 2H), 2.66–2.58 (m, 1H), 2.06–1.86 (m, 2H), 0.84 (s, 9H), 0.01 (s, 3H); ^{13}C NMR (75 MHz, $CDCl_3$) δ 204.5, 142.1, 138.6, 132.1, 129.7, 128.5, 126.6, 66.6, 44.0, 35.9, 31.8, 28.7, 25.9, 18.3, -5.4; IR (neat film NaCl) 2952, 2927, 2855, 1679, 1253, 1111 cm^{-1}; HRMS (ESI) calcd for $[C_{18}H_{28}O_2Si + Na]^+$ 327.1756, found 327.1755.

General Procedure for the Hydroacylation of Aldehydes 1i, 1j, 1m, 1n: Aldehyde (0.30 mmol), amine **4** (13 mg, 0.075 mmol, 25 mol %), aniline (33 mg, 0.36 mmol), benzoic acid (4.4 mg, 0.036 mmol), triphenylphosphine (8.0 mg, 0.03 mmol) and $PhCF_3$ (0.30 mL) were added to a 1 dram vial with a magnetic stir bar, and brought into a nitrogen atmosphere glove box. Chlorobis(cyclooctene)rhodium (I) dimer (11.0 mg, 0.015 mmol) was added. The resulting solution was stirred for 36 h at 100 °C and the reaction vial was removed from the glove box. Et_2O (1 mL) and 1 M aqueous HCl (0.5 mL) were added, and the mixture was vigorously stirred for 10 min. To the mixture was added H_2O (5 mL). The aqueous layer was thoroughly extracted with Et_2O (4 × 15 mL). Combined organic layers were washed with brine (10 mL), dried over anhydrous Na_2SO_4 and concentrated in vacuo. Silica gel chromatography (EtOAc:Hex) gave the ketones **2** in the reported yields.

7-Methyl-7,8-dihydro-5*H*-pyrrolo[1,2-a]azepin-9(6*H*)-one (2i): See general procedure for the hydroacylation of aldehydes **1i, 1j, 1m, 1n.** Reaction was carried out with 48 mg (0.29 mmol) of aldehyde **1i**. The crude mixture was purified by silica gel flash column chromatography (1:1 EtOAc:Hex) to afford 30 mg (63% yield) of ketone **2i** as light yellow oil. R_f 0.25 (1:3 EtOAc:Hex). ^{1}H NMR (300 MHz, $CDCl_3$) δ 6.99 (dd, J = 3.9, 1.8 Hz, 1H), 6.78 (t, J = 2.1 1H), 6.13 (dd, J = 4.1, 2.4 Hz, 1H), 4.28–4.09 (m, 2H), 2.78–2.61 (m, 2H), 2.31–2.12 (m, 2H), 1.68–1.58 (m, 1H), 1.07 (d, J = 6.6 Hz); ^{13}C NMR (75 MHz, $CDCl_3$) δ 190.5, 134.2, 128.1, 117.0, 108.7, 47.9, 47.4, 35.2, 27.6, 22.2; IR (neat film NaCl) 3053, 2985, 1646, 1526, 1421, 1265 cm^{-1}; HRMS (ESI) calcd for $[C_{10}H_{13}NO + Na]^+$, *m/z* 186.0895, found 186.0898.

8-Methyl-8,9-dihydro-6*H*-azepino[1,2-a]indol-10(7*H*)-one (2j): See general procedure for the hydroacylation of aldehydes **1i, 1j, 1m, 1n.** Reaction was carried out with 42 mg (0.20 mmol) of aldehyde **1j**. The crude mixture was purified by silica gel flash column chromatography (1:3 EtOAc:Hex) to afford 28 mg (66% yield) of ketone **2j** as colorless oil. R_f 0.35 (1:3 EtOAc:Hex). ^{1}H NMR (300 MHz, $CDCl_3$) δ 7.70 (d, *J* = 7.8 Hz, 1H), 7.37 (d, *J* = 3.9 Hz, 2H), 7.25 (s, 1H), 7.19–7.10 (m, 1H), 4.40–4.35 (m, 2H), 2.91 (dd, *J* = 14.5, 4.1 Hz, 1H), 2.76 (dd, *J* = 14.2, 8.9 Hz, 1H), 2.39–2.21 (m, 2H), 1.82–1.72 (m, 1H), 1.14 (d, *J* = 6.6 Hz, 3H); ^{13}C NMR (75 MHz, $CDCl_3$) δ 193.7, 139.0, 126.2, 125.3, 123.2, 120.6, 110.2, 108.5, 48.6, 42.6, 35.5, 28.1, 22.1; peak at 139.0 ppm corresponds to two carbons; this was confirmed by recording ^{13}C NMR in CD_3OD, see spectra; ^{13}C NMR (75 MHz, CD_3OD) δ 196.4, 140.8, 140.0, 127.6, 126.8, 124.1, 121.9, 111.8, 109.4, 43.7, 36.7, 29.6, 22.5; one of the NMR signals for aliphatic carbons is obscured by solvent NMR peaks; IR (neat film NaCl) 3053, 2986, 1663, 1518, 1421, 1266 cm^{-1}; HRMS (ESI) calcd for $[C_{14}H_{15}NO + Na]^+$, *m/z* 236.1046, found 236.1051.

3-Methyl-3,4-dihydronaphthalen-1(2*H*)-one (2k): Aldehyde **1k** (49.5 mg, 0.30 mmol), amine **4** (13.2 mg, 0.075 mmol, 25 mol %), aniline (0.36 mmol), benzoic acid (3.6 mg, 0.03 mmol), and triphenylphosphine (3.9 mg, 0.015 mmol) were added to a 1 dram vial with a magnetic stir bar, and brought into a nitrogen atmosphere glove box. $PhCF_3$ (0.60 mL) and chlorobis(cyclooctene)rhodium (I) dimer (5.4 mg, 0.0075 mmol) were added. The resulting solution was stirred for 15 h at 100 °C and the reaction vial was removed from the glove box. CH_2Cl_2 (2 mL) and 1 M aqueous HCl (1.0 mL) were added, and the mixture was vigorously stirred for 10 min. The organic layer was concentrated with

silica gel in vacuo. Silica gel chromatography with Hex:MeOH (98:2) provided **2k** as a colorless oil (15.0 mg, 0.094 mmol, 30%). This separation of **2k** from side products in the crude reaction mixture was challenging, and we attribute the low yield to this factor. R_f 0.39 (2:1 CH_2Cl_2:Hex). The characterization data are consistent with those previously reported.[30]

The reaction was repeated with aldehyde (34.8 mg, 0.22 mmol), amine **4** (35.4 mg, 0.20 mmol, 0.9 equiv) and accordingly scaled amounts of other reagents. ^{1}H NMR analysis of reaction mixture after HCl workup with 4'-methoxyacetophenone as an internal standard showed 65% yield of **2k**.

3-Phenyl-3,4-dihydronaphthalen-1(2*H*)-one (2l): Aldehyde **1l** (66.8 mg, 0.30 mmol), amine **4** (53.1 mg, 0.30 mmol, 100 mol %), aniline (0.36 mmol), benzoic acid (3.6 mg, 0.03 mmol), and triphenylphosphine (3.9 mg, 0.015 mmol) were added to a 1 dram vial with a magnetic stir bar, and brought into a nitrogen atmosphere glove box. $PhCF_3$ (0.60 mL) and chlorobis(cyclooctene)rhodium (I) dimer (5.4 mg, 0.0075 mmol) were added. The resulting solution was stirred for 15 h at 100 °C and the reaction vial was removed from the glove box. CH_2Cl_2 (1 mL) and 1 M aqueous HCl (0.6 mL) were added, and the mixture was vigorously stirred for 10 min. The organic layer was concentrated with silica gel in vacuo. Silica gel chromatography with CH_2Cl_2:Hex (2:1) provided **2l** as a colorless oil (38.9 mg, 0.18 mmol, 58%). R_f 0.33 (2:1 CH_2Cl_2:Hex). The characterization data are consistent with those previously reported.[14]

6-Methyl-6,7-dihydroindolizin-8(5*H*)-one (2m): See general procedure for the hydroacylation of aldehydes **1i, 1j, 1m, 1n.** Reaction was carried out with 60 mg (0.4

mmol) of aldehyde **1m**. The crude mixture was purified by silica gel flash column chromatography (1:1 EtOAc:Hex) to afford 40 mg (67% yield) of ketone **2m** as light yellow oil. R_f 0.25 (1:3 EtOAc:Hex). ^{1}H NMR (300 MHz, $CDCl_3$) δ 7.01 (dd, *J* = 4.2, 1.5 Hz, 1H), 6.84 (t, *J* = 2.1 Hz, 1H), 6.25 (dd, *J* = 4.2, 2.4 Hz, 1H), 4.15 (ddd, *J* = 12.3, 4.2, 1.2 Hz, 1H), 3.72 (dd, *J* = 12.3, 9.9 Hz, 1H), 2.65 (ddd, *J* = 16.7, 4.0, 1.5 Hz, 1H), 2.59–2.46 (m, 1H), 2.29 (dd, *J* = 16.6, 10.8 Hz, 1H), 1.14 (d, *J* = 6.6 Hz, 3H); ^{13}C NMR (75 MHz, $CDCl_3$) δ 187.1, 130.1, 125.8, 113.8, 110.4, 51.6, 44.4, 30.4, 18.3; IR (neat film NaCl) 3053, 2985, 1662, 1558, 1420, 1265 cm^{-1}; HRMS (CI) calcd for $[C_9H_{11}NO + H]^+$, *m/z* 150.0913, found 150.0926.

7-Methyl-7,8-dihydropyrido[1,2-a]indol-9(6*H*)-one (2n): See general procedure for the hydroacylation of aldehydes **1i, 1j, 1m, 1n.** Reaction was carried out with 60 mg (0.30 mmol) of aldehyde **1n**. The crude mixture was purified by silica gel flash column chromatography (1:3 EtOAc:Hex) to afford 41 mg (69% yield) of ketone **2n** as a colorless solid. MP 116 °C, R_f 0.35 (1:3 EtOAc:Hex). ^{1}H NMR (300 MHz, $CDCl_3$) δ 7.75–7.72 (m, 1H), 7.39–7.37 (m, 2H), 7.27 (s, 1H), 7.20–7.14 (m, 1H), 4.41–4.36 (m, 1H), 3.81–3.73 (m, 1H), 2.84–2.77 (m, 1H), 2.70–2.59 (m, 1H), 2.46 (ddd, *J* = 16.5, 11.1, 0.9 Hz, 1H), 1.25 (dd, *J* = 6.6, 0.9 Hz, 1H); ^{13}C NMR (75 MHz, $CDCl_3$) δ 190.2, 137.2, 133.2, 126.8, 125.6, 123.4, 121.1, 110.3, 105.5, 48.0, 45.2, 30.1, 18.6; IR (neat film NaCl) 3053, 2986, 1675, 1527, 1421, 1265 cm^{-1}; HRMS (ESI) calcd for $[C_{13}H_{13}NO + Na]^+$, *m/z* 222.0889, found 222.0887.

1-Benzosuberone (2o): Aldehyde **1o** (81.7 mg, 0.51 mmol), amine **3** (58.6 mg, 0.54 mmol, 100 mol %), aniline (56 mg, 0.60 mmol), benzoic acid (6.1 mg, 0.05 mmol), and

triphenylphosphine (6.6 mg, 0.025 mmol) were added to a 1 dram vial with a magnetic stir bar, and brought into a nitrogen atmosphere glove box. $PhCF_3$ (2.50 mL) and chlorobis(cyclooctene)rhodium (I) dimer (9.0 mg, 0.0125 mmol) were added. The resulting solution was stirred for 20 h at 100 °C and the reaction vial was removed from the glove box. Aqueous HCl (3.0 mL, 1M) were added, and the mixture was vigorously stirred for 10 min. The organic layer was separated and concentrated in vacuo. Silica gel chromatography on silica gel (20:1 Hex:EtOAc) afforded **2o** as a colorless oil (41.5 mg, 0.26 mmol, 51%). R_f 0.22 (30:1 Hex:EtOAc). The characterization data are consistent with those previously reported.[31]

2-Ethyl-2,3-dihydro-1*H*-inden-1-one (2p): Aldehyde (161.1 mg, 1.00 mmol), amine **3** (15.9 mg, 0.13 mmol, 13 mol %), aniline (112 mg, 1.2 mmol), benzoic acid (12 mg, 0.1 mmol), and triphenylphosphine (13.1 mg, 0.05 mmol) were added to a 1 dram vial with a magnetic stir bar in the nitrogen atmosphere of the glove box. $PhCF_3$ (3.0 mL) and chlorobis(cyclooctene)rhodium (I) dimer (18.0 mg, 0.025 mmol) were added. The resulting solution was stirred for 16 h at 100 °C and reaction vial was removed from glovebox. Aqueous HCl (3.0 mL, 1M) was added, and the mixture was vigorously stirred for 10 min. The organic phase was separated and concentrated in vacuo. Column chromatography on silica gel (30:1 Hex:EtOAc) afforded **2p** as a colorless oil (39.9 mg, 0.25 mmol, 25%). R_f 0.22 (30:1 Hex:EtOAc). The characterization data are consistent with those previously reported.[32]

3-Methyl-5-(pyrrolidin-1-yl)pyridin-2-amine (4): A mixture of 2-amino-5-iodopicoline[33] (1.17 g, 5 mmol), pyrrolidine (1.07 g, 15 mmol), K_2CO_3 (1. 38 g, 10 mmol),

CuI (95 mg, 0.5 mmol), and L-proline (115 mg, 1 mmol) in 5 mL of DMSO was heated in a vial at 75 °C.[34] The reaction was monitored by TLC. Upon completion, the cooled mixture was diluted with 30 mL ethyl acetate and was filtered through a pad of celite. The celite pad was washed with ethyl acetate (50 mL). The combined organic layer was washed with water (3 × 20 mL), brine (15 mL), dried over Na_2SO_4, and concentrated in vacuo. The residual paste was purified by silica gel flash chromatography (97.8:2:0.2 EtOAc:MeOH:Et_3N) to afford 580 mg (65%) of picoline **4**. R_f 0.10 (20:1 EtOAc:MeOH), pale yellow solid. MP 129–130 °C. ^{1}H NMR (300 MHz, $CDCl_3$) δ 7.37 (d, J = 2.7 Hz, 1H), 6.7 (d, J = 2.7 Hz, 1H), 3.88 (s, 2H), 3.17 (t, J = 6.6 Hz, 4H), 2.12 (s, 3H), 1.98–1.94 (m, 4H); ^{13}C NMR (75 MHz, $CDCl_3$) δ 148.2, 139.2, 128.7, 123.4, 117.6, 48.1, 25.1, 17.5; IR (neat film NaCl) 3377, 3175, 2906, 2829, 1646, 1476, 1437, 1335, 1255, 1172,1140 cm^{-1}; HRMS (ESI) calcd for $[C_{10}H_{15}N_3 + Na]^+$, *m/z* 200.1158, found 200.1155.

(*S*)-3-(6-Amino-5-methylpyridin-3-yl)-4-benzyl-5,5-diphenyloxazolidin-2-one (5): 2-Amino-5-iodo-3-picoline[31] (234 mg, 1 mmol), (*S*)-(–)-5-benzyl-4,4-diphenyl-1,3-oxazolidinone (329 mg, 1 mmol), copper (I) iodide (19 mg, 0.1 mmol), potassium phosphate (636 mg, 3 mmol), *N,N'*-dimethylethylenediamine (22 μL, 0.2 mmol) toluene (2 mL) and a magnetic stir bar were placed in 1 dram vial. The vial was flushed with nitrogen and capped. The reaction mixture was stirred at 100 °C for 24 hours, diluted with CH_2Cl_2 (10 mL) and washed with saturated aqueous NH_4Cl (10 mL). The organic phase was separated, dried over Na_2SO_4, and concentrated in vacuo. Purification by column chromatography on silica gel (EtOAc) followed by recrystallization from $PhCF_3$ afforded **5** as light yellow crystals (154 mg, 0.35 mmol, 35%). R_f 0.25 (EtOAc); MP 239–240 °C;

^{1}H NMR (300 MHz, $CDCl_3$) δ 7.80 (d, *J* = 2.4 Hz, 1H), 7.58–7.55 (m, 2H), 7.43–7.18 (m, 9H), 7.04–7.02 (m, 2H), 6.64 (dd, *J* = 1.8 Hz, 5.4 Hz, 2H), 5.21 (t, *J* = 6.6 Hz, 1H), 4.39 (br s, 2H), 2.74 (d, *J* = 6.6 Hz, 2H), 1.99 (s, 3H); ^{13}C NMR (75 MHz, $CDCl_3$) δ 156.0, 155.6, 143.2, 142.0, 139.2, 137.1, 135.0, 129.5, 129.3, 128.9, 128.8, 127.5, 126.9, 126.6, 125.8, 117.4, 88.0, 68.2, 37.8, 17.8 (two signals in the aromatic region are not resolved); HRMS (ESI) calcd for $[C_{28}H_{25}N_3O_2 + H]^+$ 436.2020, found 436.2015. $[\alpha]_D^{25}$ –234 (c = 0.68, $CHCl_3$).

Supporting Information. NMR spectra for new compounds and new preparations of known compounds, assignment diagram for **2g**, and HPLC chromatograms for (±)-**2a** and (–)-**2a** are provided. This material is available free of charge via the Internet at http://pubs.acs.org.*

* http://pubs.acs.org/doi/suppl/10.1021/jo300779q/suppl_file/jo300779q_si_002.pdf

Part 2: Three hydrogen bond donor catalysts

Chapter 3: Introduction

Over the last couple of decades hydrogen bond catalysis has become a fast growing area of research.[1] Various functionalities, including thiourea, hydroxyl, amide, guanidine and other groups, were successfully employed and a wide variety of reactions were carried out including enantioselective transformations. The first example of hydrogen bonding catalysis was reported back in 1942, many decades before the boom in this area. Wassermann reported the acceleration of the Diels-Alder reaction of cyclopentadiene with *p*-benzoquinone by phenol (Scheme 1) as well as by a number of carboxylic acids.[2]

Scheme 1. First hydrogen bond catalyzed reaction.

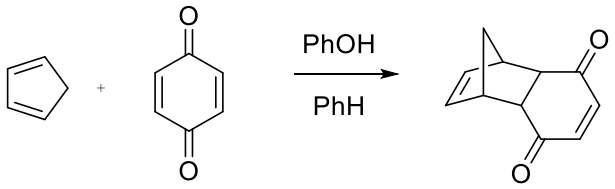

Eighteen years later, Eaton *et al.* noted significant acceleration of the Diels-Alder reaction between anthracene and maleic anhydride by aluminum chloride (Scheme 2); a factor of greater than 2 x 10^5 was observed.[3] Both reactions presumably involve coordination of the catalyst to a carbonyl oxygen of the dienophile by either a hydrogen

Scheme 2. Lewis acid catalyzed Diels-Alder reaction.

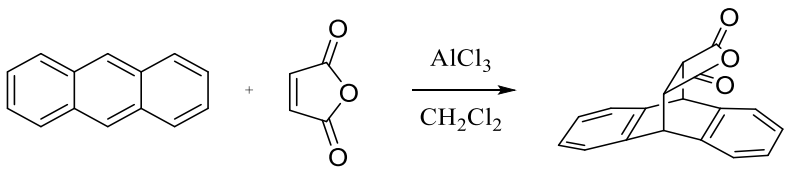

bond or a Lewis acid-base interaction. This increases the electrophilicity of the dienophile and leads to a reaction rate acceleration. It is interesting to note that the first report was left seemingly unnoticed, whereas the second was followed by a rapid development of Lewis acid catalysts, including chiral ones for carrying out enantioselective transformations.[4]

Jacobsen's thioureas

The failure to capitalize on Wassermann's earlier report was probably due to the perception that hydrogen bonding is not sufficiently activating or directional. As a result little work was carried out in this area untill Jacobsen's discovery of the enantioselective Strecker reaction in 1997.[5] In this seminal contribution Jacobsen *et al.* showed that *N*-allyl imines react with HCN in the presence of a chiral thiourea catalyst to afford α-aminonitriles with high enantioselectivities (Scheme 3). Interestingly, the authors first intended to use thiourea derivatives as chiral ligands for metal ions in order to perform Lewis acid catalysis, but found that the metal-free ligand provided higher enantioselectivity. Later the reaction was expanded to hydrocyanation of a wider range of aldimines[6] as well as more sterically demanding methylketoimines[7] using a chiral urea catalyst (Scheme 4).

Scheme 3. Thiourea-catalyzed Strecker reaction.

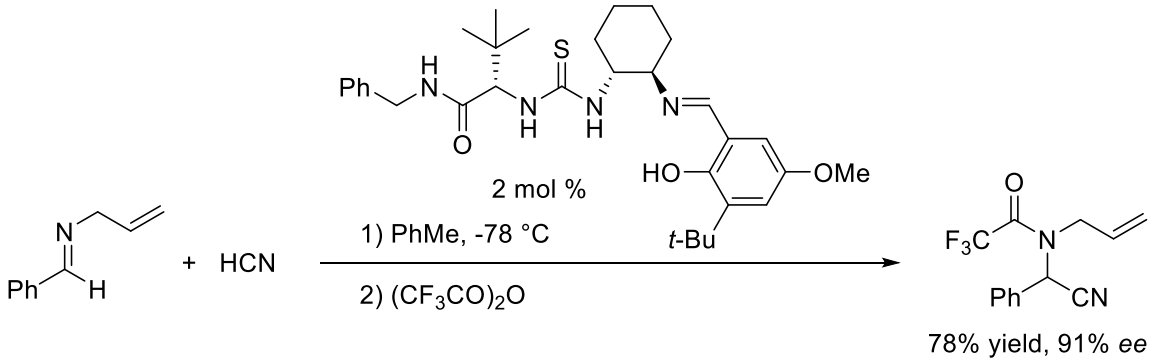

Scheme 4. Expanded scope of the Strecker reaction.

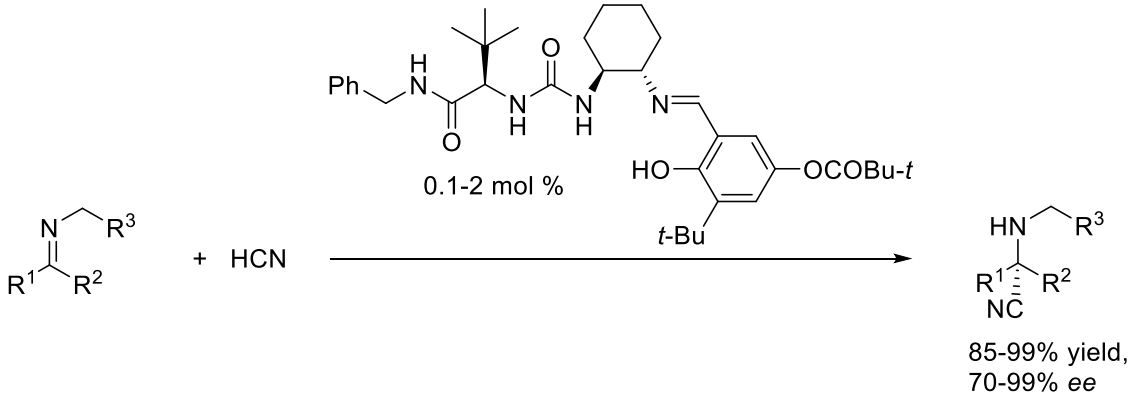

The mechanism of the Strecker reaction was investigated and it was found to obey Michaelis-Menten kinetics. This indicated that reversible substrate-catalyst coordination occurs prior to the rate limiting step. The imines were found to exist as a mixture of *E* and *Z*-isomers, but upon titration with the catalyst only the *Z*-compound's signals shifted in the ^{1}H NMR spectra due to binding. A cyclic *Z*-imine, 3,4-dihydroisoquinoline, was also found to be a highly active substrate. This led the authors to conclude that the *Z*-imine is the reactive species. By modifying the catalyst's structure, they showed that only the urea's N–H bonds are essential. Lastly, the structure of the free catalyst and its complex with the

Z-imine were studied by ^{1}H NMR using the nuclear Overhauser effect and computations. All of this led to a proposal in which the transition state consists of a *Z*-imine bound to the two N–H bonds of the urea in the catalyst "pocket" and HCN approaches from the diaminocyclohexane side of the complex (Scheme 5). Although this mechanistic hypothesis proved to be wrong later (see below), it enabled a better catalyst to be designed by increasing the size of the amide portion of the catalyst (i.e., the opposite side of where HCN attacks). This new thiourea catalyst (Scheme 5, right) provided higher enantioselectivities compared to the previously reported urea catalyst, especially with challenging substrates.

Scheme 5. Proposed transition state for the thiourea-catalyzed Strecker reaction and a new better catalyst.

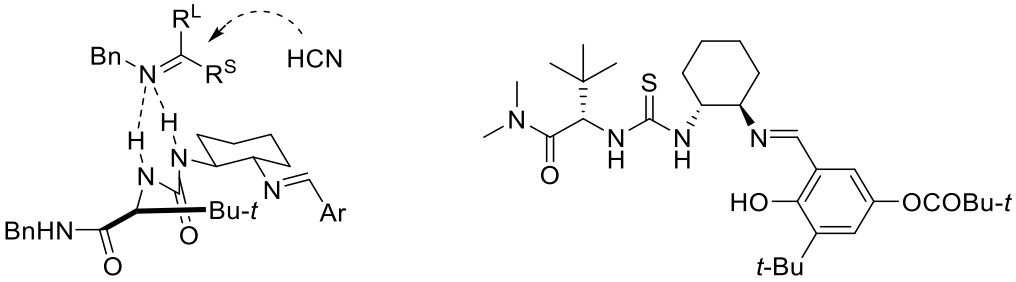

Jacobsen *et al.* later applied their catalysts to other nucleophilic addition reactions of imines that previously could not be achieved by other methods. Examples include the Mannich reaction with silyl enol ethers,[8] hydrophosphorylation,[9] aza-Baylis-Hillman[10] and nitro-Mannich reactions[11] (not shown). Further, they discovered that the diaminocyclohexane portion of the catalyst is not required for enantioinduction, enabling

simpler thioureas to be used for the catalytic syntheses of unnatural amino acids via the Strecker reaction (Scheme 6).[12]

Scheme 6. Synthesis of unnatural amino acids with an optimized Strecker reaction catalyst.

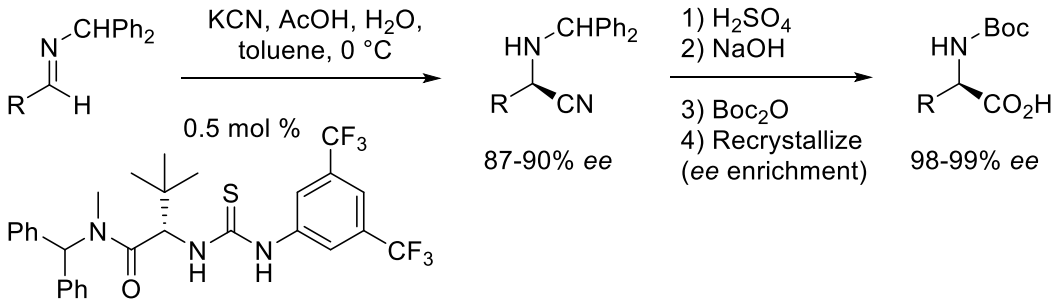

The following additional experimental data are not supported by the originally proposed mechanism (Scheme 5): 1. Both activity and enantioselectivity are sensitive to the structure of the amino acid portion of the catalyst. 2. Imines with electron donating groups react faster, suggesting that imine basicity is important. 3. Reaction with DCN leads to nearly quantitative incorporation of deuterium into the product, while H-D exchange of the two N–H's in the thiourea takes place more slowly than the hydrocyanation.[13] These observations suggested that the reaction proceeds via an iminium cation formed by protonation of the imine by hydrogen cyanide. Detailed computational studies showed that the lowest energy pathway starts with catalyst-promoted imine protonation by HNC with formation of a catalyst-bound isocyanide-iminium cation ion pair (Scheme 7). Structural rearrangement of this ion pair (i.e., cyanide to isocyanide via a π-bound CN^- intermediate) occurs in the rate limiting step, followed by the ion pair collapse in the C–C bond forming step.

Scheme 7. Revised mechanism for the thiourea-catalyzed Strecker reaction.

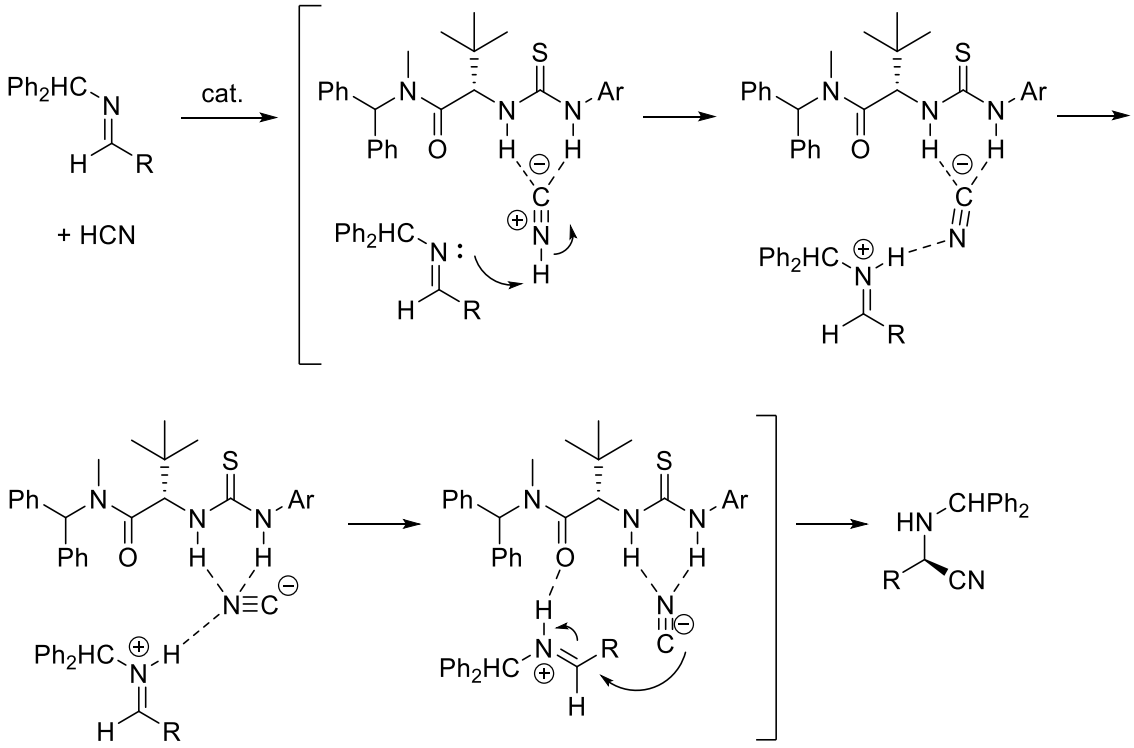

Bifunctional catalysis

A further step forward in the field was made by Takemoto, who introduced a bifunctional catalyst containing a thiourea moiety and an amine group. This catalyst reportedly activates both the electrophile and nucleophile, and brings them together in a spatially organized manner. This is illustrated for the Michael reaction shown in Scheme 8.[14] This bifunctional catalyst proved to be very versatile and efficient in a variety of additional transformations.[15]

Scheme 8. Bifunctional catalyst in a Michael addition reaction.

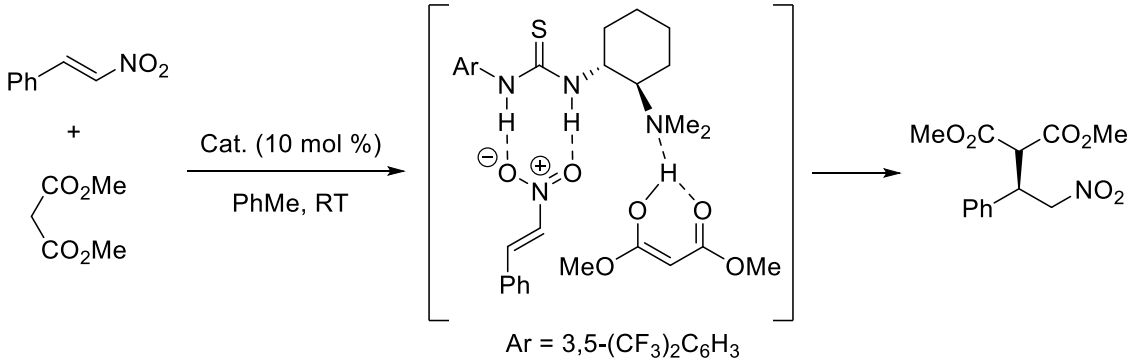

Interestingly, the proposed mechanism above was questioned by Papai *et al.* based upon detailed computational studies.[16] A new pathway (B in Scheme 9) was found in which the nucleophile protonates the amine site of the catalyst, and the resulting ammonium ion then activates the electrophile. Both pathways were found to be feasible and account for the observed enantioselectivity, but the transition state for route B was calculated to be 2.7 kcal/mol more favorable in the gas phase and 1.9 kcal/mol in solution than for route A.

Scheme 9. Two possible pathways for the Michael addition reaction and the computed energies for the key intermediates and transition states.

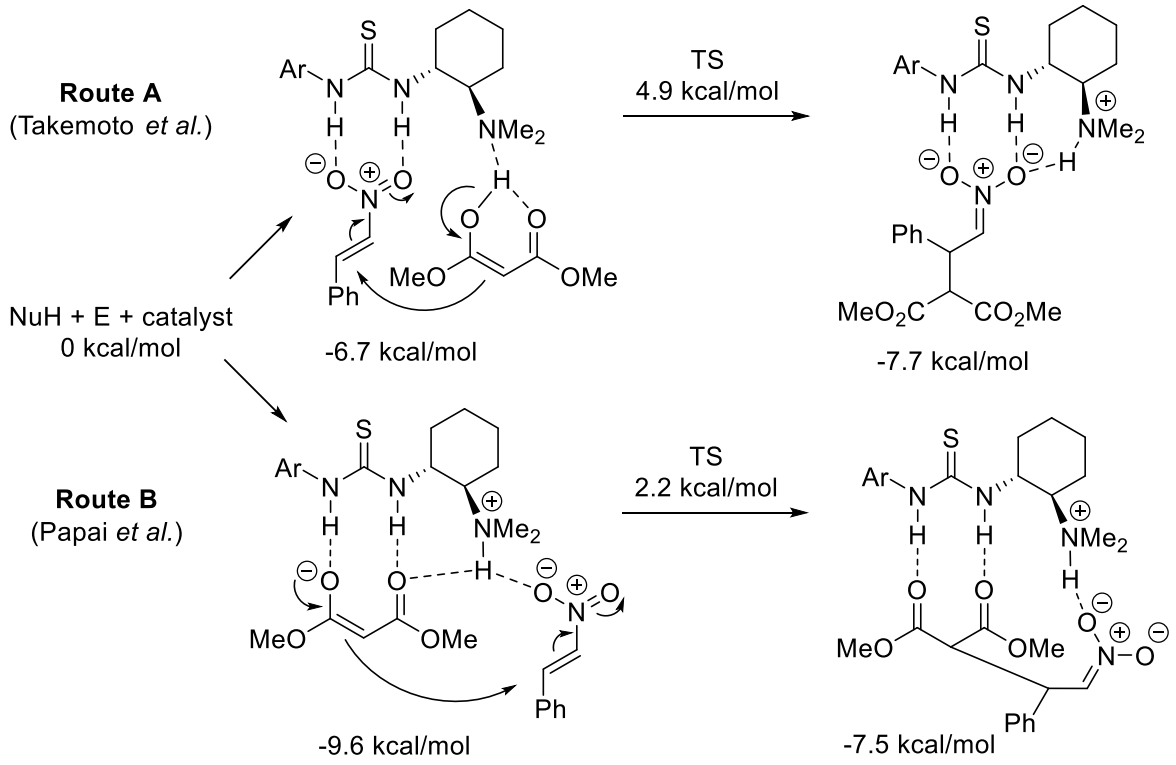

This was rationalized as being due to a significant disruption of the hydrogen bonding network and the spatial reorganization required for route A. Another simple explanation that can be envisioned is that coordination of the electrophile to the more acidic quaternary ammonium salt (activation) and the interaction of the nucleophile with the less acidic thiourea moiety (deactivation), would lead to a faster reaction than vice versa. It was also proposed that the latter pathway (B) may be operational in other reactions with a bifunctional thiourea catalyst (i.e., in reactions with a nucleophile capable of base activation and a strongly polarized electrophile). For instance, Papai *et al.* proposed an

alternative mechanism for an asymmetric conjugate addition of nitroalkanes to chalcones in the presence of a cinchone-derived bifunctional thiourea that was originally discovered by Soos *et al*. (Scheme 10).[17]

Scheme 10. Michael reaction with a bifunctional catalyst and a revised mechanism by Papai et al.

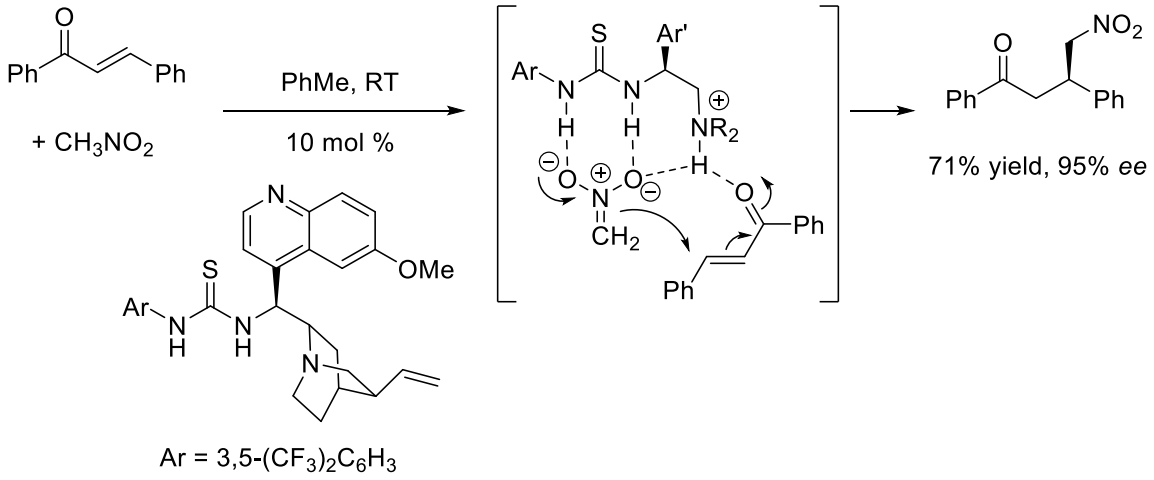

Himo *et al*. predicted that a similar reaction pathway takes place in the Henry reaction catalyzed by a similar cinchone-derived thiourea (Scheme 11).[18] This transformation was originally developed by Hiemstra *et al.*, who used a non-derivatized cinchone as a catalyst (R = OH).[19] Substitution of the mildly acidic phenolic OH group of the natural product (R = OH) with an electron deficient and more acidic thiourea arm (R = ArNHC(S)NH, where Ar = 3,5-$(CF_3)_2C_6H_3$) dramatically increased the scope and enantioselectivity (i.e., from 24-35% *ee* to 85-92% *ee*) of this transformation. [20]

Scheme 11. Henry reaction with a bifunctional catalyst and the Papai mechanism.

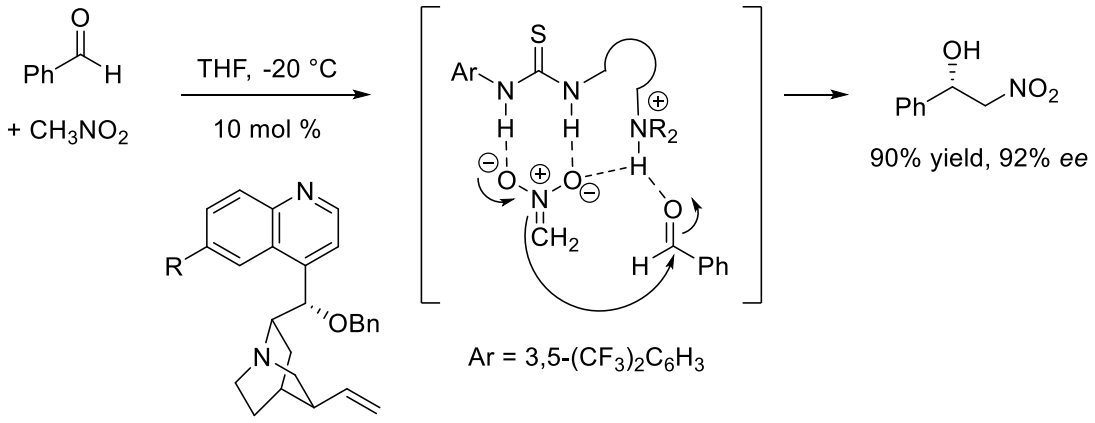

In summary, all of the reactions described above in Schemes 7, 8, 10 and 11 were originally designed so that the thiourea moiety of the catalyst would stabilize the developing negative charge on the electrophile's heteroatom in the transition state of the reaction (i.e., pathway A in Scheme 9). However, computations indicate that the role of the hydrogen bond donor is to stabilize the anion resulting from the deprotonation of the nucleophile (i.e., pathway B in Scheme 9). The electrophile is activated by a hydrogen bond between the protonated side of the catalyst and the heteroatom of the electrophile for reactions in Schemes 8, 10 and 11 or by protonation in case of the Strecker reaction in Scheme 7. Since, both the nucleophile and electrophile are bound to the catalyst, a rigid spatial arrangement results which can lead to good enantioselectivity. It is worth noting, however, that in most calculations the difference between the two pathways is only a few kcal/mol, but given the high complexities of these systems and the extensive charge separation, the reliability of these computations is uncertain. Experimental studies are typically limited to the absolute configuration of the major enantiomer of the product,

binding measurements of the substrates to the catalysts, and kinetic investigations,[21] none of which have established the reaction pathway (except for the Strecker reaction in Scheme 7).

Anion binding catalysis

Hydrogen bonding catalysts are poor choices for S_N2 reactions because alkyl halides undergo little or no binding to them. A number of S_N1 reactions, however, have been reported, including enantioselective transformations. These processes are similar to those discussed above in that the negative charge is stabilized in the rate determining step. They stand out, however, in the way that the enantioselectivity is induced in the final product – solely via ion-pair interactions.[22] The first report of such a reaction came from Jacobsen *et al.* on an enantioselective acyl-Pictet-Spengler cyclization of indoles onto *N*-acyliminium ions (Scheme 12).[23] This reaction was known to proceed via electrophilic aromatic substitution in the acyliminium intermediate, but the role of the thiourea was not clear at the time. To broaden the substrate scope of thiourea-catalyzed acyliminium reactions, as well as to elucidate the mechanism of these reactions, hydroxylactams were investigated and the acyliminium intermediates were formed *in situ* (Scheme 13).[24] NMR showed a fast and irreversible formation of the chlorolactam. The tertiary derivative (R = Me) was found to be more reactive than the secondary compound (R = H), which indicated that a S_N1 mechanism takes place. It was proposed that the observed enantioselectivity is induced via noncovalent interactions of the thiourea-chloride chelate with the acyliminium cation in a

Scheme 12. Thiourea-catalyzed acyl-Pictet-Spengler reaction.

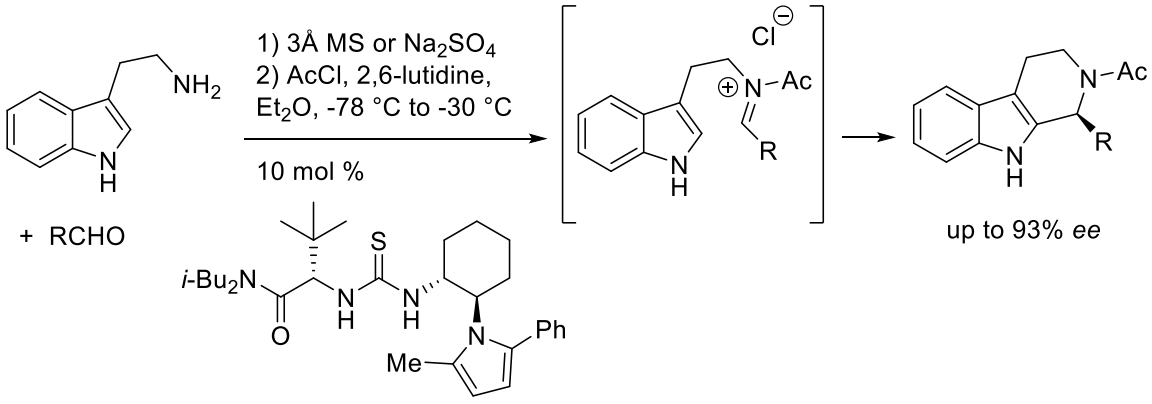

Scheme 13. The proposed mechanism for the thiourea-catalyzed Pictet-Spengler-type reaction.

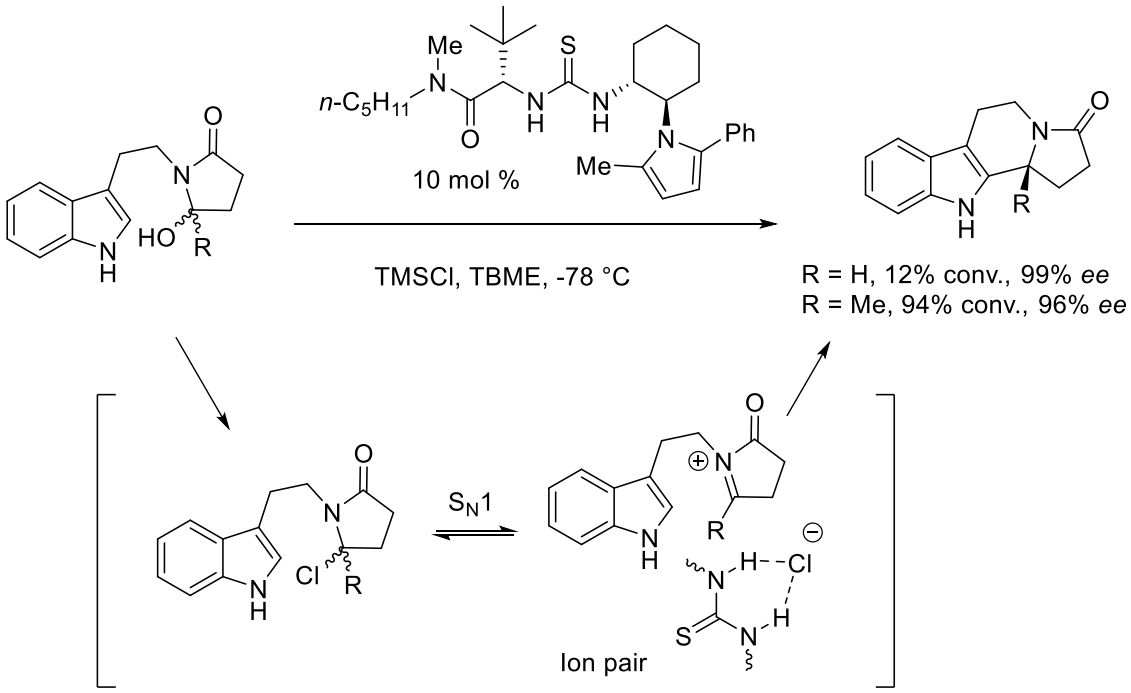

tight ion pair. This hypothesis is supported by the strong binding observed between the thiourea catalyst and chloride, as well as by the decrease in *ee* (and binding affinities) going

from Cl to Br to I. Both of the reactions illustrated in Schemes 12 and 13 are also very sensitive to the nature of the solvent and high enantioselectivities are only achieved in ethereal solvents. This can be accounted for the precipitation of the ammonium hydrochloride by-product in ethereal solvents in the former case and the interaction of HCl with TBME in the latter as these remove the chloride ion from the reaction mixture and liberate the thiourea catalyst.

Jabobsen *et al.* designed a number of additional S_N1 reactions in which the enantioselectivity is induced via ion-pairing of a cation intermediate and a thiourea-anion complex. For example, addition of silyl ketene acetals to planar oxocarbenium cations generated from 1-chloroisochromanes proceeded with 74-95% enantioselectivity (Scheme 14).[25]

Scheme 14. A thiourea-catalyzed S_N1 reaction of 1-chloroisochromane with a silyl ketene acetal.

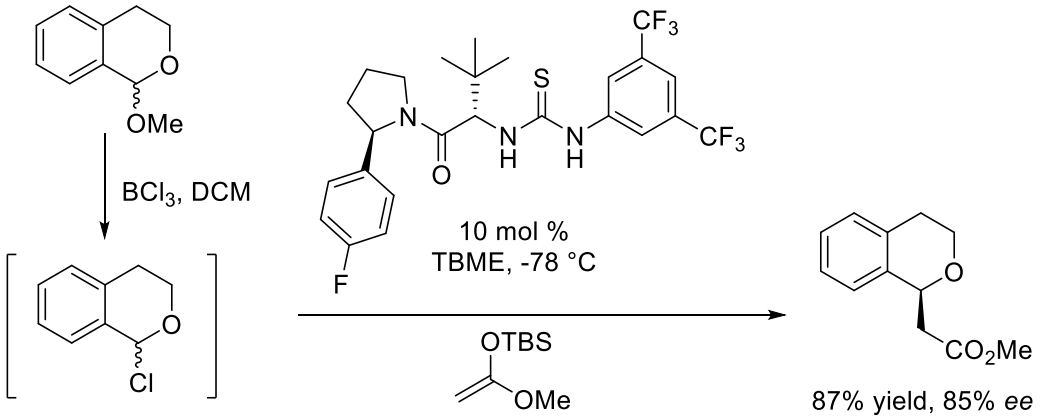

Jacobsen *et al.* also proposed ion-paring in a reaction discovered by Takemoto *et al.* that includes the addition of acylquinolinium salts to vinyl boronic acids (Scheme 15), even

though the inventors originally suggested that the role of the thiourea is to control the *E/Z* ratio of the amide bond in the acylquinolinium salts.[26]

Scheme 15. Thiourea-catalyzed Petasis reaction and a proposed ion-pairing mechanism.

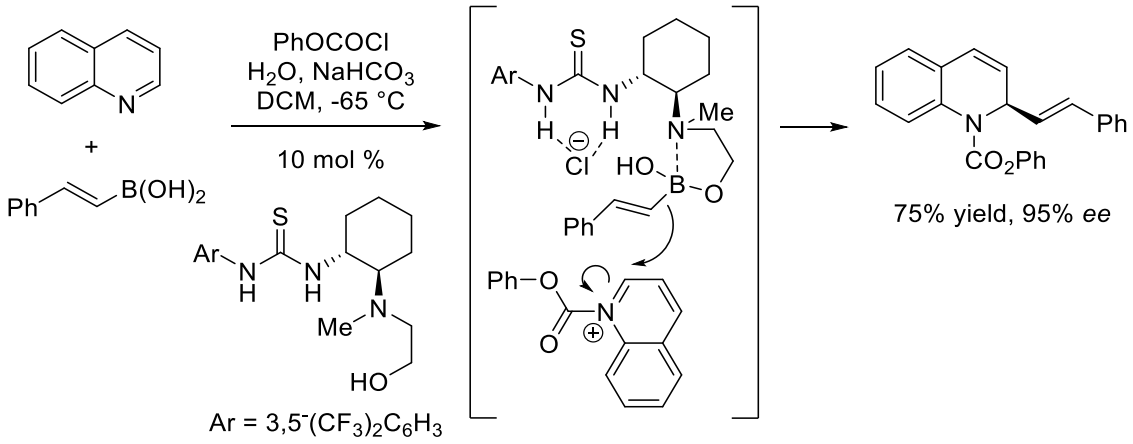

A very interesting example of inducing enantioselectivity via an ion pair is the protio-Pictet-Spengler cyclization discovered by Jacobsen *et al.* (Scheme 16).[27] This reaction is catalyzed by both benzoic acid and a thiourea. The former is a weak Bronsted acid whereas the latter serves as a hydrogen bond catalyst. More specifically, the thiourea increases the acidity of $PhCO_2H$ by binding to its conjugate base (this proposal was first introduced by Schreiner *et al.* for the non-asymmetric alcoholysis of styrene oxides)[28] and the resulting chiral anion induces enantioselectivity in the product via an ion-pair interaction with the iminium intermediate.

Scheme 16. Cooperative catalysis in the protio-Pictet-Spengler cyclization along with the proposed mechanism.

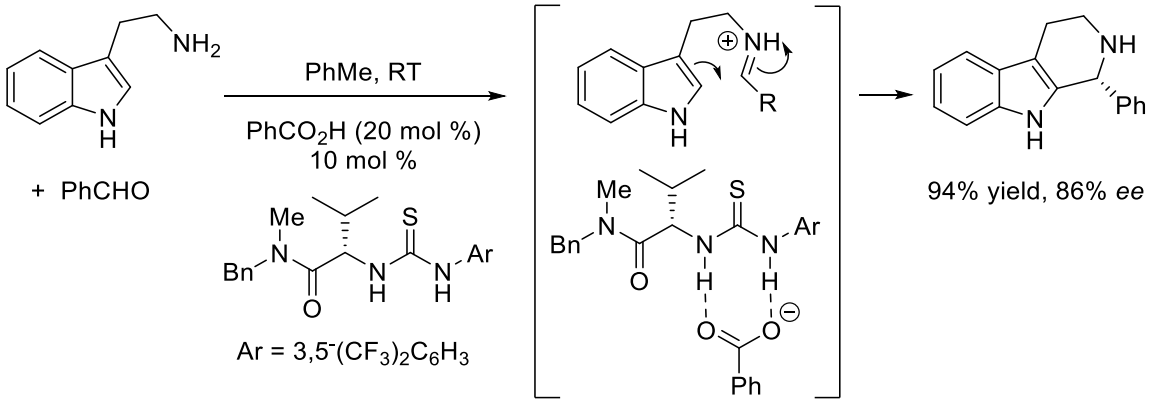

OH Hydrogen bonding catalysts

All the reactions discussed above are catalyzed by N–H hydrogen bond donors in the form of (thio)ureas. Other common types of catalysts are O–H hydrogen bond donors such as BINOL and TADDOL. The former compound has been used in the Baylis-Hillman reaction and its aza analog. For example, Schaus *et al.* followed up on the work by Ikegami *et al.*[29] and developed an enantioselective Baylis-Hillman reaction co-catalyzed by a chiral biphenol and triphenylphosphine (Scheme 17).[30] It was proposed that hydrogen bonding stabilization of the intermediate enolate by the biphenol accelerated the reaction and induced the enantioselective addition of the aldehyde.

Scheme 17. Biphenol-catalyzed Baylis-Hillman reaction.

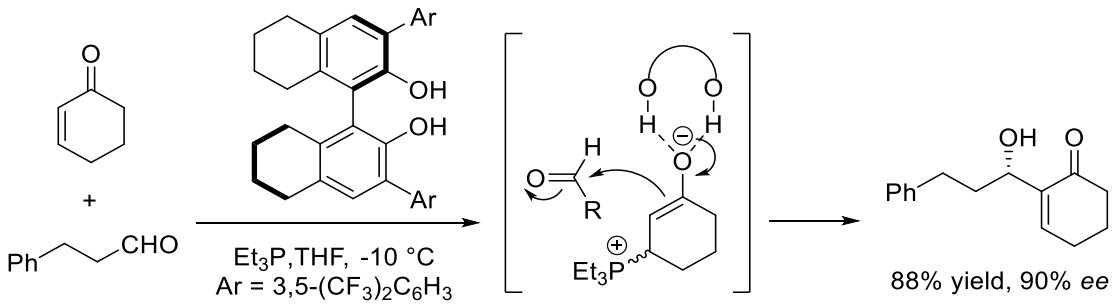

An outstanding result was achieved by Rawal *et al.* who performed an enantioselective hetero-Diels-Alder reaction in the presence of TADDOL, a simple aliphatic alcohol (Scheme 18).[31] The scope of this transformation was subsequently expanded to all-carbon Diels-Alder reactions using acroleins as the dienophiles (i.e., C=C is reacting instead of C=O).[32] Based on the crystal structure of the diol, it was proposed that the carbonyl group of the dienophile interacts with the catalyst by a single hydrogen bond and that the transition state is also stabilized by a π–π* donor-acceptor interaction with the electron rich naphthyl ring. The intermolecular hydrogen bond is strengthened by the intramolecular O–H···O–H interaction and accelerates the reaction by lowering the LUMO energy of the aldehyde, whereas the π–π* interaction shields one face of the dienophile and induces enantioselectivity.

Scheme 18. TADDOL-catalyzed Diels-Alder reaction.

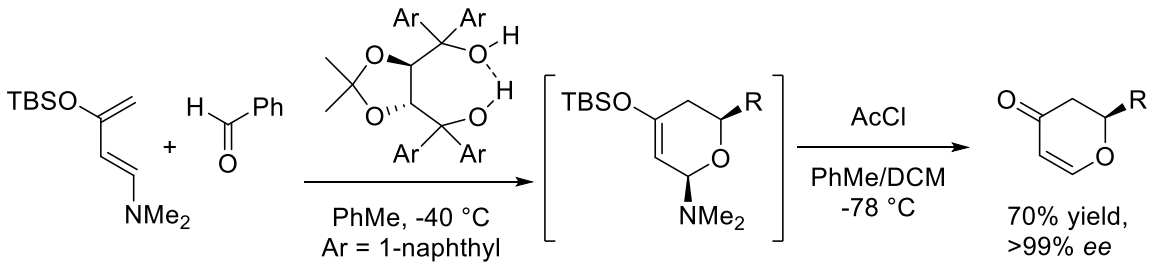

Three hydrogen bond donor catalysts

The catalysts discussed above were all designed to stabilize the developing negative charge in the transition state of a reaction with one or two hydrogen bonds. In principle, if a negative charge forms on an oxygen atom, than three lone pairs are present on the oxyanion center and a three hydrogen bond donor might make for a more efficient catalyst. The additional hydrogen bond in such a case will also provide more rigidity to the transition state structure, which could be exploited to provide better stereochemical control of the products.

Enzymes often utilize hydrogen bonds to catalyze biochemical reactions and oxyanions are common intermediates in these processes. For instance, an oxyanion intermediate is formed during peptide syntheses carried out in ribosomes when an amino group of an amino acid reacts with an ester group of the growing peptide,[33] or in the reverse process (i.e., hydrolysis) catalyzed by serine proteases.[34] The pocket in the enzyme structure that stabilizes the negative charge on oxygen is termed an "oxyanion hole".[35] Interestingly, many enzymes have two hydrogen bond donors in their oxyanion hole (e.g., those

mentioned above), but there are a few that contain three which is termed a "three-pronged oxyanion hole". Acetylcholinesterase (AChE)[36] is an important example as it plays a key role in the peripheral and central nervous systems by removing the neurotransmitter acetylcholine (ACh, 2-acetoxy-*N,N,N*-trimethylethanaminium). Rapid clearing of ACh from the synapses is essential for proper muscle function, and AChE is one of the most efficient enzymes found in nature. It catalyzes hydrolytic destruction of ACh with a rate that is close to the diffusion-controlled limit. An X-ray structure of the enzyme complex with a transition state analog (*N,N,N*-trimethyl-3-trifluoroacetylanilinium) showed three hydrogen bonds to the electron deficient carbonyl group.[37] Computations also revealed the presence of three hydrogen bonds in all of the transition structures and intermediates in the enzymatic reaction pathway.[38] These results indicate that the enzyme most likely uses all three hydrogen bonds in its oxyanion hole.

Reports on three hydrogen bond donor catalysts are limited. Moran *et al.* investigated xanthone-derived bifunctional hydrogen bonding catalysts to mimic two- and three-pronged oxyanion holes.[39] The authors studied the effect of catalyst structures on the rate, substrate-catalyst association and enantioselectivity of the Michael addition reaction between ethanethiol and an unsaturated amide (Scheme 19). Computations indicated that the amide and the urea N–H's of the catalysts act as hydrogen bond donors to stabilize the negative charge on the carbonyl oxygen in the transition state of the reaction, whereas the basic amine group activates ethanethiol by binding to its acidic S–H group. Although, it was reported that the three hydrogen bond donors are generally more reactive catalysts than the analogous two hydrogen bond donors, this difference could not be solely attributed to

the additional hydrogen bond. Indeed, the compounds also differ in acidity (urea *vs.* amide) and the position of the basic site (i.e., the linkage length).

Scheme 19. Two examples of bifunctional catalysts and the half-times of the catalytic Michael addition reaction.

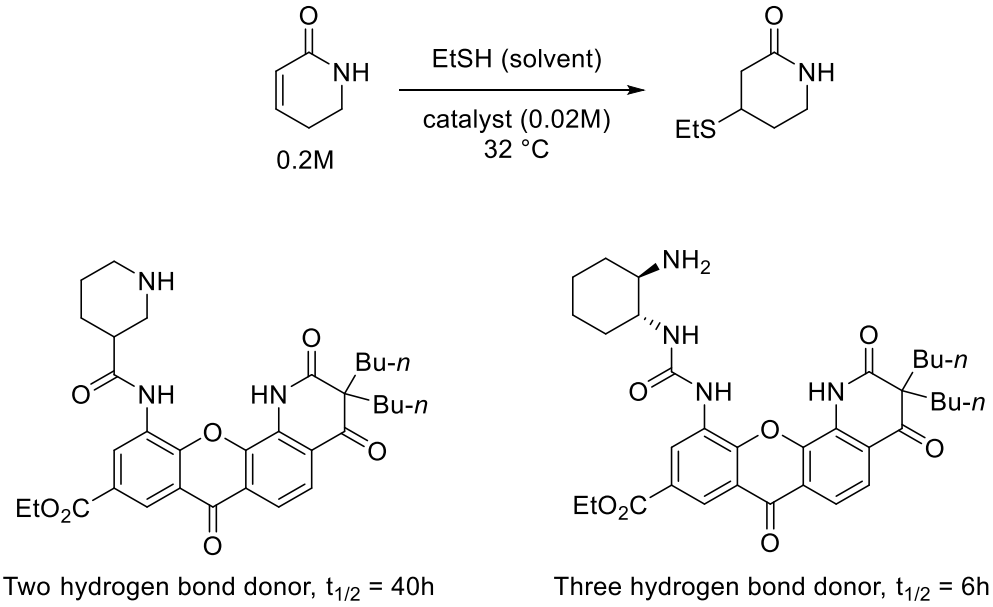

Shea *et al.* investigated the reactivity of a thiophosphoric triamide – a phosphorous analog of Schreiner's thiourea[40] with three N–H bonds (Scheme 20).[41] The catalyst showed small improvements in catalytic activity over the thiourea in a Baylis-Hillman reaction and a Friedel-Crafts reaction of β-nitrostyrene with *N*-methylindol (i.e., factors of 1.3 and 2.6, respectively), but it is not clear if these are due to the additional hydrogen bond or other differences between the two catalysts.

Scheme 20. A new three hydrogen bond donor catalyst and its comparison to the corresponding thiourea.

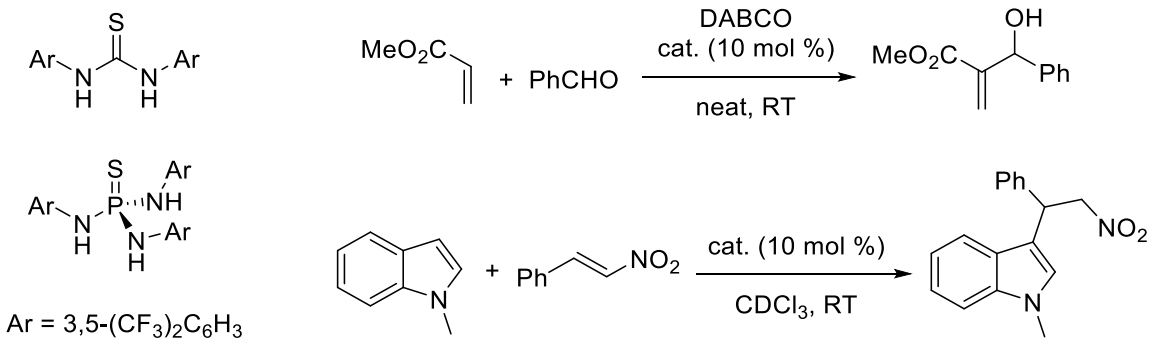

It is interesting to further investigate three hydrogen bond donors as catalysts and compare them to analogous two hydrogen bond donors. This may lead to the development of new and potentially useful hydrogen bonding catalysts as well as additional insights into the mode of action of enzymes with three-pronged oxyanion holes.

Chapter 4: Three hydrogen bond donor catalysts: oxyanion hole mimics and transition state analogs*

Nucleophilic addition reactions are often catalyzed by oxy-anion holes in enzyme-catalyzed processes.[1] Thousands of X-ray crystal structures indicate that nature typically makes use of two hydrogen bonds to facilitate these transformations.[2] Inspired by this observation, chemists mimicked this behavior and developed a wide variety of hydrogen bond catalysts.[3] The most successful and widely employed of these species are thioureas (RNHC(S)NHR). These compounds accelerate reactions by binding to a substrate and increasing its electrophilicity or alternatively by coordinating to an anionic leaving group and generating a reactive carbenium ion intermediate.[4] Transition state analogs for these processes are characterized herein, and the first report of a new catalyst class that makes use of three O–H hydrogen bond donors is described.[5,6]

Thioureas have two NH bonds which play a critical role in their effectiveness as hydrogen bond catalysts. Their acidities also can be enhanced with substituents, and this is important as well since more acidic derivatives are better (i.e., more reactive) catalysts.[7] Oxygen acids are inherently more acidic than their nitrogen analogs, however, because oxygen is more electronegative than nitrogen. Several enzymes also have been identified that use three hydrogen bonds in their oxyanion holes for catalysis.[8] This suggests to us

* Reproduced from: Beletskiy, E. V.; Schmidt, J; Wang, X.-B.; Kass, S. R. *J. Am. Chem. Soc.*, **2012**, *134*, 18534–18537.

that compounds with three hydrogen bond donors might be an effective new catalyst class, and that candidates with three OH groups are particularly attractive targets.

To explore whether a three hydrogen bond donor can confer an energetic and kinetic advantage over a two hydrogen bond donor, 1,3,5-triarylbenzene **1** was synthesized as illustrated in Scheme 1. In this compound the peripheral aromatic rings are known to be twisted with respect to the central one.[9] As a result, all three OH groups can be on one side of the central benzene ring or two hydroxyl substituents can be on one side and the third on the other (i.e., syn and anti, respectively). The rotation barrier is large enough in both cases to prevent the two rotamers from interconverting at room temperature. Isomerization does take place in refluxing mesitylene and upon cooling both isomers can be separated by medium pressure liquid chromatography.

Scheme 1. Synthesis of triarylbenzene **1**.

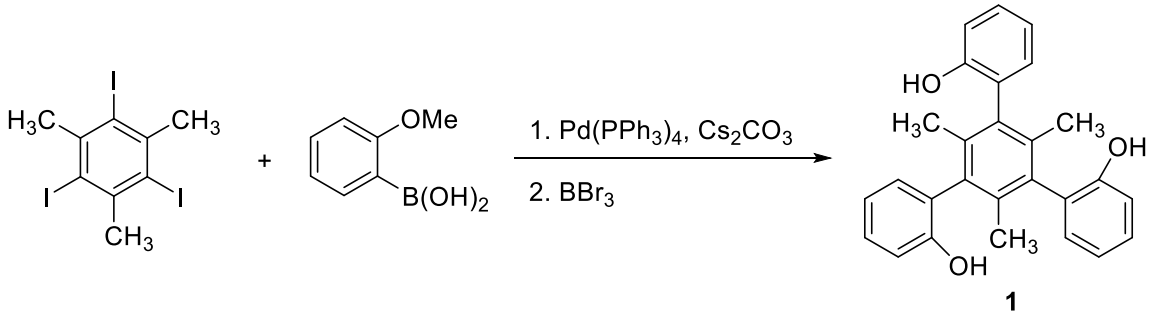

Syn- and *anti*-**1** readily form complexes with chloride ion upon electrospray ionization (ESI).[10] These small molecule clusters can be viewed as transition state analogs for oxyanion holes and hydrogen bond catalysts. To determine if *syn*-**1** • Cl^- and *anti*-**1** • Cl^-

are distinct species or whether they interconvert upon ESI, their multiphoton infrared action spectra were recorded with a Fourier transform mass spectrometer equipped with an optical parametric oscillator (OPO)/optical parametric amplifier (OPA) laser system that previously has been described (Fig. 1).[11] The two spectra are distinct indicating that the two isomers do not interconvert upon ESI.

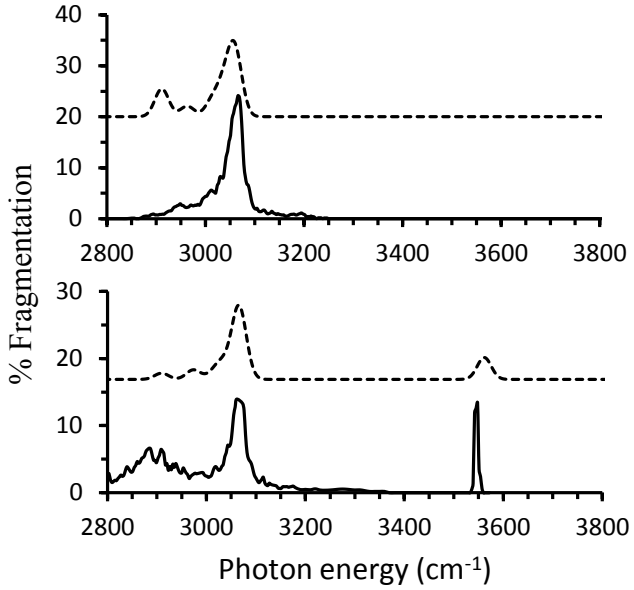

Figure 1. . IR action spectra of syn-**1** • Cl^- (top) and anti-**1** • Cl^- (bottom) from 2700 – 4000 cm^{-1}. B3LYP/aug-cc-pVDZ predictions are shown as dotted lines; see the Supporting Information for more details.

An absorbance is observed at 3545 cm^{-1} in the spectrum of *anti*-**1** • Cl^- but not from the syn isomer. This feature corresponds to a free O–H stretch which is expected for *anti*-**1** • Cl^- since one chloride anion cannot coordinate simultaneously with all three hydroxyl groups in this compound. The absence of this band, and any other above 3100 cm^{-1}, in the

spectrum of *syn*-**1** • Cl^- indicates that all three of the OH substituents form hydrogen bonds with the chloride ion in this isomer. In accord with these observations, the most favorable computed M06-2X/aug-cc-pVDZ structures[12,13] for the *anti*- and *syn*-**1** cluster ions have two and three hydrogen bonds to Cl^-, respectively (Fig. 2). Fragmentation of these complexes to *anti*- or *syn*-**1** and Cl^- are predicted by density functional theory (M06-2X/maug-cc-pVT(+d)Z//M06-2X /aug-cc-pVDZ)[14] to be endothermic by 40.3 and 47.2 kcal mol^{-1} at 298 K, respectively.[15] This 6.9 kcal mol^{-1} difference is largely due to the presence of three hydrogen bonds in the syn complex and only two in the anti species.

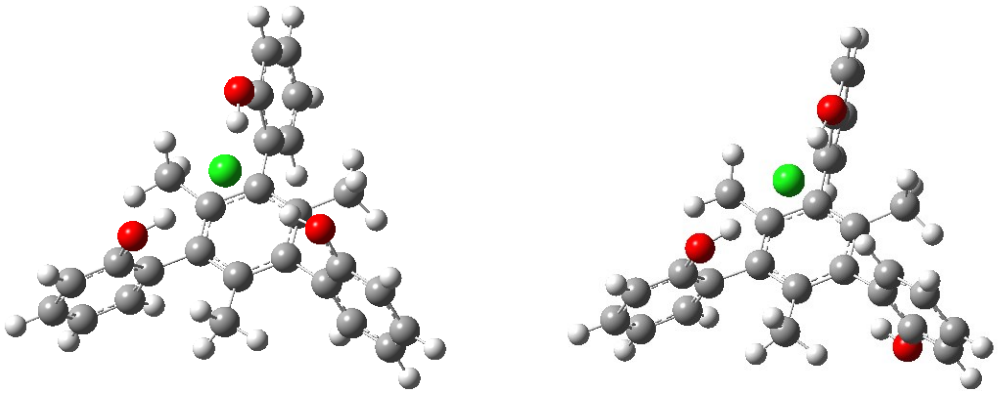

Figure 2. Computed M06-2X/aug-cc-pVDZ structures for *anti*-**1** • Cl^- (left) and *syn*-**1** • Cl^- (right). The OH •• Cl^- and O •• Cl^- distances are 2.116 and 2.121 Å (OH–Cl) and 3.067 and 3.071 Å (O–Cl) for *anti*-**1** • Cl^- and 2.145, 2.145, and 2.146 Å (OH–Cl) and 3.089, 3.089, and 3.090 Å (O–Cl) for *syn*-**1** • Cl^-.

To characterize these cluster ions further and obtain an experimental measure of the hydrogen bond interaction energies with Cl^-, PhOH • Cl^-, *anti*-**1** • Cl^- and *syn*-**1** • Cl^-

generated by ESI were recorded at 20 K with a F_2 laser at 157 nm (7.867 eV, Fig. 3).[16] The spectra of the *anti*- and *syn*-**1** complexes with Cl^- are different as expected, indicating once again that the two ions are distinct and do not interconvert upon ESI. Based upon the rapidly rising onset energies for all three species, estimates for the adiabatic electron detachment energies (ADEs) of 4.15 (PhOH • Cl^-), 4.65 (*anti*-**1** • Cl^-), and 4.80 eV (*syn*-**1** • Cl^-) were obtained. These values are all larger than that for Cl^- (ADE = 3.6131 eV).[17,18] and are well reproduced by M06-2X/maug-cc-pVT(+d)Z//M06-2X/aug-cc-pVDZ computations which give values of 3.88, 4.67, and 4.72 eV, respectively. The experimental differences with respect to Cl^- (i.e., ADE(cluster) – ADE (Cl^-)) are 12.4, 23.9, and 27.4 kcal mol^{-1}, respectively, and reflect the stabilization of the chloride anion by 1-3 hydrogen bonds. These values can not be equated to the hydrogen bond strengths or the disassociation enthalpies and correspond to lower limits for these quantities because electron detachment of the anions leads to neutral clusters that have stabilizing OH • chlorine atom interactions. This is a result of the large difference in the HCl (103.2 kcal mol^{-1}) and PhO–H (88.1 kcal mol^{-1}) bond dissociation energies.[19] As a result, ADE(PhOH • Cl^-) - ADE(Cl^-) = 12.4 kcal mol^{-1} is significantly smaller than the measured 26.0 ± 2.0 kcal mol^{-1} dissociation enthalpy for PhOH • Cl^-.[20] The 3.5 kcal mol^{-1} energy difference between the ADEs of a*nti*-**1** • Cl^- and *syn*-**1** • Cl^-, however, is a measure of the stabilization resulting from an additional hydrogen bond. It also indicates that there is a thermodynamic preference for three hydrogen bonds to Cl^- rather than two.

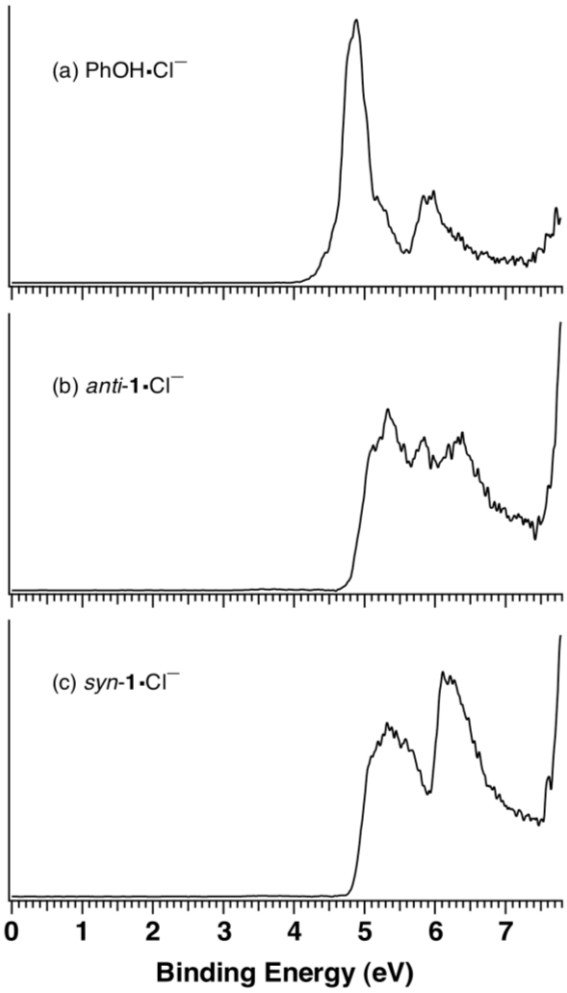

Figure 3. Low temperature (20 K) photoelectron spectra of PhOH • Cl^- (a), anti-**1** • Cl^- (b) and syn-**1** • Cl^- (c) at 157 nm (7.867 eV).

Given the biological importance of anion binding in ion channels and anion transporters,[21] and the physiological role of chloride anion in stabilizing membrane potentials, regulating cell volume, and inhibiting synapses,[22] the association constants of *anti*- and *syn*-**1** with halide anions were measured in acetonitrile by UV or ^{1}H NMR spectroscopy at 23˚C (Table 1). The binding constant for *syn*-**1** with Cl^- is 1.3 x 10^5 M^{-1}

which is quite large (~100 times larger than for catechol (i.e., K = 1015 M^{-1} for 1,2-$(HO)_2C_6H_4$) and ~1000 times bigger than for resorcinol (i.e., K = 145 M^{-1} for 1,3-$(HO)_2C_6H_4$))[23] and reflects a strong association, particularly since acetonitrile is a polar solvent. A much smaller value of 240 M^{-1} was measured for *anti*-**1**, which leads to a syn to anti ratio of 529 : 1. This syn binding preference presumably reflects its ability to form three hydrogen bonds whereas the anti structure can only form one or two. The free energy difference in binding for the two rotamers is 3.7 kcal mol^{-1}, which is virtually the same as the ΔADE of the cluster ions (i.e., 3.5 kcal mol^{-1}).

Table 1. Binding constants and selectivities for syn- and anti-**1**.

cmpd	K (M^{-1})			selectivity		
	Cl^-	Br^-	I^-	Cl^-/Br^-	Cl^-/I^-	Br^-/I^-
syn-**1**	1.27 x 10^5	4270	102	30	1250	42
anti-**1**	240	39	4.8	6.2	50	8.1
syn/ anti	529	109	21	4.8	25	5.2

Bromide and iodide ions were also examined and the binding constants to *anti*- and *syn*-**1** were determined. Each of the association constants are smaller for these less basic halide anions, but the values are larger for the syn isomer and the syn/anti ratios range from 529 (Cl^-) to 21 (I^-). The syn isomer is more selective than *anti*-**1**, which is important if such a compound is to be used as an anion sensor.[24]

Taken together, our results indicate that *syn*-**1** might be a good hydrogen bond catalyst and a better one than *anti*-**1**. That is, a compound capable of forming three hydrogen bonds to a substrate in a reaction transition state maybe more effective than an analogous two hydrogen bond donor. To test this possibility, *anti*- and *syn*-**2**[9] which have 1-pentyl groups para to all three OH substituents in **1** were used in the Friedel-Crafts reaction between β-nitrostyrene and *N*-methylindole (Scheme 2);[25] **1** was not used because of its limited solubility.

Scheme 2. Friedel-Crafts reaction catalyzed by syn- and anti-triphenols.

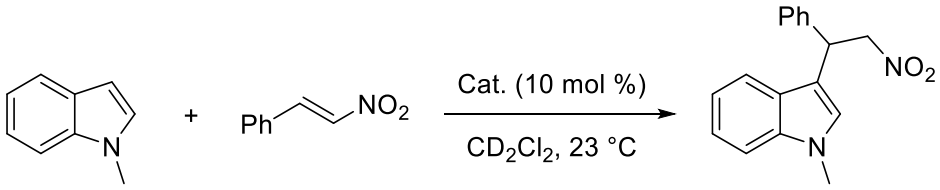

Second-order rate constants were measured by ^{1}H NMR spectroscopy and the reaction catalyzed by *syn*-**2** was observed to proceed 100 times faster than that for *anti*-**2**; the

background reaction occurs ~3 times slower than when *anti*-**2** is used as the catalyst and correcting for this increases the syn/anti ratio to ~160. This indicates that the three hydrogen bond donor is a more effective catalyst in this instance than its analogous two hydrogen bond donor. This is the first such non-enzymatic report, and it provides a kinetic reason for why enzymes might adopt three hydrogen bonds versus two in their oxyanion holes. Catalysts such as **1** or **2** that can form three hydrogen bonds in the transition state are consequently a promising new class of enzyme mimics and hydrogen bond catalysts.

Supporting Information

Experimental and computational sections, binding constant determinations, kinetic data, calculated structures (xyz coordinates) and energies, a ChemDraw picture of *syn*-**2**, and complete ref. 6 are provided. This material is available free of charge via the Internet at http://pubs.acs.org.[*]

Concentration dependence of *syn*-2 catalytic activity[†]

^{1}H NMR studies showed that triol *syn*-**2** undergoes self-association under the reaction conditions that were employed for the transformation illustrated in Scheme 2. Chemical shifts of the OH proton of the triol at different concentrations in a CD_2Cl_2 solution containing 0.25M β-nitrostyrene are shown in Table 2.

[*] http://pubs.acs.org/doi/suppl/10.1021/ja3085862/suppl_file/ja3085862_si_001.pdf
[†] Not included in the *J. Am. Chem. Soc.* publication.

To investigate the effect of *syn*-**2** self-association on its catalytic activity, we studied the reaction in Scheme 2 at three different catalyst loadings (i.e., 25 mM, 12.5 mM, and 0.25 mM). Reaction rates were measured and the experimental details are provided in the supporting information of the published manuscript; the data at each concentration were obtained the same way. A summary of the kinetic data are given in Table 3, linear least squares fits of the data are provided in Figure 4, and the background corrected reaction rate constants are shown in Table 4. It is readily apparent that the reaction rate is linearly dependent on the catalyst concentration, and this first-order dependence is consistent with k_{syn}/k_{anti} being due to the catalytic reactivity of the monomers.

Table 2. Chemical shifts of the phenolic hydrogens at different concentrations of syn-**2** in a CD_2Cl_2 solution containing 0.25M β-nitrostyrene.

Entry	*syn*-**2**, mM	δ_{OH}, ppm
1	25	5.889
2	12.5	5.868
3	6.25	5.851
4	2.5	5.827
5	0.25	5.726
6	0.125	5.681

Table 3. Second-order kinetic data for the Friedel-Crafts reaction of N-methylindole and β-nitrostyrene at 23 °C.

Catalyst loading	Time, h	Yield, %	$\ln([A][B]_0/[A]_0[B])$
12.5 mM *syn*-**2**	4.77	3.03	0.0208
	23.72	13.9	0.1032
	31.75	18.8	0.1448
	49.4	26.1	0.2133
	72.04	34.8	0.3070
	97.3	43.2	0.4134
	123.8	49.5	0.5067
	168.6	58.7	0.6713
	216	68.3	0.8963
0.25 mM *syn*-**2**	23.28	0.47	0.0031
	49.3	1.01	0.0068
	71.68	1.36	0.0091
	143.95	2.44	0.0165
	196.5	3.49	0.0238
	269.5	4.54	0.0312
	337	5.68	0.0394
	389.4	6.42	0.0447

Figure 4. Linear least squares fits of the kinetic data given in Table 4 for 12.5 mM (left) and 0.25 mM (right) syn-**2** concentrations.

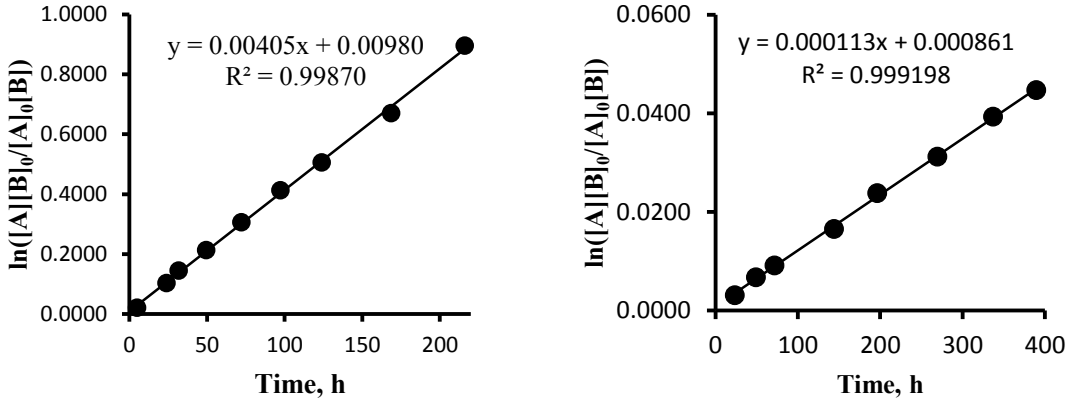

Table 4. Catalytic reaction rate constants for the Friedel-Crafts reaction of β-nitrostyrene with N-methylindole at varying concentrations of syn-**2**.

Entry	*syn*-**2**, mM	Rate constant, $M^{-1}h^{-1}$ *	Relative rate
1	25	$1.56 \cdot 10^{-2}$	1.00
2	12.5	$7.94 \cdot 10^{-3}$	0.51
3	0.25	$1.7 \cdot 10^{-4}$	0.011

* Reaction rate constants were corrected for the background (non-catalyzed) process by subtracting the latter rate constant (i.e., $k_0 = 5.9 \cdot 10^{-5}$ $M^{-1}h^{-1}$) from the observed values for the catalyzed transformation.

Chapter 5: Three hydrogen bonds in catalysis*

Herein, we report the first quantitative study on the influence of a third hydrogen bond on catalysis. In order to determine the effect of three hydrogen bonds, we measured the relative catalytic activity of two catalysts, with two and three acidic hydrogens. We chose 1,3,5-trisubstituted benzene rings as the core structure for the catalysts (Scheme 1)[1] because it is rigid and prevents intramolecular hydrogen bonding, and has C_3 symmetry for proper comparison of **1** *vs.* **2**. As acidic substituents, we chose 2-hydroxyphenyl (**a**) and 8-hydroxy-1-naphthalyl (**b**) groups. In the latter case the OH's presumably are closer to each other than in the former species, and consequently the two derivatives provide catalysts with different cavity sizes. Their ^{1}H NMR spectra show that both **1a** and **2a** exhibit free rotation about the Ar–Ar bonds, whereas in the naphthols (i.e., **1b** and **2b**) this rotation is slow on the NMR timescale. Two conformers are observed for **1b** and **2b** and their rotation barriers are estimated to be *ca.* 15-20 kcal/mol based upon the coalescence temperatures† of their OH chemical shifts.[2] Relative ratios of the conformers in dilute toluene-d_8 solutions are 50 (*syn*) : 50 (*anti*) for triol **1b** and 69 (*syn*) : 31 (*anti*) for diol **2b**. These numbers are slightly higher than the expected statistical ratios of 25 (*syn*) : 75 (*anti*) and 50 (*syn*) : 50 (*anti*), respectively, which means that there is a weak stabilization of the *syn* conformer (*ca.* 0.5 kcal/mol) relative to the *anti* species.

* To be submitted: Beletskiy, E. V.; Kass, S. R., *manuscript in preparation.*
† See the experimental section for details.

Scheme 1. Model hydrogen bond donor catalysts.

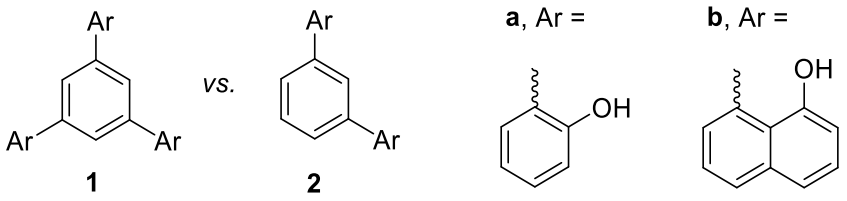

The first reaction we investigated was a ring-opening of an epoxide with a nucleophile. We rationalized that the nucleophile should be strong enough to react with an epoxide, but not too basic to coordinate with our catalysts. Reactions of styrene oxide with amines ($PhNH_2$, Et_2NH)[3] displayed small reactivity differences with **1** and **2** (i.e. less than 2 fold), probably due to catalyst inhibition by the basic amine reagent. We next turned to a more nucleophilic but less basic reagent and explored the reactivity of thiophenol (Scheme 2).[4] No reaction was observed between styrene oxide (**3a**) and PhSH in toluene-d_8 at 80 °C after 2 h, however, addition of a trialkylamine base induced a very slow reaction at ambient temperature. Interestingly, 5 mol % loadings of the catalyst were sufficient to significantly accelerate this transformation, even though thiophenol is expected to be more acidic than both **1** and **2** when Ar = **a** or **b** since its pK_a is 10.3 in DMSO,[5a] whereas that for phenol and 1-naphthol are 18.0[5b] and 16.2,[5c] respectively. Virtually no acceleration was observed, however, when CD_3CN was used as the solvent, but the background reaction without the catalyst occurred quickly.

Scheme 2. Catalytic ring-opening reactions of epoxides with thiophenol.

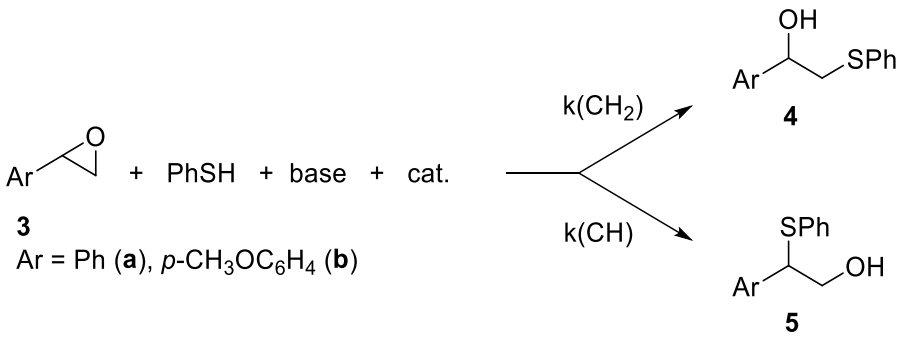

NMR analysis of the reaction mixture showed the formation of two products resulting from nucleophilic attack at the CH_2 and CH positions of the epoxide (i.e., **4** or **5**, respectively). We found that the reaction co-catalyzed with bulky bases (*i*-Pr_2NEt or PMP) proceeded smoothly according to 2nd order kinetics: the reaction was typically followed for 24-48 hours and in some cases this corresponded to more than 3 half-lifes. ^1H NMR studies showed no significant binding of *i*-Pr_2NEt to PhSH, which is consistent with the 1st order dependence on PhSH and the epoxide, and the 2nd order overall dependence of the reaction. When less bulky bases such as Et_3N and 2,6-lutidine were used, the reaction was accelerated by our catalysts and significant differences between **1b** and **2b** were observed (i.e., *ca.* 4-8 fold for the rates at less than 3% conversion), but a second order dependence was not observed and the reaction rate increased with time. We speculate that this is due to a side reaction leading to a stronger base (e.g., ring-opening of the epoxide by the amine to afford a zwitterionic alkoxide ion).

We were delighted to observe up to a 15 fold difference between the triol and diol catalytic rates (i.e., relative rates corrected for the non-catalyzed reaction (k_1/k_2), Table 1).

Table 1. Relative triol (**1**) and diol (**2**) catalytic rates in the ring-opening of **3** with thiophenol.[a]

Entry	Epoxide	Catalysts	Triol/Diol[b] $k_1/k_2(CH_2)$	Triol/Diol[b] $k_1/k_2(CH)$
1	3a	**a**, 5 mol %	4.2 (4.3)	7.6 (7.6)
2	3a	**a**, 1.67 mol %	3.2 (3.5)	5.3 (5.6)
3	3a	**b**, 5 mol %	6.2 (6.8)	9.3 (9.9)
4	3b	**b**, 5 mol %	6.2 (7.1)	11.8 (12.5)
5	3b	**b**, 1.67 mol %	5.0 (8.1[c])	9.7 (12.6)
6	3b	**b**, 0.83 mol %	nd	7.8 (12.4)
7[d]	3b	**b**, 5 mol %	6.6 (8.1)	13.5 (14.6)
8[e]	3b	**b**, 5 mol %	nd	10.4 (11.3)
9[f]	3b	**b**, 5 mol %	5.1 (6.3)	8.3 (9.0)

[a] Conditions: Rreactions were run in NMR tubes at 23 °C using 0.5 M styrene oxide, 0.5 M PhSH, and 0.125 M *i*–Pr_2NEt in toluene–d_8. Second order rate constants ($M^{-1}\cdot h^{-1}$) were determined by ^1H-NMR. See the supporting information for the rate constants. [b] Here and below: relative rates for triol *vs.* diol catalyzed reactions. The numbers in brackets are corrected for the background (uncatalyzed) process as follows: $k_1/k_2 = (k_{triol}-k_0)/(k_{diol}-k_0)$. [c] This number has a large error due to the comparable rates of the background and the diol-catalyzed processes. [d] Entry 7: 0.25 M base. [e] Entry 8: 0.042 M base. [f] Entry 9: 0.05 M base, base = 1,2,2,6,6–pentamethylpiperidine (PMP).

To address whether the acceleration was due to the formation of three hydrogen bonds, the following possibilities were considered: 1) the triol has a higher tendency to aggregate and the dimer is responsible for its enhanced activity, 2) the base inhibits the catalysts, but this effect is larger for the diol 3) statistics favor the reactivity of **1** by a factor of 3 due to presence of three pairs of hydroxyl groups as compared to only one pair in **2**. The first hypothesis was addressed by carrying out the reaction at lower catalyst loadings (i.e., lower concentrations). A non-first order dependence of the reaction rate on the catalyst concentration was observed in each case, which is presumably due to a complex mechanism for this transformation. However, dilution increases the monomer/dimer ratio of **1**, whereas **2** only was found to aggregate weakly. Consequently, if one assumes that **1** and **2** react via the same mechanism and that the dimer of **1** is the most active species, then the **1**/**2** relative rate would decrease. For the phenolic catalysts **1a** and **2a**, the background corrected k_1/k_2 relative reaction rates were found to decrease by *ca.* 25% when the catalyst loading was reduced by a factor of three (i.e., entry 1 *vs.* 2). This behavior can be ascribed to the formation of a more active dimer of **1a** at higher concentrations, so the actual enhancement of the reaction rate by a third hydrogen bond in the monomer might be small. However, the relative reactivity of naphthols **1b** and **2b** is concentration independent (i.e, entries 4–6), which suggests that aggregation is not an issue in this case. In addition, the relative rates (k_1/k_2) are larger with the naphthols than with the phenols (entry 3 *vs.* 2), even though the latter species are the more efficient catalysts. We attribute these differences to the smaller cavity size in the naphthol derivatives and the greater importance of all three acidic OH groups in this case.

To address the second possibility, we ran the reaction with different base concentrations (entries 4, 7 and 8). The relative rate k_1/k_2 for the naphthols increased by *ca.* 15% when the base loading was doubled (i.e., entry 7) and decreased by *ca.* 10% when it was cut in third (i.e., entry 8). These results indicate that large changes in the base concentration (i.e., a factor of 6) have only a small impact on k_1/k_2 (i.e., *ca.* 25%). Consequently, our data indicates that the reactivity differences between the triol (**1b**) and the diol (**2b**) are due to the third hydrogen bond to the reagents.

The relative **1b**/**2b** rates k_1/k_2 change significantly for formation of **4** and **5**. For **4a** and **4b** it is same within experimental error (6.8 and 7.1, respectively). However, for **5a** and **5b**, it is 9.9 and 12.5, respectively. This suggests that the negative charge on the epoxide oxygen increases in the transition state in the order **4** < **5a** < **5b**, and that the stabilization by the third hydrogen bond follows this trend as well. This can be ascribed to the increasing electron donating abilities of the substituents adjacent to the reaction site (i.e., H (**4**) < Ph (**5a**) < *p*-$CH_3OC_6H_4$ (**5b**)) and thus the higher extent of C–O bond breakage in the transition state. Interestingly, this trend makes the ring-opening reaction more selective with the **1b** compared to **2b**: for **3a** the CH : CH_2 selectivity increases from 41 : 59 for the diol catalyst to 51 : 49 for the triol (entry 3) and for **3b** it goes from 75 : 25 to 85 : 15 (entry 4).

We next turned our attention to the activation of carbonyl compounds and investigated the Henry reaction of aldehydes with nitromethane in the presence of a base with and without our catalysts (Table 2).[6] No acceleration was observed in the catalyzed reactions when Et_3N or DABCO (0.125 M) was used as the base. In fact, a slight rate retardation was observed presumably due to coordination of the bases to the acidic hydroxyl groups of the

catalysts. When a bulky base such as *i*-Pr_2NEt or PMP was employed, a significant acceleration of the reaction was observed when **1b** and **2b** were used. We were pleased to observe **1b**/**2b** corrected relative rates (k_1/k_2) in the range of 4.1–6.9 (Table 2), whereas **1a**/**2a** gave less than a 2.5 fold difference.

Table 2. Henry reaction rates.[a]

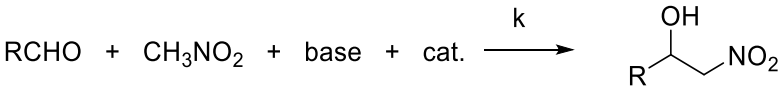

Entry	R	No cat. (k_0)	Triol **1b** (k_1)	Diol **2b** (k_2)	k_1/k_2
1	Ph	$4.4\cdot10^{-4}$	$1.2\cdot10^{-2}$	$3.05\cdot10^{-3}$	**4.0 (4.6)**
2	Ph	$1.1\cdot10^{-3}$	$1.84\cdot10^{-2}$	$4.68\cdot10^{-3}$	**3.9 (4.9)**
3[b]	Ph	$6.2\cdot10^{-4}$	$1.38\cdot10^{-2}$	$3.80\cdot10^{-3}$	**3.6 (4.1)**
4	Ar[c]	$1.7\cdot10^{-4}$	$3.3\cdot10^{-3}$	$7.94\cdot10^{-4}$	**4.2 (5.0)**
5	CH_3	$6.2\cdot10^{-4}$	$2.32\cdot10^{-2}$	$3.88\cdot10^{-3}$	**6.0 (6.9)**

[a] Conditions: aldehyde (0.5 M), CH_3NO_2 (1.5 M), base (0.125 M), catalyst (5 mol %) in toluene–d_8 at 23 °C. Second order rate constants were determined by ^1H NMR. Base = *i*–Pr_2NEt (entry 1), PMP (entries 2–5). [b] CH_3NO_2 (0.5 M). [c] Ar = *p*–$CH_3OC_6H_4$.

Unlike the epoxide reaction (Table 1), the values of k_1/k_2 did not change on going from benzaldehyde (4.9, entry 2) to anisaldehyde, which has an electron donating OMe group (5.0, entry 4). A nonconjugated acetaldehyde, however, gave a higher value (6.9, entry 5). Since conjugation is lost in the reaction, it is reasonable that with the aromatic aldehydes

the transition state is earlier than with acetaldehyde. Consequently, in the latter case there is a larger negative charge on the oxygen atom in the transition state and the effect of the third hydrogen bond is bigger.

We studied the binding of the Henry reaction reagents to the catalysts **1b** and **2b** by ^{1}H NMR.[7] It was estimated that for entry 2 44% of triol **1b** and 31% for diol **2b** are bound to PhCHO. This 1.4 fold difference is significantly less than the statistical value of 3 presumably because **1b** is larger than **2b**. Assuming that the role of the catalyst is to activate PhCHO, the actual acceleration due to the third hydrogen bond is 4.9/1.4 = 3.5 for entry 2. If the same relative binding to acetaldehyde (1.4 fold) is assumed, then the third hydrogen bond acceleration is 4.9 for entry 5. It should be noted, however, that an alternative mechanism (i.e., deprotonation of CH_3NO_2 by the base followed by coordination of the newly formed nitronate anion to the catalyst and the aldehyde to the resulting ammonium cation (see Chapter 3, Scheme 11)) maybe more favorable.

The activation of 1,2–unsaturated ketones was also studied.[8] Methyl vinyl ketone (MVK) reacted under Henry reaction conditions with $k_1/k_2 = 5.3$ (6.7 if corrected for the non-catalyzed reaction) (Table 3, entry 1). Acrolein was also reacted with nitromethane in a Michael fashion (i.e., attack on C=C versus C=O), however the relative rate value was smaller – 4.2 (4.8) (entry 2). Our catalysts were insufficiently activating for other substrates (methyl acrylate, 2-cyclohexen-1-one), so we explored other nucleophiles. Other nitroalkanes gave lower relative rates for **1b** and **2b**. That is, a more reactive α-nitrotoluene showed only a 2.9 (4.1) fold difference for the reaction with MVK (entry 3), and the rate

of benzoylnitromethane addition (R^1 = PhCO, not shown) was not at all affected by the addition of **1b**.

Table 3. Reaction rates for the Michael addition of nitroalkenes.*

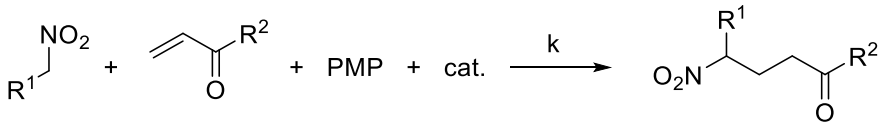

Entry	R^1	R^2	No cat. (k_0)	Triol **1b** (k_1)	Diol **2b** (k_2)	k_1/k_2[b]
1[b]	H	CH_3	$4.4 \cdot 10^{-4}$	$9.10 \cdot 10^{-3}$	$1.73 \cdot 10^{-3}$	**5.3 (6.7)**
2[c]	H	H	$2.1 \cdot 10^{-3}$	$5.22 \cdot 10^{-2}$	$1.24 \cdot 10^{-2}$	**4.2 (4.8)**
3[d]	Ph	CH_3	$1.32 \cdot 10^{-2}$	$9.54 \cdot 10^{-2}$	$3.33 \cdot 10^{-2}$	**2.9 (4.1)**

* Conditions: reactions were run in NMR tubes in toluene–d_8 at 23 °C. Second order rate constants are given in $M^{-1} \cdot h^{-1}$. [b] 0.5 M ketone, 1.5 M CH_3NO_2, 0.125 M PMP. [c] 0.15 M aldehyde, 1.5 M CH_3NO_2, 0.015 M PMP. [d] 0.5 M ketone, 0.5 M $PhCHNO_2$, 0.01 M PMP.

We investigated the reactions of a variety of unsaturated carbonyl compounds (i.e., MVK, acrolein, chalcone, 2-cyano-3-phenylacrylate and the benzylidene derivative of Meldrum's acid) in the presence and absence of a base with the following nucleophiles: PhSH, PhOH, meldrum's acid, malononitrile and pyrazole (reactions were carried out in toluene-d_8 similarly to other transformations described here), but there was little or no acceleration when **1b** was added compared to the non-catalyzed transformations. The only case, where an acceleration was observed was in the Michael addition of aniline to MVK,[9]

but k_1/k_2 = 2.0 (2.3) was low. A bulkier and less coordinating (to **1b** and **2b**) reagent 2,6-di-*iso*-propylaniline provided a higher k_1/k_2 of 3.7 (4.1).

Finally, we studied the activation of β-nitrostyrene. Its reaction with nitromethane[10] in the presence of PMP showed a small difference between the non-catalyzed and **1b**-catalyzed reactions (only a factor of 2.7 with a 4 mol % loading of **1b**). However, the reaction with *N*-methylindole,[11] although slow, showed a significant effect of the third hydrogen bond (Scheme 3) as the relative rate of **1b** and **2b** was 13.6 (19 if corrected for the background process).

Scheme 3. Friedel-Crafts reaction of β-nitrostyrene with N-methylindole.[a]

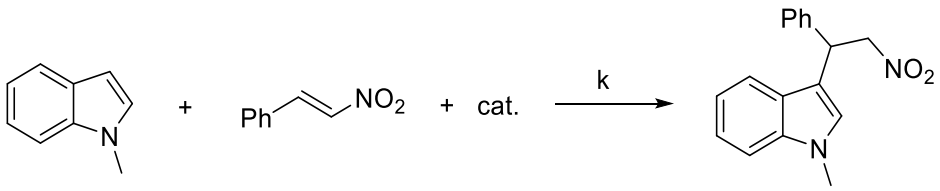

[a] Conditions: N-methylindole (0.75 M), β-nitrostyrene (0.25 M), **1b** or **2b** (10 mol %) in CD_2Cl_2, 23 °C. Second-order kinetics gives $k_1 = 1.62 \cdot 10^{-3}$ $M^{-1} \cdot h^{-1}$, $k_2 = 1.19 \cdot 10^{-4}$ $M^{-1} \cdot h^{-1}$, $k_0 = 3.5 \cdot 10^{-5}$ M^{-1} h^{-1} and **k_1/k_2 = 13.6 (19)**.

In conclusion, catalytic activities of triols and diols were compared in order to determine the effect of the third hydrogen-bond on catalysis. Triols **1** based on a 1,3,5-trisubstituted benzene core and diols **2** (1,3-disubstituted) were chosen as the model compounds. Significant accelerations (4-19 fold) were observed for the activation of epoxides, aldehydes, unsaturated carbonyl compounds and β-nitrostyrene using triol **1b** compared to

diol **2b** at 23 °C. Moreover, the three hydrogen-bond donor catalyst **1b** promoted a more selective ring-opening reaction of epoxides with thiophenol.

Experimental

General. All reactions were carried out using flame-dried glassware under a nitrogen or argon atmosphere except where aqueous solutions were employed as reagents. Unless noted otherwise, all chemicals were purchased from Sigma-Aldrich and used as received. Analytical thin layer chromatography (TLC) was carried out using 0.20 mm silica plates from Macherey-Nagel and the compounds were visualized using UV light. Flash chromatography was performed with a Biotage Isolera One using 200–400 mesh (particle size 0.04 – 0.075 mm) silica gel purchased from Sorbent Technologies. Proton (300 and 500 MHz) and carbon (75 and 125 MHz) NMR spectra were obtained on Varian or Bruker FT NMR instruments. The spectra are reported as δ values in ppm relative to the residual protio-containing solvent or tetramethylsilane. Coupling constants are reported in Hz, and multiplicities are indicated as follows: s (singlet), d (doublet), t (triplet), m (multiplet), dd (doublet of doublets), dt (doublet of triplets), ddd (doublets of doublets of doublets), app (apparent) and br (broad). High-resolution mass spectra (HRMS) in electrospray (ESI) experiments were performed on a Bruker BioTOF II.

Synthesis of new compounds.

Scheme S1. Synthesis of triol **1b** and diol **2b**.

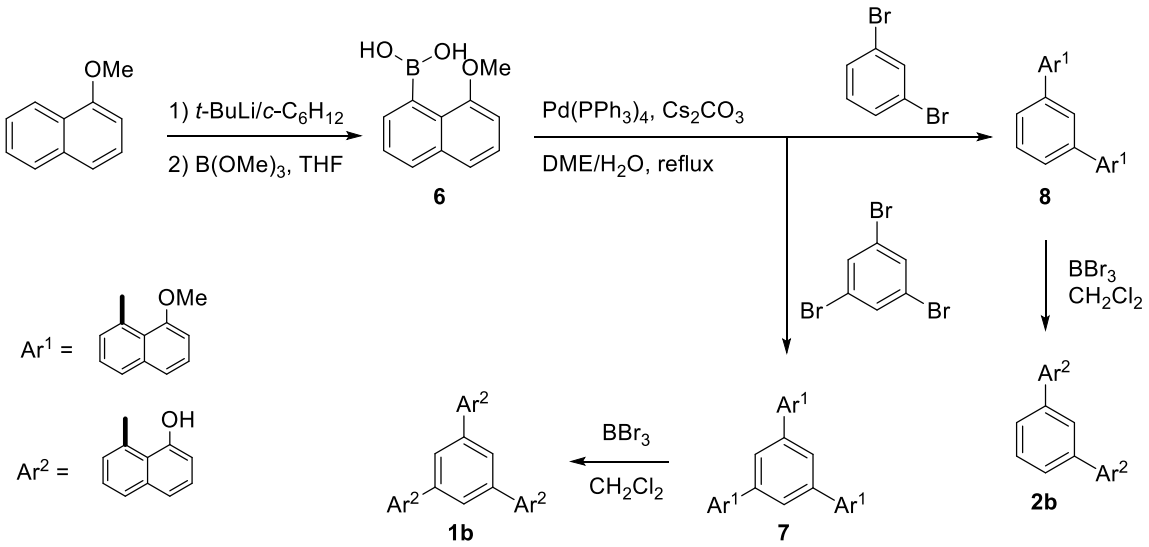

Boronic acid 6. To a –15 °C solution of 1-methoxynaphthalene (7.90 g, 50.0 mmol) in cyclohexane (50 mL) was added *t*-BuLi (1.7 M, 35 mL, 60 mmol) dropwise under nitrogen. The resulting yellow solution was allowed to warm up to room temperature and stirred for 40 h to form a yellow suspension. Nitrogen was flowed through the system continuously to evaporate some of the hydrocarbon solvent (*ca.* 40 mL). Upon cooling to –78 °C, THF (100 mL) was added and then trimethyl borate (11.2 mL, 100 mmol) was rapidly added. The resulting reaction mixture was stirred overnight as it warmed to room temperature. Aqueous ammonium chloride (15 g in 50 mL H_2O) was added and the bilayer mixture was stirred for 1 h. Ethyl acetate (100 mL) was added and the organic layer was separated, washed with brine (20 mL), dried over Na_2SO_4 and concentrated in vacuo. The resulting

solid was recrystallized twice from toluene to afford 2.41 g (24%) of **6** as a white powder (mp 147–148 °C with decomposition). ^{1}H NMR (500 MHz, acetone-d_6) δ 7.76 (dd, J = 3.3, 6.3 Hz, 1H), 7.46–7.43 (m, 3H), 7.39 (t, J = 8.5 Hz, 1H), 6.90 (d, J = 7.5 Hz, 1H), 6.70 (s, 2H), 3.97 (s, 3H); ^{13}C NMR (75 MHz, acetone-d_6) δ 157.2, 135.4, 129.2, 128.6, 128.0, 127.1, 126.9, 121.7, 105.34, 56.1 (carbon attached to boron not observed). HRMS (ESI) calcd for $[C_{11}H_{11}BO_3 + 2CH_3OH - 2H_2O + Na]^+$ 253.1012, found 253.0997.

Triol 1b. A round-bottomed flask was charged with boronic acid **6** (2.30 g, 11.4 mmol), 1,3,5-tribromobenzene (756 mg, 2.40 mmol), cesium carbonate (7.82 g, 24.0 mmol), dimethoxyethane (20 mL) and water (10 mL). Nitrogen was bubbled through the mixture with stirring for 30 min and then tetrakis(triphenylphosphine)palladium(0) (217 mg, 0.24 mmol) was added. The resulting bilayer solution was refluxed with vigorous stirring for 15 h under nitrogen. The organic layer was separated, dried over Na_2SO_4, and concentrated in vacuo. Silica gel chromatography (CH_2Cl_2–Hexanes, 12 : 88 to 100 : 0) afforded 1.10 g (85%) of the trimethyl ether **7** as a white solid (R_f = 0.52 (CH_2Cl_2–Hexanes, 50 : 50)). ^{1}H NMR (300 MHz, $CDCl_3$) mixture of *syn* and *anti* conformers (integrations as observed to the total of 30H) δ 7.78 (d, J = 9.3 Hz, 3H), 7.49–7.37 (m, 15H), 6.81 (d, J = 7.5 Hz, 3H), 3.70 (br s, 6.5H), 3.58 (s, 2.5H). HRMS (ESI) calcd for $[C_{39}H_{30}O_3 + Na]^+$ 569.2093, found 569.2067.

To a 0 °C solution of **7** (1.08 g, 1.98 mmol) in CH_2Cl_2 (10 mL) was added boron tribromide (0.76 mL, 8.0 mmol) dropwise under nitrogen. The resulting solution was stirred at room temperature overnight. Water (10 mL) was added at 0 °C and the resulting mixture was stirred at room temperature for 30 min. Ethyl acetate (30 mL) was added and

the organic layer was separated, washed with brine (10 mL), dried over Na_2SO_4 and concentrated in vacuo. The resulting solid was dissolved in a minimum amount of ethyl acetate, added to the top of a short plug of silica gel and eluted with CH_2Cl_2. This solution was evaporated in vacuo and the resulting solid was crystallized with toluene to afford 828 mg (82%) of **1b** as a white powder (R_f = 0.35 (EtOAc–DCM, 3 : 97), mp 291–293 °C). ^{1}H NMR (500 MHz, $CDCl_3$) 50:50 mixture of *syn* and *anti* conformers δ 7.84 (app t, *J* = 7.7 Hz, 3H *syn* + *anti*), 7.68 (s, 2H *anti*), 7.67 (s, 1H *anti*), 7.63 (s, 3H *syn*), 7.49–7.29 (m, 12H *syn* + *anti*), 6.98 (d, *J* = 7.5 Hz, 1H *anti*), 6.86 (d, *J* = 7.5 Hz, 2H *anti*), 6.82 (d, *J* = 8.0 Hz, 3H *syn*), 5.92 (s, 3H *syn*), 5.66 (s, 1H *anti*), 5.64 (s, 2H *anti*); ^{1}H NMR (300 MHz, toluene-d_8, 94 °C) δ 7.63–7.59 (m, 3H), 7.34 (s, 3H), 7.30 (d, *J* = 8.1 Hz, 3H), 7.21–7.11 (m, 9H), 6.65 (app br s, 3H), 5.40 (br s, 3H); ^{13}C NMR (75 MHz, acetone-d_6) δ 155.3, 144.5 (br), 143.7 (br), 142.7, 139.4 (br), 139.2, 137.5, 130.1, 129.6, 129.4, 128.6, 127.8, 126.3, 123.3, 121.5, 112.1, 112.0 (br) (nineteen signals are not resolved). HRMS (ESI) calcd for $[C_{36}H_{24}O_3 + Na]^+$ 527.1623, found 527.1611.

Diol 2b. A round-bottomed flask was charged with boronic acid **6** (505 mg, 2.51 mmol), 1,3-dibromobenzene (236 mg, 1.00 mmol), cesium carbonate (1.63 g, 5.00 mmol), dimethoxyethane (6 mL) and water (2 mL). Nitrogen was bubbled through the mixture with stirring for 15 min and then tetrakis(triphenylphosphine)palladium(0) (69 mg, 0.060 mmol) was added. This bilayer solution was refluxed with vigorous stirring for 15 h under nitrogen before allowing it to cool to room temperature. Ethyl acetate (30 mL) was added and the organic layer was dried over Na_2SO_4 and concentrated in vacuo. Silica gel chromatography (CH_2Cl_2–Hexanes, 8 : 92 to 50 : 50) afforded 304 mg (78%) of dimethyl

ether **8** as a white solid (R_f = 0.34 (CH_2Cl_2–Hexanes, 33 : 67). ^{1}H NMR (300 MHz, $CDCl_3$) mixture of *syn* and *anti* conformers (integrations as observed to the total of 22H) δ 7.79 (dd, *J* = 1.0, 8.0 Hz, 2H), 7.51–7.24 (m, 12H), 6.80 (app br s, 2H), 3.61 (s, 2.9H), 3.55 (s, 3.1H). HRMS (ESI) calcd for $[C_{28}H_{22}O_2 + Na]^+$ 413.1517, found 413.1513.

To a solution of **8** (290 mg, 0.74 mmol) in CH_2Cl_2 (4 mL) was added boron tribromide (0.16 mL, 1.7 mmol) dropwise at 0 °C under nitrogen. The resulting solution was stirred at room temperature overnight. Water (5 mL) was added at 0 °C and the resulting mixture was stirred at room temperature for 1 h. Ethyl acetate (30 mL) was added and the organic layer was separated, washed with water (10 mL) and brine (10 mL), dried over Na_2SO_4 and concentrated in vacuo. Silica gel chromatography (CH_2Cl_2–Hexanes, 16 : 84 to 100 : 0) afforded 235 mg (88%) of **2b** as a white solid that was crystallized with toluene (R_f = 0.23 (CH_2Cl_2–Hexanes, 66 : 33), mp 169–170 °C). ^{1}H NMR (500 MHz, $CDCl_3$) 59:41 mixture of *syn* and *anti* conformers δ 7.87 (d, *J* = 8.5 Hz, 2H *anti*), 7.84 (d, *J* = 8.5 Hz, 2H *syn*), 7.69 (s, 1H *anti*), 7.65 (br s, 2H *syn*), 7.59–7.28 (m, 11H *anti* + 10H *syn*), 6.93 (d, *J* = 7.0 Hz, 2H *anti*), 6.85 (d, *J* = 6.5 Hz, 2H *syn*), 5.46 (s, 2H *syn*), 5.34 (s, 2H *anti*); ^{13}C NMR (75 MHz, $CDCl_3$) mixture of *syn* and *anti* conformers δ 152.7, 142.5, 142.3, 136.7, 135.7, 135.4, 130.5, 130.1, 129.1, 128.9, 128.4, 128.3, 128.2, 126.8, 126.5, 125.0, 121.7, 121.3, 121.2, 111.9, 111.5 (seven signals are not resolved); ^{1}H NMR (300 MHz, toluene-d_8, 94 °C) rapid interconversion of *syn* and *anti* conformers δ 7.60 (dd, *J* = 1.2, 8.4 Hz, 2H), 7.31–7.28 (m, 3H), 7.24–7.21 (m, 2H), 7.18–7.12 (m, 5H), 7.06 (d, *J* = 1.2 Hz, 2H), 6.66 (app br s, 2H), 5.15 (s, 2H); ^{13}C NMR (75 MHz, toluene-d_8, 94 °C) δ 154.0, 143.6, 137.5, 137.0, 130.8, 129.0, 127.2, 125.3, 123.0, 121.7, 112.5 (three signals are not resolved). HRMS

(ESI) calcd for $[C_{26}H_{18}O_2 + Na]^+$ 385.1204, found 385.1213. The rotation barrier about the Ar–Ar bond in **1b** and **2b** was estimated to be 15-20 kcal/mol based on the coalescence temperature (i.e., *ca.* 70 °C) of the two hydroxyl group signals in **2b** (i.e., 5.53 ppm (2H) and 5.26 ppm (1H) at 22 °C) in the ^{1}H NMR spectrum (300 MHz, toluene-d_8).

Scheme S2. Synthesis of alchohols **4b** and **5b**.

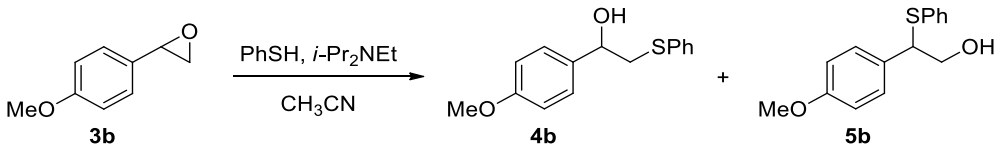

Alcohols 4b and 5b. To a solution of epoxide **3b**[12] (154 mg, 1.03 mmol) in acetonitrile (1.0 mL) was added *i*-Pr_2NEt (9 μL, 0.05 mmol) and thiophenol (102 μL, 1.00 mmol). This mixture was kept under nitrogen at room temperature for 40 h and then was concentrated in vacuo. Silica gel chromatography (EtOAc–Hexanes, 8 : 92 to 60 : 40) afforded 84 mg (32%) of **4b** and 98 mg (38%) of **5b** as colorless viscous oils.

Alcohol 4b. R_f = 0.33 (EtOAc–Hexanes, 33 : 67). ^{1}H NMR (300 MHz, $CDCl_3$) δ 7.41–7.37 (m, 2H), 7.32–7.18 (m, 5H), 6.89–6.84 (m, 2H), 4.67 (ddd, *J* = 3.3, 5.7, 9.0 Hz, 1H), 3.78 (s, 3H), 3.27 (dd, *J* = 3.9, 13.5 Hz, 1H), 3.08 (dd, *J* = 9.0, 13.8 Hz, 1H), 2.86 (d, *J* = 2.4 Hz, 1H); ^{13}C NMR (75 MHz, $CDCl_3$) δ 159.3, 135.0, 134.2, 130.0, 129.0, 127.1, 126.6, 113.9, 71.3 (CH), 55.2 (CH_3), 43.7 (CH_2). HRMS (ESI) calcd for $[C_{15}H_{16}O_2S + Na]^+$ 283.0769, found 283.0781.

Alcohol 5b. R_f = 0.23 (EtOAc–Hexanes, 33 : 67). ^{1}H NMR (300 MHz, $CDCl_3$) δ 7.35–7.29 (m, 2H), 7.27–7.18 (m, 5H), 6.86–6.81 (m, 2H), 4.27 (t, *J* = 6.9 Hz, 1H) , 3.85 (app

dt, J = 2.1, 6.6 Hz, 2H), 3.76 (s, 3H), 2.18 (t, J = 6.5 Hz, 1H); ^{13}C NMR (126 MHz, $CDCl_3$) δ 159.1, 133.7, 132.5, 130.7, 129.1, 128.9, 127.5, 114.1, 65.2, 55.3, 55.2. HRMS (ESI) calcd for $[C_{15}H_{16}O_2S + Na]^+$ 283.0769, found 283.0755.

Kinetics for the reaction of styrene oxides with thiophenol in the presence of a base and a hydrogen bond catalyst.

General details for epoxide ring-opening reactions. Stock solutions of styrene oxide (**3a** or **b**) and thiophenol in toluene-d_8 (both *ca.* 0.50 M) were prepared and an aliquot was added to the solid catalysts in a screw-capped 1 dram vial. The mixture was heated till the catalysts were dissolved (no reaction occurred during this operation as confirmed by ^{1}H NMR), except for entries 2, 5 and 6 in which **1a** and **2a** were soluble at room temperature. After a rapid cooling to ambient temperature with cold water, the base was added with a microliter syringe. After shaking, the solutions were transferred into NMR tubes, the head space was flushed with nitrogen for 30 seconds and the reactions were followed by ^{1}H NMR at 23 ± 1 °C (ambient temperature). It should be noted that slight variations in ambient temperature have little effect on the reaction rate since we found that at 0 °C the reaction is only *ca*. 20 % slower.

Table S1. Two pathways of the ring-opening reaction of styrene oxides with thiophenol: rates and relative rates of triol (k_1) vs. diol (k_2) catalyzed reactions.[a]

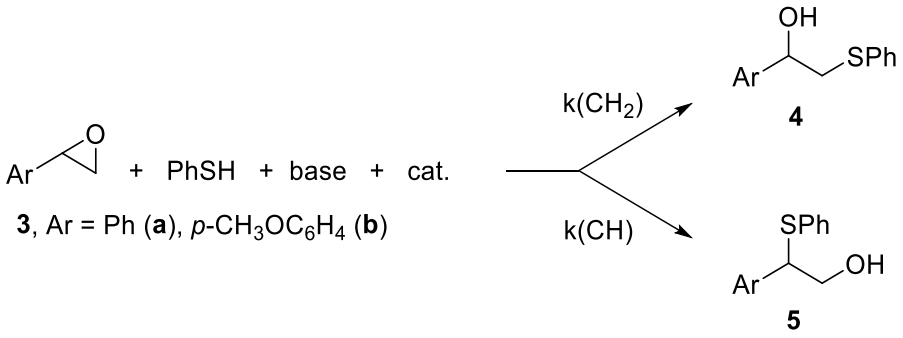

Entry	Styrene oxide	Catalyst	$k(CH_2)$[b]	**k_1/k_2 (CH_2)[c]**	$k(CH)$[b]	**k_1/k_2 (CH)[c]**
1	**3a**	**1,2a**	$k_1 = 7.73 \cdot 10^{-2}$ $k_2 = 1.85 \cdot 10^{-2}$ $k_0 = 5.3 \cdot 10^{-4}$	**4.2 (4.3)**	$k_1 = 1.29 \cdot 10^{-1}$ $k_2 = 1.71 \cdot 10^{-2}$ $k_0 = 2.2 \cdot 10^{-4}$	**7.6 (7.6)**
2	**3a**	**1,2a**	$k_1 = 1.72 \cdot 10^{-2}$ $k_2 = 5.36 \cdot 10^{-3}$ $k_0 = 5.3 \cdot 10^{-4}$	**3.2 (3.5)**	$k_1 = 1.91 \cdot 10^{-2}$ $k_2 = 3.61 \cdot 10^{-3}$ $k_0 = 2.2 \cdot 10^{-4}$	**5.3 (5.6)**
3	**3a**	**1,2b**	$k_1 = 2.96 \cdot 10^{-2}$ $k_2 = 4.78 \cdot 10^{-3}$ $k_0 = 5.3 \cdot 10^{-4}$	**6.2 (6.8)**	$k_1 = 3.05 \cdot 10^{-2}$ $k_2 = 3.29 \cdot 10^{-3}$ $k_0 = 2.2 \cdot 10^{-4}$	**9.3 (9.9)**
4	**3b**	**1,2b**	$k_1 = 3.61 \cdot 10^{-2}$ $k_2 = 5.84 \cdot 10^{-3}$ $k_0 = 9.1 \cdot 10^{-4}$	**6.2 (7.1)**	$k_1 = 2.09 \cdot 10^{-1}$ $k_2 = 1.78 \cdot 10^{-2}$ $k_0 = 1.1 \cdot 10^{-3}$	**11.8 (12.5)**
5	**3b**	**1,2b**	$k_1 = 1.04 \cdot 10^{-2}$ $k_2 = 2.09 \cdot 10^{-3}$ $k_0 = 9.1 \cdot 10^{-4}$	**5.0 (8.1)**	$k_1 = 4.36 \cdot 10^{-2}$ $k_2 = 4.48 \cdot 10^{-3}$ $k_0 = 1.1 \cdot 10^{-3}$	**9.7 (12.6)**
6	**3b**	**1,2b**	nd[d]	–	$k_1 = 2.1 \cdot 10^{-2}$ $k_2 = 2.7 \cdot 10^{-3}$ $k_0 = 1.1 \cdot 10^{-3}$	**7.8 (12.4)**
7	**3b**	**1,2b**	$k_1 = 5.3 \cdot 10^{-2}$ $k_2 = 8.0 \cdot 10^{-3}$ $k_0 = 1.7 \cdot 10^{-3}$	**6.6 (8.1)**	$k_1 = 3.1 \cdot 10^{-1}$ $k_2 = 2.3 \cdot 10^{-2}$ $k_0 = 1.9 \cdot 10^{-3}$	**13.5 (14.6)**
8	**3b**	**1,2b**	nd	–	$k_1 = 6.5 \cdot 10^{-2}$ $k_2 = 6.2 \times 10^{-3}$ $k_0 = 5.3 \cdot 10^{-4}$	**10.4 (11.3)**
9	**3b**	**1,2b**	$k_1 = 2.51 \cdot 10^{-2}$ $k_2 = 4.93 \cdot 10^{-3}$ $k_0 = 1.1 \cdot 10^{-3}$	**5.1 (6.3)**	$k_1 = 1.59 \cdot 10^{-1}$ $k_2 = 1.91 \cdot 10^{-2}$ $k_0 = 1.7 \cdot 10^{-3}$	**8.3 (9.0)**

[a] Conditions: styrene oxide (0.5M), thiophenol (0.5 M), base and catalyst (5 mol % all entries except 1.7 mol % in entries 2 and 5, and 0.83 mol % in entry 6) all in toluene-d_8. Base = *i*-Pr_2NEt (0.122

M in entries 1-6, 0.240 M in entry 7, 0.040 M in entry 8), 1,2,2,6,6-pentamethylpiperidine (PMP, 0.050 M, entry 9). [b] Second-order rate constants (M^{-1} h^{-1}): k_1 is for the triol catalyzed reaction (i.e., **1**), k_2 is for the diol (**2**) process and k_0 corresponds to the non-catalyzed background reaction. [c] Triol/diol relative catalytic rates, numbers in brackets are background corrected (i.e., $(k_1–k_0)/(k_2–k_0)$). [d] nd = not determined.

Second order kinetics analysis was applied: $k_{overall}t = 1/[\mathbf{3}] – 1/[\mathbf{3}]_0 = ([\mathbf{3}]_0 – [\mathbf{3}])/[\mathbf{3}][\mathbf{3}]_0 = ([\mathbf{4}] + [\mathbf{5}])/ [\mathbf{3}][\mathbf{3}]_0$ or since $[\mathbf{3}]_0 = 0.5$ M and $k_{overall} = k(CH_2) + k(CH)$ this breaks into two equations for each reaction pathway: $0.5k(CH_2)t = [\mathbf{4}]/[\mathbf{3}]$ and $0.5k(CH)t = [\mathbf{5}]/[\mathbf{3}]$. The [**4**]/[**3**] and [**5**]/[**3**] ratios were determined from the normalized signal intensities of the products and the starting material by ^{1}H NMR. The following signals were used for this purpose: **3a**, 2.57 ppm (dd, *J* = 4.0, 5.5 Hz, 1H); **4a**, 4.50 ppm (dd, *J* = 4.0, 9.0 Hz, 1H); **5a**, 4.11 ppm (t, *J* = 7.0 ppm, 1H);[13] **3b**, 2.63 ppm (dd, *J* = 4.0, 6.0 Hz, 1H); **4b**, 4.54 ppm (dd, *J* = 4.0, 8.5 Hz, 1H); **5b**, 4.15 ppm (t, *J* = 7.0 Hz, 1H). The second-order reaction rates were determined from the plots of [**4**]/[**3**] and [**5**]/[**3**] versus time where the slopes are $0.5k(CH_2)$ and $0.5k(CH)$, respectively. The reported uncertainties correspond to the statistical errors of the linear least squares fits. Entry 4 (Table S1) was repeated to check the reproducibility of the data and gave the same results.

Entry 1 (Table S1). Thiophenol (154 μL, 1.50 mmol) was added to **3a** (freshly distilled, 180 mg, 1.50 mmol) in 2.67 mL of toluene-d_8. Triol **1a** (8.9 mg, 0.025 mmol) and diol **2a** (6.4 mg, 0.025 mmol) were each dissolved in 1.00 mL portions of this solution by heating them in 1 dram screw-capped vials. After cooling to ambient temperature, *i*-Pr_2NEt (22 μL, 0.125 mmol) was added to each vial and the contents were mixed by shaking before being transferred into a series of NMR tubes. The head space in each tube was flushed with nitrogen, and the reactions were followed by ^{1}H NMR at 23 ± 1 °C (Table S2). Rate

constants obtained from linear least squares analyses (Figure S1) are: $k_1(CH_2)$ = (7.73 ± 0.15) • 10^{-2} M^{-1} h^{-1} and $k_2(CH_2)$ = (1.85 ± 0.04) • 10^{-2} M^{-1} h^{-1} (triol/diol relative rate is 4.2 ± 0.1); $k_1(CH)$ = (1.29 ± 0.05) • 10^{-1} M^{-1} h^{-1} and $k_2(CH)$ = (1.71 ± 0.05) • 10^{-2} M^{-1} h^{-1} (triol/diol relative rate is 7.6 ± 0.3).

Table S2. Second-order kinetic data for the reaction of styrene oxide (**3a**) with thiophenol in the presence of i-Pr_2NEt and 5 mol % of triol **1a** or diol **2a**.

Entry	Triol **1a** catalyzed			Diol **2a** catalyzed		
	Time (h)	[**4a**]/[**3a**]	[**5a**]/[**3a**]	Time (h)	[**4a**]/[**3a**]	[**5a**]/[**3a**]
1	1.35	0.0436	0.0740	1.37	0.0116	0.0108
2	2.85	0.0958	0.157	2.90	0.0243	0.0226
3	5.68	0.205	0.334	5.71	0.0499	0.0461
4	8.08	0.303	0.510	8.12	0.0739	0.0685

Figure S1. Linear least squares fits of the kinetic data given in Table S2. Triol **1a** catalyzed reaction (left) and diol **2a** catalyzed reaction (right).

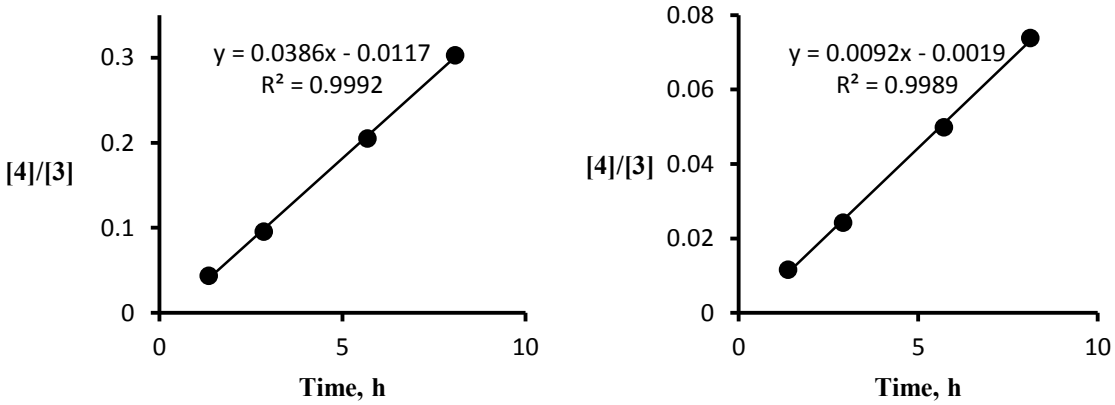

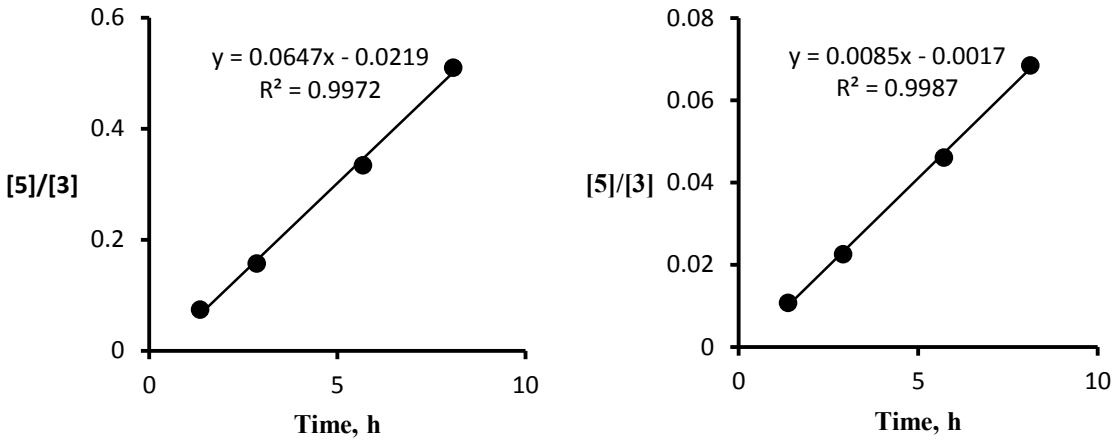

Entry 2 (Table S1). Thiophenol (154 μL, 1.50 mmol) was added to **3a** (freshly distilled, 180 mg, 1.50 mmol) in 1.77 mL of toluene-d_8. 0.70 mL portions of this solution were added to the solutions of triol **1a** and diol **2a** in toluene-d_8 (both 0.30 mL, 0.083 mmol). *i*-Pr_2NEt (22 μL, 0.125 mmol) was added to each vial and the contents were mixed by shaking before being transferred into a series of NMR tubes. The head space in each tube was flushed with nitrogen, and the reactions were followed by ^1H NMR at 23 ± 1 °C (Table S3). Rate

Table S3. Second-order kinetic data for the reaction of styrene oxide (**3a**) with thiophenol in the presence of i-Pr_2NEt and 1.7 mol % of triol **1a** or diol **2a**.

Entry	Triol **1a** catalyzed			Diol **2a** catalyzed		
	Time (h)	[**4a**]/[**3a**]	[**5a**]/[**3a**]	Time (h)	[**4a**]/[**3a**]	[**5a**]/[**3a**]
1	2.13	nd	0.0136	2.25	nd	0.0030
2	6.30	0.0431	0.0444	6.40	0.0169	0.0091
3	23.85	0.179	0.199	23.92	0.0625	0.0388
4	48.25	0.403	0.452	48.28	0.129	0.0859

constants obtained from linear least squares analyses (Figure S2) are: $k_1(CH_2)$ = (1.72 ± 0.05) • 10^{-2} M^{-1} h^{-1} and $k_2(CH_2)$ = (5.36 ± 0.07) • 10^{-3} M^{-1} h^{-1} (triol/diol relative rate is 3.2 ± 0.1); $k_1(CH)$ = (1.91 ± 0.07) • 10^{-2} M^{-1} h^{-1} and $k_2(CH)$ = (3.61 ± 0.10) • 10^{-3} M^{-1} h^{-1} (triol/diol relative rate is 5.3 ± 0.2).

Figure S2. Linear least squares fits of the kinetic data given in Table S3. Triol **1a** catalyzed reaction (left) and diol **2a** catalyzed reaction (right).

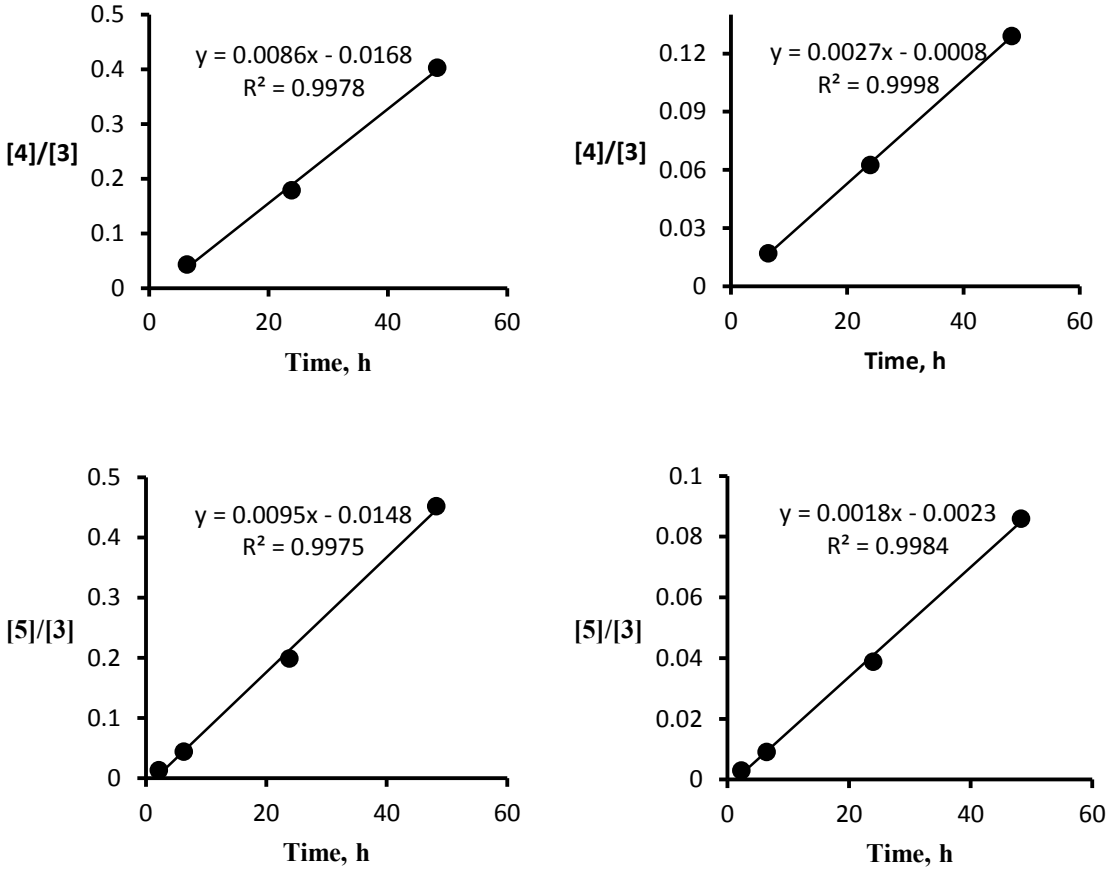

Entry 3 (Table S1). Thiophenol (154 μL, 1.50 mmol) was added to **3a** (freshly distilled, 180 mg, 1.50 mmol) in 2.67 mL of toluene-d_8. Triol **1b** (12.6 mg, 0.025 mmol) and diol **2b** (9.1 mg, 0.025 mmol) were each dissolved in 1.00 mL portions of this solution by heating them in 1 dram screw-capped vials. The remaining stock solution was used for monitoring the background reaction. After cooling to ambient temperature, *i*-Pr_2NEt (22 μL, 0.125 mmol) was added to each vial and the contents were mixed by shaking before being transferred into a series of NMR tubes. The head space in each tube was flushed with nitrogen, and the reactions were followed by ^1H NMR at 23 ± 1 °C (Table S4). Rate

Table S4. Second-order kinetic data for the reaction of styrene oxide (**3a**) with thiophenol in the presence of i-Pr_2NEt and triol **1b** or diol **2b**.

Entry	Triol **1b** catalyzed			Diol **2b** catalyzed		
	Time (h)	[**4a**]/[**3a**]	[**5a**]/[**3a**]	Time (h)	[**4a**]/[**3a**]	[**5a**]/[**3a**]
1	3.69	0.0498	0.0552	3.80	0.00765	0.00604
2	7.68	0.107	0.118	7.75	0.0164	0.0111
3	30.15	0.422	0.451	30.25	0.0639	0.0440
4	54.95	0.790	0.827	55.00	0.126	0.0873
5	73.0	1.08	1.12	73.02	0.174	0.120

constants obtained from linear least squares analyses (Figure S3) are: $k_1(CH_2) = (2.96 \pm 0.04) \cdot 10^{-2}$ M^{-1} h^{-1} and $k_2(CH_2) = (4.78 \pm 0.13) \cdot 10^{-3}$ M^{-1} h^{-1} (triol/diol relative rate is 6.2 ± 0.2); $k_1(CH) = (3.05 \pm 0.03) \cdot 10^{-2}$ M^{-1} h^{-1} and $k_2(CH) = (3.29 \pm 0.09) \cdot 10^{-3}$ M^{-1} h^{-1} (triol/diol relative rate is 9.3 ± 0.3). One point was recorded for the background reaction:

time = 73.1 h, [**4**]/[**3**] = 0.0192 and [**5**]/[**3**] = 0.00791. This gives $k_0(CH_2) = 5.3 \bullet 10^{-4}$ M^{-1} h^{-1} and $k_0(CH) = 2.2 \bullet 10^{-4}$ M^{-1} h^{-1}.

Figure S3. Linear least squares fits of the kinetic data given in Table S4. Triol **1b** catalyzed reaction (left) and diol **2b** catalyzed reaction (right).

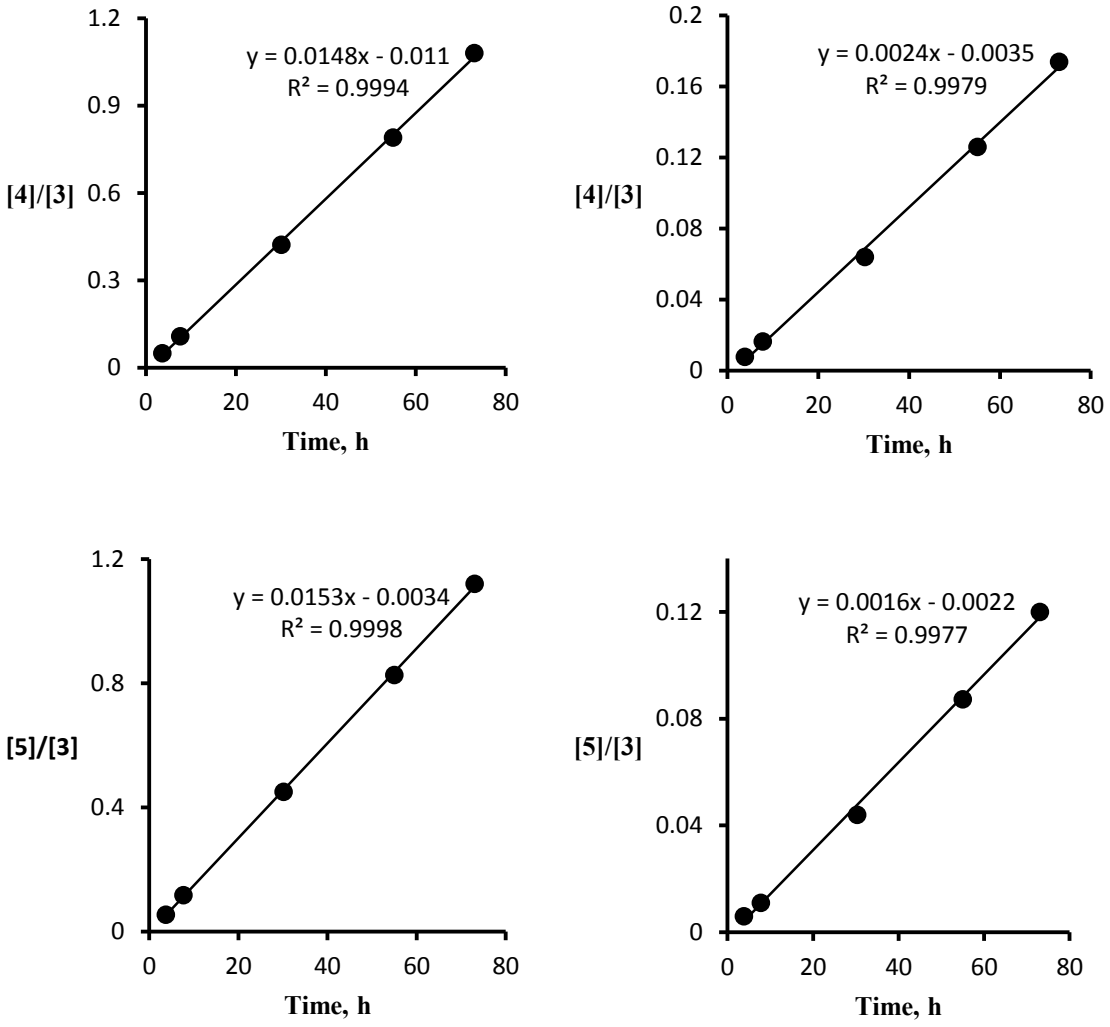

Entry 4 (Table S1). Thiophenol (154 μL, 1.50 mmol) was added to **3b** (225 mg, 1.50 mmol) in 2.63 mL toluene-d_8. Triol **1b** (12.6 mg, 0.025 mmol) and diol **2b** (9.1 mg, 0.025 mmol) were each dissolved in 1.00 mL portions of this solution by heating them in 1 dram screw-capped vials. The remaining stock solution was used for monitoring the background reaction. After cooling to ambient temperature, *i*-Pr_2NEt (22 μL, 0.125 mmol) was added to each vial and the contents were mixed by shaking before being transferred into a series of NMR tubes. The head space in each tube was flushed with nitrogen, and the reactions were followed by ^1H NMR at 23 ± 1 °C (Table S5). Single point second order analysis

Table S5. Second-order kinetic data for the reaction of p-methoxystyrene oxide (**3b**) with thiophenol in the presence of i-Pr_2NEt (0.122 M) and 5 mol % of triol **1b** or diol **2b**.

Entry	Triol **1b** catalyzed			Diol **2b** catalyzed		
	Time (h)	[**4b**]/[**3b**]	[**5b**]/[**3b**]	Time (h)	[**4b**]/[**3b**]	[**5b**]/[**3b**]
1	0.97	0.0173	0.111	1.05	nd	0.00867
2	2.00	0.0341	0.220	3.05	0.00816	0.0249
3	2.98	0.0475	0.326	5.42	0.0148	0.0454
4	3.95	0.0665	0.428	7.72	0.0218	0.0680
5	5.30	0.0906	0.556	23.76	0.0719	0.242
6	7.63	0.133	0.814	30.38	0.0948	0.316
7	23.85	0.428	2.50			

showed that the diol catalyzed reaction was accelerating after 4 h, so only entries 1-4 were used for the analysis. Rate constants obtained from linear least squares analyses (Figure S4) are: $k_1(CH_2) = (3.61 \pm 0.02) \cdot 10^{-2}$ M^{-1} h^{-1} and $k_2(CH_2) = (5.84 \pm 0.14) \cdot 10^{-3}$ M^{-1} h^{-1}

(triol/diol relative rate is 6.2 ± 0.2); $k_1(CH) = (2.09 \pm 0.01) \cdot 10^{-1}$ M^{-1} h^{-1} and $k_2(CH) = (1.78 \pm 0.05) \cdot 10^{-2}$ M^{-1} h^{-1} (triol/diol relative rate is 11.8 ± 0.4). Two points were recorded

Figure S4. Linear least squares fits of the kinetic data given in Table S5. Triol **1b** catalyzed reaction (left) and diol **2b** catalyzed reaction (right).

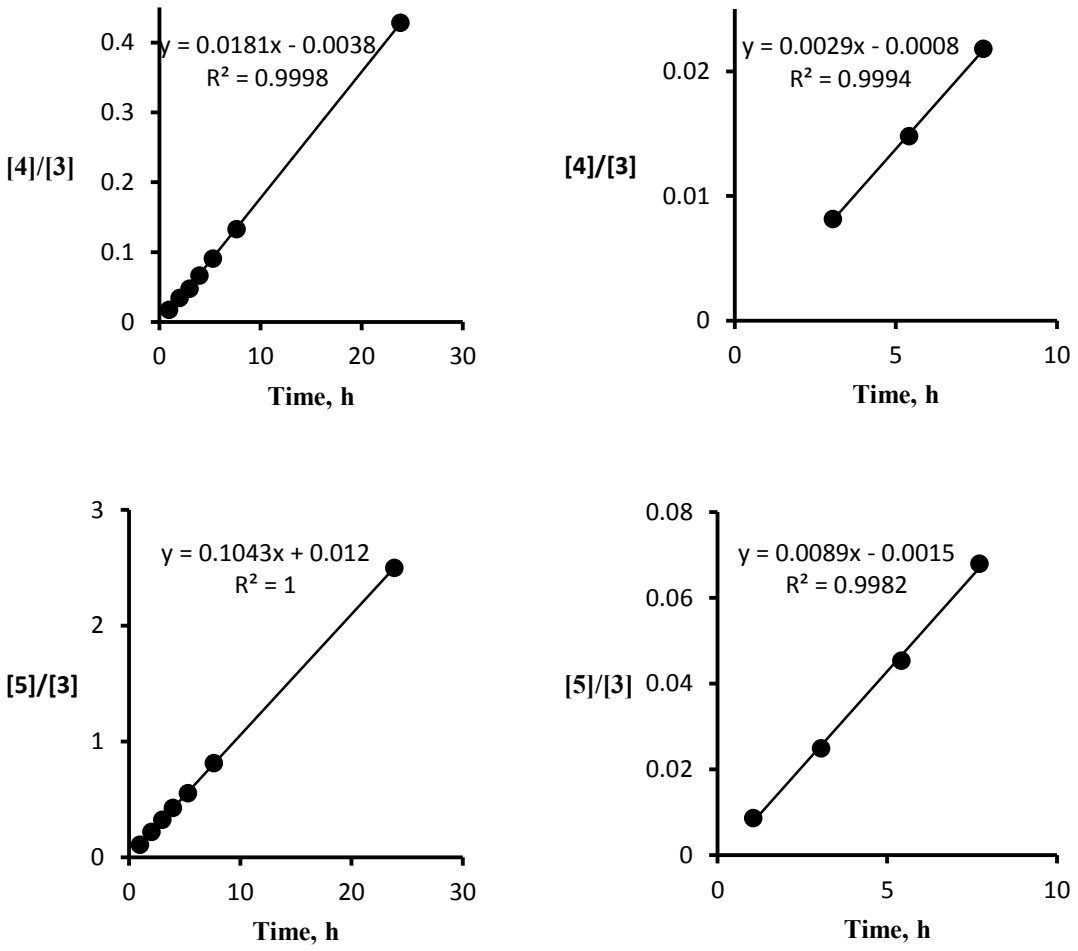

for the background reaction: time = 7.45 h, [**4**]/[**3**] = 0.0035 and [**5**]/[**3**] = 0.0046, this gives $k_0(CH_2) = 9.4 \cdot 10^{-4}$ M^{-1} h^{-1} and $k_0(CH) = 1.2 \cdot 10^{-3}$ M^{-1} h^{-1}; time = 26.05 h, [**4**]/[**3**] = 0.0116

and [**5**]/[**3**] = 0.0148, this gives $k_0(CH_2) = 8.9 \cdot 10^{-4}$ M^{-1} h^{-1} and $k_0(CH) = 1.1 \cdot 10^{-3}$ $M^{-1}h^{-1}$; average – $k_0(CH_2) = 9.1 \cdot 10^{-4}$ M^{-1} h^{-1} and $k_0(CH) = 1.1 \cdot 10^{-3}$ M^{-1} h^{-1}.

Entry 4 repeated (Table S1). To check the reproducibility of the results, entry 4 was repeated. New batches of hydrogen-bonding catalysts were used (triol **1b** was purified by both silica gel chromatography and recrystallization from toluene) and a different commercial source of thiophenol (Acros) was used. Data are reported in Table S6. Single

Table S6. Second-order kinetic data for the reaction of p-methoxystyrene oxide (**3b**) with thiophenol in the presence of i-Pr_2NEt (0.122 M) and 5 mol % of triol **1b** or diol **2b**.

Entry	Triol **1b** catalyzed			Diol **2b** catalyzed		
	Time (h)	[**4b**]/[**3b**]	[**5b**]/[**3b**]	Time (h)	[**4b**]/[**3b**]	[**5b**]/[**3b**]
1	1.79	0.0265	0.182	1.87	nd	0.0153
2	2.77	0.0427	0.283	2.84	0.0081	0.0236
3	4.76	0.0766	0.483	4.82	0.0134	0.0402
4	7.09	0.116	0.710	7.16	0.0205	0.0621
5	9.23	0.155	0.927	9.29	0.0268	0.0817
6	23.84	0.424	2.453	23.86	0.0763	0.239

point second order analysis showed that the diol catalyzed reaction was significantly speeding up after entry 5, so only entries 1-5 were used in the plots. Rate constants obtained from linear least squares analyses (Figure S5) are: $k_1(CH_2) = (3.62 \pm 0.03) \cdot 10^{-2}$ M^{-1} h^{-1} and $k_2(CH_2) = (5.83 \pm 0.10) \cdot 10^{-3}$ M^{-1} h^{-1} (triol/diol relative rate is 6.2 ± 0.1); $k_1(CH) = (2.06 \pm 0.01) \cdot 10^{-1}$ M^{-1} h^{-1} and $k_2(CH) = (1.79 \pm 0.02) \cdot 10^{-2}$ M^{-1} h^{-1} (triol/diol relative rate is 11.5 ± 0.2). Two points were recorded for the background reaction: time = 9.37 h, [**5**]/[**3**]

Figure S5. Linear least squares fits of the kinetic data given in Table S6. Triol **1b** catalyzed reaction (left) and diol **2b** catalyzed reaction (right).

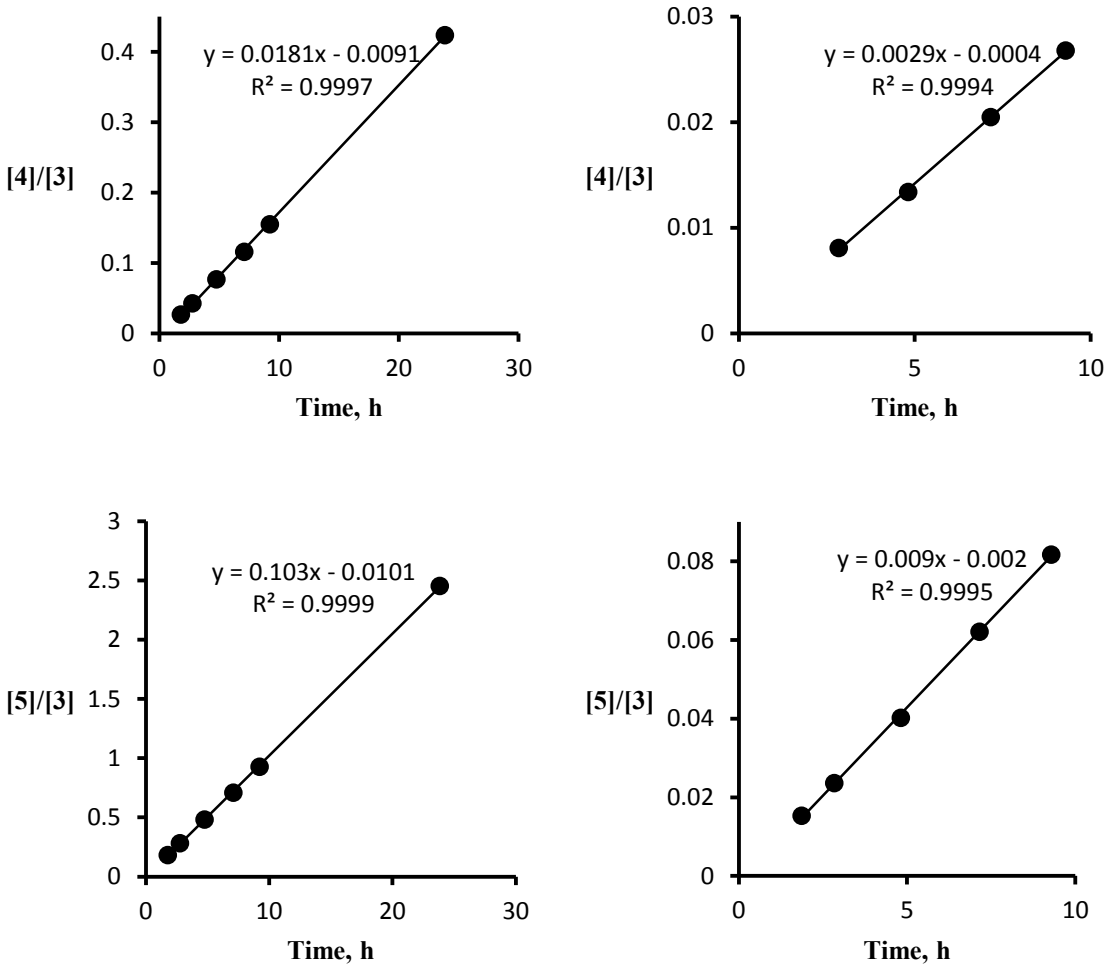

= 0.0054, this gives $k_0(CH) = 1.2 \bullet 10^{-3}$ M^{-1} h^{-1}; time = 23.92 h, [**4**]/[**3**] = 0.0115, [**5**]/[**3**] = 0.0148, this gives $k_0(CH_2) = 9.6 \bullet 10^{-4}$ M^{-1} h^{-1} and $k_0(CH) = 1.2 \bullet 10^{-3}$ M^{-1} h^{-1}; average – $k_0(CH_2) = 9.6 \bullet 10^{-4}$ M^{-1} h^{-1} and $k_0(CH) = 1.2 \bullet 10^{-3}$ M^{-1} h^{-1}. Note: although the rate constants calculated by linear regressions perfectly match for both experiments, single point analyses gave slightly different values (up to 7% deviation).

Entry 5 (Table S1). Thiophenol (154 μL, 1.50 mmol) was added to **3b** (225 mg, 1.50 mmol) in 1.73 mL of toluene-d_8. 0.70 mL of this solution was added to solutions of triol **1b** and diol **2b** (both 0.30 mL, 0.083 mmol). *i*-Pr_2NEt (22 μL, 0.125 mmol) was added to each vial and the contents were mixed by shaking before being transferred into a series of NMR tubes. The head space in each tube was flushed with nitrogen, and the reactions were followed by ^1H NMR at 23 ± 1 °C (Table S7). Rate constants obtained from linear least squares analyses (Figure S6) are: $k_1(CH_2) = (1.04 \pm 0.04) \cdot 10^{-2}$ M^{-1} h^{-1} and $k_2(CH_2) = (2.09 \pm 0.05) \cdot 10^{-3}$ M^{-1} h^{-1} (triol/diol relative rate is 5.0 ± 0.1); $k_1(CH) = (4.36 \pm 0.01) \cdot 10^{-2}$ M^{-1} h^{-1} and $k_2(CH) = (4.48 \pm 0.08) \cdot 10^{-3}$ M^{-1} h^{-1} (triol/diol relative rate is 9.7 ± 0.2).

Table S7. Second-order kinetic data for the reaction of p-methoxystyrene oxide (**3b**) with thiophenol in the presence of i-Pr_2NEt (0.122 M) and 1.7 mol % of triol **1b** or diol **2b**.

Entry	Triol **1b** catalyzed			Diol **2b** catalyzed		
	Time (h)	[**4b**]/[**3b**]	[**5b**]/[**3b**]	Time (h)	[**4b**]/[**3b**]	[**5b**]/[**3b**]
1	3.19	0.0169	0.0695	3.26	0.0038	0.0064
2	6.30	0.0335	0.139	6.36	0.0065	0.0125
3	24.0	0.125	0.524	24.03	0.0253	0.0526

Figure S6. Linear least squares fits of the kinetic data given in Table S7. Triol **1b** catalyzed reaction (left) and diol **2b** catalyzed reaction (right).

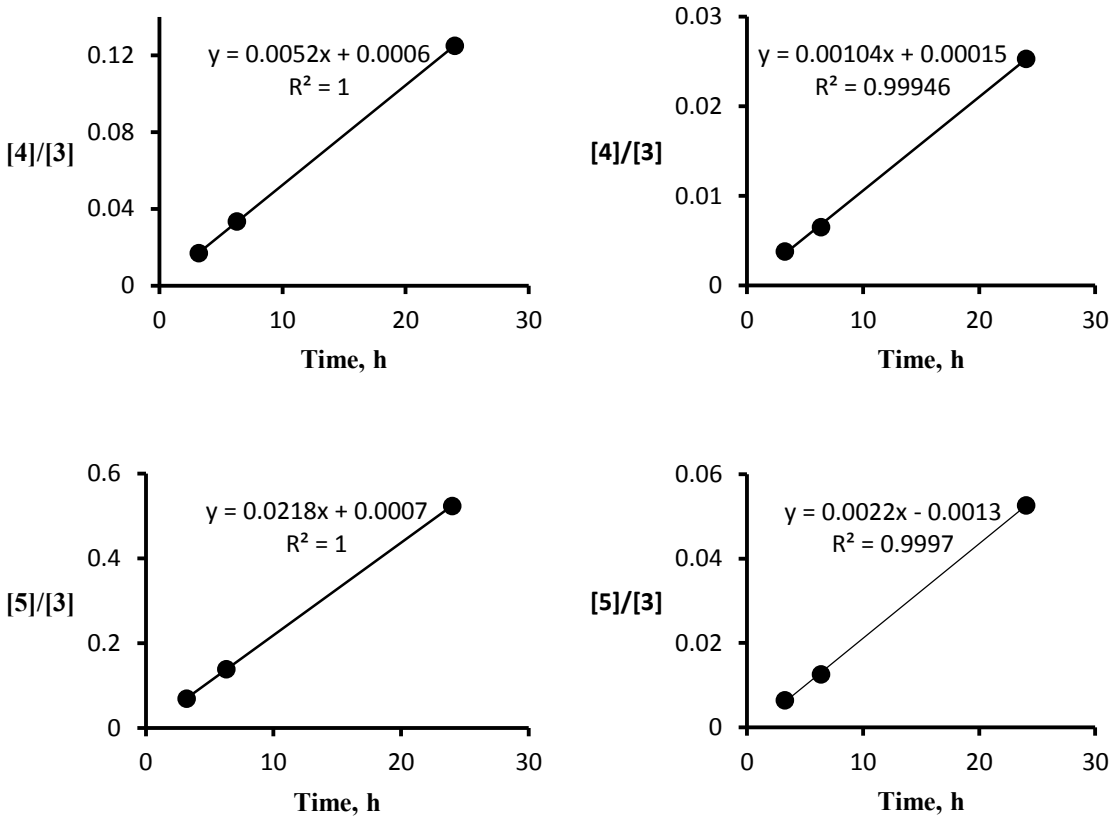

Entry 6 (Table S1). Thiophenol (154 μL, 1.50 mmol) was added to **3b** (225 mg, 1.50 mmol) in 2.18 mL of toluene-d_8. 0.85 mL portions of this solution were added to the solutions of triol **1b** and diol **2b** in toluene-d_8 (both 0.15 mL, 0.042 mmol). *i*-Pr_2NEt (22 μL, 0.125 mmol) was added to each vial and the contents were mixed by shaking before being transferred into a series of NMR tubes. The head space in each tube was flushed with nitrogen, and the reactions were followed by ^1H NMR at 23 ± 1 °C (Table S8). Single point second order analysis for entry 3 compared to entries 1-2 indicated that the triol catalyzed

reaction became *ca.* 20–25% faster and that the diol catalyzed process increased in speed by *ca.* 40-50%. Linear analyses for entries 1-2 provides: $k_1(CH) = 2.1 \bullet 10^{-2}$ M^{-1} h^{-1} and $k_2(CH) = 2.7 \bullet 10^{-3}$ M^{-1} h^{-1} (triol/diol relative rate is 7.8).

Table S8. Second-order kinetic data for the reaction of p-methoxystyrene oxide (**3b**) with thiophenol in the presence of i-Pr_2NEt (0.122 M) and 0.83 mol % of triol **1b** or diol **2b**.

Entry	Triol **1b** catalyzed		Diol **2b** catalyzed	
	Time (h)	[**5b**]/[**3b**]	Time (h)	[**5b**]/[**3b**]
1	6.12	0.055	6.20	0.0075
2	23.77	0.240	23.84	0.0312
3	95.9	1.17	95.75	0.182

Entry 7 (Table S1). Thiophenol (154 μL, 1.50 mmol) was added to **3b** (225 mg, 1.50 mmol) in 2.63 mL of toluene-d_8. Triol **1b** (12.6 mg, 0.025 mmol) and diol **2b** (9.1 mg, 0.025 mmol) were each dissolved in 1.00 mL portions of this solution by heating them in 1 dram screw-capped vials. The remaining stock solution was used for monitoring the background reaction. After cooling to ambient temperature, *i*-Pr_2NEt (43 μL, 0.250 mmol) was added to each vial and the contents were mixed by shaking before being transferred into a series of NMR tubes. The head space in each tube was flushed with nitrogen, and the reactions were followed by ^{1}H NMR at 23 ± 1 °C (Table S9). Linear analyses for entries 1-2 provides: $k_1(CH_2) = 5.3 \bullet 10^{-2}$ M^{-1} h^{-1} and $k_2(CH_2) = 8.0 \bullet 10^{-3}$ M^{-1} h^{-1} (triol/diol relative rate is 6.6); $k_1(CH) = 3.1 \bullet 10^{-1}$ M^{-1} h^{-1} and $k_2(CH) = 2.3 \bullet 10^{-2}$ M^{-1} h^{-1} (triol/diol relative rate is 13.5). One point was recorded for the background reaction: time = 24.5 h, [**4**]/[**3**] =

0.0208 and [**5**]/[**3**] = 0.0233. This gives $k_0(CH_2) = 1.7 \cdot 10^{-3}$ $M^{-1} \cdot h^{-1}$ and $k_0(CH) = 1.9 \cdot 10^{-3}$ $M^{-1} \cdot h^{-1}$.

Table S9. Second-order kinetic data for the reaction of p-methoxystyrene oxide (**3b**) with thiophenol in the presence of i-Pr_2NEt (0.240 M) and 5 mol % of triol **1b** or diol **2b**.

Entry	Triol **1b** catalyzed			Diol **2b** catalyzed		
	Time (h)	[**4b**]/[**3b**]	[**5b**]/[**3b**]	Time (h)	[**4b**]/[**3b**]	[**5b**]/[**3b**]
1	1.17	0.0304	0.195	1.27	0.0065	0.0155
2	3.68	0.0975	0.583	3.72	0.0163	0.0432

Entry 8 (Table S1). Thiophenol (154 μL, 1.50 mmol) was added to **3b** (225 mg, 1.50 mmol) in 2.63 mL of toluene-d_8. Triol **1b** (12.6 mg, 0.025 mmol) and diol **2b** (9.1 mg, 0.025 mmol) were each dissolved in 1.00 mL portions of this solution by heating them in 1 dram screw-capped vials. The remaining stock solution was used for monitoring the background reaction. After cooling to ambient temperature, *i*-Pr_2NEt (7.0 μL, 0.040 mmol) was added to each vial and the contents were mixed by shaking before being transferred into a series of NMR tubes. The head space in each tube was flushed with nitrogen, and the reactions were followed by ^{1}H NMR at 23 ± 1 °C (Table S10). Single point second order analysis showed that the diol catalyzed reaction was speeding up for entry 4 by *ca.* 30%, so only entries 1-3 were used in the plots. Rate constants obtained from linear least squares analyses (Figure S7) are: $k_1(CH) = (6.5 \pm 0.1) \cdot 10^{-2}$ M^{-1} h^{-1} and $k_2(CH) = (6.2 \pm 0.1) \cdot 10^{-3}$ M^{-1} h^{-1} (triol/diol relative rate is 10.4 ± 0.2). One point was recorded for the

background reaction: time = 24.0 h, [**5**]/[**3**] = 0.0064. This gives k_0(CH) = 5.3 • 10^{-4} M^{-1} h^{-1}.

Table S10. Second-order kinetic data for the reaction of p-methoxystyrene oxide (**3b**) with thiophenol in the presence of i-Pr_2NEt (0.040 M) and 5 mol % of triol **1b** or diol **2b**.

Entry	Triol **1b** catalyzed			Diol **2b** catalyzed		
	Time (h)	[**4b**]/[**3b**]	[**5b**]/[**3b**]	Time (h)	[**4b**]/[**3b**]	[**5b**]/[**3b**]
1	2.25	0.0139	0.0977	2.28	nd	0.0067
2	4.52	0.0271	0.187	4.37	nd	0.0133
3	6.13	0.0364	0.239	6.19	0.0057	0.0188
4	23.9	0.129	0.806	23.95	0.0394	0.100

Figure S7. Linear least squares fits of the kinetic data given in Table S10. Triol **1b** catalyzed reaction (left) and diol **2b** catalyzed reaction (right).

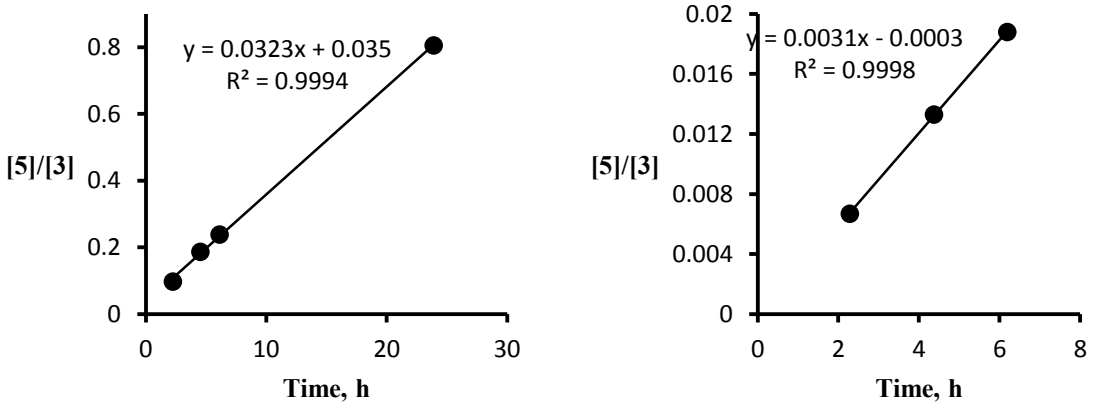

Entry 9 (Table S1). Thiophenol (154 μL, 1.50 mmol) was added to **3b** (225 mg, 1.50 mmol) in 2.63 mL of toluene-d_8. Triol **1b** (12.6 mg, 0.025 mmol) and diol **2b** (9.1 mg,

0.025 mmol) were each dissolved in 1.00 mL portions of this solution by heating them in 1 dram screw-capped vial. The remaining stock solution was used for monitoring the background reaction. After cooling to ambient temperature, PMP (9.0 μL, 0.050 mmol) was added to each vial and the contents were mixed by shaking before being transferred into a series of NMR tubes. The head space in each tube was flushed with nitrogen, and the reactions were followed by ^{1}H NMR at 23 ± 1 °C (Table S11). Rate constants obtained from linear least squares analyses (Figure S8) are: $k_1(CH_2) = (2.51 \pm 0.04) \cdot 10^{-2}$ M^{-1} h^{-1} and $k_2(CH_2) = (4.93 \pm 0.06) \cdot 10^{-3}$ M^{-1} h^{-1} (triol/diol relative rate is 5.1 ± 0.1); $k_1(CH) = (1.59 \pm 0.02) \cdot 10^{-1}$ M^{-1} h^{-1} and $k_2(CH) = (1.91 \pm 0.03) \cdot 10^{-2}$ M^{-1} h^{-1} (triol/diol relative rate is 8.3 ± 0.1). One point was recorded for background reaction: time = 25.15 h, [**4**]/[**3**] = 0.0139 and [**5**]/[**3**] = 0.0213. This gives $k_0(CH_2) = 1.1 \cdot 10^{-3}$ M^{-1} h^{-1} and $k_0(CH) = 1.7 \cdot 10^{-3}$ M^{-1} h^{-1}.

Table S11. Second-order kinetic data for the reaction of p-methoxystyrene oxide (**3b**) with thiophenol in the presence of PMP (0.050 M) and 5 mol % of triol **1b** or diol **2b**.

Entry	Triol **1b** catalyzed			Diol **2b** catalyzed		
	Time (h)	[**4b**]/[**3b**]	[**5b**]/[**3b**]	Time (h)	[**4b**]/[**3b**]	[**5b**]/[**3b**]
1	1.07	0.0143	0.104	1.10	nd	0.0088
2	2.18	0.0287	0.204	2.23	0.0048	0.0177
3	4.22	0.0542	0.380	4.26	0.0091	0.0341
4	6.01	0.0771	0.533	–	–	–
5	25.04	0.315	2.026	25.04	0.0607	0.236

Figure S8. Linear least squares fits of the kinetic data given in Table S11. Triol **1b** catalyzed reaction (left) and diol **2b** catalyzed reaction (right).

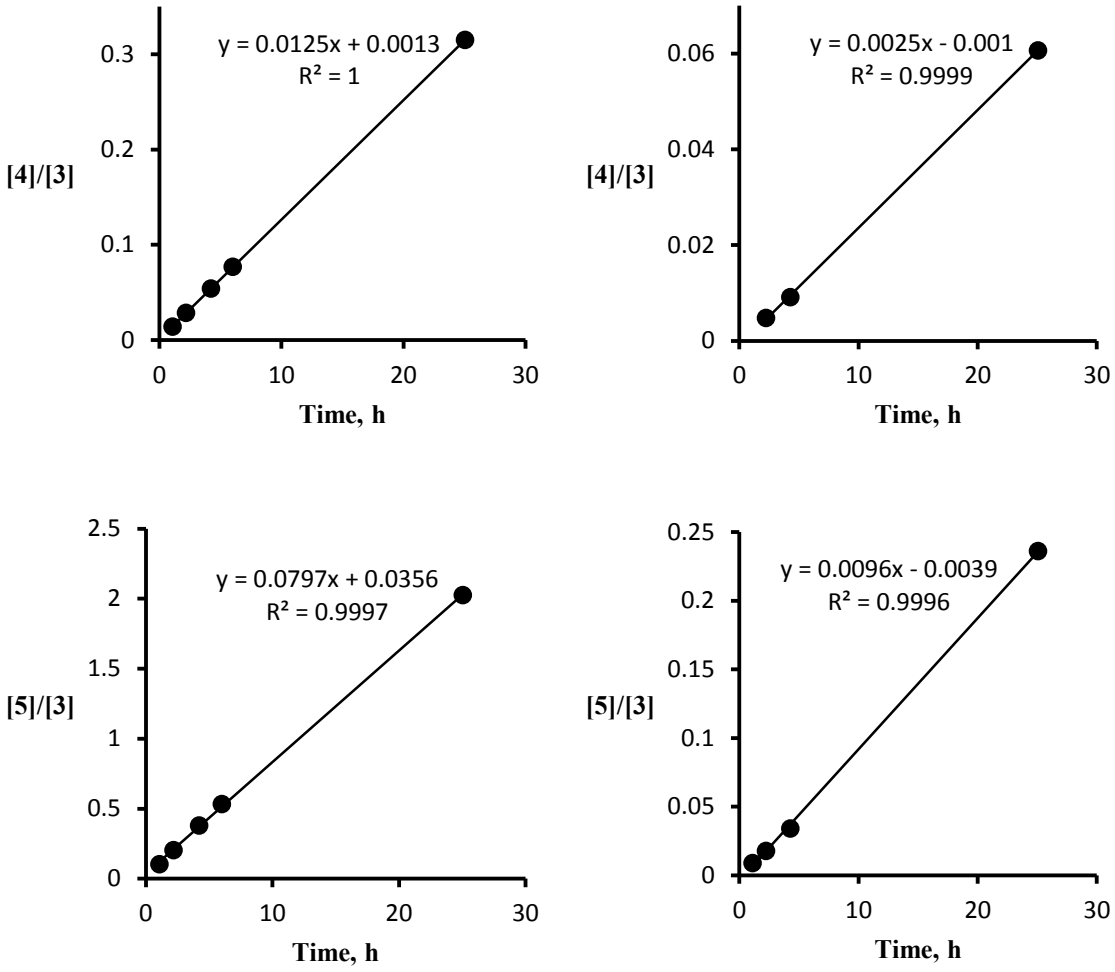

Kinetics for the reaction of aldehydes with nitromethane in the presence of a base and a hydrogen bond catalyst (Henry reaction).

General details for the Henry reaction (Table 2). Reactions were carried out at 23 ± 1 °C with an aldehyde (0.5 M), nitromethane (1.5 M except entry 3 where it was 0.5 M), a

base (0.125 M) and a hydrogen-bonding catalyst (0.025 M) all in toluene-d_8. The reaction progress was monitored by ^{1}H NMR using normalized peak intensities of the starting aldehyde and the resulting product. Second order rate constants were determined from the following equation: $\ln(A/B) - \ln(A_0/B_0) = k(A_0-B_0)t$, where A is the aldehyde concentration and B is the nitromethane concentration. That is, the plot of Y where $Y = (\ln(A/B) - \ln(A_0/B_0))/(A_0 - B_0)$ versus time affords a straight line, and the slope corresponds to the second order rate constant. The reported uncertainties are the statistical errors of the linear least squares fits.

Entry 1 (Table 2). Benzaldehyde (160 mg, 1.51 mmol) and nitromethane (freshly distilled, 280 mg, 4.59 mmol) were mixed in 2.61 mL of toluene-d_8. Triol **1b** (12.6 mg, 0.025 mmol) and diol **2b** (9.1 mg, 0.025 mmol) were each dissolved in 1.00 mL portions of this solution by heating them in 1 dram screw-capped vials. The remaining stock solution was used for monitoring the background reaction. After cooling to ambient temperature, *i*-Pr_2NEt (22 μL, 0.125 mmol) was added to each vial including the one for the background process, the contents were mixed by shaking and transferred into NMR tubes. The head space in each sample was flushed with nitrogen for 30 seconds and the reactions were followed by ^{1}H NMR at 23 ± 1 °C (Table S12). Approximate initial concentrations A_0 = 0.50 M for the aldehyde and B_0 = 1.52 M for nitromethane were used for the calculations. Product resonances at 4.10 ppm (dd, J = 10 Hz, 13 Hz, 1H), 5.07 ppm (dd, J = 3.0 Hz, 10 Hz, 1H) or 3.79 ppm (dd, J = 3.0 Hz, 13 Hz, 1H) depending on the positioning of the broad OH resonance,[14] and the aldehyde signal at 9.70 ppm (s, 1H) were used to determine the yield. Second order kinetic analyses showed that the triol catalyzed reaction slowed down

after 6 h, whereas the diol catalyzed and background processes sped up after 29 h. Entries 1-2 were used obtaining k_1, entries 1-4 for k_2 and entries 1-3 for k_0. Rate constants obtained from the linear least squares analyses (Figure S9) are: $k_1 = (1.2 \pm 0.1) \cdot 10^{-2}$ M^{-1} h^{-1}, $k_2 = (3.05 \pm 0.05) \cdot 10^{-3}$ M^{-1} h^{-1} (triol/diol relative rate is 4.0 ± 0.3) and $k_0 = 4.4 \cdot 10^{-4}$ M^{-1} h^{-1}.

Table S12. Second-order kinetic data for the reaction of benzaldehyde with nitromethane in the presence of i-Pr_2NEt and triol **1b** or diol **2b**.*

Entry	Triol **1b**			Diol **2b**			No catalysis		
	T (h)	% y	Y, M^{-1}	T (h)	% y	Y, M^{-1}	T (h)	% y	Y, M^{-1}
1	3.07	5.29	0.03607	3.10	1.17	0.00776	6.15	0.36	0.00237
2	6.07	10.34	0.07308	6.09	2.39	0.1598	22.12	1.38	0.0916
3	22.05	30.58	0.2539	22.07	9.12	0.06389	29.15	1.87	0.01246
4	29.08	36.14	0.3156	29.1	12.18	0.08725	46.0	3.22	0.02165
5	45.9	47.54	0.4657	45.95	19.86	0.1508	-	-	-
6	69.7	54.81	0.5838	69.7	29.81	0.2458	-	-	-

* % y = % yield

Figure S9. Linear least squares fits of the kinetic data given in Table S12. Triol **1b** catalyzed (left), diol **2b** catalyzed (middle) and non-catalyzed (right) processes.

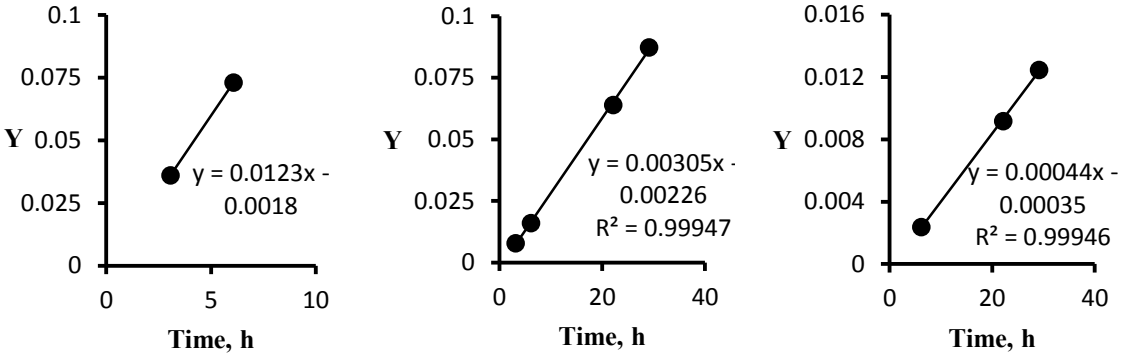

Entry 2 (Table 2). Benzaldehyde (161 mg, 1.52 mmol) and nitromethane (freshly distilled, 279 mg, 4.57 mmol) were mixed in 2.61 mL of toluene-d_8. Triol **1b** (12.6 mg, 0.025 mmol) and diol **2b** (9.1 mg, 0.025 mmol) were each dissolved in 1.00 mL portions of this solution by heating them in 1 dram screw-capped vials. The remaining stock solution was used for monitoring the background reaction. After cooling to ambient temperature, PMP (23 μL, 0.125 mmol) was added to each vial including the one for the background process, the contents were mixed by shaking and transferred into NMR tubes. The head space in each sample was flushed with nitrogen for 30 seconds and the reactions were followed by ^{1}H NMR at 23 ± 1 °C (Table S13). Approximate initial concentrations A_0 = 0.51 M for the aldehyde and B_0 = 1.52 M for nitromethane were used for the calculations. Single point analyses showed that the diol catalyzed reaction was speeding up after 8 h, so entries 1-3 were used to obtain k_2. Rate constants obtained from the linear least squares

analyses (Figure S10) are: $k_1 = (1.84 \pm 0.01) \cdot 10^{-2}$ M^{-1} h^{-1}, $k_2 = (4.68 \pm 0.08) \cdot 10^{-3}$ M^{-1} h^{-1} (triol/diol relative rate is 3.9 ± 0.1) and $k_0 = 1.1 \cdot 10^{-3}$ M^{-1} h^{-1}.

Table S13. Second-order kinetic data for the reaction of benzaldehyde with nitromethane in the presence of PMP and triol **1b** or diol **2b**.

Triol **1b**			Diol **2b**			No catalysis		
T (h)	% yield	Y, M^{-1}	T (h)	% yield	Y, M^{-1}	T (h)	% yield	Y, M^{-1}
3.80	9.83	0.0692	3.88	2.46	0.0164	7.62	1.31	0.00869
5.80	14.65	0.1069	5.83	3.75	0.0253	23.42	3.89	0.02627
7.82	19.37	0.1466	7.85	5.14	0.0350	-	-	-
23.28	44.92	0.4287	23.31	16.89	0.1254	-	-	-

Figure S10. Linear least squares fits of the kinetic data given in Table S13. Triol **1b** catalyzed (left), diol **2b** catalyzed (middle) and non-catalyzed (right) processes.

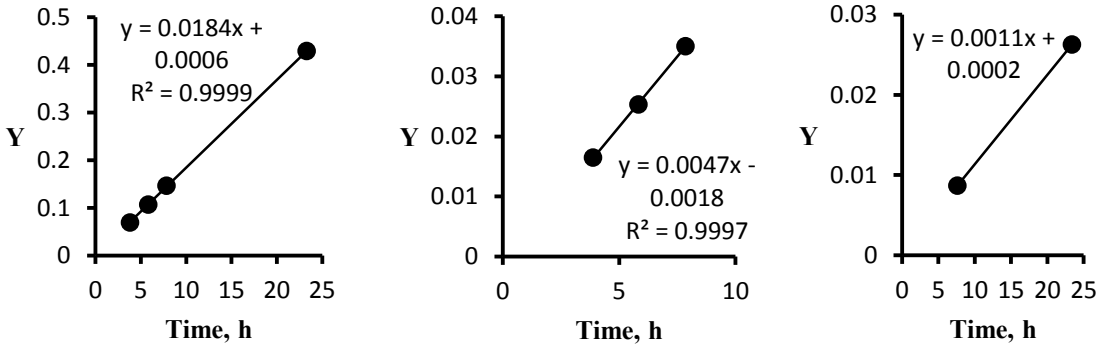

Entry 3 (Table 2). Benzaldehyde (160 mg, 1.51 mmol) and nitromethane (freshly distilled, 92.4 mg, 1.51 mmol) were mixed in 2.77 mL of toluene-d_8. Triol **1b** (12.6 mg, 0.025 mmol) and diol **2b** (9.1 mg, 0.025 mmol) were each dissolved in 1.00 mL portions

of this solution by heating them in 1 dram screw-capped vials. The remaining stock solution was used for monitoring the background reaction. After cooling to ambient temperature, PMP (23 μL, 0.125 mmol) was added to each vial including the one for the background process, the contents were mixed by shaking and transferred into NMR tubes. The head space in each sample was flushed with nitrogen for 30 seconds and the reactions were followed by ^{1}H NMR at 23 ± 1 °C (Table S14). Approximate initial concentrations A_0 = 0.50 M for the aldehyde and B_0 = 0.50 M for nitromethane were used for the calculations. Y = (product/aldehyde) • 2. The triol catalyzed reaction was slowing down after 22 h, so entries 1-3 were used for obtaining k_1. Rate constants obtained from the linear least squares analyses (Figure S11) are: $k_1 = (1.38 \pm 0.04) \cdot 10^{-2}$ M^{-1} h^{-1} and $k_2 = (3.80 \pm 0.06) \cdot 10^{-3}$ M^{-1} h^{-1} (triol/diol relative rate is 3.6 ± 0.1). A single point analysis gives $k_0 = 6.2 \cdot 10^{-4}$ M^{-1} h^{-1}.

Table S14. Second-order kinetic data for the reaction of benzaldehyde with nitromethane (0.5 M) in the presence of PMP and triol **1b** or diol **2b**.

Entry	Triol **1b**		Diol **2b**		No catalysis	
	Time (h)	Y, M^{-1}	Time (h)	Y, M^{-1}	Time (h)	Y, M^{-1}
1	3.95	0.0540	4.02	0.0139	47.83	0.0280
2	7.26	0.1004	7.34	0.0253	-	-
3	22.54	0.3103	22.58	0.0807	-	-
4	47.78	0.5843	47.80	0.1798	-	-

Figure S11. Linear least squares fits of the kinetic data given in Table S14. Triol **1b** catalyzed (left) and diol **2b** catalyzed (right) reactions.

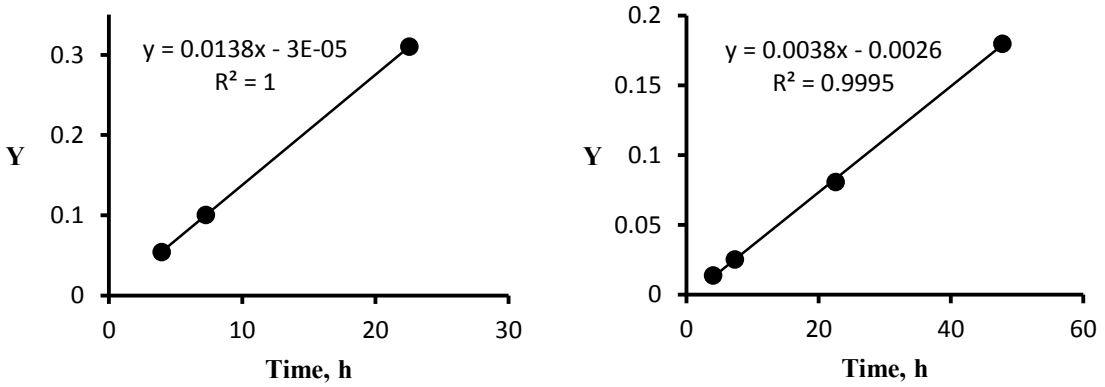

Entry 4 (Table 2). *p*-Methoxybenzaldehyde (freshly distilled, 205 mg, 1.50 mmol) and nitromethane (freshly distilled, 283 mg, 4.64 mmol) were mixed in 2.57 mL of toluene-d_8. Triol **1b** (12.6 mg, 0.025 mmol) and diol **2b** (9.1 mg, 0.025 mmol) were each dissolved in 1.00 mL portions of this solution by heating them in 1 dram screw-capped vials. The remaining stock solution was used for monitoring the background reaction. After cooling to ambient temperature, PMP (23 μL, 0.125 mmol) was added to each vial including the one for the background process, the contents were mixed by shaking and transferred into NMR tubes. The head space in each sample was flushed with nitrogen for 30 seconds and the reactions were followed by ^{1}H NMR at 23 ± 1 °C (Table S15). Approximate initial concentrations A_0 = 0.50 M for the aldehyde and B_0 = 1.55 M for nitromethane were used for the calculations. A product peak at 4.31 ppm (dd, J = 10 Hz, 13 Hz, 1H)[15] and a resonance at 9.71 ppm (s, 1H) for the aldehyde were used to determine the yield. The triol catalyzed reaction slowed down after 8 h whereas the diol catalyzed process speeded up

after 31 h. Rate constants obtained from the linear least squares analyses (Figure S12) are: $k_1 = (3.3 \pm 0.3) \cdot 10^{-3}$ M^{-1} h^{-1}, $k_2 = (7.94 \pm 0.14) \cdot 10^{-4}$ M^{-1} h^{-1} (triol/diol relative rate is 4.2 ± 0.4) and $k_0 = 1.7 \cdot 10^{-4}$ M^{-1} h^{-1}.

Table S15. Second-order kinetic data for the reaction of p-methoxybenzaldehyde with nitromethane in the presence of PMP and triol **1b** or diol **2b**.*

Entry	Triol **1b**			Diol **2b**			No catalysis		
	T (h)	% y	Y, M^{-1}	T (h)	% y	Y, M^{-1}	T (h)	% y	Y, M^{-1}
1	4.27	2.29	0.01500	4.35	0.58	0.00376	23.68	0.70	0.00454
2	8.24	4.25	0.02821	8.32	1.12	0.00728	53.0	1.45	0.00945
3	23.54	9.46	0.06513	23.60	2.97	0.01955	-	-	-
4	31.50	11.12	0.07748	31.55	3.83	0.02535	-	-	-
5	52.9	13.94	0.09916	52.95	5.93	0.03982	-	-	-

* % y = % yield

Figure S12. Linear least squares fits of the kinetic data given in Table S15. Triol **1b** catalyzed (left), diol **2b** catalyzed (middle) and non-catalyzed (right) processes.

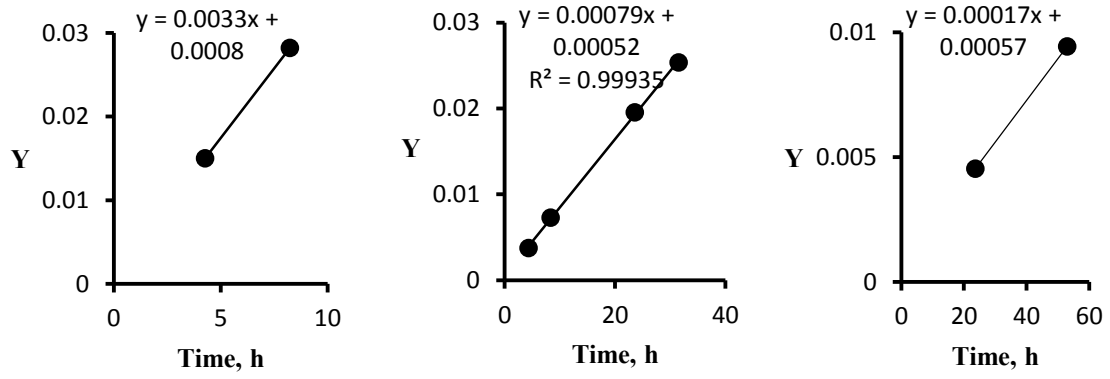

Entry 5 (Table 2). Triol **1b** (12.6 mg, 0.025 mmol) and diol **2b** (9.1 mg, 0.025 mmol) were each dissolved in a mixture of nitromethane (freshly distilled, 80 μL, 1.50 mmol), PMP (23 μL, 0.125 mmol) and toluene-d_8 (0.60 mL) by heating them in 1 dram screw-capped vials. Acetaldehyde (94.5%, containing 5.55 wt % trimer according to the ^{1}H NMR, 95.7 mg, 2.05 mmol) was dissolved in toluene-d_8 (1.09 mL) in a 1 dram screw-capped vial and 0.30 mL portions were then added to each of the three reaction vials. After shaking, the contents were transferred into NMR tubes and the head space in each sample was flushed with nitrogen for 30 seconds. The tubes were capped and covered with a septa to prevent evaporation of acetaldehyde, and the reactions were followed by ^{1}H NMR at 23 ± 1 °C (Table S16). Approximate initial concentrations A_0 = 0.51 M for acetaldehyde and B_0 = 1.50 M for nitromethane were used for the calculations. A product peak at 3.86 ppm (dd, J = 9.0 Hz, 12.5 Hz, 1H)[16] and the resonance at 9.29 ppm (q, J = 2.5Hz, 1H) of the aldehyde were used to determine the yield. After 24 h, side-products were observed in the triol and

Table S16. Second-order kinetic data for the reaction of acetaldehyde with nitromethane in the presence of PMP and triol **1b** or diol **2b**.

Entry	Triol **1b** catalyzed			Diol **2b** catalyzed			Non-catalyzed		
	Time, h	% yield	Y, M^{-1}	Time, h	% yield	Y, M^{-1}	Time, h	% yield	Y, M^{-1}
1	1.20	4.09	0.0280	1.25	0.756	0.00507	7.50	0.66	0.0044
2	2.26	6.95	0.0486	2.38	1.33	0.00894	24.4	2.23	0.0151
3	3.78	11.63	0.0841	3.90	2.17	0.01468	-	-	-
4	7.26	20.97	0.1630	7.37	4.10	0.02810	-	-	-
5	10.75	29.8	0.2494	10.83	6.06	0.04211	-	-	-

diol catalyzed processes, presumably due to a reaction of the product with another molecule of acetaldehyde. Rate constants obtained from the linear least squares analyses (Figure S13) are: $k_1 = (2.32 \pm 0.04) \cdot 10^{-2}$ M^{-1} h^{-1} and $k_2 = (3.88 \pm 0.05) \cdot 10^{-3}$ M^{-1} h^{-1} (triol/diol relative rate is 6.0 ± 0.1). A single point analysis gives $k_0 = 6.2 \cdot 10^{-4}$ M^{-1} h^{-1} (entry 2).

Figure S13. Linear least squares fits of the kinetic data given in Table S16. Triol **1b** catalyzed (left) and diol **2b** catalyzed (right) reactions.

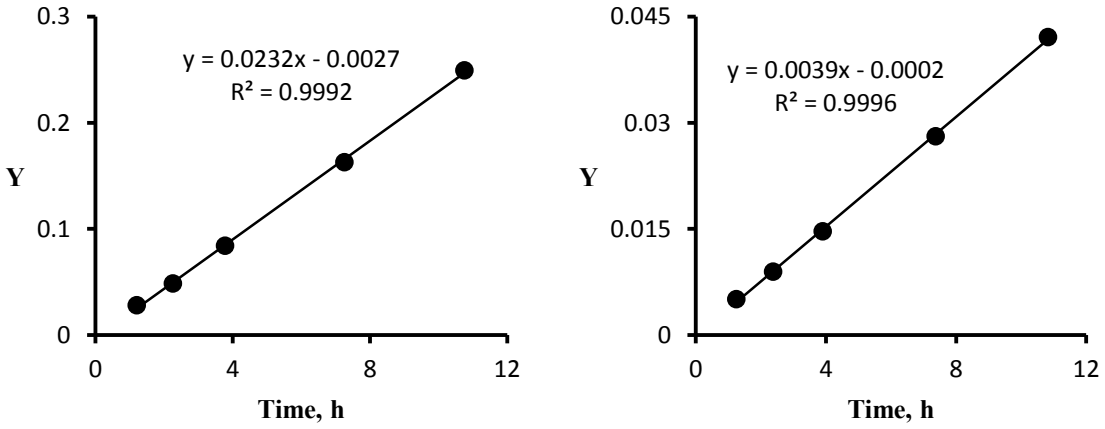

^{1}H NMR binding studies of triol 1b and diol 2b to the Henry reaction reagents.[17]

We studied the binding of triol **1b** and diol **2b** to each of the reactants in the Henry reaction separately. Dilute solutions of the triol and diol in toluene-d_8 were titrated with one of the reagents (R) and ^{1}H NMR spectra were recorded. The proton chemical shifts of the hydroxyl groups were used to plot $1/\Delta\delta$ versus $1/[R]$, where $\Delta\delta = \delta - \delta_0$ and δ_0 is the chemical shift of the unbound substrate whereas δ is the observed value upon the addition of R. Linear plots are consistent with a 1:1 binding model and given that $1/\Delta\delta = 1/(K \cdot$

$\Delta\delta_{max} \cdot [R]) + 1/\Delta\delta_{max}$, where $\Delta\delta_{max}$ corresponds to the difference of the chemical shifts of the bound and unbound substrate, the binding constant K was obtained from the ratio of the intercept to the slope; $\Delta\delta_{max}$ can be obtained from the inverse of the intercept. Binding to each substrate as a percentage was also estimated under reaction concentrations from $\Delta\delta/\Delta\delta_{max}$.

Binding results to PMP (0.122M), PhCHO (0.50 M) and CH_3NO_2 (1.5 M) are summarized in table S17 and were obtained from the titration data in Tables S18-S22. Both triol **1b** and diol **2b** are observed as a mixture of *syn* and *anti*-conformers due to slow interconversion on the NMR scale. Monitoring the chemical shift dependence on reagent concentration provided binding constants to both conformers of **2b**, *syn*-**1b**, and to the non-equivalent top and bottom sites of *anti*-**1b** (i.e., binding to the lone OH or the two equivalent OH groups on the opposite side of the central benzene ring). Binding of PhCHO (Table S21) and CH_3NO_2 (Table S22) to the lone OH of *anti*-**1b** and *anti*-**2b** were found to be weak, whereas the bulky PMP base did not show any binding to *syn*-**1b** but was found to bind weakly to the 2 OH's on the same side of *anti*-**1b**. It also binds weakly to *syn*-**2b** and more strongly to the single OH group of *anti*-**1b** and *anti*-**2b** (Tables S19 and S20). Based on these results the binding to each reagent in the Henry reaction mixture was calculated for each conformer by assuming that each process is independent of the others (Table S17). The ratio of *syn : anti* conformers of the non-bound **1b** and **2b** was assumed to be independent of other reagents in the solution and equal to that found in solutions of triol **1b** (52 (*syn*) :48 (*anti*)) and diol **2b** (67 (*syn*):33 (*anti*)) alone. This and the data in Table S17 (i.e., binding percentage of the individual conformers) were used to calculate

the total bindings (i.e., all conformers) of triol **1b** and diol **2b** to PhCHO and were found to be 44% and 31%, respectively, which gives the difference of *ca.* 1.4 fold between triol and diol binding to PhCHO.

Table S17. PMP (0.122 M), benzaldehyde (0.5 M) and nitromethane (1.5 M) bindings to conformers of triol **1b** and diol **2b** separately and together (the Henry reaction conditions, Table S12, entry 2).

Substrate	Individual binding			Henry reaction mixture			
	PMP	PhCHO	CH_3NO_2	Free	PMP	PhCHO	CH_3NO_2
syn-**1b**	0%	59%	40%	32%	0%	46%	21%
anti-**1b**-2H	20%	56%	37%	32%	8%	41%	19%
anti-**1b**-1H	34%	0%	0%	66%	34%	0%	0%
syn-**2b**	20%	56%	37%	32%	8%	41%	19%
anti-**2b**	50%	0%	0%	50%	50%	0%	0%

Binding of diol 2b to PMP. Diol **2b** (4.2 mg, 12 mmol) was dissolved in 1.00 mL of toluene-d_8. The resulting solution (12 mM, 67 (*syn*) : 33 (*anti*) by NMR) was titrated with neat PMP. Due to the disappearance of all of the OH signals upon addition of the base, the binding constant was estimated based upon the shift of the most upfield signals in the aromatic region (i.e., the aromatic hydrogen resonance *para* to the OH group). The *syn*-conformer resonances moved downfield (Table S18) and the plot of the data (Figure S14) afforded $\Delta\delta_{max} = 0.55 \pm 0.01$ ppm and $K_{syn} = 2.1 \pm 0.1$ M^{-1}, which indicates that at 0.122 M PMP (i.e., the concentration used in the Henry reaction, Table 2, entry 2) $\Delta\delta/\Delta\delta_{max}$ x

100% = 20% or 20% of the *syn*-conformer of **2b** is bound. Binding of the *anti*-conformer was estimated from the change in the total *syn : anti* ratio (Table S19). The average of the data in entries 2-4 provides K_{anti} = 8.3 M^{-1}. At 0.122 M PMP (% unbound *anti* / % *anti*) x 100% = 21.5/42.6 x 100% = 50% or 50% of the *anti*-conformer of **2b** is bound.

Table S18. Titration data for the binding of PMP to the syn-conformer of diol **2b**.

Entry	total PMP added, μL	[PMP], M	1/[PMP], M^{-1}	$\Delta\delta_{syn}$, ppm	$1/\Delta\delta_{syn}$
1	0	0	-	0	-
2	11	0.0592	16.9	0.060	16.7
3	23	0.122	8.20	0.112	8.93
4	34	0.179	5.59	0.149	6.71
5	57	0.293	3.41	0.208	4.81
6	80	0.403	2.48	0.247	4.05

Figure S14. Double-reciprocal plot for the binding of the *syn*-conformer of **2b** to PMP.

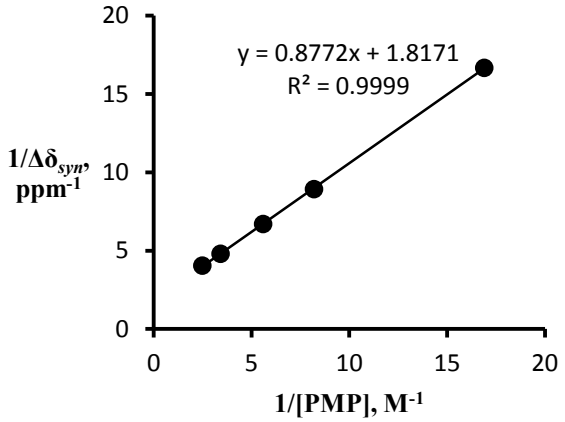

Table S19. Titration data for the binding of PMP to the anti-conformer of diol **2b**.*

Entry	[PMP], M	% *syn*	% unbound *syn*	% unbound *anti*	% bound *anti*	K_{anti}, M^{-1}
1	0	66.9	66.9	33.1	0	-
2	0.0592	61.0	53.4	26.4	12.6	8.0
3	0.122	57.4	42.7	21.1	21.5	8.3
4	0.179	56.2	35.1	17.4	26.4	8.5
5	0.293	53.5	20.6	10.2	36.3	12
6	0.403	46.3	7.1	3.5	50.2	35

* All % given represent the % of the total concentration of **2b**, % unbound *syn* = % *syn*/(K_{syn} · [PMP]); % unbound *anti* = % unbound *syn* · 33.1/66.9; % bound *anti* = 100% – % *syn* – % unbound *anti*; K_{anti} = (% bound *anti*)/(% unbound *anti* · [PMP]).

Binding of triol 1b to PMP. Triol **1b** (6.0 mg, 12 mmol) was dissolved in 1.00 mL of toluene-d_8. The resulting solution (12 mM, 54 (*syn*) : 46 (*anti*)) was titrated with PMP. Due to the disappearance of the OH signals after the addition of the base, binding was estimated by the shifting of the most upfield signal in the aromatic region (i.e., the aromatic hydrogen *para* to the OH group). The signal for the *syn*-conformer changed insignificantly indicating no appreciable binding; the resonance for the *anti*-conformer moved downfield for the 2 OH side (Table S20) and upfield for the single hydroxyl group side. The plot of the former data (Figure S15) afforded $\Delta\delta_{max}$ = 0.51 ± 0.02 ppm and K_{anti} = 2.0 ± 0.1 M^{-1}, which indicates that at 0.122 M PMP (i.e., the concentration used in the Henry reaction, Table 2, entry 2) $\Delta\delta/\Delta\delta_{max}$ = 20% or 20% of the *anti*-conformer of **1b** is bound (i.e., that is the same as that for the *syn*-conformer of 2**b**). The chemical shift for the single hydroxyl group side

of free **1b** was not observed due to spectral overlap and so the binding constant was assumed to be half that of the *anti*-conformer of **2b** (i.e., the statistical difference and this K = 8.3/2 = 4.1 M^{-1}). This indicates that 34% of *anti*-**1b** is bound at 0.122 M PMP.

Table S20. Titration data for the binding of PMP to triol **1b**.

Entry	PMP added, μL	[PMP], M	1/[PMP], M^{-1}	$\Delta\delta_{anti}$, ppm	$1/\Delta\delta_{anti}$, ppm^{-1}
1	0	0	-	0	-
2	11	0.0592	16.9	0.054	18.5
3	23	0.122	8.20	0.101	9.90
4	34	0.179	5.59	0.135	7.41
5	57	0.293	3.41	0.186	5.38

Figure S15. Double-reciprocal plot for the binding of two OH's on the same side of the *anti*-conformer of **1b** to PMP.

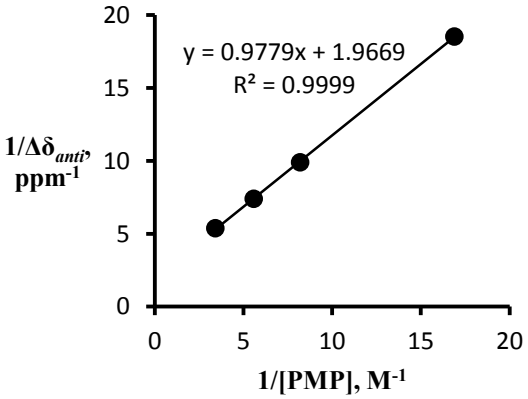

Binding to PhCHO. A solution of triol **1b** in toluene-d_8 (0.75 mL, 3.3 mM) was titrated with PhCHO. Binding was estimated based on the downfield shift of the OH signals for

the *syn* (3 OH) and *anti* (2 OH) conformers (Table S21). Small changes in the *anti*-conformer lone OH chemical shift indicated weak binding to this site. The plots of the data (Figure S16) afforded $\Delta\delta_{max} = 1.32 \pm 0.05$ ppm and $K_{syn} = 2.8 \pm 0.1$ M^{-1}, indicating that at

Table S21. Titration data for the binding of benzaldehyde to triol **1b**.

Entry	PhCHO added, μL	[PhCHO], M	δ_{syn}, ppm	δ_{anti}, ppm (2 OH)	$\Delta\delta_{syn}$, ppm	$\Delta\delta_{anti}$, ppm
1	0	0	5.720	5.330		
2	10	0.129	6.076	5.783	0.356	0.453
3	20	0.256	6.264	6.033	0.544	0.703
4	30	0.378	6.391	6.204	0.671	0.874
5	40	0.498	6.505	6.349	0.785	1.019
6	50	0.615	6.579	6.496	0.859	1.166

Figure S16. Double-reciprocal plots for the binding of the *syn* conformer of **1b** to benzaldehyde (left) and the two OH side of the *anti*-conformer of **1b** to benzaldehyde (right).

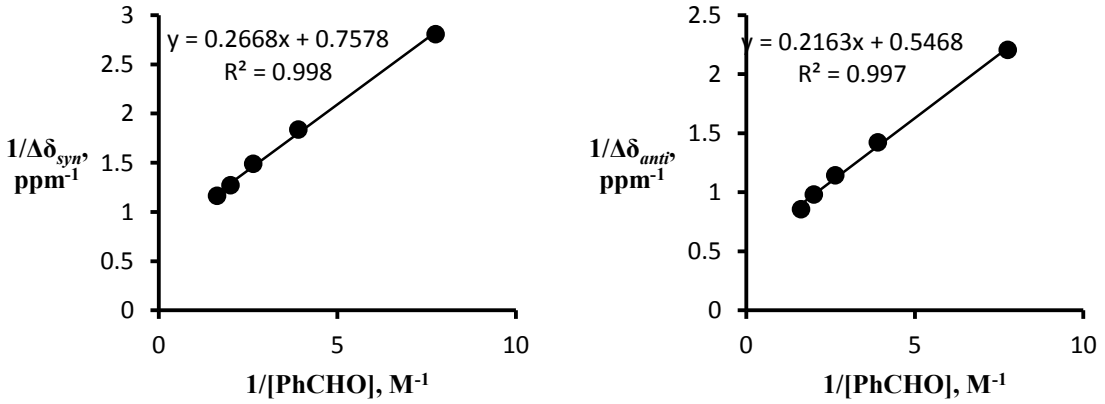

0.50 M PhCHO (i.e., the concentration used in the Henry reaction, Table 2, entry 2) $\Delta\delta/\Delta\delta_{max}$ x 100% = 0.77/1.32 x 100% = 59% or 59% of the *syn*-conformer of **1b** is bound; and $\Delta\delta_{max}$ = 1.83 ± 0.10 ppm and K_{anti} = 2.5 ± 0.2 M^{-1}, indicating that at 0.50 M PhCHO $\Delta\delta/\Delta\delta_{max}$ x 100% = 1.02/1.83 x 100% = 56% or 56% of the *anti*-conformer of **1b** is bound.

Binding of the *syn* conformer of diol **2b** to PhCHO was estimated to be the same as that for the *anti*-conformer of triol **1b** (i.e., 56%).

Binding to CH_3NO_2. A solution of triol **1b** in toluene-d_8 (0.70 mL, 0.2 mM) was titrated with nitromethane. Binding was estimated based on the downfield shift of the OH group signals for the *syn* (3 OH) and the *anti* (2 OH) conformers (Table S22). Small changes in

Table S22. Titration data for the binding of nitromethane to triol **1b**.

Entry	CH_3NO_2 added, μL	$[CH_3NO_2]$, M	δ_{syn}, ppm	δ_{anti}, ppm	$\Delta\delta_{syn}$, ppm	$\Delta\delta_{anti}$, ppm
1	0	0	5.680	5.295	-	-
2	3.0	0.079	5.738	5.353	0.058	0.058
3	6.0	0.157	5.788	5.405	0.108	0.110
4	10.0	0.260	5.841	5.466	0.161	0.171
5	20.0	0.513	6.053	5.669	0.373	0.374
6	30.0	0.759	6.127	5.726	0.447	0.431
7	40.0	0.998	6.191	5.804	0.511	0.509

the *anti*-conformer lone OH chemical shift indicated weak binding to this site. The plots of the data (Figure S17) afforded $\Delta\delta_{max}$ = 1.7 ± 0.7 ppm and K_{syn} = 0.44 ± 0.18 M^{-1}, indicating that at 1.50 M nitromethane (i.e., concentration used in the Henry reaction, Table 2, entry 2) $\Delta\delta/\Delta\delta_{max}$ x 100% = 0.68/1.7 x 100% = 40 ± 16% which is the amount of the bound *syn*-

conformer of **1b**; and $\Delta\delta_{max}$ = 1.9 ± 0.6 ppm and K_{anti} = 0.39 ± 0.12 M^{-1}, indicating that at 1.50 M nitromethane $\Delta\delta/\Delta\delta_{max}$ = 0.71/1.9 = 37 ± 11% which is the amount of the bound *anti*-conformer of **1b**.

Figure S17. Double-reciprocal plots for the binding of the *syn* conformer of **1b** to nitromethane (left) and the two OH side of the *anti*-conformer of **1b** to nitromethane (right).

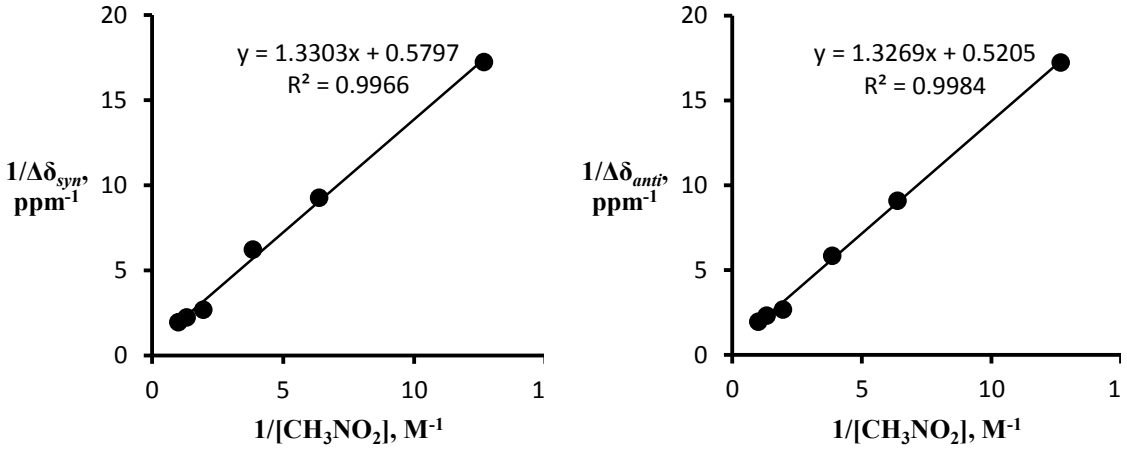

Binding of the *syn*-conformer of diol **2b** to CH_3NO_2 was estimated to be the same as that for the *anti*-conformer of triol **1b** (i.e., 37%).

Kinetics of the reaction of 1,2-unsaturated carbonyl compounds with nitroalkanes in the presence of a base and a hydrogen bond catalyst.

Entry 1 (Table 3). Methyl vinyl ketone (MVK) (freshly distilled over $NaHCO_3$, 108.3 mg, 1.54 mmol) and nitromethane (freshly distilled, 286 mg, 4.69 mmol) were mixed in

2.63 mL of toluene-d_8. Triol **1b** (12.6 mg, 0.025 mmol) and diol **2b** (9.1 mg, 0.025 mmol) were each dissolved in 1.00 mL portions of this solution by heating them in 1 dram screw-capped vials. The remaining stock solution was used for monitoring the background reaction. After cooling to ambient temperature, PMP (23 μL, 0.125 mmol) was added to each vial including the one for the background process, the contents were mixed by shaking and transferred into NMR tubes. The head space in each sample was flushed with nitrogen for 30 seconds and the reactions were followed by ^{1}H NMR at 23 ± 1 °C (Table S23). Approximate initial concentrations A_0 = 0.51 M for the ketone and B_0 = 1.56 M for nitromethane were used for the calculations. The product peak at 3.76 ppm (t, J = 6.8 Hz, 2H)[18] and the resonance at 5.33 ppm (dt, J = 10.5, 0.7 Hz, 1H) for MVK were used to determine the yield. This reaction was complicated by the formation of a by-product which was assigned as 5-nitrononan-2,8-dione based on the splitting pattern of its resonance at 4.24–4.20 ppm (i.e., a quintet-like multiplet corresponding to 1H)[19]; this compound corresponds to the addition of two molecules of MVK to nitromethane. To determine the rate of the reaction, consequently, the yield of this by-product (y2) was added to the yield of the product (y1) and a second order analyses was used as for the Henry reaction described above. The change in the concentration of MVK due to the side reaction was ignored, but only the entries with low y2 (≤ 2%) were used to obtain the rate constants. Since only two experimental points were used in the triol reaction analyses, the XY-intercept was added to the plot as an additional point to estimate the uncertainty. The rate constants obtained from the linear least squares analysis (Figure S18) are: k_1 = (9.10 ±

0.09) • 10^{-3} M^{-1} h^{-1}, k_2 = (1.73 ± 0.01) • 10^{-3} M^{-1} h^{-1} (triol/diol relative rate is 5.3 ± 0.1) and k_0 = (4.4 ± 0.1) • 10^{-4} M^{-1} h^{-1}.

Table S23. Second-order kinetic data for the reaction of MVK with nitromethane in the presence of PMP and triol **1b** or diol **2b**.

Entry			Triol **1b**		
	Time (h)	% y1	% y2	% y1+2	Y
1	4.04	5.43	0.01	5.44	0.03619
2	7.70	9.40	0.79	10.19	0.07010
3	23.50	19.9	5.16	25.04	0.1932
4	47.55	27.4	10.8	38.2	0.3314
Entry			Diol **2b**		
	Time (h)	% y1	% y2	% y1+2	
1	4.15	1.14	0.0	1.14	0.00736
2	7.80	2.05	0.0	2.05	0.01332
3	22.58	5.50	0.25	5.75	0.03833
4	47.62	10.66	1.18	11.84	0.08243
Entry			No catalysis		
	Time (h)	% y1	% y2	% y1+2	
1	7.48	0.53	0.0	0.53	0.0034
2	22.68	1.51	0.0	1.51	0.00978
3	47.70	3.21	0.0	3.21	0.02103

Figure S18. Linear least squares fits of the kinetic data given in Table S23. Triol **1b** catalyzed (left), diol **2b** catalyzed (middle) and non-catalyzed (right) processes.

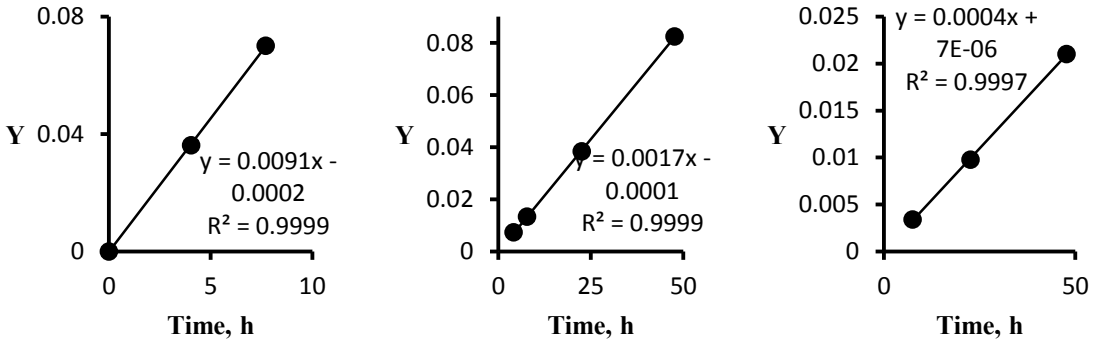

Entry 2 (Table 3). Nitromethane (freshly distilled, 275 mg, 4.50 mmol) and PMP (8.1 μL, 0.045 mmol) were mixed in 2.74 mL of toluene-d_8. Triol **1b** (12.6 mg, 0.025 mmol) and diol **2b** (9.1 mg, 0.025 mmol) were each dissolved in 1.00 mL portions of this solution by heating them in 1 dram screw-capped vials. The remaining stock solution was used for monitoring the background reaction. After cooling to ambient temperature, acrolein (dried over anhydrous $CaSO_4$ and K_2CO_3, 10.0 μL, 0.150 mmol) was added to each vial, the contents were mixed by shaking and then transferred into NMR tubes. The head space in each sample was flushed with nitrogen for 30 seconds and the reactions were followed by ^{1}H NMR at 23 ± 1 °C (Table S24). Approximate initial concentrations A_0 = 0.50 M for the aldehyde and B_0 = 1.50 M for nitromethane were used for the calculations. The product peak at 3.71 ppm (t, J = 6.8 Hz, 2H)[20] and the resonance at 6.00 ppm (ddd, J = 8.0, 10, 17.5 Hz, 1H) for the aldehyde were used to determine the yield. The observed pseudo first-order rate constants (i.e., due to 10 fold excess of CH_3NO_2) were calculated from the slopes of

plots of LN versus time (Figure S19), where LN = – ln(1 – y/100) and y is the yield, to afford: $k_1 = (7.83 \pm 0.06) \cdot 10^{-2}$ h^{-1}, $k_2 = (1.87 \pm 0.06) \cdot 10^{-2}$ h^{-1} (triol/diol relative rate is 4.2 ± 0.1) and $k_0 = (3.1 \pm 0.1) \cdot 10^{-3}$ h^{-1}. Second order rate constants reported in Table 3

Table S24. Pseudo first-order kinetic data for the reaction of acrolein with nitromethane in the presence of PMP and triol **1b** or diol **2b**.

Entry	Triol **1b**			Diol **2b**			No atalysis		
	T (h)	% yield	LN	T (h)	% yield	LN	T (h)	% yield	LN
1	1.12	8.81	0.0922	1.15	2.82	0.0286	1.21	0.740	0.00743
2	2.44	18.21	0.2010	2.45	5.58	0.0574	2.49	1.04	0.0105
3	4.81	31.70	0.3813	4.82	9.75	0.1026	4.84	1.88	0.0190
4	8.13	47.45	0.6434	8.12	14.75	0.1596	8.15	2.82	0.0286

Figure S19. Linear least squares fits of the kinetic data given in Table S24: triol **1b** catalyzed (left), diol **2b** catalyzed (middle) and non-catalyzed (right) processes.

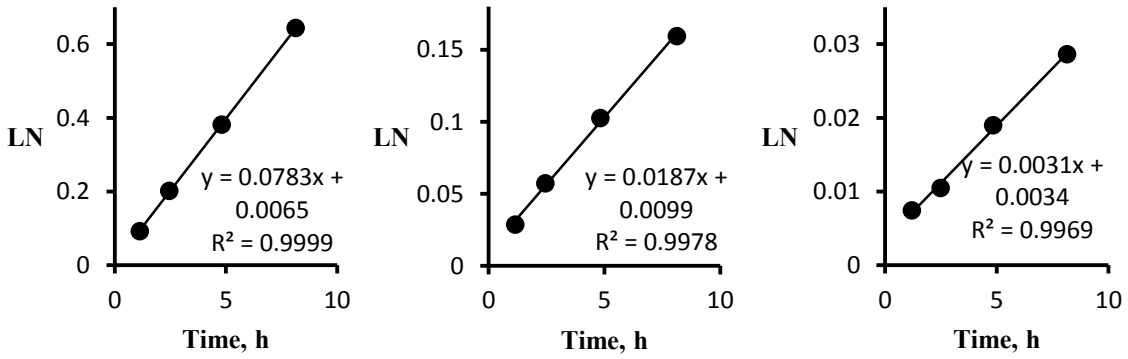

were obtained by dividing the pseudo first-order constants over nitromethane concentration (1.5 M): $k_1 = (5.22 \pm 0.04) \cdot 10^{-2}$ M^{-1} h^{-1}, $k_2 = (1.24 \pm 0.04) \cdot 10^{-2}$ M^{-1} h^{-1} and $k_0 = (2.1 \pm 0.1) \cdot 10^{-3}$ M^{-1} h^{-1}.

Entry 3 (Table 3). Triol **1b** (12.6 mg, 0.025 mmol) and diol **2b** (9.1 mg, 0.025 mmol) each were dissolved in 1.00 mL of a 10 mM PMP solution in toluene-d_8 by heating them in 1 dram screw-capped vials. After cooling to ambient temperature, MVK (freshly distilled over $NaHCO_3$, 41 μL, 0.50 mmol) and α-nitrotoluene (53 μL, 0.50 mmol) were added to each vial including the one for monitoring the background reaction, the contents were mixed by shaking and then transferred into NMR tubes. The head space in each sample was flushed with nitrogen for 30 seconds and the reactions were followed by ^1H NMR at 23 ± 1 °C (Table S25). Approximate initial concentrations $A_0 = 0.45$ M for the

Table S25. Second-order kinetic data for the reaction of MVK with α-nitrotoluene in the presence of PMP and triol **1b** or diol **2b**.

Entry	Triol **1b**		Diol **2b**		No catalysis	
	Time (h)	P/S	Time (h)	P/S	Time (h)	P/S
1	1.34	0.0527	1.34	0.0198	1.38	0.0075
2	2.42	0.0957	2.40	0.0354	2.43	0.0139
3	4.73	0.1953	4.72	0.0705	4.75	0.0263
4	6.77	0.2853	6.76	0.101	6.78	0.0401

ketone and $B_0 = 0.45$ M for the nitroalkane were used for the calculations. The product peak at 1.51 ppm (s, 3H) and the resonance at 1.75 ppm (s, 3H)[21] for MVK were used to

determine the product to starting material ratio (P/S). Second order rate constants were calculated as the slope in the plot of Y versus time, where Y = (P/S)·(1/0.45) (Figure S20) to afford: $k_1 = (9.55 \pm 0.11) \cdot 10^{-2}$ M^{-1} h^{-1}, $k_2 = (3.33 \pm 0.09) \cdot 10^{-2}$ M^{-1} h^{-1} (triol/diol relative rate is 2.86 ± 0.03) and $k_0 = (1.32 \pm 0.05) \cdot 10^{-2}$ M^{-1} h^{-1}.

Figure S20. Linear least squares fits of the kinetic data given in Table S25. Triol **1b** catalyzed (left), diol **2b** catalyzed (middle) and non-catalyzed (right) processes.

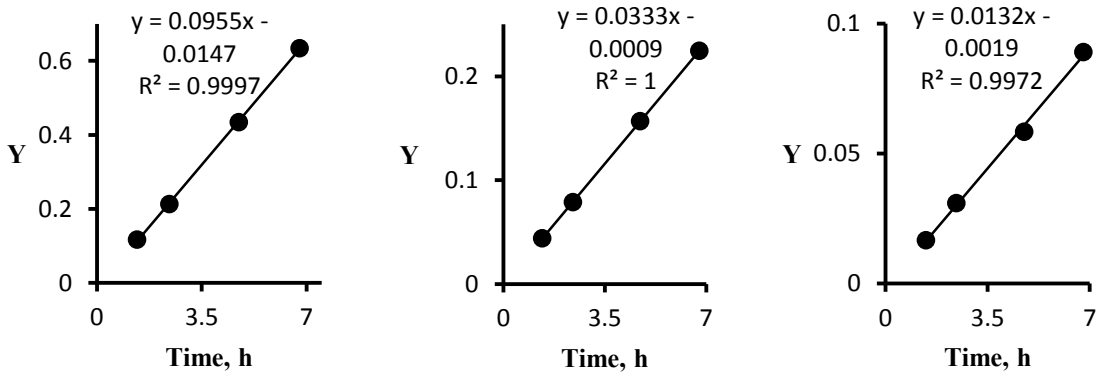

Kinetics for the Friedel-Crafts reaction of β-nitrostyrene with *N*-methylindole in the presence of a hydrogen bond catalyst.

N-Methylindole (397 mg, 3.03 mmol) and β-nitrostyrene (149 mg, 1.00 mmol) were dissolved in 3.40 mL of CD_2Cl_2 (Scheme S3). Triol **1b** (12.6 mg, 0.025 mmol) and diol **2b** (9.6 mg, 0.0265 mmol) were each dissolved in 1.80 mL portions of this solution. The reaction was followed by ^{1}H NMR at 23 ± 1 °C (Table S26) and the yield was determined from the normalized peak intensities of the product at 4.98 ppm (dd, J = 8.5, 12.5 Hz, 1H)[22]

Scheme S3. Friedel-Crafts reaction of β-nitrostyrene with N-methylindole in the presence of triol **1b** or diol **2b**.

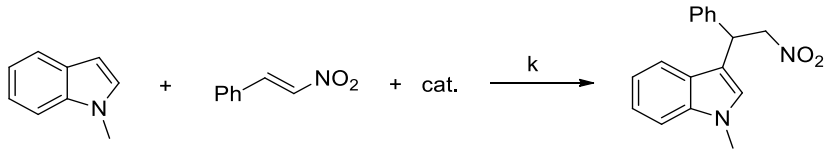

Table S26. Second-order kinetic data for the reaction of β-nitrostyrene with N-methylindole in the presence of triol **1b** or diol **2b**.

Entry	Time (h)	Triol **1b** catalyzed		Diol **2b** catalyzed	
		% yield	Y, M^{-1}	% yield	Y, M^{-1}
1	48.7	5.9	0.0807		
2	71.0	8.3	0.115	0.73	0.096
3	95.1	11.4	0.162	1.01	0.0134
4	160	17.5	0.261	1.58	0.0210
5	240	23.5	0.366	2.20	0.0293
6	336	30.1	0.497	2.87	0.0384

and the combined methyl resonances of the product and *N*-methylindole at 3.74 ppm (s, 3H) and 3.80 ppm (s, 3H), respectively. Approximate initial concentrations A_0 = 0.25 M for β-nitrostyrene and B_0 = 0.76 M for *N*-methylindole were used for the calculations. Second order rate analysis was applied (i.e., as for the Henry reaction described above) and showed that reactions slowed down after 160 h, so entries 1-4 were used for the calculations. Rate constants obtained from the linear least square analyses (Figure S20) are: $k_1 = (1.62 \pm 0.05) \cdot 10^{-3}$ M^{-1} h^{-1} and $k_2 = (1.19 \pm 0.07) \cdot 10^{-4}$ M^{-1} h^{-1} (corrected to a 9.1

mg loading by multiplying by 9.1/9.6 for the proper comparison). The background rate (k_0 = 3.5 • 10^{-5} M^{-1} h^{-1}) was estimated from a single point at 266 h and an observed yield of 0.70%. The triol/diol relative rate is 13.6 ± 1.0 and it becomes 19 upon correction for the non-catalyzed process.

Figure S20. Linear least squares fits of the kinetic data given in Table S26. Triol **1b** catalyzed (left) and diol **2b** catalyzed (right) reactions.

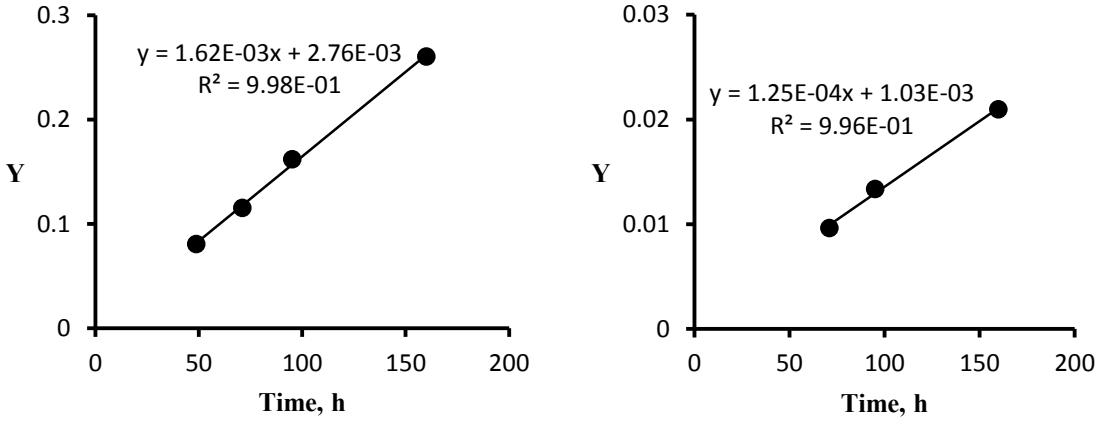

Kinetics for the reaction of methyl vinyl ketone (MVK) with an amine in the presence of a hydrogen bond catalyst.

Reaction of MVK with aniline. Aniline (137 μL, 1.50 mmol) was dissolved in 2.86 mL of toluene-d_8. Triol **1b** (12.6 mg, 0.025 mmol) and diol **2b** (9.1 mg, 0.025 mmol) were each dissolved in 1.00 mL portions of this solution by heating them in 1 dram screw-capped vials. The remaining stock solution was used for monitoring the background reaction.

MVK (41 μL, 0.50 mmol) was added to each vial, the contents were mixed by shaking and then transferred into NMR tubes. The head space in each sample was flushed with nitrogen for 30 seconds and the reactions were followed by ^{1}H NMR at 23 ± 1 °C (Table S27). Product to starting material ratios (P/S) were determined based on the intensities of the normalized signals for *N*-phenyl-4-amino-2-butanone at 2.01 ppm (t, J = 6.3 Hz, 2H) and MVK at 1.73 (s, 3H). Second order rate constants were determined from a single point as k = (P/S)/(0.5t). The triol/diol relative rate is 2.0 and upon correction for the background process it is 2.3.

Table S27. Second-order kinetic data for the reaction of MVK with aniline in the presence of triol **1b** or diol **2b**.

	Triol **1a**			Diol **2a**			No catalysis	
Time (h)	P/S	k_1, $M^{-1}\cdot h^{-1}$	Time (h)	P/S	k_2, $M^{-1}\cdot h^{-1}$	Time (h)	P/S	k_0, $M^{-1}\cdot h^{-1}$
1.61	0.278	0.345	1.60	0.137	0.171	1.60	0.0270	0.034

Reaction of MVK with 2,6-di-*iso*-propylaniline. Di-*i*-Pr-aniline (283 μL, 1.50 mmol) was dissolved in 2.72 mL of toluene-d_8. Triol **1b** (12.6 mg, 0.025 mmol) and diol **2b** (9.1 mg, 0.025 mmol) were each dissolved in 1.00 mL portions of this solution by heating them in 1 dram screw-capped vials. The remaining stock solution was used for monitoring the background reaction. MVK (41 μL, 0.50 mmol) was added to each vial, the contents were mixed by shaking and then transferred into NMR tubes. The head space in each sample were flushed with nitrogen for 30 seconds and the reactions was followed by ^{1}H NMR at

23 ± 1 °C (Table S28). Product to starting material ratios (P/S) were determined based on the intensities of the normalized signals for *N*-(2,6-di-*iso*-propylphenyl)-4-amino-2-butanone at 2.90 ppm (t, J = 5.7 Hz, 2H) and MVK at 1.73 (s, 3H). A single point determination provided the background rate $k_0 = 1.1 \cdot 10^{-3}$ $M^{-1} \cdot h^{-1}$. Linear least squares fits of P/S versus time (Figure S21) afforded $k_1 = (3.66 \pm 0.01) \cdot 10^{-2}$ $M^{-1} \cdot h^{-1}$ and $k_2 = (9.86 \pm 0.07) \cdot 10^{-3}$ $M^{-1} \cdot h^{-1}$ from the slopes divided by the initial concentration of MVK (i.e., 0.50 M). The triol/diol relative rate is 3.71 ± 0.03 which becomes 4.1 upon correcting for the non-catalyzed process.

Table S28. Second-order kinetic data for the reaction of MVK with 2,6-di-*iso*-propylaniline in the presence of triol **1b** or diol **2b**.

Entry	Triol **1a**		Diol **2a**		No catalysis	
	Time (h)	P/S	Time (h)	P/S	Time (h)	P/S
1	2.23	0.0389	2.32	0.0110	-	-
2	4.72	0.0829	4.77	0.0225	-	-
3	7.25	0.1288	7.28	0.0361	-	-
4	24.65	0.4483	24.67	0.1211	24.72	0.0130

Figure S21. Linear least squares fits of the kinetic data given in Table S28. Triol **1b** catalyzed (left) and diol **2b** catalyzed (right) reactions.

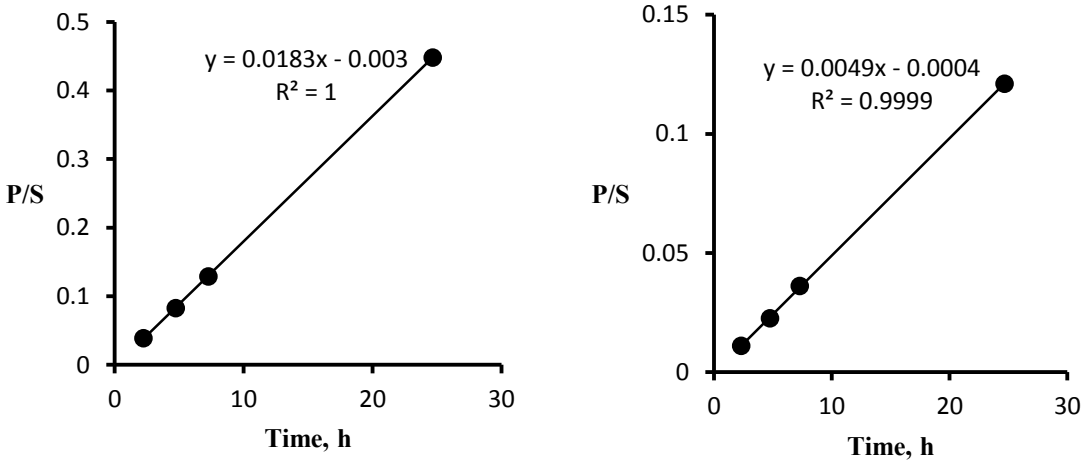

Part 3: Functionalized 1,3,5-triarylbenzenes as anion receptors

Chapter 6: Anion receptors and their applications

The first reports on anion chelation appeared in the late 1960's and included the chelation of methoxide with a bidentate Lewis acid,[1] and the encapsulation of chloride anions by a diammonium cation (Scheme 1).[2] It was not until the 1990's, however, that the importance of anion receptors was recognized and a variety of functionalities including metal-based complexes, multicharged cations and hydrogen bond donors such as amides, ureas, thioureas, phenols, pyrroles and others were used to bind anions.[3]

Scheme 1. Early examples of an anion binding.

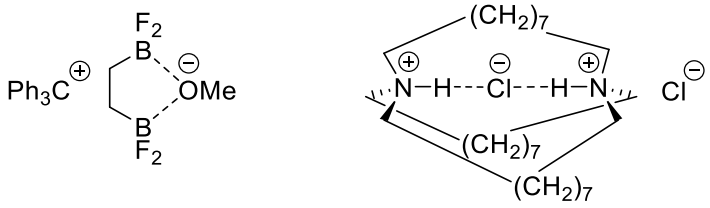

In the past few decades anion receptors have found applications in various fields of the chemical sciences: in catalysis for enantioselective S_N1 reactions (discussed in Chapter 3), in analysis for detection of anions in various solutions, including biosamples, in healthcare as antibiotics or anticancer drugs and for treating diseases associated with malfunctioning

anion channels, and possibly in the environment as reagents for treating nuclear waste (discussed in this Chapter).

Anion receptors as optical probes

The most obvious application of an anion receptor is as an analytical probe for this species. Anions play a critical role in nature, living organisms and industrial processes. Development of their analyses in aqueous solutions and especially for biosamples is very important. Most common methods of detection are optical and electrochemical. In an optical detection method the spectral properties of the probe, such as absorption or fluorescence intensities, change upon addition of the anion of interest, allowing for qualitative and often quantitative determinations.[4] A few examples of molecular receptors used as optical probes for phosphate and phosphorylated molecules are discussed here and the electrochemical method of detection is introduced in the next subchapter.

Hamachi *et al.* developed a highly selective fluorescence receptor for nucleoside polyphosphates (Scheme 2).[5] A dinuclear zinc complex of a xanthene-based receptor shows no fluorescence due to formation of a deconjugated structure, however complexation to a polyphosphate restores the conjugation in the xanthene subunit and produces strong fluorescence. No changes were observed upon addition of other anions including dihydrogen phosphate.

Scheme 2. A highly selective fluororeceptor for polyphosphates.

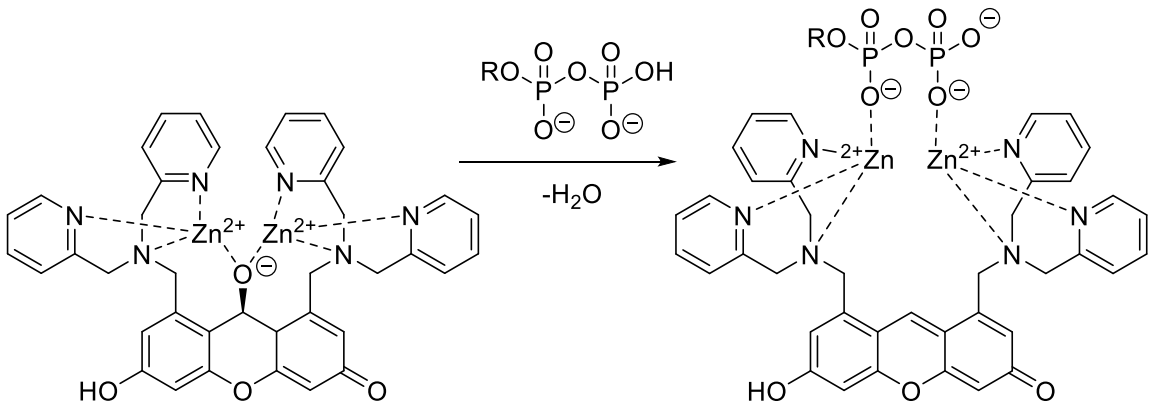

Another example of optical sensing was shown by Pierre *et al.* who discovered an adenosine triphosphate (ATP) selective luminescent probe (Scheme 3).[6] The terbium containing molecule demonstrated a decrease in luminescence upon addition of ATP. No change was observed upon addition of adenosine diphosphate or monophosphate. The authors ascribed the luminescence quench to π-π stacking of the purine necleoside to the phenacridine in the receptor and the photoelectron transfer between the two aromatic systems. The anion selectivity was ascribed to the higher charge of ATP compared to the other two nucleosides and the resulting strong electrostatic interaction with the triply charged receptor. However, given the known ability of amides to serve as anion receptors[7] and presumably their enhanced binding affinity upon complexation to the Lewis acid (terbium), it is possible that ATP also interacts with the amide portion of the receptor via multiple hydrogen bonds.

Scheme 3. A selective luminescence probe for ATP and its proposed mechanism of action.

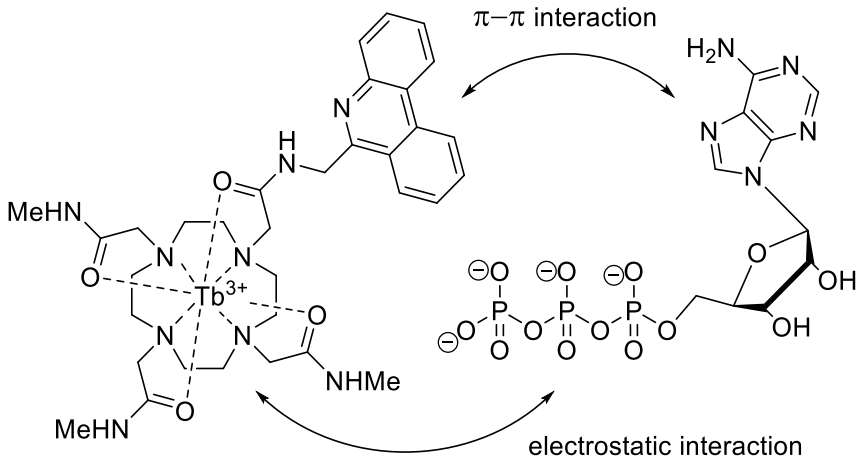

Another approach for optical sensing of an analyte is the use of indicator-displacement assays (IDA).[8] This method employs a combination of a receptor and an indicator that reversibly bind to each other. Once an analyte is introduced into the system, it causes displacement of the indicator and a change in the optical signal (color, absorbance, fluorescence, etc.). This approach does not require incorporation of a chromosphere or fluorophore into the receptor, thus significantly simplifying its design and synthesis. An example of this approach was demonstrated by Kim *et al.* who discovered a highly selective colorimetric assay for phosphate at neutral pH in water (Scheme 4).[9] A dinuclear zinc complex was used as the receptor and a pH-sensitive dye, pyrocatechol violet, as the indicator. The receptor-indicator complex has a blue color which changes to yellow upon addition of phosphate. Moreover, other anions cause little or no change in the UV absorption and no change in the assay color, allowing for a selective naked-eye detection of phosphate. Although interesting from a scientific point of view, practical applications of

this method are questionable due to no possibility for quantitative analysis and the cost of a non-reusable probe.

Scheme 4. Colorimetric phosphate sensing assay.

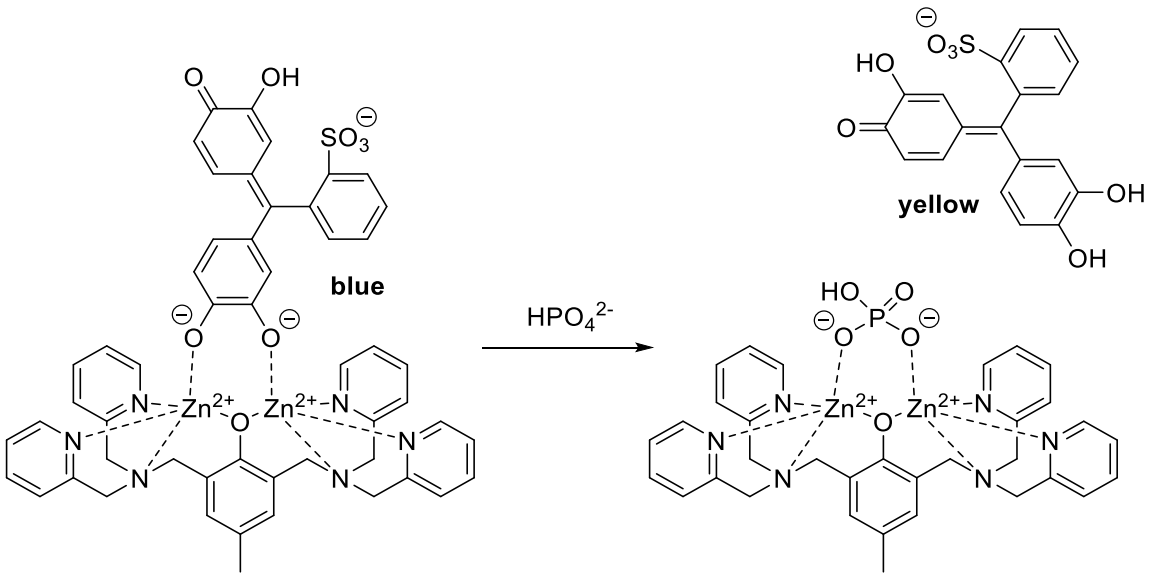

In these three examples (Schemes 2, 3 and 4) the sensing selectivity is achieved due to the high binding selectivity of the receptors to the anion of interest. Interestingly, Anslyn *et al.* developed receptor arrays in which individual components are not necessarily selective for an analyte, but the combined response of all of the components in the array provides selective recognition (i.e., mammalian tongue mimics).[10]

Anion receptors as ionophores in ion-selective electrodes

The above examples all utilized receptors as probes or assays for anions. Ionophore based ion selective electrodes (ISE), on the other hand, can be reused many times and thus act as sensors.[11] They were introduced over 40 years ago and since then have gained very high importance in chemical sensing.

ISE can be used for detecting anions or cations. In both cases the key component of the ISE is an ion selective membrane, which in turn consists of a hydrophobic polymeric material, a plasticizer, an ionic site and an ionophore. A typical example of an ion selective electrode is the one proposed by Song *et al.* for selective detection of dibasic phosphate (Figure 1).[12] The reported membrane was made of polyvinyl chloride (PVC) as a polymeric matrix (33%) and *o*-nitrophenyloctyl ether (*o*-NPOE) as a plasticizer (66%). Addition of *o*-NPOE lowers the glass transition temperature of PVC and provides a rubber-like homogenous structure of the polymeric membrane. This is important as it allows the

Figure 1. A representative example of an anion-selective membrane of an ISE in an analyzed solution ($X^- = 1/2\ HPO_4^{2-}$).

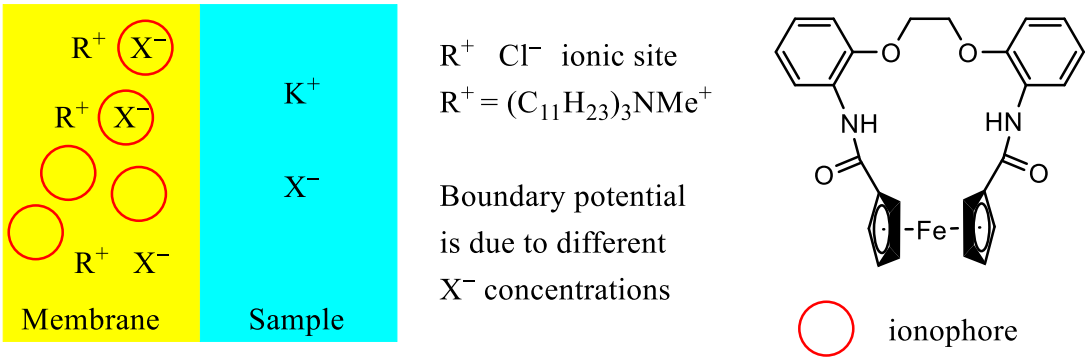

ionophore, ionic site and anions to move freely inside the membrane, which is necessary for a quick and sample-dependent response from the ISE. The non-polar nature of PVC and *o*-NPOE prevents their binding to anions so they do not interfere with the selective binding of the ionophore.

In an ISE used for anion detection (i.e., X^-), the ionophore ideally is a compound that binds strongly and selectively to X^-. A chloride salt of a hydrophobic cation is typically used as the ionic site. A marcocyclic ferrocene-based amide was employed by Song *et al.*as the ionophore and tridodecylmethyl ammonium chloride as the ionic site (Figure 1, X^- = 1/2 HPO_4^{2-}). The chloride anion exchanges easily with X^- from the solution and binds to the ionophore since it is used in 3-10 fold excess over the ionic site. It is important, however, that although the anions can migrate between the membrane and the analyzed solution, the hydrophobic cation of the ionic site stays in place. In this way the concentration of the free X^- in the membrane is very small and determined by the ionophore-X^- binding affinity and is independent of the X^- concentration in the analyzed solution, since the ionophore and the ionic site are at constant concentrations. The phase boundary potential between the solution and the membrane is thus determined only by the concentration of X^- in solution.

To carry out an analysis with an ISE, it is placed in a solution of interest and a potentiometric measurement is made using a cell such as in Figure 2. The resulting EMF is the sum of all the phase boundary potentials in the electric circuit, but the only sample dependent phase boundary potential is the one between the membrane of the ISE and the

analyzed solution. Thus, the EMF is only dependent on the anion concentration in solution. It is important, that both the binding affinity and the selectivity of the ionophore to X^- are

Figure 2. An electrochemical cell for potentiometric measurement with an ISE (reproduced from ref. 11).

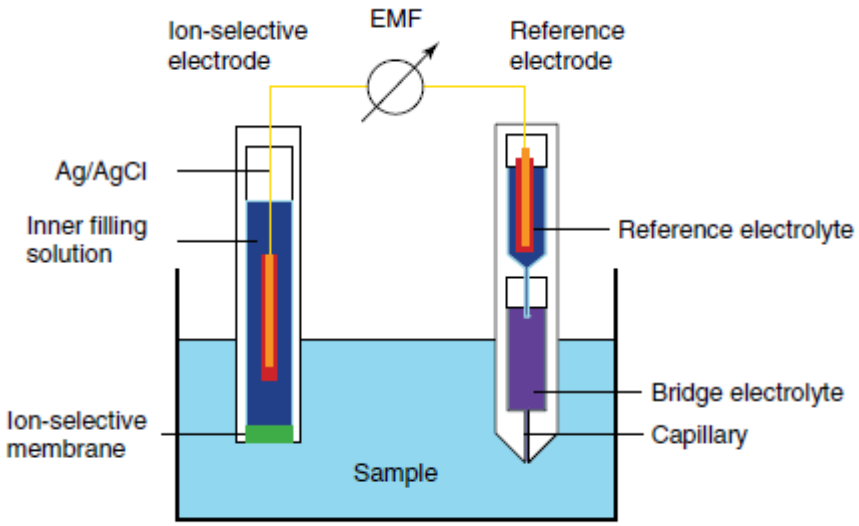

high for these measurements (Figure 1), otherwise the exchange of free X^- (resulting from a low binding affinity) or ionophore-bound X^- (resulting from a low binding selectivity) with other anions would occur and alter the phase boundary potential. Selectivity coefficients are determined as $K_{X/Y}^{pot} = a_X / a_Y$, where a_X is the activity of a 10^{-2} M solution of the anion of interest and a_Y is the activity of an interfering anion that would provide the same response. The selectivities $\log K_{HPO_4^{2-}/Y}^{pot}$ of the HPO_4^{2-} ISE (Figure 1) were reported: Cl^-, -2.92; OAc^-, -1.66; NO_3^-, -2.19; SCN^-, -0.50; SO_4^{2-}, -1.45.

In addition to a high binding affinity and selectivity, other requirements for an ionophore receptor are its solubility in a nonpolar polymer matrix and a neutral charge. A neutral receptor is preferred over a cationic one because the latter has an unbound counterion that can easily exchange with ions in an analyzed solution. The latter two requirements work against achieving high binding affinities because decreasing the polarity and the absence of a positive charge typically weakens interactions with anions. In this respect, ISE receptors differ from optical receptors, which are often charged and are used in polar aqueous solvents. The nature of the detection selectivity is another difference in these two methods: for an ISE it does not only consist of the ionophore binding selectivity, but it also depends on the distribution selectivity of the anions between the aqueous solution and the membrane. This makes it particularly difficult to design an ISE for anions with high hydration energies such as phosphate or sulfate.

Anion receptors as HPLC supports

Anion receptors have been utilized in stationary phases for the separation of anionic analytes.[13] Sessler *et al.* found that HPLC with a calix[4]pyrrole-modified silica gel stationary phase (Scheme 5) gives excellent separation of 5'-adenosine phosphates (ATP, ADP, AMP) and oligonucleotides.[14] The calix[4]pyrrole units in the stationary phase presumably interact with these compounds by hydrogen bonding to the phosphate groups and the more of the latter substituents, the longer the observed retention times.

Scheme 5. Anion receptor modified silica gels for HPLC separation of 5'-adenosine phosphates (left) and oligonucleotides (right).

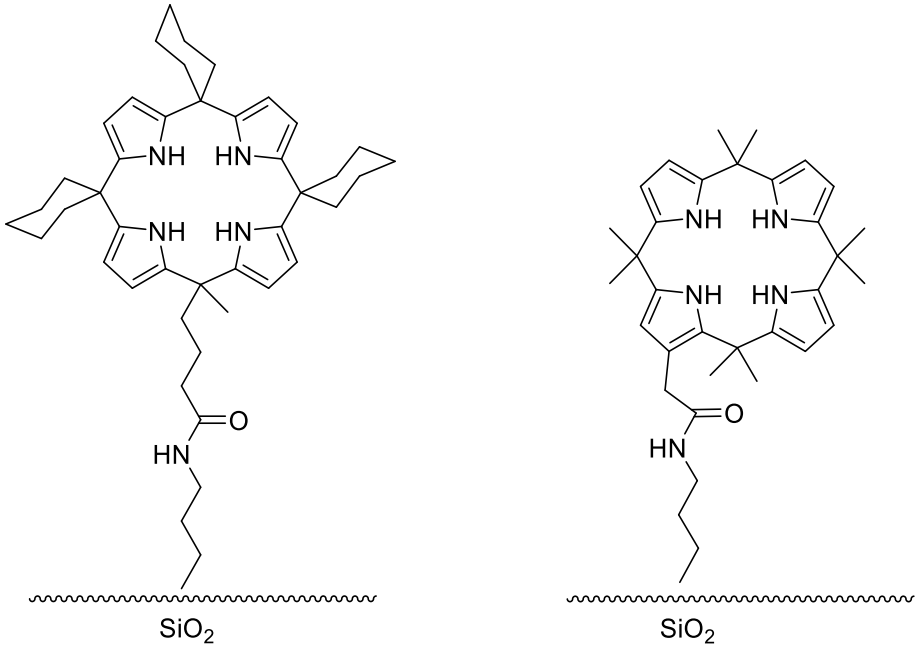

Chloride receptors as trans-membrane transporters and drugs

Anions play critical roles in living organisms. Their concentrations in cells are regulated by specialized proteins that allow them to cross hydrophobic phospholipid bilayer membranes. Chloride ion is the most abundant and important anion as it is responsible for maintaining pH, cell volumes and membrane potentials, as well as transmitting nerve impulses.[15] Its transport across cellular membranes is regulated by chloride-ion channels that allow this anion to flow down its electrochemical gradient, and by ABC transporters (ATP-binding cassette transporters) that utilize the hydrolysis energy of ATP to transfer chloride against the electrochemical gradient.[16] The channel responsible for chloride

transport in the epithelia is the cystic fibrosis transmembrane conductance regulator (CFTR).[17] A mutation of the CFTR leads to the disease, cystic fibrosis. It arises from stopping the anion flow and a slowing of the water flow in airways of the lungs. This leads to lethal bacteria accumulation in dehydrated mucus clogs. As this fatal disease is one of the most prevalent genetic disorders among Caucasians,[18] and a number of other genetic diseases are associated with a malfunctioning chloride-ion channel,[19] anion transport studies are very important.

Artificial anion transporters have been proposed to replace the function of CFTR.[20] For example, Cheng *et al.* showed that introduction of a synthetic analog of the natural product squalamine (GL-172, Scheme 6) into cystic fibrosis epithelial cells facilitates chloride transport through the membrane. They proposed that this compound might have therapeutic applications for patients with cystic fibrosis.[21]

Scheme 6. Squalamine and its synthetic analog GL-172.

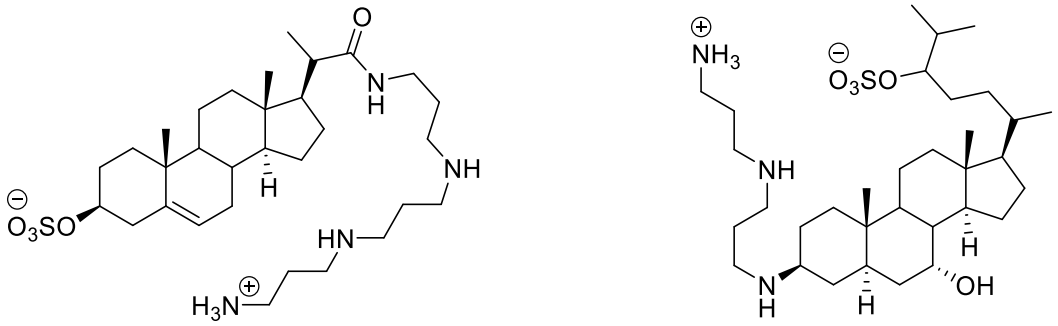

GL-172 Squalamine

Squalamine was also found to possess significant antimicrobial activity against both *Gram*-negative and *Gram*-positive bacteria, and presumably is involved in the immune system of the dogfish shark from which it was isolated.[22] Anion transporters, consequently were proposed to act as antibacterial and antifungal therapeutics by increasing the ion flow through cell membranes, and squalamine synthetic analogs have been studied in this regard.[23] Microorganism resistance to this type of therapeutic is expected to be reduced since the drug does not need to enter the cell thereby eliminating enzymatic degradation and export processes. In addition, the positive charge on the polyamine moiety may lead to stronger interactions with negatively charged bacterial membranes over neutral mammalian ones. This would provide cell selectivity and diminish drug toxicity. Electrostatic interactions between positively charged ammonium and negatively charged sulfonate groups presumably favors self-association and formation of Cl^--permeable pores in the cell membrane. H^+/Cl^- symport (i.e., the simultaneous transport of H^+ and Cl^- through a phospholipid bilayer) leads to reduced pH gradients and cell death. Kinetic studies suggested that the dimer of GL-172 is the active transporter. However, the monomer was found to be the major membrane-bound species. In order to overcome this problem, a number of "connected" dimer analogs of GL-172 were synthesized (not shown).[24] These compounds displayed activities comparable to that of GL-172 and are insensitive to the linking sequence of the monomers. This strongly suggests that a receptor is not involved in their biological action, and provides further support for the membrane pore mechanism.

Anion transporters are also promising candidates for cancer treatment. For example, prodigiosins (Scheme 7), a family of natural products, attracted enormous attention due to their anticancer as well as immunosuppressive and antibiotic activity.[25] Obatoclax is a less toxic synthetic analog developed by Gemin X (recently acquired by Cephalon) which shows promising activity against lung cancer and is in phase II clinical trials.[26]

Scheme 7. Prodigiosin I, its HCl adduct and its synthetic analog Obatoclax.

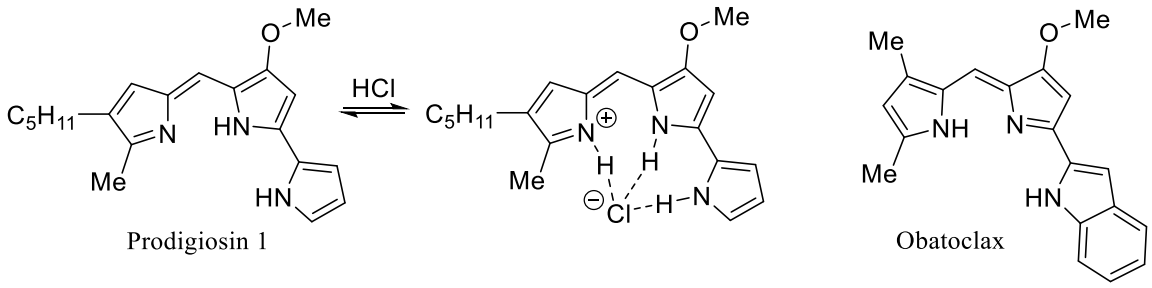

Prodigiosin 1 Obatoclax

Apoptosis (programmed cell death) is involved in the action of prodiogisins and Obatoclax, however the exact mechanism of action remains controversial.[27] Various possibilities have been proposed and perhaps more than one pathway is involved. For example, these compounds were found to inhibit the anti-apoptosis proteins BCL-2[28] and to induce copper-mediated DNA cleavage.[29] Most interestingly, it was suggested that prodigiosins decrease the pH of the already more acidic cancer cell cytoplasm via H^+/Cl^- symport and trigger apoptosis.[30] Indeed, the protonated form of prodiogisin (Scheme 7) is capable of forming three hydrogen bonds to chloride anion, and the complex can bypass the lipid bilayer. Sessler *et al.* found that activity of a family of prodigiosins and their synthetic analogs against A549 human lung cancer and PC3 human prostate cells has a

strong correlation with their H^+/Cl^- ion symport transfer rates.[31] More recently Quesada *et al.* obtained the same result for Obatoclax and its derivatives.[32] Acidification of the cytosol is argued to cause apoptosis,[33] therefore discharging pH gradients between the cytosol (pH = 7.2) and acidic compartments in the cell such as the lysosomes (pH = 4.8) maybe one of the mechanisms of action for prodigiosins.

Tamjamines share a similar structural scaffold with the prodigiosins and also possess anticancer and antimicrobial properties, but are easier to synthesize (Scheme 8).[34] Unlike prodigiosins ($pK_a \sim 7.2$), tamjamines ($pK_a \sim 10$) are more basic and are protonated at the physiological pH value.[35] Due to this inability to release H^+, they are poor H^+/Cl^- symporters. Nevertheless, Quesada *et al.* showed that these compounds are capable of Cl^-/HCO_3^- antiport (i.e., simultaneous transport of Cl^- and HCO_3^- in opposite directions across a phospholipid bilayer) and their efficiency in this regard correlates with their activity against the GLC4 lung cancer cell line.[36] Transport of bicarbonate also explains their ability to neutralize acidic compartments in cells and cause apoptosis.

Scheme 8. Examples of the tambjamine family of natural products and synthetic analogs used in a lipophilicity study.

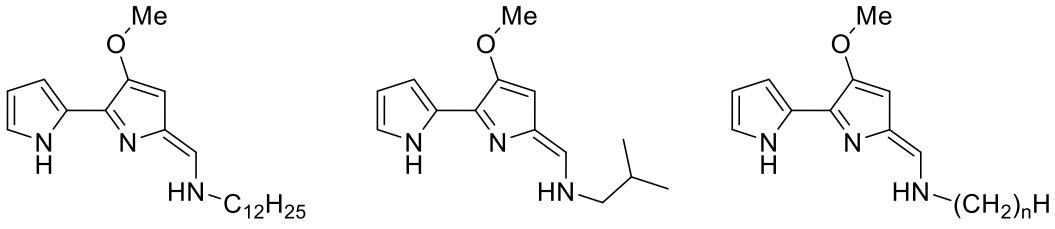

BE-18591 Tambjamine C n = 1-12

Quesada *et al.* explored the role of the lipophilicity of tambjamine analogs on their transport ability.[37] Compounds with varying hydrocarbon chain length were synthesized (Scheme 8), as well as compounds with branched hydrocarbon chains and a more lipophilic benzyloxy group instead of methoxy group (not shown). This approach enabled the lipophilicity to be varied without impacting the binding affinity of the compounds. Chloride loaded vesicles were placed in bicarbonate solutions and Cl^-/HCO_3^- antiport was observed. The initial chloride efflux rate (in percent per second) as a measure of the transport efficiency was plotted against log*P* (i.e., the logarithm of water/*n*-octanol partition coefficient), as a measure of the lipophilicity (Figure 3). As expected, it was found that an initial increase in lipophilicity leads to more efficient transport. After a certain point, however, the transport efficiency drops, indicating that log*P* ~ 4.2 is the optimal lipophilicity value within the tamjamine family for efficient anion transport.

Figure 3. Transport efficiency of tambjamines as a function of their lipophilicity (reproduced from ref. 37, compounds **1-10** represent n = 1-10 in Scheme 8; **11** is for n = 12 and **12-16** are not shown).

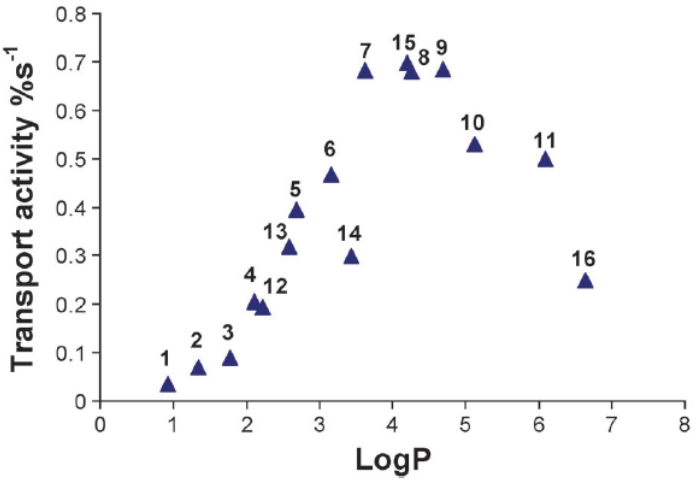

Inspired by a correlation between transport efficiency and anticancer activity of prodigiosins and tambjamines, efforts have been made to design synthetic transporters.[38] Gale *et al.* introduced simple but very efficient tren-based tris-(thio)urea anion transporters (Scheme 9, left).[39] Binding affinities to anions, Cl^-/NO_3^- and Cl^-/HCO_3^- antiport rates, and activities against various types of cancer cell lines were measured. Similar effects of the lipophilicity on the transport efficiency were found as in case of tambjamines; fluorination of the aryl group causes significant increases in the transport efficiency of the urea derivatives (i.e., orders of magnitude). Too much fluorine in the more lipophilic thiourea derivatives, however, causes a drop in their transport abilities. This was explained as being due to the low concentration of the highly lipophilic species in the aqueous phase or at the polar surface of the lipid bilayer. The highest transport rate was achieved for a urea

derivative with log*P* ~ 7.6, and it is an order of magnitude higher than that for a thiourea with similar lipophilicity. This can be rationalized by the stronger binding affinity of ureas compared to their thiourea analogs.

Scheme 9. Tren- and indole-based synthetic anion transporters.

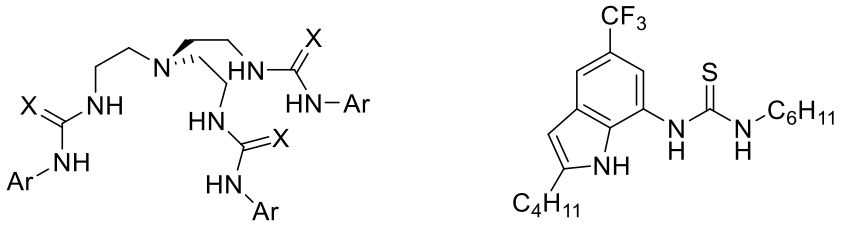

Ar = Ph, 4-F-C_6H_4, C_6F_5,
4-$CF_3C_6H_4$, 3,5-$(CF_3)_2C_6H_3$
X = O, S

In order for a compound to be a potential orally active drug, it generally needs to obey "Lipinski's rule of five". This phenomenological rule states that a drug candidate should have a molecular mass of less than 500, no more than 5 hydrogen bond donors and no more than 10 acceptors, and a log*P* of less than 5. All of these numbers are multiple of five, and this gives the name to the rule.[40] Consequently, Gale *et al.* explored lower molecular weight mono(thio)urea receptors. An indole-based thiourea (Scheme 9, right) showed high activity towards cancer cells, but much reduced toxicity against non-cancerous human cells.[41]

Another interesting anion transporter was reported by Smith *et al.* who installed a urea moiety into a phospholipid structure (Scheme 10).[42] Two molecules of the compound when incorporated on both sides of the phospholipid layer transported chloride via a relay mechanism.

Scheme 101. A phospholipid-based chloride transporter.

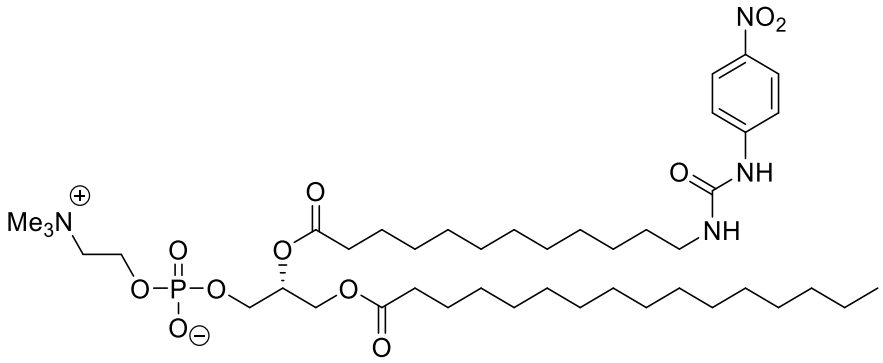

Therapeutic applications of phosphate transporters

Other anions that are potentially useful targets for selective transport in living organisms include bicarbonate and phosphate.[43] To date bicarbonate transporters, such as tambjamines (Scheme 8) or tren-based thioureas (Scheme 9), act mostly as Cl^-/HCO_3^- antiporters as discussed above. As for phosphate anions, they are extremely important in living organisms because they are part of energy storage molecules (ATP), genetic information storage (DNA and RNA), the cell membrane phospholipid bilayer, skeletal bones, take part in cell signaling, and serve as a buffer in serum and urine.[44] Transport of inorganic phosphate, consequently, is crucial for living organisms.[45] High serum concentrations of this anion (hyperphosphatemia) is a major problem in patients with chronic kidney disease[46] as it increases the rate of death from cardiovascular events[47] and causes bone and joint destruction.[48] Besides dietary restrictions, removal of phosphate from the body is a way of treating hyperphosphatemia. During hemodialysis, phosphate transfer from intracellular spaces to the plasma is the rate limiting step, which makes this procedure

ineffective for phosphate clearance because the largest amounts of this anion are contained in the cytoplasm of the cells.[49] No reports to the best of our knowledge have appeared in the literature regarding inorganic phosphate artificial transporters (i.e., agents that increase the transport rate from intracellular spaces) and their potential therapeutic applications.

Many nucleotide analogs have activity against HIV, hepatitis and herpes viruses, but due to their hydrophilicity, these compounds often require a transporter to penetrate through cellular membranes.[50] Sessler *et al.* designed a sapphyrin-based receptor for 5'-guanosine monophosphate (GMP) capable of transporting it through a model membrane system (Scheme 11).[51] This receptor is monoprotonated at physiological pH, and utilizes hydrogen bonding to bind GMP. The N–H bonds of saphyrin bind to the phosphate group and the cytosine nucleoside moiety recognizes its complimentary partner (i.e., GMP). An

Scheme 11. Guanosine monophosphate and its artificial transporter.

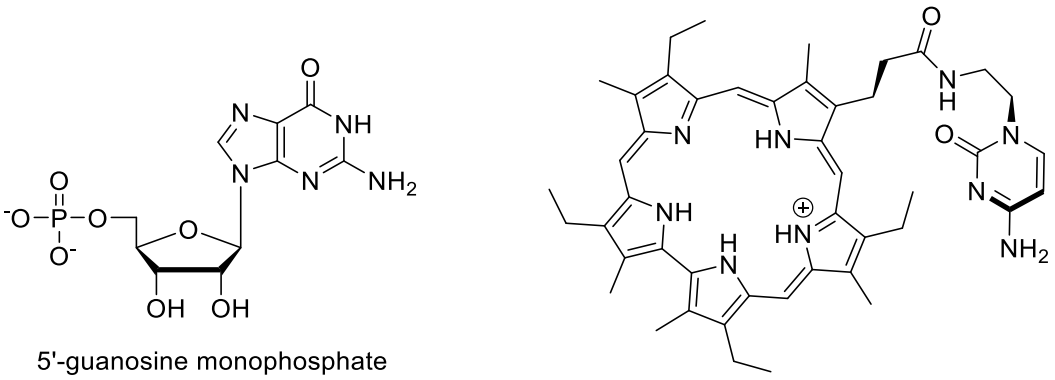

analogous neutral calix[4]pyrrole receptor (not shown) showed promising results as an ionophore in an ISE for mononucleotides.

Hamachi *et al.* designed a tetranuclear zinc complex capable of intracellular delivery of short phosphorylated peptides (Scheme 12).[52] Binding of the metallocenters to the peptide anionic phosphate site was found to be crucial for transport and was inhibited by addition of pyrophosphate anion. One dinuclear zinc arm presumably is used for binding to the peptide in analogy to Scheme 4, while the second arm interacts with the cellular membrane phospholipids to enhance the transport properties.

Scheme 12. A transmembrane transporter for short phosphorylated peptides.

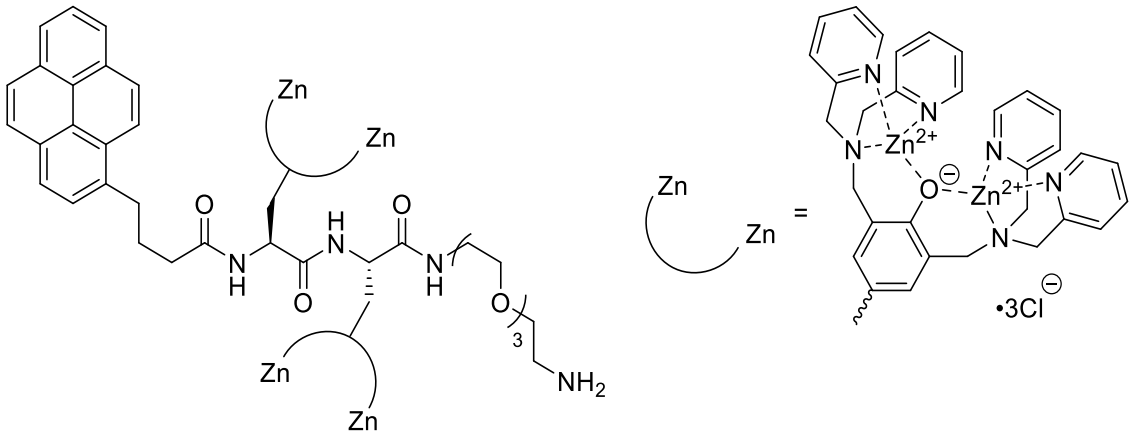

Related to phosphate transport is the ability of certain phosphate receptors to coordinate to the outer surface of a phospholipid bilayer resulting in the inward translocation of the phospholipid.[53] For example, phosphatidylserine (PS) is a component of phospholipid membranes and its distribution is controlled by a special enzyme, aminophospholipid flippase. Normally PS is located on the inner side of the cellular membrane and its appearance in the outer layer is usually due to apoptosis and activates cell capture and destruction by macrophages, or, in case of erythrocytes, it causes blood coagulation. Smith

et al. showed that a synthetic choline-derived PS scramblase (Scheme 13) significantly increases thrombin production in erythrocytes.[53] It was proposed that this artificial scramblase interacts with PS by hydrogen bonding and that the two urea groups bind to the two formaly charged phosphate oxygen atoms. An electrostatic interaction between the ammonium cation of the scramblase and the carboxylate anion in PS also leads to their association.

Scheme 13. Phosphatidylserine (left) and its artificial scramblase (right).

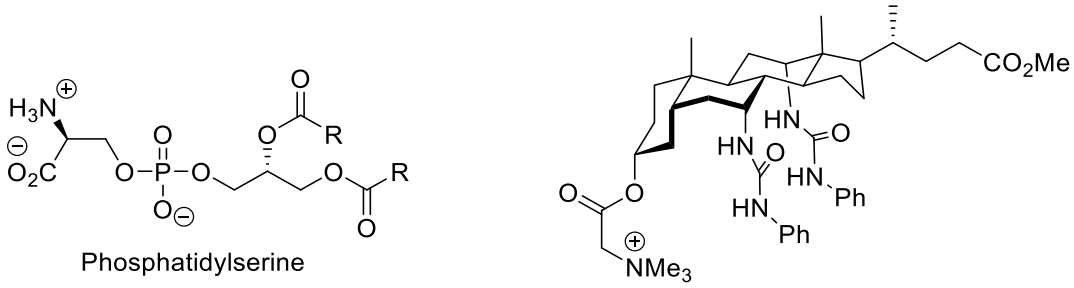

In addition to blood coagulation enhancement, other applications were proposed for scramblases. A dipicolylamine-zinc-derived complex (Scheme 14, left) showed high activity against the Gram-positive bacterium *S. aureus*, which are resistant to the antibiotics vancomycin and oxacillin, and low toxicity against mammalian cells.[54] The mechanism of differentiation was ascribed to the fact that the outer surface of mammalian cell membranes are mostly constructed of zwitterionic phospholipids, whereas the microbial one has a substantial amount of anionic phospholipids. Due to the ability of scramblases to bind phosphate anions (see Scheme 4), it induces the transport of negatively charged

phospholipids to the inner surface of the bilayer and depolarizes the bacterial cell membrane thereby disrupting its functions.

Scheme 14. Phospholipid binding antibacterial compound (left) and microbial and tumor imaging agent (right).

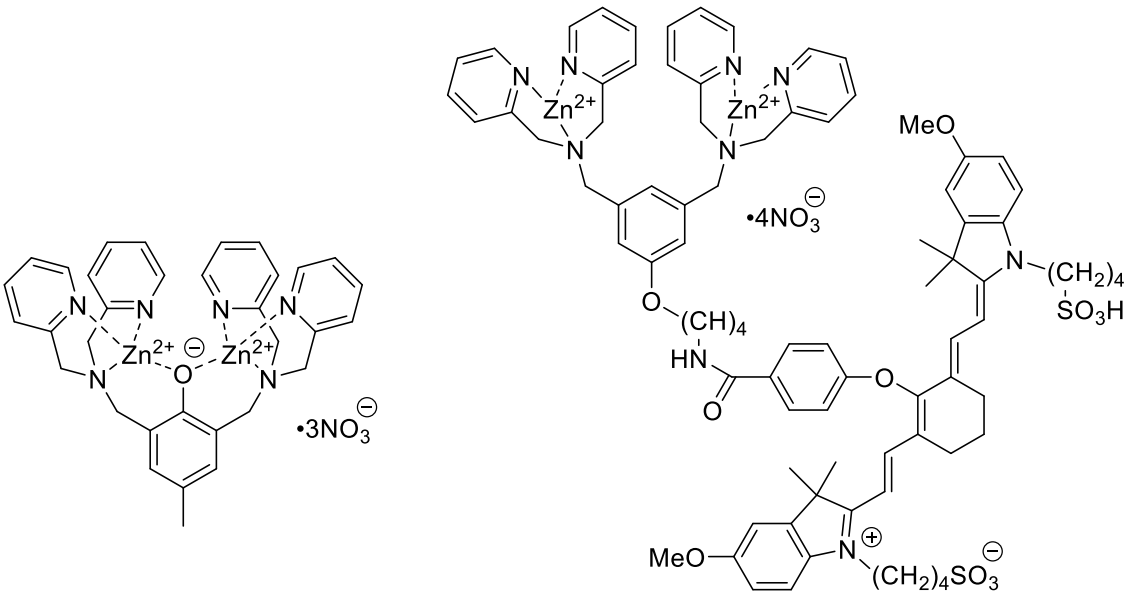

A similar compound with a chromophore attached (Scheme 14, right) was used for fluorescent imaging of bacterial infections[55] and tumors[56] in living mice. In both cases, accumulation of the imaging agent is based on its interaction with negatively charged phospholipid molecules in the outer layer of bacterial or necrotic tumor cells. In the latter case, the negatively charged PS molecules appear on the surface due to apoptosis.

In conclusion, anion transporters are promising candidates for the treatment of "channelopathies" – diseases associated with dysregulation of anion transport through cell membranes, and can also serve as antibiotics, anticancer drugs, and blood coagulants.

Chloride transporters have received the most attention to date, but the transport of phosphate, bicarbonate and other anions is also crucial for living organisms and presumably will also be harnessed for therapeutic applications. For an anion transporter to be developed into an oral drug, it needs to possess strong binding to the anion of interest, optimal lipophilicity for maximal transport efficiency and obey "the rule of five".

Other therapeutic applications

Sapphyrins are pentapyrrole porphyrin-like macrocycles (Scheme 15), and are singlet-oxygen producing photosensitizers. These compounds have attracted significant attention due to their ability to selectively accumulate in cancerous cells and catalyze the photo-cleavage of DNA.[57] Sessler *et. al.* studied the binding properties of the monoprotonated

Scheme 15. Sapphyrin, a strong phosphate binder possessing anticancer activity.

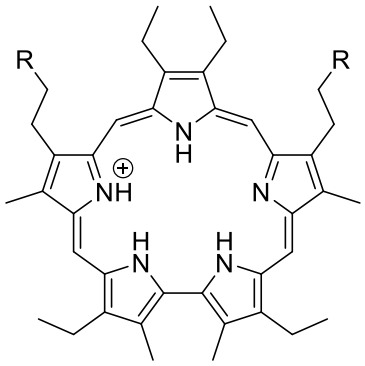

forms of these compounds to various anions.[58] Phosphate, mononucleotides, and DNA were all found to bind strongly, and in the last instance this was proposed to play a critical role in the photocleavage event.

Anion receptors for selective extraction

Extraction of anions may be useful for removing toxic, interfering or otherwise hazardous species from waste water.[59] For example, it was proposed that the radioactive waste from nuclear weapons production could be disposed by incorporation in transportable glass "logs" (i.e., vitrification), but the nitrate rich waste contains small amounts of sulfate that interferes with this process.[60] Its extraction is particularly difficult due to the very high hydration energy of SO_4^{2-}.[61] Nevertheless, Bowman-James *et al.* designed receptors (Scheme 16) that enabled aqueous solutions of sulfate to be extracted into an organic solvent in the presence of the much more lipophilic nitrate anion.[62] These

Scheme 16. Receptors for selective sulfate extraction.

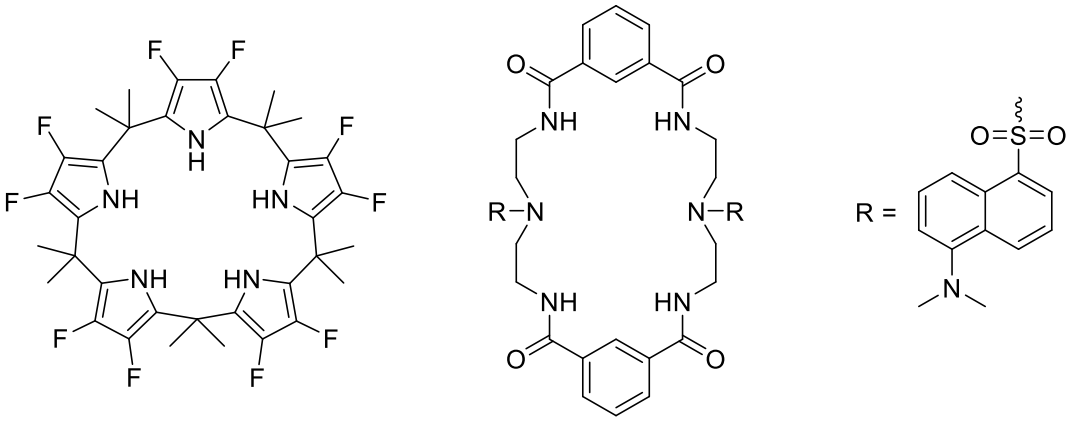

receptors bind sulfate strongly due to multiple hydrogen bond interactions and were used together with a lipophilic ammonium salt to extract sulfate (^{35}S-labelled) into chloroform and toluene even in the presence of a 100-fold excess of nitrate.

Another tetrahedral anion, pertechnetate (i.e., TcO_4^-), is the most stable form of the radioactive isotope ^{99}Tc produced in nuclear waste from fission of ^{235}U and ^{239}Pu (it comprises 6% of the total fission product yield).[63] Due to its long half-life ($t_{1/2} = 2.13 \times 10^5$ years), high mobility in the superficial layers of the Earth's crust, and ease of entering the food chain, it is one of the most dangerous radioactive pollutants known. An artificial receptor that can extract or separate this anion from nuclear waste consequently would be of considerable value. Due to the relatively large size of TcO_4^- and the diffuse charge density it is particularly difficult to design a receptor for this soft base. Beer *et al.* nevertheless reported a neutral receptor capable of extracting pertechnetate.[64] Conditions simulating nuclear waste were used and when the sodium nitrate rich aqueous solution at pH = 11 was treated with a dichloromethane solution of a tripodal receptor (Scheme 17, left), 70% of the TcO_4^- was extracted. Recently, Amendola *et al.* made further progress in the field by discovering a receptor for TcO_4^- in aqueous solution.[65] The hexaprotonated form of an azacryptand receptor (Scheme 17, right) was found to encapsulate TcO_4^- efficiently ($K = 3.2 \bullet 10^5\ M^{-1}$) in water at pH = 2.0. Moreover, high selectivities over nitrate and chloride were observed.

Scheme 17. Pertechnetate anion receptors; tripodal amide used for extraction (left) and an azacryptand that binds in aqueous solution (right).

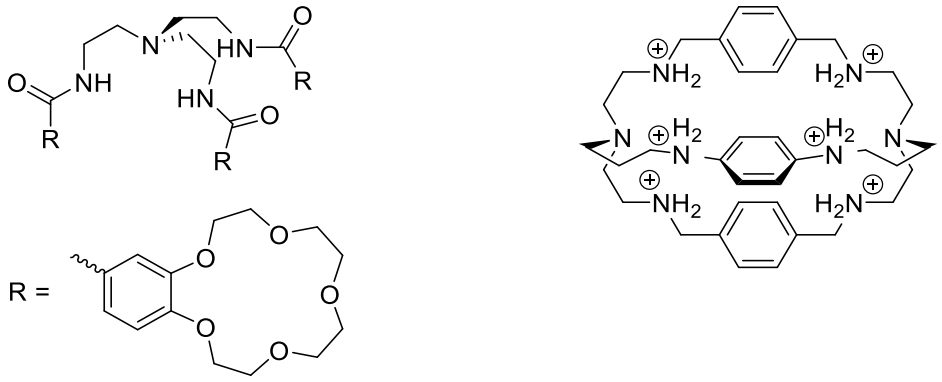

Anion receptors as part of ion-pair receptors

Ion pair receptors combine anion and cation recognition sites in their molecular structure.[66] These compounds, just like anion receptors may be used for the analytical detection of anions, anion transport, salt extraction or solubilization, but the countercation will participate in all of these processes. In addition, ion-pair receptors can be used for zwitterion recognition. An advantage of dual binding of an anion and cation over typical anion receptors is that the former tend to have larger binding affinities because of the electrostatic attraction to the counterion.

An example of the use of an ion-pair receptor for extraction of radioactive pertechnetate anion was given above (Scheme 17, left). The analogous receptor without the crown ethers (not shown) has the same binding affinity to Bu_4N^+ TcO_4^- as the ion-pair receptor, but the latter has a 20 fold stronger binding and a 2.4 fold higher selectivity over Cl^- for the sodium

salts. This is presumably due to electrostatic interactions and structural reorganizations of the ion-pair receptor after complexation with Na^+. As a result, the ion-pair receptor showed a much higher distribution coefficient of TcO_4^- between a 2.35 M aqueous $NaNO_3$ solution and dichloromethane compared to its analog without the crown ethers (2.3 *vs.* 0.1).

Sessler *et al.* prepared a polymeric material capable of capturing alkali halides from water.[67] The methyl methacrylate-based copolymer (Scheme 18) containing crown ether and calix[4]pyrrole units for cation and anion binding respectively, extracts KF and KCl from aqueous solutions into methylene chloride. Interestingly, KCl is extracted much more efficiently than NaCl, suggesting possible applications, such as treatment of hyperkalemia, a dangerous condition involving elevated serum potassium concentrations.

Scheme 18. Polymeric material for KCl extraction.

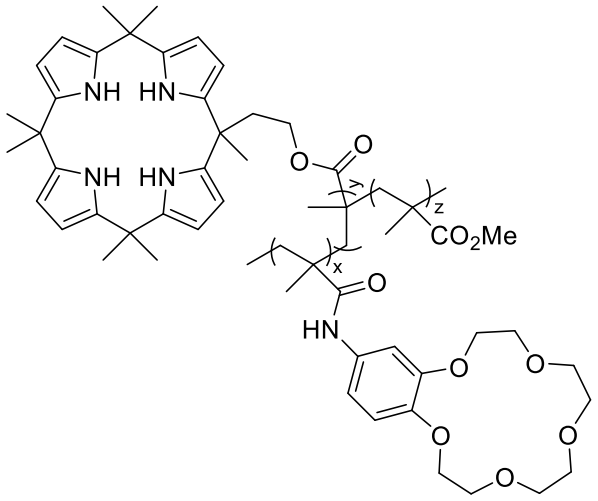

Another example of cooperative binding was given by Kubo *et al.* who studied diphenyl phosphate binding to a thiourea-containing crown ether (Scheme 19, left).[68] Addition of

potassium cation increases the binding to diphenyl phosphate by 19 fold in acetonitrile presumably due to the conformational change of the crown ether upon complexation of the cation and some electrostatic stabilization. In a similar study, Kim *et al.* investigated a fluorescent calix[4]arene-based receptor (Scheme 19, right).[69] Due to a lack of binding, the free receptor displays negligible changes in its fluorescence spectrum upon addition of

Scheme 19. Ion-pair receptors for potassium diphenyl phosphate (left) and potassium dihydrogen phosphate (right). Reproduced from ref. 66.

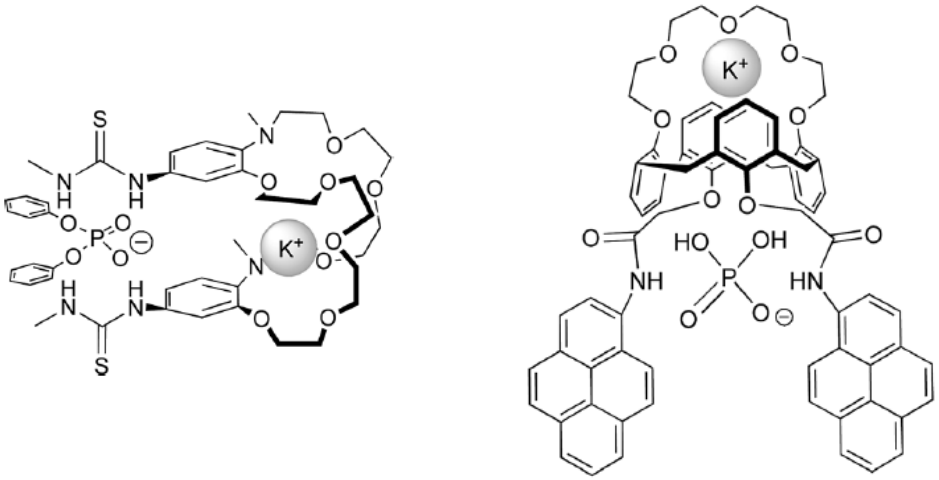

anions, but this situation changes when K^+ is added. Complexation to K^+ induces conformational changes in the receptor that enable better interaction between the two pyrenyl groups and cause an increase in fluorescence. Due to electrostatic interactions with the bound K^+, subsequent complexation of $H_2PO_4^-$ to the amide groups via hydrogen bonding becomes favored. It increases the distance between the pyrenyl groups and causes

a decrease in fluorescence back to the free receptor level. This behavior mimics a 2-bit INHIBIT logic gate (i.e., "on" for one input (K^+) and "off" for two inputs ($K^+ + H_2PO_4^-$)).

Conclusion

The most important applications of anion receptors were outlined. Although, the abilities of these compounds to bind anions and/or transport them through cellular membranes are already being used for sensing anions and treating cancer, improvements such as increasing detection selectivity and/or biological activity and compatibility are still desired. Other applications in medicine and environmental chemistry still need to be developed for practical use. Utilizing hydrogen bonds to bind anions has proven to be an excellent strategy for designing ionophores in ion selective electrodes, artificial anion transporters for medicinal applications, and reagents for anion extraction. The specific compounds were often designed just as anion receptors first, but then their molecular structures were modified for a particular application. Exploring new hydrogen bond donor receptors is thus an important area of chemical research, as it may lead to applications in the areas of human health and the environment.

Chapter 7: Functionalized 1,3,5-triphenylbenzene as a selective receptor for dihydrogen phosphate in aqueous solutions

Introduction

Phosphate is an essential anion in living organisms. Its derivatives are incorporated in energy storage molecules (ATP), genetic information storage (DNA and RNA), cell membrane phospholipid bilayers and skeletal bones. They take part in cell signaling as well as serving as a buffer in serum and urine.[1] Serum phosphate concentrations are regulated by the parathyroid hormone, and excess amounts are removed by the kidneys. Abnormal phosphate levels usually indicate kidney or parathyroid gland problems, or a vitamin D imbalance.[2] All of these issues require treatment and effect a large number of people (i.e., according to the U.S. Department of Health and Human Services, over 10% of Americans have some level of chronic kidney disease, and over 100,000 people in the U.S. develop primary hyperparathyroidism each year).[3] Consequently, routine monitoring of phosphate levels is very important and would be carried out on every blood sample drawn if a suitable method were available. To put this in perspective, chloride is monitored in each blood sample because there is a suitable method for this anion, and millions of such analyses are carried out each year in the U.S. Phosphate is currently measured using a colorimetric method discovered over 40 years ago.[4] Beckman Coulter among others produce a number of analyzers for quantifying inorganic phosphate in serum and urine. According to this company's manual, the devices provide high precision, but certain improvements such as

eliminating the use of H_2SO_4 (a strong and corrosive acid), increasing the lifetime and storage temperature of the reagent (which currently needs to be refrigerated and only lasts 30 days), expanding the linearity range, and lowering the cost are needed. Maybe most significantly, the current method is slow, making it incompatible with real time measurements and unsuitable for routine blood determinations.

Phosphate is also a common component of fertilizers, detergents and medicinal drugs. Pollution due to this anion is known to cause eutrophication (i.e., the ecosystem response to excess nutrients) in natural water sources, including an increase in green or blue algal blooms with toxin-producing cyanobacteria strains that threaten other aquatic organisms and drinking water safety.[5] According to EPA information, at least one-third of the 123,000 U.S. lakes that are 10 acres or more in size contain cyanobacteria. In fact, in some lakes such as Lake Erie, the eutrophication is so massive that it can be seen from outer space. Consequently, phosphate and its derivatives need to be monitored in waste products and natural waters at concentrations of ≥ 0.01 mg/L. Even at this low concentration, this anion can cause dramatic changes in streams.[6] The currently EPA-approved method for measuring this ion utilizes an ascorbic acid modification of the colorimetric method noted above. This slow procedure (i.e., manual mixing of reagents followed by a 10 minute waiting period) is problematic for field measurements and, as already noted, is not useful for real time sampling.

A solution to these problems is to develop a phosphate ion-selective electrode (ISE). ISE's are typically easy to use, can be reused multiple times and provide quick responses. They also have long lifetimes and low costs (see Chapter 6). These qualities make this

approach desirable for use in health care clinics, field studies and industrial monitoring of environmental conditions. To implement this method a dihydrogen phosphate receptor (the ionophore) is needed. Due to the high hydration energy and low basicity of phosphate, however, it is a challenge to achieve selectivity over common interfering anions such as Cl^- (which is more lipophilic) and OAc^- (which is more basic).[7] Although a few selective phosphate receptors are known and some examples were given in the Chapter 6, all of them are positively charged and cannot be used as ionophores in ISEs, since any non-bound counteranion would rapidly exchange with ions in solution. As a result, no adequate phosphate ISE has been developed to date. This is undoubtedly the reason why phosphate measurements are not routinely carried out on every blood sample.

According to the U. S. Department of Health and Human Services over 871,000 people in the U. S. in 2009 were treated for end stage renal disease, also known as the fifth stage of the already mentioned chronic kidney disease. These people suffer from total and permanent kidney failure, a condition that, among others, results in hyperphosphatemia (i.e., high serum phosphate concentrations).[8] Hyperphosphatemia is the major problem for people with this disease, as it increases the rate of death from cardiovascular events[9] and causes bone and joint destruction.[10] Phosphate binders are used to reduce phosphate levels.[11] Current methods of treatment include ingesting relatively large amounts of ion exchange resins (i.e., 8 g a day or the equivalent of forty 200 mg pills).[12] The extraction of phosphate from the intestines with the currently employed resins such as Sevelamer (Scheme 1) is not efficient enough to decrease the serum phosphate level to $\leq$ 5.5 mg/dL as recommended by the National Kidney Foundation, and combinations with calcium

binders raise a risk of hypercalcemia.[13] Concentrations typically plateau at ca. 6.5 mg/dL upon treatment with Sevelamer, and it takes a month long period to reach this rather high level.[14] Consequently, more efficient binders are required. To increase the efficiency and decrease the dose of the drugs, higher binding selectivity is needed. In particular, selectivity over acetate and other fatty acid anions that represent over 90% of the total intra-intestinal anion concentration is required.[15] Incorporation of a selective and strong phosphate binder together with a potassium binder (i.e., the most abundant cation in the intestine) in a polymer matrix (Scheme 1, in analogy to the work by Sessler *et al.* represented in Scheme 18, Chapter 6) may provide a drug that would be much more efficient than Sevelamer.

Scheme 1. Sevelamer (left), a polyamine drug (amino-groups are partially protonated at physiological pH) for hyperphosphatemia treatment, and a possible alternative (right).

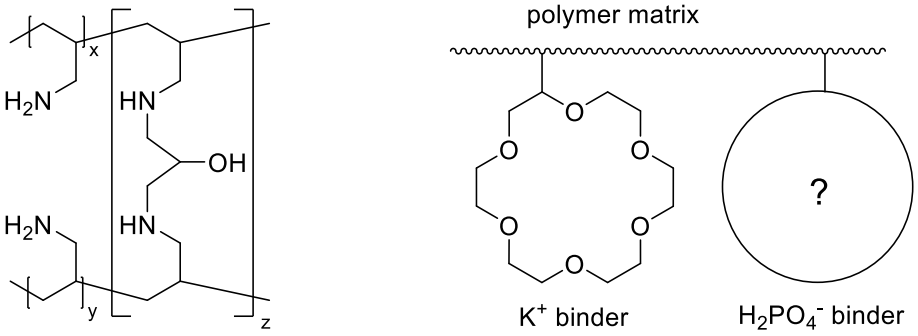

As indicated, both sensing and extraction applications require strong binding to phosphate and selectivity over acetate, so presumably receptors that possess these qualities could be utilized for both applications. Other useful properties of certain phosphate binders were discussed in Chapter 6 and include antibiotic and blood coagulant activities that are

due to targeting the phospholipids in the cellular membrane bilayer and scrambling their positioning in between the inner and the outer layers. All these important applications make the problem of designing a selective phosphate receptor of a high interest.

Different types of interactions have been used in developing anion receptors.[16] Electrostatic attraction or complexation to a metal may lead to strong binding, but often lack selectivity. Moreover, charged ionophores are not suitable for use in ISE. Utilizing more directional interactions, such as hydrogen bonding, in principle allows one to adjust the binding pocket of the receptor to the size and shape of the anion of interest, thus providing a more selective binding reagent.

During our investigation of hydrogen bond donors based on a 1,3,5-triphenyl benzene core, we were inspired by the work of Tobe *et al.*[17] and decided to explore the corresponding tris-thioureas as plausible anion receptors (Scheme 2). Herein we report our

Scheme 2. Comparison of the literature report and our work.

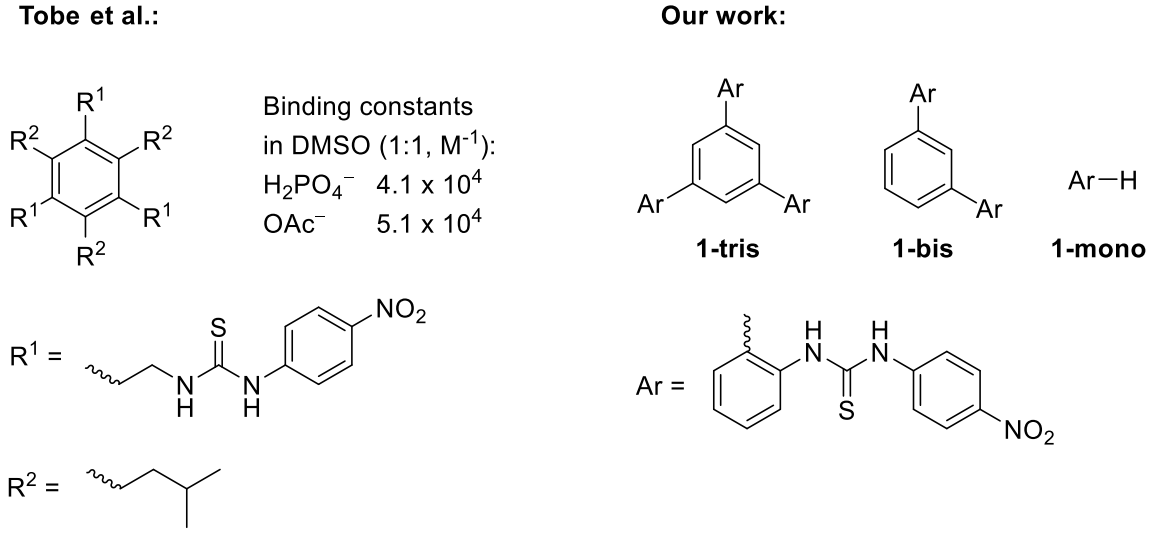

findings with 4-nitrophenyl derivative **1-tris**. In order to see the influence of each consecutive thiourea arm on binding we studied analogs **1-bis** and **1-mono** with two and one arm, respectively.

Results and discussion

Synthesis: The synthesis of the bis-amine (**4-bis**) precursor to **1-bis** was previously reported and was carried out by coupling 1,3-dibromobenzene with the pivaloyl-protected 2-aminophenylboronic acid and then deprotecting both amine groups (Scheme 3). We used the same procedure to prepare **4-tris**, and the resulting amines **4** were easily converted into

Scheme 3. Synthesis of receptors **1** and **2**.

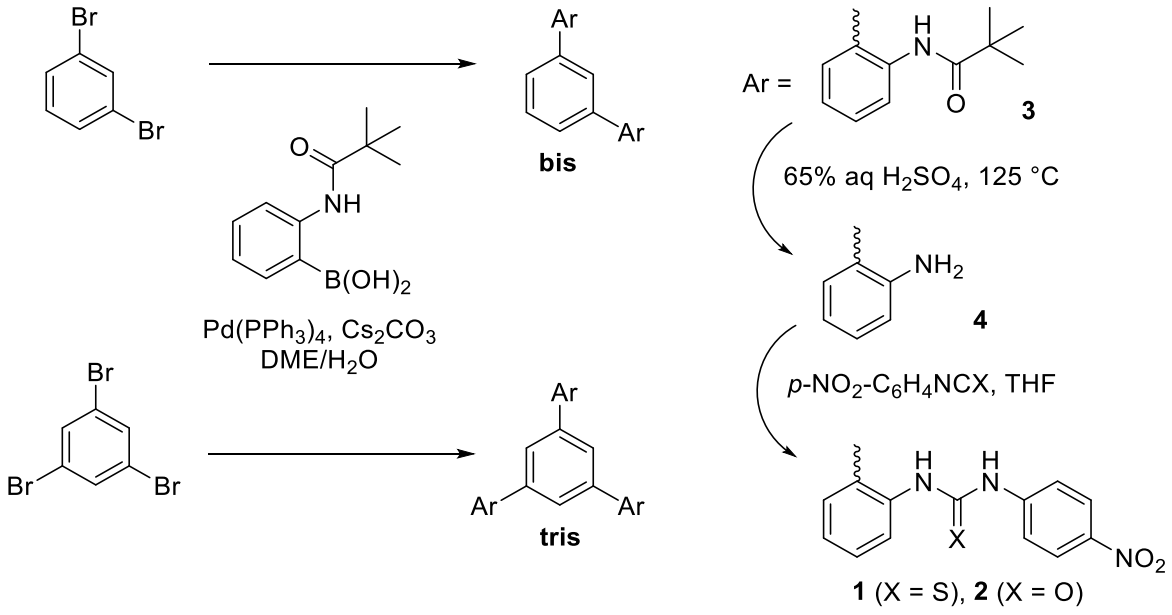

their corresponding thioureas (**1**) upon reaction with *p*-nitrophenylisothiocyanate. Alternatively, the trisurea (**2-tris**) was made by utilizing *p*-nitrophenylisocyanate.

Anion binding studies: To probe the hydrogen bonding interactions of thioureas with anions, clusters of **1-tris**, **1-bis** and **1-mono** with dihydrogen phosphate ($H_2PO_4^-$), acetate (OAc^-) and chloride (Cl^-) were examined in the gas phase by negative ion photoelectron spectroscopy. The adiabatic detachment energies (ADEs) were assigned from the rapidly rising onset region of the spectra and were found to follow the following trend: ADE(**1-mono**) < ADE(**1-bis**) < ADE(**1-tris**) (Table 1). Thus, each new thiourea arm provides additional stabilization due to more hydrogen bonding.

Table 1. Adiabatic detachment energies (eV) for anion clusters of **1** in the gas phase.[a]

Anion	Free anion[b]	**1-mono**	**1-bis**	**1-tris**
$H_2PO_4^-$	4.57 ± 0.01	4.64	5.25	5.38
OAc^-	3.38 ± 0.05	4.50	5.10	5.54
Cl^-	3.61	4.75	5.25	5.64

[a] Estimated uncertainties are 0.1 eV. [b] See ref. 18.

The ADEs can not be used to compare the hydrogen bonding energies of the anion clusters, however, because they are also dependent on the stabilization energies of the corresponding radical clusters. Interestingly, the ADE of the $H_2PO_4^-$ cluster of **1-mono** is within the experimental error of that for the free anion. This indicates that **1-mono** interacts with

$H_2PO_4^{\bullet}$ as strongly as it does with $H_2PO_4^-$. This is unprecedented and different than for OAc^- and Cl^-, who's ADEs are significantly lower than for their **1-mono** clusters. Given that the bond dissociation energy of $H–OPO_3H_2$ is greater than those for H–OAc and H–Cl (i.e., 122 > 113 > 103 kcal/mol) it is reasonable to expect that dihydrogen phosphate radical would interact with the thiourea more strongly than the other two radicals and thus have the smallest ADE difference between the free anion and its cluster.

Interactions of thioureas with dihydrogen phosphate and acetate in 0.5% wet DMSO (*v/v*) were studied by UV-visible spectroscopy. All the thiourea compounds showed a broad band with $\lambda_{max} \approx 356$ nm. Addition of $H_2PO_4^-$ and OAc^- caused changes in the spectra in the range of 300-500 nm, and the wavelength with the largest change in absorption was used for binding analyses (see below for details). Job plots indicated a 1:1 binding stoichiometry for both anions, but also a consecutive 1:2 binding with OAc^-. Titrations with $H_2PO_4^-$ in the 0–1 equivalent range caused absorption changes that were linearly dependent on the anion concentration, indicating quantitative complexation and very strong 1:1 binding. Further addition of $H_2PO_4^-$ caused smaller but still significant increases in absorption, and altogether the spectral changes did not fit a 1:1 binding curve. It was concluded that at least two processes must occur. That is, very strong 1:1 binding takes place first and is followed by deprotonation of the **1-tris**-bound $H_2PO_4^-$ cluster by the additional $H_2PO_4^-$. The resulting products are H_3PO_4 and the **1-tris**-bound HPO_4^{2-} cluster, which is analogous to a similar example previously reported (see experimental for details, Scheme S1).[19] Given that the titration plot is linear, we estimate that at least 89% of **1-tris** is bound upon addition of 1 equivalent of $H_2PO_4^-$ (i.e., quantitative within the experimental

error). This indicates that the 1:1 binding constant is more than 5 x 10^6 M^{-1}, which is larger than for similar compounds reported by Tobe *et al.* (Scheme 1). We speculate that the bigger binding affinity of **1-tris** is due to its greater rigidity and the larger acidity of a N,N'-diaryl substituted thiourea compared to an N-alkyl-N'-aryl-derivative.

Addition of 1 equivalent of OAc^- or OH^- to **1-tris** leads to the same spectral changes (Figure 1, top; for clarity, spectral differences (i.e., ΔA) are provided). The absorbance was also linearly dependent upon the OAc^- concentration when 1.0 equivalent or less was used. These facts are consistent with irreversible deprotonation of **1-tris** upon addition of OAc^-.

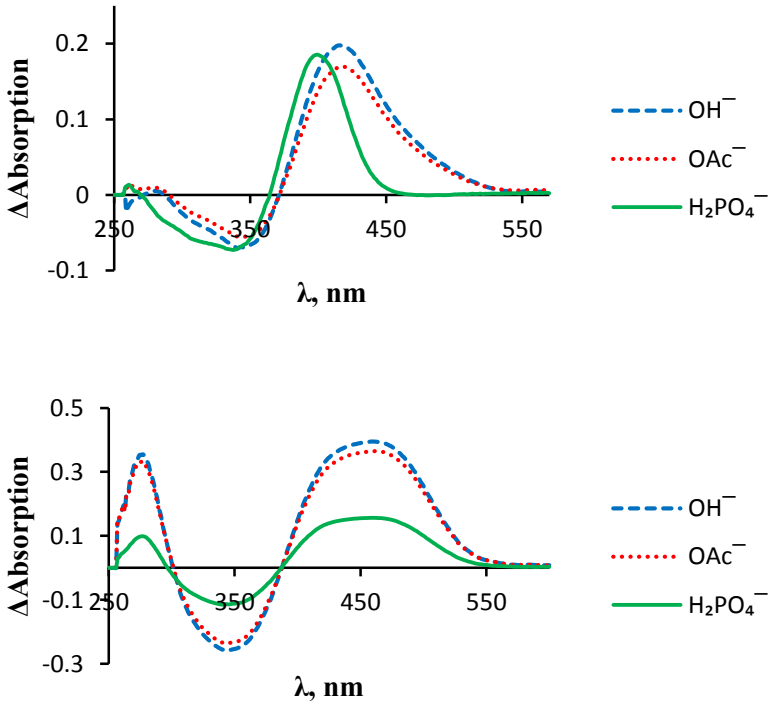

Figure 1. Absorbance changes upon the addition of 1 equivalent of Bu_4N^+ salts of OH^-, OAc^- and $H_2PO_4^-$ to **1-tris** (15 μM, top) and **1-mono** (30 μM, bottom) in 0.5% wet DMSO (*v/v*).

In contrast, $H_2PO_4^-$ leads to a narrower band with its maximum at a different wavelength, which indicates that a different type of interaction is taking place. Deprotonation of **1-mono** also takes place with OAc^- (Figure 1, bottom) and one equivalent of dihydrogen phosphate leads to similar but smaller (i.e., 39%) changes as those observed with hydroxide ion. This suggests that proton transfer takes place in this case too. The formation of the conjugate base of **1-mono** and phosphoric acid does not fit the data, but they are in accord with a 1:1 complex and afford a binding constant of $K = 4.0 \times 10^4\ M^{-1}$. This value is significantly smaller than for **1-tris** binding and suggests that at least two of the thiourea arms participate in the **1-tris**–$H_2PO_4^-$ complex. The bisthiourea (**1-bis**) behaves similarly to its mono and tris derivatives with acetate ion. That is, the spectra resulting from addition of 1 equivalent of $Bu_4N^+\ OAc^-$ and $Bu_4N^+\ OH^-$ are the same (Figure 2, top) indicating that deprotonation takes place. The smaller band in all three cases provides an estimated pK_a value for the thioureas that is 2 pK_a units less than for acetic acid in 0.5% wet DMSO (*v/v*). The addition of multiple equivalents of $H_2PO_4^-$ led to a change in the isosbestic point (i.e., the wavelength where the molar absorptivities of the free and the bound species are the same, or the x-intercept in the spectral differences plot; Figure 2, bottom) from 370 to 378 nm. These spectral changes indicate that at least two processes are taking place, and although their nature requires further investigation, it is clear that all three thioureas show different behavior with $H_2PO_4^-$. That is, **1-tris** produces very strong binding utilizing all three thiourea arms, **1-mono** shows much weaker binding presumably with proton transfer, and **1-bis** appears to undergo competitive bindings with and without proton transfer.

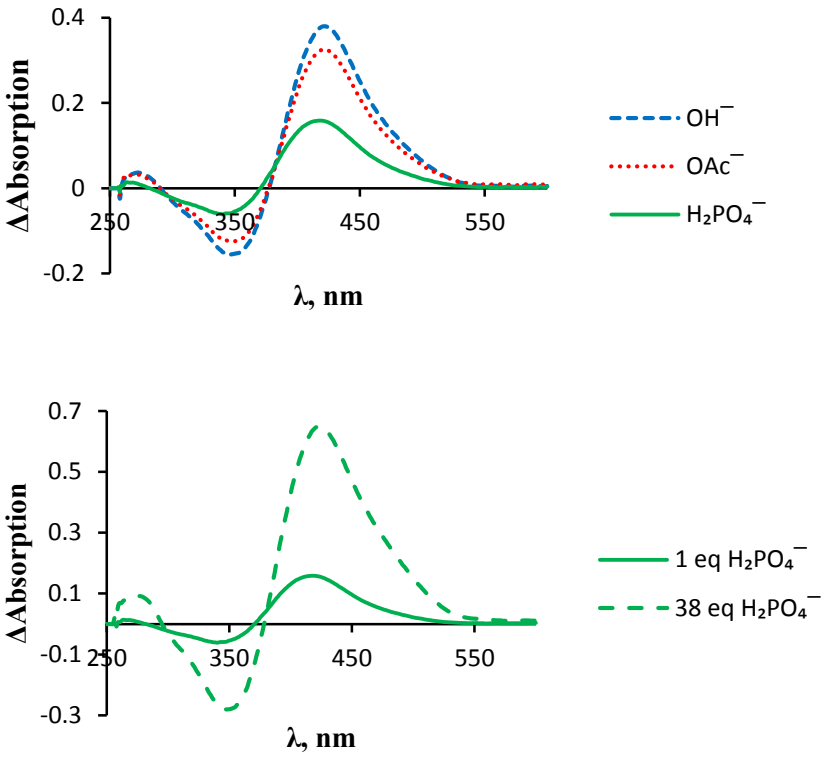

Figure 2. Absorbance changes of **1-bis** (15 μM) upon the addition of 1 equivalent of Bu_4N^+ salts of OH^-, OAc^- and $H_2PO_4^-$ (top), and 1 and 38 equivalents of $Bu_4N^+H_2PO_4^-$ (bottom) in 0.5% wet DMSO (*v/v*).

The pK_a values of **1** are unknown but we estimate that $pK_a \leq 8$ in all three cases. This is based on a correlation between the known pK_a's of a series of anilines[20] and thioureas[21] (Scheme 4). This is consistent with OAc^- (pK_a(AcOH) = 12.3) deprotonating **1**. It is unlikely that **1-mono** is more acidic than H_3PO_4 (estimated $pK_a \approx 4$)[22], but proton transfer in the **1-mono** • $H_2PO_4^-$ cluster could still occur due to the possibility of three hydrogen bonds in the resulting complex compared to only two when proton transfer does not take place (Scheme 4, bottom).

Scheme 4. Prediction of **1-mono** pK_a value in DMSO, and proposed structures for the proton transfer complexes of **1-mono** with OAc^- and $H_2PO_4^-$.

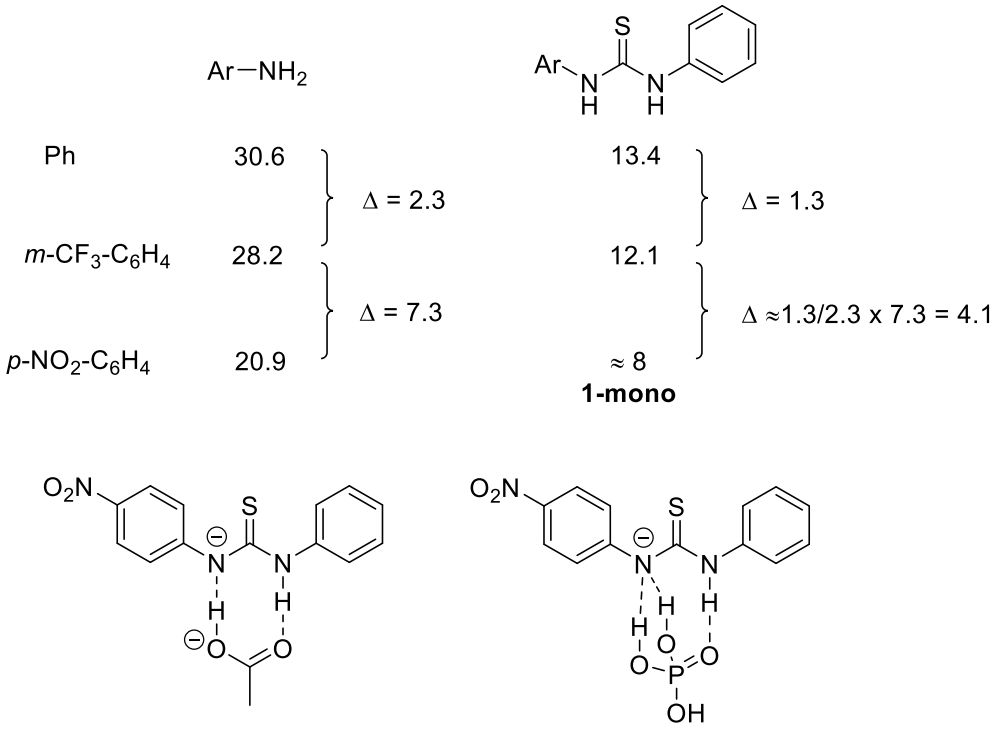

Additional support for the deprotonation of **1** was obtained from IR spectra. Interaction of **1-mono** with OAc^- led to two new bands at 1714 cm^{-1} and 1628 cm^{-1} in the C=O region upon addition of 1.5 equivalents of OAc^- to **1-mono** in DMSO-d_6. These features are assigned to free AcOH and a 1:1 AcOH–thioureido anion complex, respectively (Figure 3).

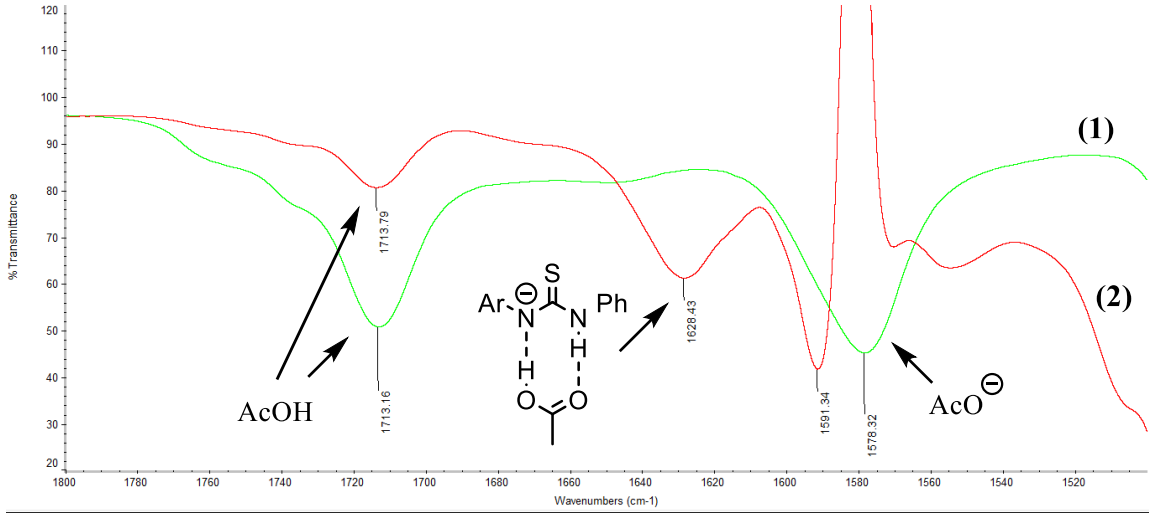

Figure 3. An 1800–1500 cm^{-1} IR spectra expansion of **(1)** AcOH and Bu_4NOAc (each 60 mM), and **(2) 1-mono** and Bu_4NOAc (60 and 90 mM, respectively). Spectra were recorded in DMSO-d_6 solutions in a 0.1 mm NaCl cell. The solvent and the Bu_4NOAc solution (90 mM) were used as the background for **(1)** and **(2)**, respectively.

The acidities of ureas are typically 5-6 pK_a units lower than those of the corresponding thioureas,[20] thus **2-tris** is expected to be significantly less acidic than **1-tris**. Upon addition of $H_2PO_4^-$ or OAc^- to **2-tris**, different spectral changes (Figure 4) than those brought about

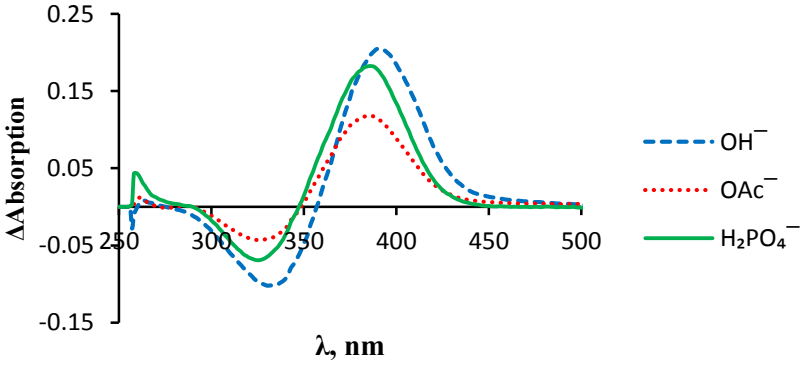

Figure 4. Absorbance changes of **2-tris** (15 μM) upon the addition of 1 equivalent of Bu_4N^+ salts of OH^-, OAc^- and $H_2PO_4^-$ in 0.5% wet DMSO (*v/v*).

by OH^- were observed. This indicates that neither $H_2PO_4^-$ nor OAc^- deprotonates **2-tris**, as expected from its lower acidity. Titration experiments showed that binding constants are too high to measure (i.e., $K \geq 5 \times 10^6\ M^{-1}$).

Since the binding affinity of **1-tris** to $H_2PO_4^-$ was very strong in 0.5% wet DMSO (*v/v*), we decided to study anion complexation in more competitive environments with higher water content. To our delight, we observed a relatively strong binding of 4000 M^{-1} to $H_2PO_4^-$ in 25% aqueous DMSO (*v/v*). The wavelength of maximal spectral difference upon addition of OAc^- shifted from 415 nm in 0.5% DMSO–H_2O to 379 nm in 25% DMSO–H_2O (Figure 5), whereas for $H_2PO_4^-$ and OH^- it did not move significantly. This indicates that the interaction with OAc^- is different, and we attribute this to binding rather than deprotonation. A single reciprocal linear least squares fit of the data give $K = 35\ M^{-1}$, and thus the $H_2PO_4^-/OAc^-$ selectivity is more than 100. To our knowledge, such a high selectivity has not been reported in an aqueous solvent. Moreover, the binding affinity of

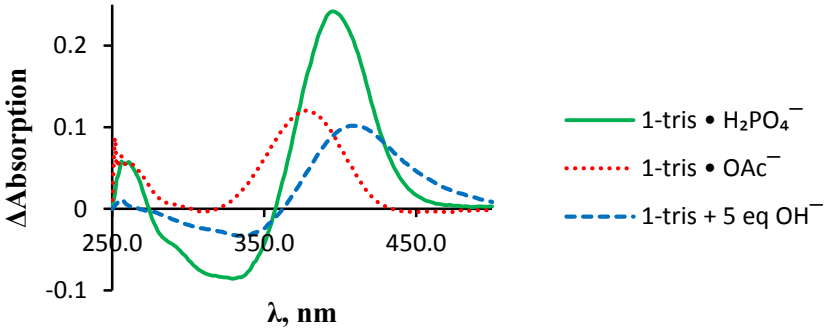

Figure 5. Absorbance changes of **1-tris** (15 μM) upon the addition of Bu_4N^+ salts of OH^-, OAc^- and $H_2PO_4^-$ in 25% aqueous DMSO (*v/v*). In case of OAc^- and $H_2PO_4^-$, ΔA_{max} are plotted (i.e., $\Delta A = A_{max} - A_0$, where A_{max} is the calculated absorption of the bound species).

1-tris to $H_2PO_4^-$ in aqueous DMSO is stronger than previously reported for any neutral receptor in this solvent mixure. This is important because neutral receptors can potentially be used as ionophores in ion-selective electrodes. Another, important anion, Cl^- showed essentially no binding to **1-tris** in this solvent mixture (i.e., K = 1.5 M^{-1}).

Additional DMSO–H_2O mixtures ranging from 0.5 to 30% water were investigated (Table 2). Interestingly, we found the logarithm of the binding affinity to $H_2PO_4^-$ is linearly correlated with the water percentage in the solvent mixture (Figure 6). For acetate, deprotonation occurred when the water content was small (i.e., < 12.5%) as indicated by the spectral changes. At higher water contents (i.e., ≥ 25%), 1:1 binding was observed. These results indicate that the relative acidities of **1-tris** and AcOH change as the water content of the solvent mixture increases, and, contrary to the 0.5% DMSO–H_2O solution, AcOH is more acidic than **1-tris** in the 25% water mixture. In the intermediate water

Table 2. Binding affinities (1:1) of **1-tris** to $H_2PO_4^-$ and OAc^- in DMSO–H_2O mixtures.

% H_2O in DMSO (*v/v*)	K (M^{-1})	
	$H_2PO_4^-$	OAc^-
0.5	≥ 5 x 10^6	deprotonation
5	2.3 x 10^5	deprotonation
12.5	7.5 x 10^4	deprotonation
20	1.5 x 10^4	nd
25	4000	35
30	1400	13

content mixtures (i.e., $12.5 \leq x < 25\%$) the pK_a values of these two species are presumably close and, as expected, the experimental data suggests competition between deprotonation and binding. That is, for both 12.5% and 20% water mixtures, the wavelength of the largest absorbance difference (i.e., λ for the largest ΔA or $A - A_0$) gradually shifts to lower wavelengthes throughout the titration with $Bu_4N^+ OAc^-$. This indicates that deprotonation prevails at lower concentrations of OAc^- while binding increases with larger amounts of this anion because, as mentioned earlier, largest absorbance change is at λ = 416 nm for the former process, and at 379 nm for the latter one (i.e., 0.5% *vs.* 25% DMSO–H_2O mixtures). In the 12.5% DMSO–H_2O mixture the titration curve could be fit to a 1:1 binding isotherm with an apparent association constant of $K = 1.4 \times 10^5\ M^{-1}$, but the titration curve could not be fit in a 20% water mixture.

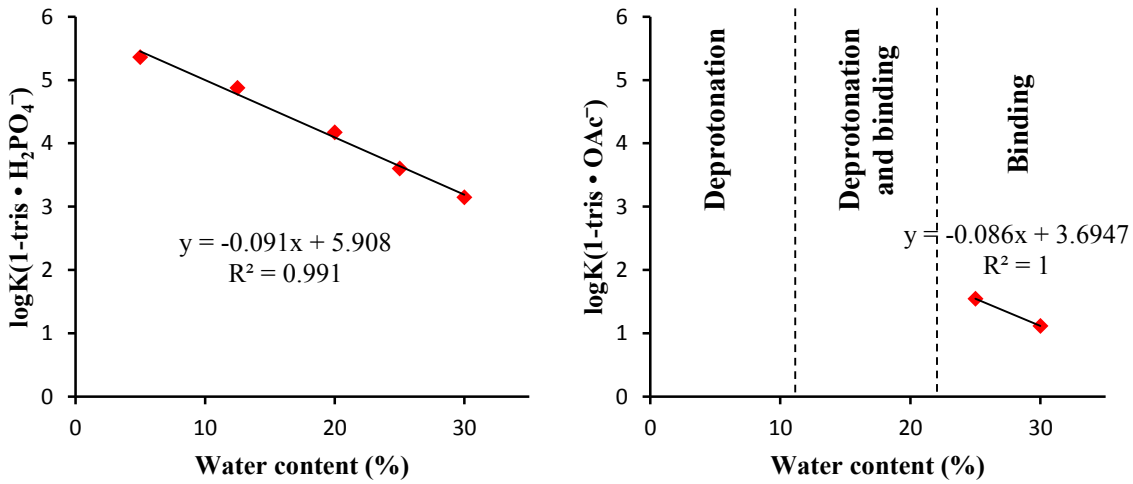

Figure 6. Logarithms of the binding constants of **1-tris** to $H_2PO_4^-$ (left) and OAc^- (right) versus the percent water in DMSO–H_2O mixtures.

Increasing the amount of water in the solvent has a similar effect on the interactions of the mono-thiourea (**1-mono**) with anions. The maximum in the spectral changes graph (i.e., $\Delta A(\lambda)$) upon addition of $H_2PO_4^-$ or OAc^- blue shifted to lower wavelengths in 25% DMSO–H_2O (Figure 7) compared to the 0.5% mixture (Figure 1, bottom), whereas for OH^- it is similar in both solvent mixtures. This observation indicates that in 25% aqueous DMSO, $H_2PO_4^-$ and OAc^- bind to **1-mono**, which supports the hypothesis of proton transfer to both of these anions in 0.5% wet DMSO.

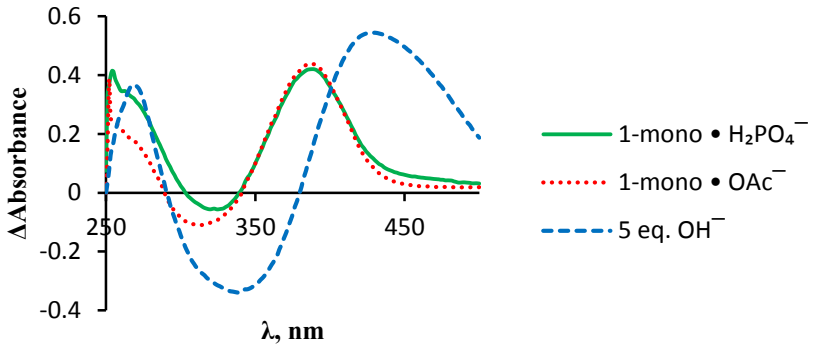

Figure 7. Absorbance changes of **1-mono** (60 μM) upon the addition of Bu_4N^+ salts of OH^-, OAc^- and $H_2PO_4^-$ in 25% aqueous DMSO (*v*/*v*). In case of OAc^- and $H_2PO_4^-$, ΔA_{max} are plotted.

Interestingly, a less acidic urea **2-tris** was found to bind to OAc^- stronger than *thio*urea **1-tris** (Table 3), which is in accordance with the previously reported tendency.[23] However, the binding affinity to $H_2PO_4^-$ is weaker for the urea compound, which gives a lower $H_2PO_4^-/OAc^-$ selectivity (i.e., 15-fold).

To establish the number of thiourea arms used to bind a specific anion, the mono, bis and tris-thiourea association constants were compared (Table 3). For OAc^-, **1-tris** only

binds this anion 3 times more strongly than **1-mono**, which is the statistically expected ratio if only one arm is used for binding. Likewise, $K_{\mathbf{1\text{-}bis}}/K_{\mathbf{1\text{-}mono}} = 2$ for $H_2PO_4^-$, indicating that one arm is used in this case too. The tris-thiourea, however, has an association constant that is more than 100-fold stronger than the statistical value (i.e., 36 M^{-1}) that would be expected if only one arm was used for binding. These results reveal that in 25% aqueous DMSO **1-bis** and **1-mono** use one arm for binding $H_2PO_4^-$ whereas **1-tris** uses all three.

Table 3. Binding constants (1:1, M^{-1}) of (thio)ureas in 25% aqueous DMSO (v/v).

Anion	**1-tris**	**1-bis**	**1-mono**	**2-tris**
$H_2PO_4^-$	4000	28	12	2300
OAc^-	35	nd	12	150
Cl^-	1	nd	nd	nd

To determine whether all six N–H bonds are used in the **1-tris** • $H_2PO_4^-$ cluster, we recorded the IR spectrum of this species and the free thiourea in DMSO-d_6 (Figure 8). The N–H stretches of **1-tris** are observed as a broad band at about 3000 cm^{-1}, which is significantly lower than literature values of thioureas in $CHCl_3$ solutions (i.e., 3450–3300 cm^{-1}).[24] This shift is presumably due to coordination of **1-tris** by the solvent. Upon addition of 1 equivalent of $H_2PO_4^-$ a new broad band at about 2700 cm^{-1} appears, but some residual absorbance besides the C–H stretches (e.g., 3160 and 3110 cm^{-1}) may still be present in the 3300–3000 cm^{-1} region. This could indicate that some N–H bonds are not interacting with

$H_2PO_4^-$ or that some of these interactions are comparable in strength with those to the solvent and therefore no apparent change is observed in the frequencies.

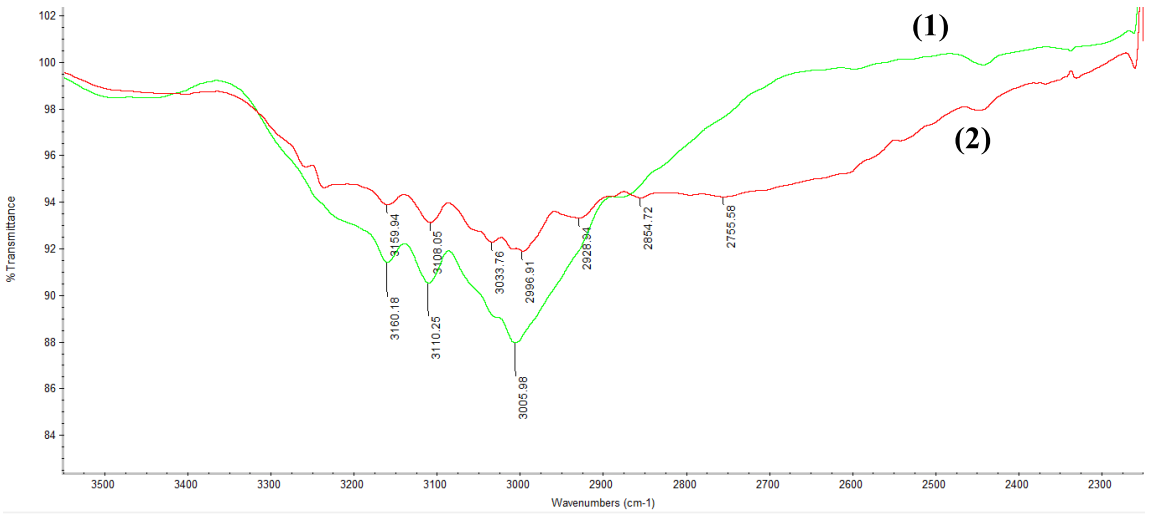

Figure 8. A 3550–2250 cm^{-1} IR spectra expansion of 10 mM **(1)1-tris** and **(2)** Bu_4N^+ $H_2PO_4^-$ • **1-tris** in DMSO-d_6 recorded using a 0.1 mm NaCl cell. The spectra were background corrected by subtracting the spectra of DMSO-d_6 **(1)** or of a 10 mM Bu_4N^+ $H_2PO_4^-$ solution in DMSO-d_6 **(2)**.

In conclusion, receptors **1** containing one, two, or three thiourea arms were synthesized, and their interactions with dihydrogen phosphate and acetate were studied in the gas phase and in solution. The tris-thiourea **1-tris** was found to bind very strongly to $H_2PO_4^-$ in 0.5% wet DMSO whereas deprotonation was observed with OAc^-; this was ascertained based upon predicted pK_a values, UV-vis and IR spectra. In 25% aqueous DMSO, it was found that OAc^- binds to **1-tris** with a weak affinity constant (i.e., K = 35 M^{-1}), whereas $H_2PO_4^-$ binds strongly (i.e., K = 4000 M^{-1}). This leads to a high $H_2PO_4^-/OAc^-$ selectivity (i.e., > 100 fold), something that has not been previously reported in aqueous solutions. As a result, the 1,3,5-triphenylbenzene core is a very promising platform for constructing dihydrogen

phosphate receptors. Analysis of the binding affinities of mono, bis, and tris-thioureas **1** showed that all three arms of **1-tris** are used to bind $H_2PO_4^-$ whereas only one is employed for OAc^-.

Analogs of 1-tris

We have synthesized derivatives of **1** with Ar = 3,5-$(CF_3)_2C_6H_3$ (**5-tris**, **bis**) and C_6H_5 (**6-tris**) (Scheme 5). These compounds have higher solubility in non-polar organic solvents

Scheme 5. Synthesis of the more soluble analogs of **1** (**5** and **6**).

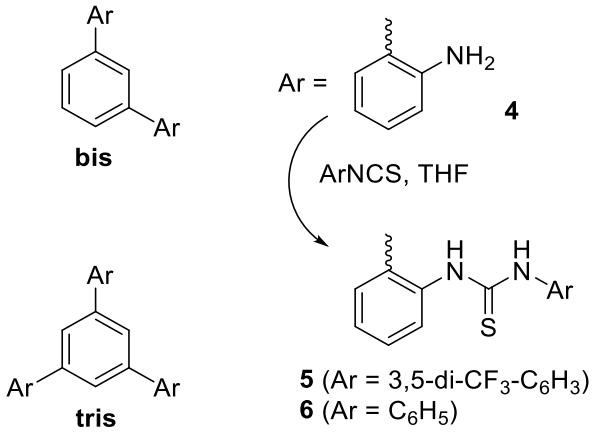

such as dichloromethane and could be investigated as ionophores for ISE, which typically utilize a non-polar polymer membrane. Binding affinities of the tris-thioureas **5-tris** and **6-tris** were found to be similar to those of **1-tris**. However, the uncertainties in the UV measurements are expected to be significantly higher due to a lack of absorption at $\lambda \geq 300$ nm. Thiourea **5-tris** was found to bind 2.5 fold stronger to $H_2PO_4^-$ in 25% aqueous DMSO

(*v/v*) than **1-tris** (i.e., K = 1.0 x 10^4 M^{-1}), whereas binding to acetate could not be measured due to the very small changes in the spectra upon addition of this anion.

Table 4. Binding constants (1:1, M^{-1}) of thioureas **5-6** in 0.5 wt % aqueous DMSO.

Anion	**5-tris**	**6-tris**
$H_2PO_4^-$	7.7 x 10^5	3.9 x 10^5
Cl^-	360	nd
$H_2PO_4^-$*	1.0 x 10^4	nd

* 25% aqueous DMSO (*v/v*).

Tris-oxalamide **7** was synthesized as an analog of urea **2-tris** (Scheme 6). Unfortunately, **7** proved to be a much weaker and less selective binder to $H_2PO_4^-$ (K = 900 M^{-1} for $H_2PO_4^-$ and K = 4.6 x 10^4 M^{-1} for OAc^- in 0.5% aqueous DMSO), but interestingly gives a new band in the visible spectrum upon addition of $H_2PO_4^-$ or OAc^- (λ_{max} = 432 nm), leading to a yellow solution.

Scheme 6. Synthesis of tris-oxalamide **7**.

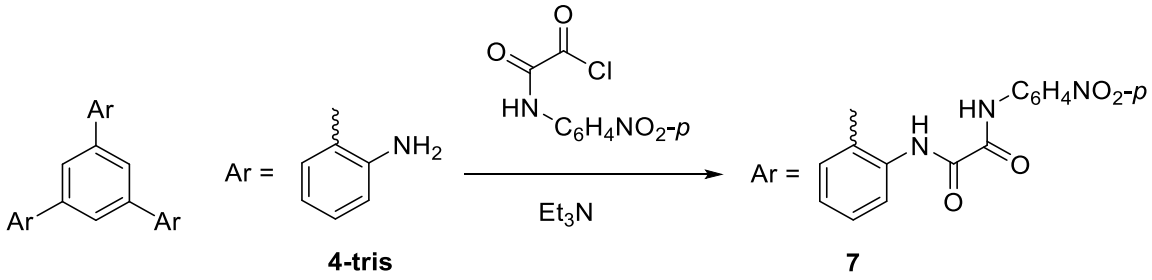

Thioureas **5-tris** and **5-bis** were found to be very soluble in non-polar organic solvents and were tested as catalysts in two reactions (Scheme 7) – the Fridel-Crafts transformation of β-nitrostyrene with *N*-methylindole, and the ring-opening reaction of styrene oxide with thiophenol in the presence of a base. Both of these processes were found to be catalyzed by **5**, but the difference between the two compounds was found to be small indicating that no more than two thiourea arms are used in these reactions.

Scheme 7. Catalytic reactions investigated with thioureas **5**.

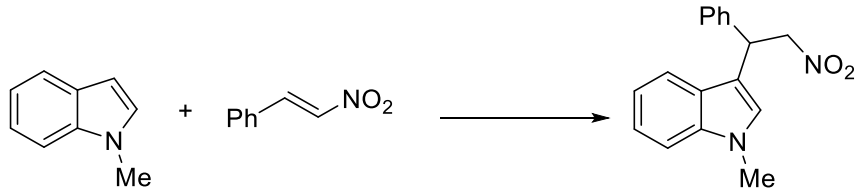

Catalyst	Reaction rate constants, $M^{-1}h^{-1}$ (23 °C)
5-tris	1.1×10^{-2}
5-bis	6.1×10^{-3}
Tris/bis	1.8
No cat.	3.5×10^{-5}

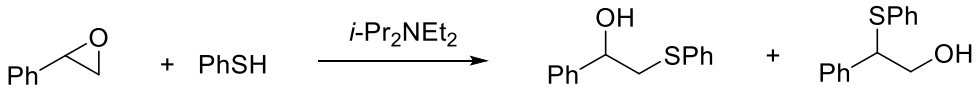

Catalyst	Rate constants of formation, $M^{-1}h^{-1}$ (23 °C)	
5-tris	7.2×10^{-2}	6.9×10^{-2}
5-bis	4.5×10^{-2}	3.4×10^{-2}
Tris/bis	1.6	2.0
No cat.	5.3×10^{-4}	2.2×10^{-4}

In conclusion, analogs of **1-tris** with CF_3 groups (**5-tris**) and non-substituted thiourea arms (**6**) were found to be more soluble in organic solvents. Moreover, **5-tris** showed a

higher affinity for $H_2PO_4^-$ in 25% aqueous DMSO (*v/v*) than **1-tris**. Both these qualities make **5-tris** a promising candidate as the ionophore in a phosphate selective electrode.

Experimental

1,3,5-tris(2-Pivaloylaminophenyl)benzene (3-tris). A round-bottomed flask was charged with 2-pivaloylaminophenylboronic acid[25] (2.66 g, 12.0 mmol), 1,3,5-tribromobenzene (945 mg, 3.0 mmol), cesium carbonate (9.78 g, 30 mmol), 1,2-dimethoxyethane (15 mL) and water (15 mL). Nitrogen was bubbled through the two layered solution with stirring over 10 min to remove oxygen from the system. Tetrakis(triphenylphosphine)palladium(0) (347 mg, 0.30 mmol) was then added and the reaction mixture was refluxed with vigorous stirring for 13 h under nitrogen. Ethyl acetate (50 mL) and water (20 mL) were added, both layers were separated, and the aqueous solution was extracted with EtOAc (20 ml). The combined organic material was washed with brine (10 mL), dried over Na_2SO_4 and concentrated under reduced pressure. Medium pressure liquid chromatography (MPLC) on silica gel of the residue with ethyl acetate : hexanes (15 : 85 to 67 : 33) afforded 1.47 g (81%) of **3-tris** as a white solid (R_f = 0.19 (EtOAc : hexanes, 33 : 67)). ^{1}H NMR (500 MHz, acetone-d_6) δ 8.01 (br s, 3H), 7.96 (d, J = 8.0 Hz, 3H), 7.49 (s, 3H), 7.41 (dd, J = 1.5 and 7.5 Hz, 3H), 7.38 (dt, J = 1.5 and 8.0 Hz, 3H), 7.26 (dt, J = 1.0 and 7.5 Hz, 3H), 1.04 (s, 9H). ^{13}C NMR (75 MHz, acetone-d_6) δ 177.1, 141.2, 137.0, 135.6, 131.1, 130.5, 129.6, 126.2, 125.4, 40.5, 28.2. HRMS-ESI: calcd for $C_{39}H_{45}N_3O_3Na$ $(M + Na)^+$ 626.3359, found 626.3365.

1,3,5-tris(2-Aminophenyl)benzene (4-tris). A round-bottomed flask equipped with a condenser was charged with tris-amide **3** (1.44 g, 2.39 mmol) and 65% aqueous sulfuric acid (prepared by mixing 10 mL of conc. H_2SO_4 and 10 mL water). The resulting mixture was heated at 125 °C under nitrogen for 17 h. It was then allowed to cool to room temperature, poured into water (20 mL), and the aqueous solution was made basic (i.e., pH = 9) with *ca.* 200 mL of 30% aqueous ammonia. The resulting suspension was extracted with EtOAc (2 x 50 mL) and the combined organic layers were dried over Na_2SO_4 and concentrated under reduced pressure to afford 827 mg (99%) of **4-tris** as a pale yellow powder (R_f = 0.26 (EtOAc : hexanes, 67 : 33)). Its spectral data are consistent with those that have been previously reported.[26]

1,3,5-tris[2-(3-(4-Nitrophenyl)thioureido)phenyl]benzene (1-tris). To a mixture of **4-tris** (70 mg, 0.20 mmol) and 4-nitrophenylisothiocyanate (130 mg, 0.72 mmol) was added dry THF (0.5 mL) under nitrogen. The solution was stirred for 16 h and concentrated under reduced pressure. Medium pressure liquid chromatography (MPLC) on silica gel of the residue with ethyl acetate : hexanes (12 : 78 to 100 : 0) afforded 137 mg (77%) of **1-tris** as a yellow powder. ^{1}H NMR (500 MHz, acetone-d_6) δ 9.38 (br s, 6H), 7.98 (d, J = 8.5 Hz, 6H), 7.59 (s, 3H), 7.58 (d, J = 8.5 Hz, 6H), 7.50 – 7.43 (m, 9H), 7.34 (t, J = 7.5 Hz, 3H). ^{13}C NMR (75 MHz, acetone-d_6) δ 181.7, 146.9, 144.9, 140.6, 139.9 136.4, 132.0, 130.3, 130.1, 129.7, 129.2, 125.0, 124.5. HRMS-ESI: calcd for $C_{45}H_{33}N_9O_6S_3Na$ $(M + Na)^+$ 914.1608, found 914.1618.

1,3-bis[2-(3-(4-Nitrophenyl)thioureido)phenyl]benzene (1-bis). To a mixture of 1,3-bis(2-aminophenyl)benzene (**4-bis**, 52 mg, 0.20 mmol) and 4-nitrophenylisothiocyanate

(79 mg, 0.44 mmol) was added dry THF (0.5 mL) under nitrogen. The solution was stirred for 22 h and concentrated under reduced pressure. Medium pressure liquid chromatography (MPLC) on silica gel of the residue with ethyl acetate : hexanes (12 : 78 to 100 : 0) afforded 124 mg (100%) of **1-bis** as a yellow powder (R_f = 0.24 (EtOAc : hexanes, 50 : 50)). ^{1}H NMR (500 MHz, acetone-d_6) δ 9.36 (br s, 2H), 9.25 (br s, 2H), 8.04 (d, J = 9.5 Hz, 4H), 7.61 (d, J = 8.5 Hz, 4H), 7.59 (s, 1H), 7.52 (d, J = 7.5 Hz, 2H), 7.49 (app s, 3H), 7.44 (d, J = 9.0 Hz, 2H), 7.43 (t, J = 9.0 Hz, 2H), 7.33 (t, J = 7.0 Hz, 2H). ^{13}C NMR (75 MHz, acetone-d_6) δ 181.8, 147.1, 144.8, 140.4, 140.0, 136.5, 132.1, 130.6, 130.2, 130.0, 129.7, 129.3, 129.0, 125.0, 124.2. HRMS-ESI: calcd for $C_{32}H_{24}N_6O_4S_2Na$ $(M + Na)^+$ 643.1193, found 643.1195.

1-(4-Nitrophenyl)-3-phenylthiourea (1-mono). To a mixture of aniline (91 μL, 1.0 mmol) and 4-nitrophenylisothiocyanate (180 mg, 1.0 mmol) was added dry THF (1.0 mL) under nitrogen. The solution was stirred for 5 h and concentrated under reduced pressure. The residue was recrystallized from toluene to afford 189 mg (69%) of **1-mono** as a yellow powder. Its spectral data are consistent with those that have been previously reported.[27]

1,3,5-tris[2-(3-(4-Nitrophenyl)ureido)phenyl]benzene (2-tris). To a mixture of the tris-aniline **4-tris** (36.3 mg, 0.103 mmol) and 4-nitrophenylisothiocyanate (59 mg, 0.36 mmol) was added dry THF (0.5 mL) under nitrogen. The solution was stirred for 1 h and concentrated under reduced pressure. Medium pressure liquid chromatography (MPLC) on silica gel of the residue with CH_3CN : CH_2Cl_2 (10 : 90 to 20 : 80) afforded 37 mg (43%) of **2-tris** as a yellow powder (R_f = 0.42 (CH_3CN : CH_2Cl_2, 20 : 80)). ^{1}H NMR (500 MHz, acetone-d_6) δ 9.27 (br s, 3H), 8.05 (d, J = 9.5 Hz, 6H), 7.98 (br s, 3H), 7.92 (app br d, J =

5.5 Hz, 3H), 7.55 (d, J = 9.0 Hz, 6H), 7.52 (s, 3H), 7.37 (dt, J = 1.5 and 8.0 Hz, 3H), 7.22 (d, J = 7.0 Hz, 4H), 7.11 (dt, J = 1.0 and 8.0 Hz, 3H). ^{13}C NMR (75 MHz, acetone-d_6) δ 154.7, 147.3, 143.4, 141.3, 136.5, 135.8, 131.7, 130.5, 129.9, 126.3, 126.0, 125.6, 119.5. HRMS-ESI: calcd for $C_{45}H_{33}N_9O_9Na$ $(M + Na)^+$ 866.2293, found 866.2308.

1,3,5-tris[2-(3-(3,5-Trifluoromethylphenyl)thioureido)phenyl]benzene (5-tris). To a solution of tris-aniline **4-tris** (176 mg, 0.50 mmol) in dry THF (1.0 mL) was added 3,5-trifluoromethylphenylisothiocyanate (0.33 mL, 1.8 mmol) under nitrogen. The solution was stirred for 20 h and concentrated under reduced pressure. Medium pressure liquid chromatography (MPLC) on silica gel of the residue with ethyl acetate : dichloromethane (0 : 100 to 5 : 95) afforded 170 mg (29%) of **5-tris** as a white powder (R_f = 0.47 (EtOAc : DCM, 5 : 95)). ^{1}H NMR (500 MHz, $CDCl_3$) δ 9.18 (br s, 3H), 7.71 (br s, 3H), 7.66 (s, 6H), 7.56 (s, 3H), 7.51 – 7.42 (m, 12H), 7.36 (d, J = 7.5 Hz, 3H). ^{13}C NMR (75 MHz, $CDCl_3$) δ 180.1, 139.3, 138.7, 137.5, 133.0, 131.8 (q, J_{C-F} = 34 Hz), 131.1, 130.0, 129.5, 128.7, 128.3, 124.5, 122.7 (q, J_{C-F} = 271 Hz), 119.4. ^{19}F NMR (282 MHz, $CDCl_3$) δ -63.5. HRMS-ESI: calcd for $C_{51}H_{30}F_{18}N_6S_3Na$ $(M + Na)^+$ 1187.1299, found 1187.1263.

1,3-bis[2-(3-(3,5-Trifluoromethylphenyl)thioureido)phenyl]benzene (5-bis). To a solution of 1,3-bis(2-aminophenyl)benzene (130 mg, 0.50 mmol) in dry THF (1.0 mL) was added 3,5-trifluoromethylphenylisothiocyanate (0.20 mL, 1.1 mmol) under nitrogen. The solution was stirred for 16 h and concentrated under reduced pressure. Medium pressure liquid chromatography (MPLC) on silica gel of the residue with ethyl acetate : dichloromethane (0 : 100 to 5 : 95) afforded 352 mg (88%) of **5-bis** as a white powder (R_f = 0.24 (dichloromethane)). ^{1}H NMR (500 MHz, $CDCl_3$) δ 9.25 (br s, 2H), 7.76 (br s, 2H),

7.62 – 7.58 (m, 9H), 7.55 (t, J = 8.0 Hz, 1H), 7.50 – 7.47 (m, 6H), 7.41 (d, J = 8.0 Hz, 2H). ^{13}C NMR (75 MHz, $CDCl_3$) δ 180.2, 139.3, 138.1, 138.0, 133.4, 131.7 (q, J_{C-F} = 34 Hz), 131.2, 129.7, 129.5, 129.3, 128.85, 128.83, 128.4, 125.0, 122.8 (q, J_{C-F} = 271 Hz), 119.4. ^{19}F NMR (282 MHz, $CDCl_3$) δ -63.5. HRMS-ESI: calcd for $C_{36}H_{22}F_{12}N_4S_2Na$ $(M + Na)^+$ 825.0992, found 825.0987.

1,3,5-tris[2-(3-Phenylthioureido)phenyl]benzene (6-tris). To a solution of tris-aniline **4-tris** (70 mg, 0.20 mmol) in dry THF (0.4 mL) was added phenylisothiocyanate (86 μL, 0.72 mmol) under nitrogen. The solution was stirred for 16 h and more phenylisothiocyanate (86 μL, 0.72 mmol) was added. The reaction mixture was stirred for additional 16 h and concentrated under reduced pressure. Medium pressure liquid chromatography (MPLC) on silica gel of the residue with ethyl acetate : hexanes (12 : 88 to 100 : 0) afforded 103 mg (68%) of **6-tris** as a white powder (R_f = 0.25 (EtOAc : hexanes, 50 : 50)). ^{1}H NMR (500 MHz, $CDCl_3$) δ 8.63 (br s, 3H), 7.87 (br s, 3H), 7.52 – 7.46 (m, 9H), 7.40 (t, J = 8.0 Hz, 3H), 7.33 (t, J = 7.5 Hz, 3H), 7.15 – 7.03 (m, 15H). ^{13}C NMR (75 MHz, $CDCl_3$) δ 180.2, 138.8, 137.9, 137.4, 134.3, 130.9, 129.0, 128.9, 128.8, 128.6, 128.4, 126.4, 125.0. HRMS-ESI: calcd for $C_{45}H_{36}N_6S_3Na$ $(M + Na)^+$ 779.2061, found 779.2077.

1,3,5-tris[2-(2-((4-Nitrophenyl)amino)-2-oxoacetamido)phenyl]benzene (7). A solution of tris-aniline **4-tris** (36.6 mg, 0.104 mmol) and triethylamine (87 μL, 0.50 mmol) in dry DCM (3.0 mL) was added dropwise to a solution of 2-((4-nitrophenyl)amino)-2-oxoacetyl chloride[28] (105 mg, 0.46 mmol) in dry DCM (4 mL) at -13 °C under nitrogen. The mixture was stirred for 16h at ambient temperature and filtered. The precipitate was dissolved in DMSO (3 mL) and ethyl acetate (75 mL) was added. The resulting solution

was washed with water (2 x 50 mL), saturated aqueous $NaHCO_3$ (50 mL), brine (20 mL) and dried over Na_2SO_4. Concentration under reduced pressure to *ca.* 30 mL and filtration after 16 h afforded 29.5 mg (31%) of tris-oxalamide **7** as a white powder. ^{1}H NMR (500 MHz, DMSO-d_6) δ 11.22 (s, 3H), 10.25 (s, 3H), 8.07 (d, J = 9.0 Hz, 6H), 7.92 (d, J = 8.5 Hz, 3H), 7.90 (d, J = 9.0 Hz, 6H), 7.61 (s, 3H), 7.55 (d, J = 7.5 Hz, 3H), 7.47 (t, J = 7.5 Hz, 3H), 7.31 (t, J = 7.5 Hz, 3H). ^{13}C NMR (75 MHz, DMSO-d_6) δ 158.6, 157.2, 143.05, 143.02, 138.6, 134.2, 133.5, 130.0, 128.6, 128.2, 125.7, 123.9, 123.0, 120.0. HRMS-ESI: calcd for $C_{48}H_{32}N_9O_{12}$ $(M - H)^-$ 926.2176, found 926.2165.

Binding constant determinations.

Dilute non-aggregating solutions of a receptor *S* were titrated with a given anion X^- via a solution of its tetrabutylammonium salt and were monitored by UV-VIS spectrometery. Unless otherwise stated, UV absorption spectra (250-600 nm) were recorded three times for each solution and average values for each point were used; all of the spectra were background corrected by subtracting the absorption of the solvent. The wavelength with the maximum change in the concentration corrected absorption ($A_{cor} = A \cdot C_0/C$, where C and C_0 are the current and the initial receptor concentrations) was determined and then used for further analysis. Absorptions were plotted versus anion concentrations and the binding constants were determined by an iterative non-linear least squares curve fitting routine implemented in Excel using the equations below.[29] Observed and calculated absorptions are given for each titration in the corresponding Tables and Figures.

$$[SX] = \frac{K[S]_0 + K[X]_0 + 1 - \sqrt{(K[S]_0 + K[X]_0 + 1)^2 - 4K^2[S]_0[X]_0}}{2K}$$

$$A = A_0 \frac{[S]}{[S]_0} + A_{\max} \frac{[SX]}{[S]_0}$$

K: binding constant for 1:1 complex formation

[S]: free receptor concentration

$[S]_0$: total receptor concentration

[SX]: bound receptor concentration

$[X]_0$: total anion concentration

A: absorption of the solution

A_0: absorption of the initial solution (no anion added)

A_{max}: absorption of the solution if all the receptor was bound (infinite excess of anion at the initial receptor concentration)

In cases where there is a large excess of the anion, $[X] \approx [X]_0$, and the plot of of $\Delta A_{cor}/[X]$ versus ΔA_{cor} gives a straight line where the slope of the linear least squares fit of the data is the binding constant (K) and the intercept is $K \cdot \Delta A_{max}$:

$$\frac{\Delta A_{cor}}{[X]} = -\Delta A_{cor} \cdot K + K \cdot \Delta A_{\max}$$

with $\Delta A_{cor} = (A - A_0) \cdot C_0/C$, where C and C_0 are the current and the initial receptor concentrations; $\Delta A_{max} = A_{max} - A_0$.

Tris-thiourea 1 binding to $H_2PO_4^-$ in 0.5% aqueous DMSO (*v/v*). (a) Job's plot. A 100 μM solution of **1-tris** in 0.5% H_2O–DMSO (105 μL) was titrated with 0.5% H_2O–DMSO and a 100 μM solution of tetrabutylammonium dihydrogenphosphate in 0.5% H_2O–DMSO, so that the sum of the total concentrations of the two were constant (10.0 μM). UV absorptions at λ = 400 nm are given in Table S1. Since $\Delta A = A - A_0 = A_{sx}$ and ΔA is proportional to [SX], the binding stoichiometry is given at the maximum of a plot of ΔA *vs.* anion % in the mixture, where A_0 is the free receptor absorption (for a 15 μM solution A_0 = 0.265) and A_{SX} is the absorption of the bound species SX.[30] The maximum was observed at 0.5 indicating that the binding mode is 1:1 (Figure S1).

(b) Binding isoterm. A 15.0 μM solution of **1-tris** in 0.5% H_2O–DMSO (2.00 mL) was titrated with a 1.61 mM (entries 1-12) followed by a 33.9 mM (entries 13-14) solution of tetrabutylammonium dihydrogenphosphate in 0.5% H_2O–DMSO at 23 °C (Table S2). A linear dependence of the absorbance versus the number of equivalents of $H_2PO_4^-$ in the 0-0.94 range (Figure S2, left) is consistent with complete binding, and leads to A_{max} = 0.426. If one assumes that ≥ 89% of the thiourea is bound when 1 equivalent $H_2PO_4^-$ is added, then $K \geq 5 \times 10^6\ M^{-1}$. The change in absorption at higher concentrations of $H_2PO_4^-$ was ascribed to deprotonation of the receptor-bound complex by free $H_2PO_4^-$ to afford thiourea-bound HPO_4^{2-} (Scheme S1). Non-linear curve fitting of these data affords an apparent binding affinity $K_{11} = 5.2 \times 10^5\ M^{-1}$ and A_{max} = 0.544 (not shown), or an equilibrium constant K = 3.9 and A_{max} = 0.548 calculated in analogous way for this process (Figure S2, right).

Table S1. Job's plot data for the interaction of **1-tris** with $H_2PO_4^-$ (λ = 400nm).

Entry	μL solvent added	μL $H_2PO_4^-$ added	$[thiourea]_0$, μM	$[H_2PO_4^-]_0$, μM	Absorption	ΔA
1	1350	45	7.00	3.00	0.2266	0.0741
2	67	7.4	6.67	3.33	0.2268	0.0791
3	158	17.6	6.00	4.00	0.2156	0.0774
4	315	35.0	5.00	5.00	0.2032	0.0794
5	472	52.5	4.00	6.00	0.1804	0.0709
6	475	52.8	3.33	6.67	0.1641	0.0643
7	312	34.7	3.00	7.00	0.1570	0.0618

Figure S1. Job's plot for the interaction of **1-tris** with $H_2PO_4^-$.

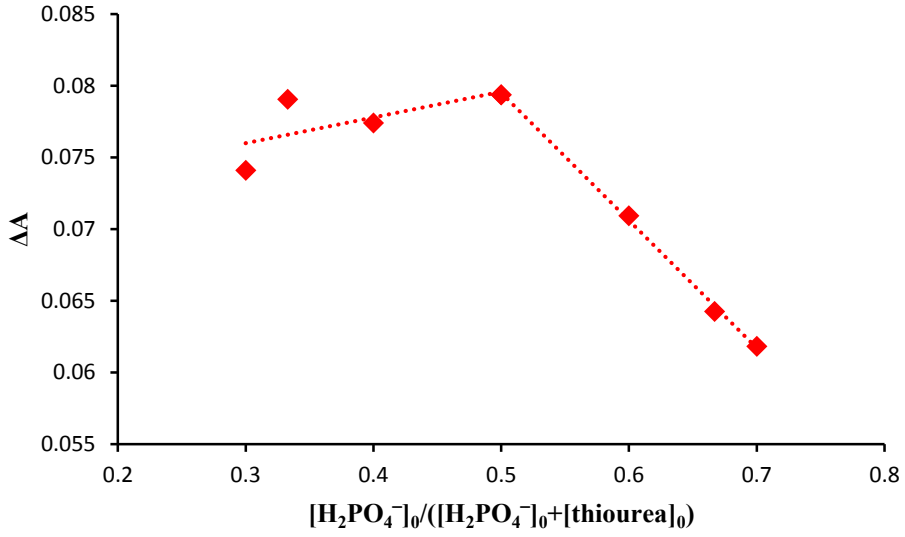

Table S2. Data for the titration of **1-tris** with $H_2PO_4^-$ in 0.5% H_2O–DMSO at 400 nm.

Entry	μL $H_2PO_4^-$ added	$[thiourea]_0$, μM	$[H_2PO_4^-]_0$, μM	Observed absorption[a]	Calculated absorption[b]
0	0	15.00	0.00	0.2400	0.2421
1	3	14.98	2.41	0.2719	0.2716
2	5	14.96	4.01	0.2916	0.2913
3	7.5	14.94	6.01	0.3175	0.3159
4	10	14.93	8.00	0.3408	0.3405
5	12.5	14.91	9.99	0.3667	0.3651
6	15	14.89	12.0	0.3902	0.3897
7	17.5	14.87	13.9	0.4116	0.4143
8	20	14.85	15.9	0.4341	0.4346
9	25	14.82	19.8	0.4723	0.4631
10	30	14.78	23.8	0.4937	0.4854
11	40	14.71	31.5	0.5108	0.5120
12	50	14.63	39.2	0.5191	0.5243
13	5	14.60	121	0.5385	0.5431
14	10	14.56	203	0.5477	0.5451

[a] Concentration-corrected absorptions. [b] From the linear (entries 0-7) and non-linear (entries 8-14) curve fits.

Scheme S1. Proposed interactions of **1-tris** with $H_2PO_4^-$.

$$\textbf{1-tris} + H_2PO_4^- \underset{}{\overset{K \geq 5 \times 10^6\ M^{-1}}{\rightleftharpoons}} \textbf{1-tris} \bullet H_2PO_4^-$$

$$\textbf{1-tris} \bullet H_2PO_4^- + H_2PO_4^- \overset{K = 3.9}{\rightleftharpoons} \textbf{1-tris} \bullet HPO_4^{2-} + H_3PO_4$$

Figure S2. Least squares fittings of the titration data in Table S2.

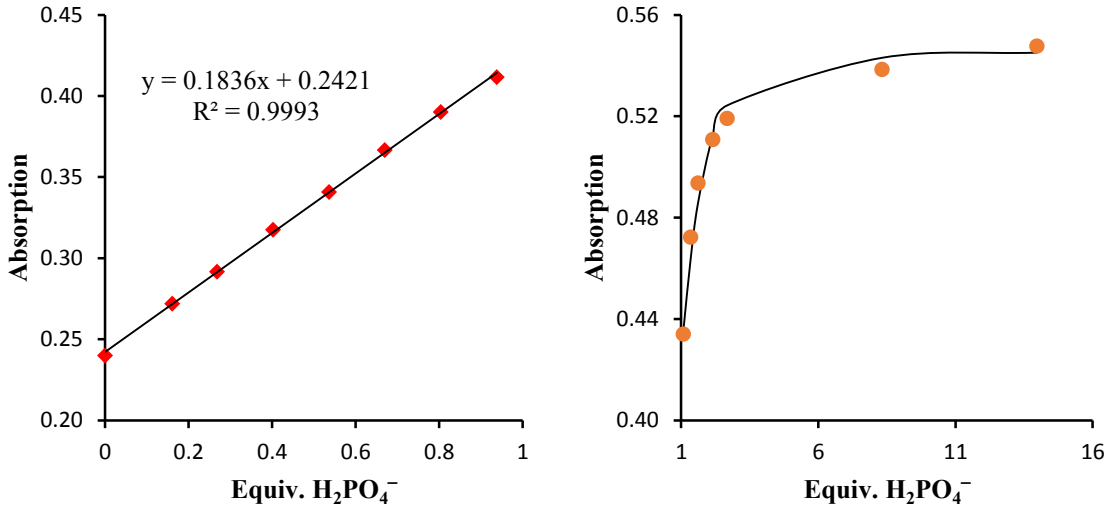

Tris-thiourea 1 interaction with OAc^- in 0.5% aqueous DMSO (*v/v*). (a) Job's plot. A 100 μM solution of **1-tris** in 0.5% H_2O–DMSO (105 μL) was titrated with 0.5% H_2O–DMSO and a 100 μM solution of tetrabutylammonium acetate in 0.5 % H_2O–DMSO, so that the sum of the total concentrations of the two were constant (10.0 μM). UV absorptions at λ = 416 nm are given in Table S3. Since $\Delta A = A - A_0 = A_{sx}$ and ΔA is proportional to [SX], the binding stoichiometry is given at the maximum of a plot of ΔA *vs.* anion % in the mixture, where A_0 is the free receptor absorption (for a 15 μM solution $A_0 = 0.102$) and A_{SX} is the absorption of the bound species SX. The maximum was observed at *ca.* 0.55 indicating that the binding mode is 1:1 and is followed by subsequent 1:2 complex formation (Figure S3).

(b) Titration data. A 15 μM solution of **1-tris** in 0.5% H_2O–DMSO (2.10 mL) was titrated with a 4.31 mM solution of tetrabutylammonium acetate in 0.5% H_2O–DMSO at

24 °C (Table S4). A linear dependence of the absorbance versus the number of equivalents of OAc^- in the 0-1.00 range (Figure S4) is consistent with irreversible deprotonation. The spectral data is also the same as observed when 1 equivalent of tetrabutylammonium hydroxide is added. A linear least squares fit affords A_{max} = 0.255. The change in absorption at higher concentrations of OAc^- was ascribed to the interaction of the other two thiourea arms and 1:2 complex formation (see Job's plot).

Table S3. Job's plot data for the interaction of **1-tris** with OAc^-.

Entry	µL solvent added	µL OAc^- added	$[thiourea]_0$, µM	$[OAc^-]_0$, µM	Absorption	ΔA
1	1350	45	7.00	3.00	0.1403	0.0159
2	67	7.4	6.67	3.33	0.1391	0.0178
3	158	17.6	6.00	4.00	0.1346	0.0201
4	315	35.0	5.00	5.00	0.1300	0.0255
5	472	52.5	4.00	6.00	0.1198	0.0254
6	475	52.8	3.33	6.67	0.1103	0.0226
7	312	34.7	3.00	7.00	0.1053	0.0212

Figure S3. Job's plot for the interaction of **1-tris** with OAc^-.

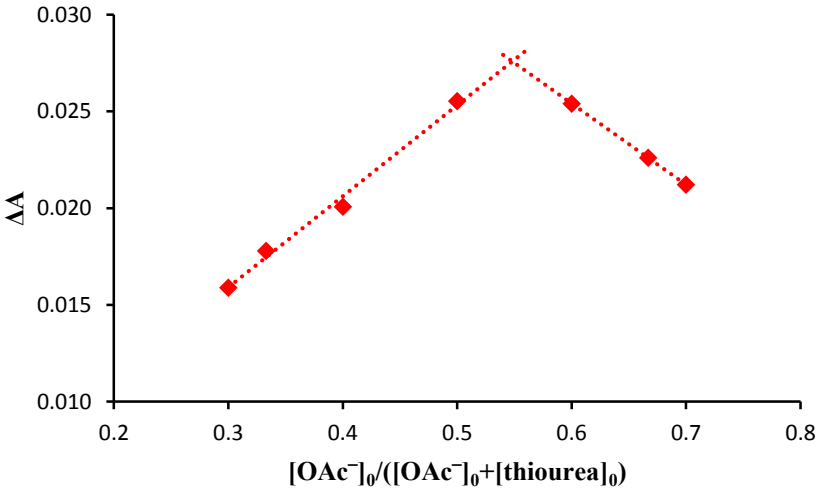

Table S4. Data for the titration of **1-tris** with OAc^- in 0.5% H_2O–DMSO at 416 nm.

Entry	µL OAc^- added	$[thiourea]_0$, µM	$[OAc^-]_0$, µM	Observed absorption*	Calculated absorption[b]
0	0	15.00	0.0	0.0895	0.0894
1	2	14.99	4.3	0.1367	0.1371
2	3	14.98	6.4	0.1599	0.1609
3	4	14.97	8.6	0.1847	0.1847
4	5	14.96	10.7	0.2091	0.2085
5	6	14.96	12.9	0.2323	0.2324
6	7	14.95	15.0	0.2543	0.2562
7	8.5	14.94	18.2	0.2848	
8	10	14.93	21.4	0.3177	
9	12	14.91	25.7	0.3454	
10	14	14.90	29.9	0.3683	
11	16	14.88	34.2	0.3888	
12	18	14.87	38.4	0.4024	
13	21	14.84	44.7	0.4111	
14	25	14.82	53.1	0.4182	
15	30	14.78	63.6	0.4257	

[a] Concentration-corrected absorptions. [b] From the linear fit.

Figure S4. Linear least squares fitting of the titration data in Table S4.

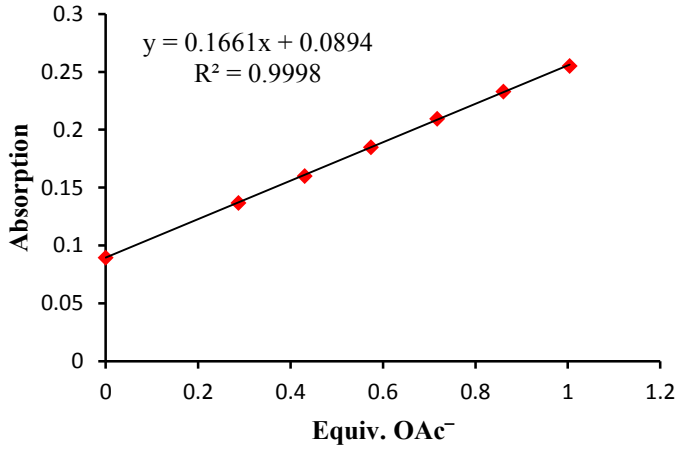

Mono-thiourea 1 binding to $H_2PO_4^-$ in 0.5% aqueous DMSO (*v/v*). A 14.3 μM solution of **1-mono** in 0.5% H_2O–DMSO (2.10 mL) was titrated with a 30.0 mM solution of tetrabutylammonium dihydrogenphosphate in 0.5% H_2O–DMSO at 23 °C (Table S5). Non-linear curve fitting of the titration data affords $K = 4.0 \times 10^4\ M^{-1}$ and $A_{max} = 0.205$ (Figure S5).

Mono-thiourea 1 interaction with OAc^- in 0.5 % aqueous DMSO (*v/v*). To a 30 μM solution of **1-mono** in 0.5% H_2O–DMSO (2.00 mL) was added a 5.0 mM solution of tetrabutylammonium hydroxide in 0.5% MeOH–DMSO (12.0 μL, 1.00 equiv.), followed by a 5.00 mM acetic acid solution in DMSO (12.0 μL, 1.00 equiv.). Less than a 10% change was observed after addition of the acetic acid, indicating that little, if any, proton transfer takes place from the acid (Figure 3 in the discussion section).

Table S5. Data for the titration of **1-mono** with $H_2PO_4^-$ in 0.5% H_2O–DMSO at 454 nm.

Entry	μL $H_2PO_4^-$ added	$[thiourea]_0$, μM	$[H_2PO_4^-]_0$, μM	Observed absorption	Calculated absorption*
0	0	14.3	0.0	0.0315	0.0315
1	1	14.3	14.3	0.0835	0.0819
2	2	14.3	28.5	0.1126	0.1129
3	3	14.3	42.8	0.1316	0.1325
4	4	14.3	57.0	0.1451	0.1456
5	5	14.3	71.3	0.1547	0.1548
6	7	14.2	99.7	0.1668	0.1668
7	10	14.2	142	0.1767	0.1767
8	15	14.2	212	0.1866	0.1848
9	20	14.2	283	0.1885	0.1889
10	30	14.1	423	0.1929	0.1926
11	50	14.0	698	0.1936	0.1946

* From the non-linear curve fit.

Figure S5. Non-linear least squares fitting of the titration data in Table S5.

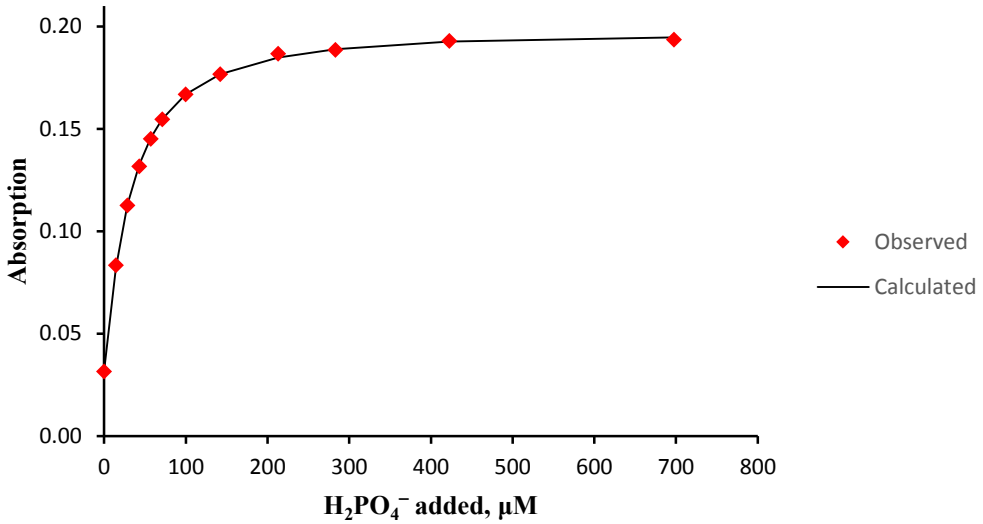

Tris-urea 2 binding to $H_2PO_4^-$ in 0.5% aqueous DMSO (*v/v*). A 15.0 µM solution of **2-tris** in 0.5% H_2O–DMSO (2.00 mL) was titrated with 2.95 mM (entries 1-10) and 14.7 mM (entries 11-15) solutions of tetrabutylammonium dihydrogenphosphate in 0.5% H_2O–DMSO at 23 °C (Table S6). In analogy to **1-tris** (Scheme S1), linearity in the range of 0-1.0 equivalents of $H_2PO_4^-$ (Figure S6, left) is consistent with $K \geq 5 \times 10^6$ M^{-1} and A_{max} = 0.528, whereas the data for subsequent titration fits into the hypothesis of **2-tris** • HPO_4^{2-} with K = 0.057 and A_{max} = 1.10 (Figure S6, right).

Tris-urea 2 binding to OAc^- in 0.5% aqueous DMSO (*v/v*). A 15.0 µM solution of **2-tris** in 0.5% H_2O–DMSO (2.00 mL) was titrated with a 3.86 mM solution of tetrabutylammonium acetate in 0.5% H_2O–DMSO at 23 °C (Table S7). A linear dependence of the absorbance versus the number of equivalents of OAc^- in the 0-1.00 range (Figure S7) is consistent with strong binding ($K \geq 5 \times 10^6$ M^{-1}), with a linear least squares

Table S6. Data for the titration of **2-tris** with $H_2PO_4^-$ in 0.5% H_2O–DMSO at 386 nm.

Entry	μL $H_2PO_4^-$ added	$[thiourea]_0$, μM	$[H_2PO_4^-]_0$, μM	Observed absorption[a]	Calculated absorption[b]
0	0	15.00	0.00	0.2997	0.3053
1	2.5	14.98	3.68	0.3613	0.3601
2	4	14.97	5.88	0.3960	0.3930
3	5	14.96	7.35	0.4163	0.4150
4	6	14.96	8.81	0.4424	0.4369
5	7	14.95	10.3	0.4590	0.4588
6	8.5	14.94	12.5	0.4921	0.4917
7	10	14.93	14.6	0.5188	0.5246
8	12.5	14.91	18.3	0.5516	0.5768
9	15	14.89	21.9	0.5758	0.6021
10	20	14.85	29.2	0.6177	0.6355
11	2.5	14.83	47.3	0.6877	0.6871
12	5	14.82	65.3	0.7321	0.7212
13	10	14.78	101.3	0.7854	0.7684
14	20	14.71	172.8	0.8327	0.8269
15	30	14.63	244	0.8557	0.8645

[a] Concentration-corrected absorptions. [b] From the linear (entries 0-7) and non-linear (entries 8-15) curve fits.

Figure S6. Least squares fittings of the titration data in Table S6.

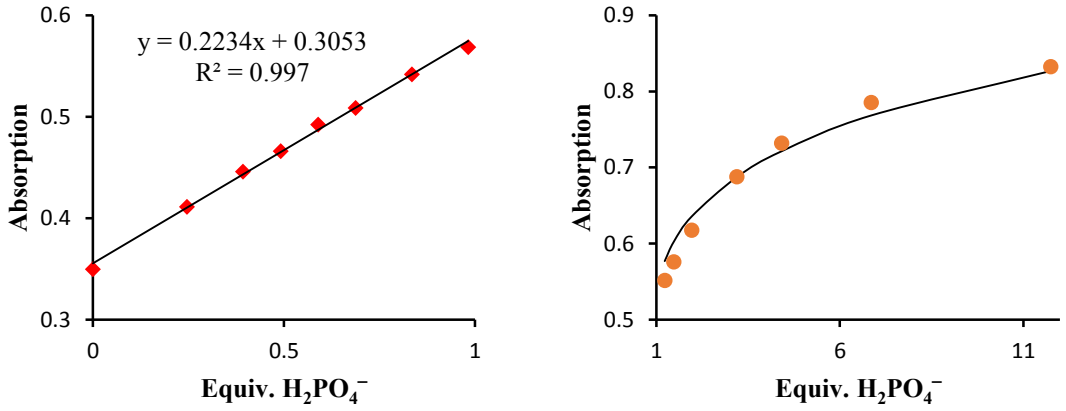

Table S7. Data for the titration of **2-tris** with OAc^- in 0.5% H_2O–DMSO at 386 nm.

Entry	µL OAc^- added	$[urea]_0$, µM	$[OAc^-]_0$, µM	Observed absorption[a]	Calculated absorption[b]
0	0	15.00	0.00	0.3048	0.3049
1	2	14.99	3.85	0.3338	0.3349
2	3	14.98	5.77	0.3504	0.3500
3	4	14.97	7.69	0.3660	0.3650
4	5	14.96	9.61	0.3800	0.3800
5	6	14.96	11.5	0.3952	0.3950
6	7.8	14.94	15.0	0.4213	0.4220
7	10	14.93	19.2	0.4481	
8	12.5	14.91	23.9	0.4756	
9	15.6	14.88	29.8	0.4958	
10	20	14.85	38.2	0.5127	
11	25	14.82	47.6	0.5193	
12	30	14.78	57.0	0.5222	
13	40	14.71	75.6	0.5263	
14	50	14.63	94.0	0.5262	

[a] Concentration-corrected absorptions. [b] From the linear fit.

Figure S7. Linear least squares fitting of the titration data in Table S7.

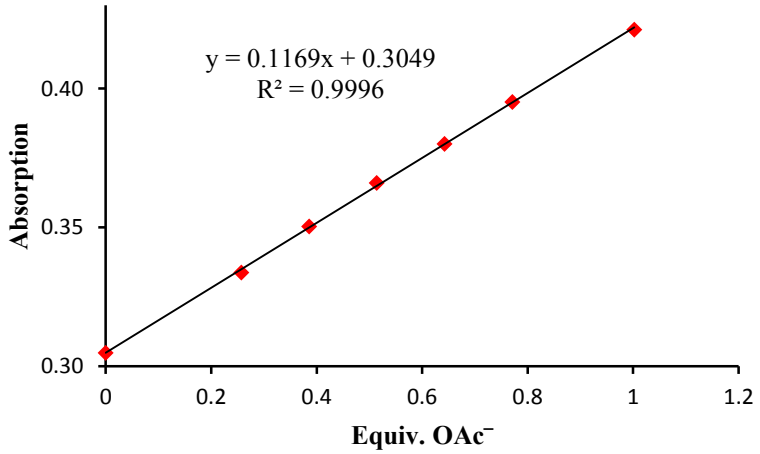

fit affording A_{max} = 0.422. The change in absorption at higher OAc^- concentrations was ascribed to sequential binding (1:2) upon interaction with the remaining two thiourea arms.

Tris-thiourea 1 binding to $H_2PO_4^-$ in 5% aqueous DMSO (*v/v*). A 15 μM solution of **1-tris** in 5% H_2O–DMSO (2.00 mL) was titrated with a 2.14 mM solution of tetrabutylammonium dihydrogenphosphate in 5% H_2O–DMSO at 24 °C (Table S8). Non-linear curve fitting of the titration data affords K = 2.3 x 10^5 M^{-1} and A_{max} = 0.549 (Figure S8).

Table S8. Data for the titration of **1-tris** with $H_2PO_4^-$ in 5% H_2O–DMSO at 399 nm.

Entry	μL $H_2PO_4^-$ added	$[thiourea]_0$, μM	$[H_2PO_4^-]_0$, μM	Observed absorption	Calculated absorption*
0	0	15.00	0	0.2619	0.2619
1	1	14.99	1.07	0.2753	0.2774
2	2	14.99	2.13	0.2901	0.2924
3	3.5	14.97	3.73	0.3122	0.3141
4	5	14.96	5.33	0.3282	0.3345
5	7.5	14.94	7.98	0.3573	0.3656
6	10	14.93	10.6	0.3841	0.3925
7	12.5	14.91	13.3	0.4104	0.4152
8	15	14.89	15.9	0.4346	0.4338
9	17.5	14.87	18.5	0.4532	0.4489
10	20	14.85	21.2	0.4691	0.4609
11	25	14.82	26.4	0.4862	0.4781
12	30	14.78	31.6	0.4933	0.4893
13	40	14.71	41.9	0.4996	0.5016
14	50	14.63	52.1	0.5019	0.5075

* From the non-linear curve fit.

Figure S8. Non-linear least squares fitting of the titration data in Table S8.

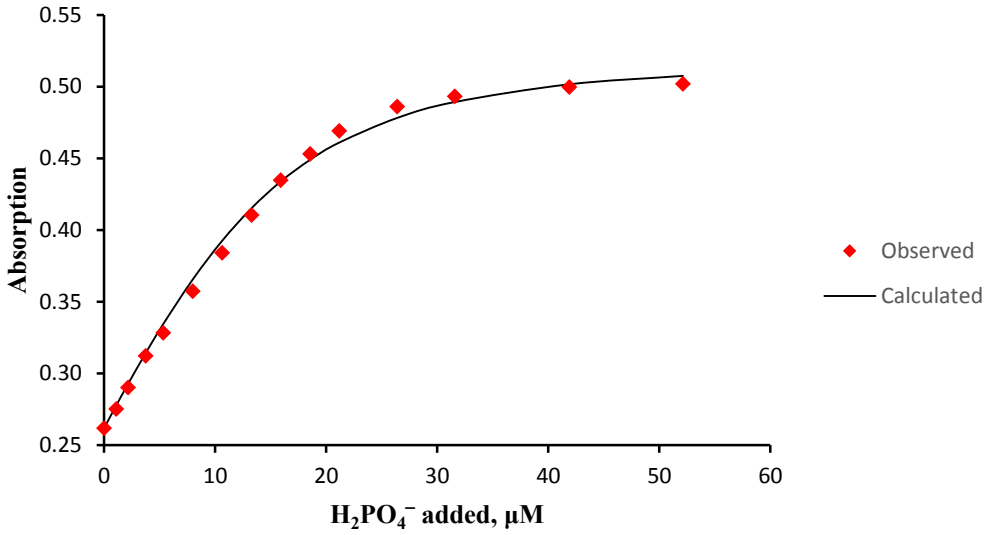

Tris-thiourea 1 interaction with OAc^- in 5% aqueous DMSO (*v/v*). A 15 µM solution of **1-tris** in 0.5% H_2O–DMSO (2.10 mL) was titrated with a 4.31 mM solution of tetrabutylammonium acetate in 0.5% H_2O–DMSO at 24 °C (Table S9). A linear dependence of the absorbance versus the number of equivalents of $H_2PO_4^-$ in the 0-0.93 range (Figure S9) is consistent with irreversible deprotonation, with a linear least square fit affording $A_{max} = 0.272$. The change in absorption at higher OAc^- concentrations of was ascribed to sequential binding or deprotonation (1:2) upon interaction with the remaining two thiourea arms.

Table S9. Data for the titration of **1-tris** with OAc^- in 5% H_2O–DMSO at 411 nm.

Entry	µL OAc^- added	$[thiourea]_0$, µM	$[OAc^-]_0$, µM	Observed absorption[a]	Calculated absorption[b]
0	0	15.00	0.0	0.1314	0.1346
1	2	14.99	4.7	0.1790	0.1772
2	3	14.98	7.0	0.2010	0.1985
3	4	14.97	9.3	0.2215	0.2198
4	5	14.96	11.7	0.2428	0.2411
5	6	14.96	14.0	0.2582	0.2625
6	7	14.95	16.3	0.2749	
7	8.5	14.94	19.8	0.2919	
8	10	14.93	23.2	0.3065	
9	13	14.90	30.2	0.3291	
10	16	14.88	37.1	0.3425	
11	20	14.85	46.3	0.3545	
12	25	14.82	57.7	0.3622	
13	30	14.78	69.1	0.3688	
14	40	14.71	91.6	0.3755	

[a] Concentration-corrected absorptions. * From the linear fit.

Figure S9. Linear least squares fitting of the titration data in Table S9.

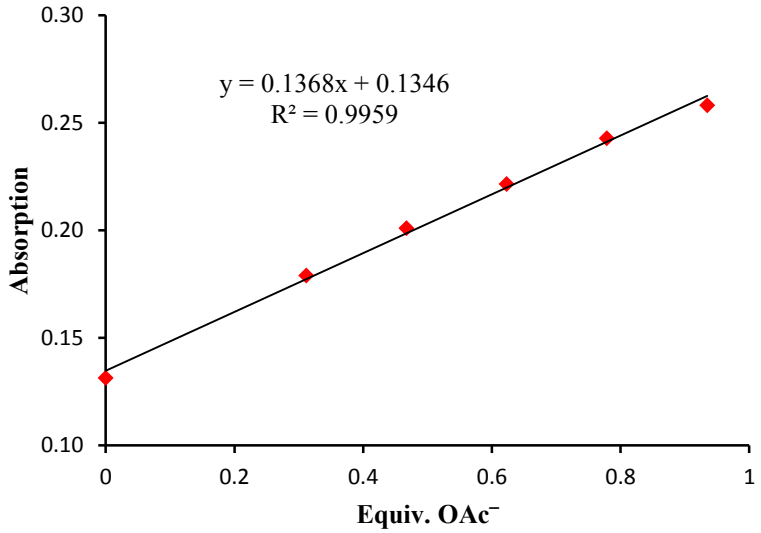

Tris-thiourea 1 binding to $H_2PO_4^-$ in 12.5% aqueous DMSO (*v/v*). A 15 μM solution of **1-tris** in 12.5% H_2O–DMSO (2.00 mL) was titrated with a 16.1 mM solution of tetrabutylammonium dihydrogenphosphate in 12.5% H_2O–DMSO at 24 °C (Table S10). Non-linear curve fitting of the titration data affords K = 7.5 x 10^4 M^{-1} and A_{max} = 0.544 (Figure S10).

Tris-thiourea 1 binding to OAc^- in 12.5% aqueous DMSO (*v/v*). A 15 μM solution of **1-tris** in 12.5% H_2O–DMSO (2.00 mL) was titrated with a 3.81 mM solution of tetrabutylammonium acetate in 12.5% H_2O–DMSO at 23 °C (Table S5). The wavelength of the maximum change in the concentration-corrected absorption of the thiourea shifted from λ = 413 nm to 406 nm. Non-linear curve fitting of the titration data affords K = 1.4 x 10^5 M^{-1} and A_{max} = 0.218 for λ = 413 nm (Figure S11).

Table S10. Data for the titration of **1-tris** with $H_2PO_4^-$ in 12.5% H_2O–DMSO at 397 nm.

Entry	μL $H_2PO_4^-$ added	$[thiourea]_0$, μM	$[H_2PO_4^-]_0$, μM	Observed absorption	Calculated absorption*
0	0	15.0	0	0.2608	0.2608
1	1	15.0	8.03	0.3315	0.3298
2	2	15.0	16.1	0.3761	0.3792
3	3	15.0	24.1	0.4086	0.4135
4	4	15.0	32.1	0.4386	0.4374
5	5	15.0	40.1	0.4563	0.4545
6	7.5	14.9	60.1	0.4865	0.4804
7	10	14.9	80.0	0.4968	0.4944
8	15	14.9	119	0.5067	0.5085
9	20	14.9	159	0.5123	0.5150
10	30	14.8	237	0.5162	0.5203
11	130	14.1	981	0.5086	0.5075
12	230	13.5	1658	0.4880	0.4862

* From the non-linear curve fit.

Figure S10. Non-linear least squares fitting of the titration data in Table S10.

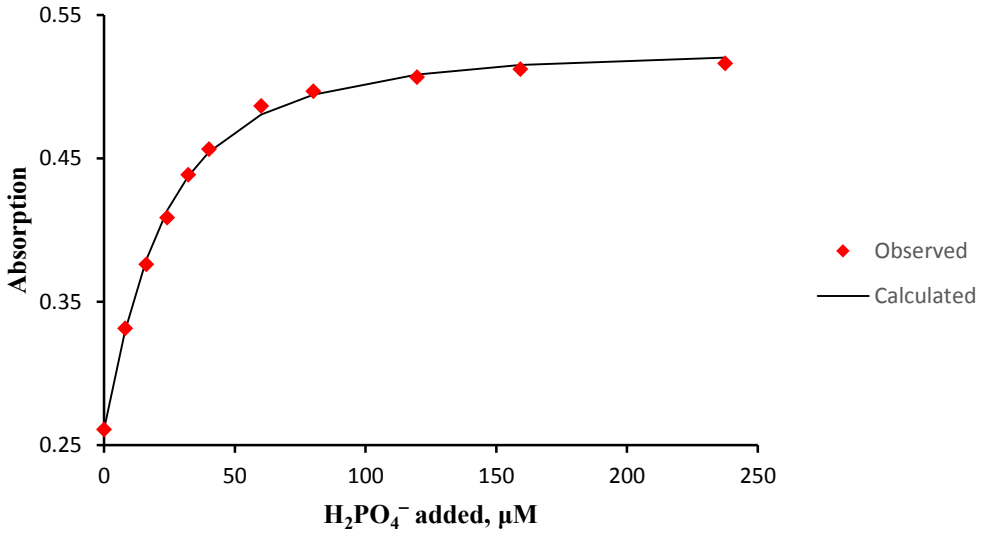

Table S11. Data for the titration of **1-tris** with OAc^- in 12.5% H_2O–DMSO at 413 nm.

Entry	µL OAc^- added	$[thiourea]_0$, µM	$[OAc^-]_0$, µM	Observed absorption	Calculated absorption*
0	0	15.00	0.1153	0.1153	0.1153
1	2	14.99	0.1362	0.1362	0.1341
2	3.5	14.97	0.1490	0.1490	0.1466
3	5	14.96	0.1579	0.1579	0.1576
4	6.5	14.95	0.1667	0.1667	0.1669
5	8	14.94	0.1726	0.1726	0.1746
6	10	14.93	0.1791	0.1791	0.1825
7	15	14.89	0.1900	0.1900	0.1944
8	20	14.85	0.1985	0.1985	0.2002
9	30	14.78	0.2070	0.2070	0.2051
10	40	14.71	0.2111	0.2111	0.2068
11	60	14.56	0.2148	0.2148	0.2073
12	80	14.42	0.2143	0.2143	0.2065

* From the non-linear curve fit.

Figure S11. Non-linear least squares fitting of the titration data in Table S11.

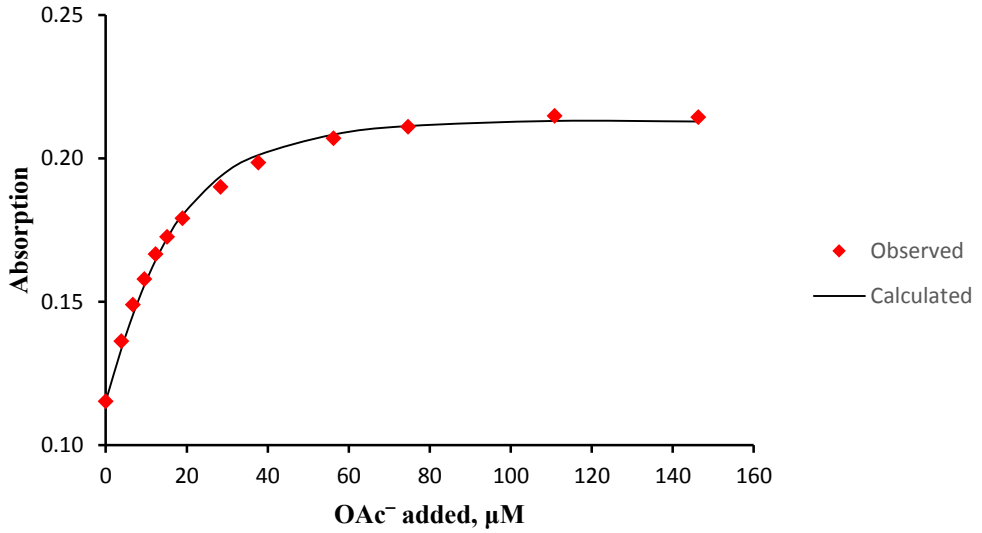

Tris-thiourea 1 binding to $H_2PO_4^-$ in 20% aqueous DMSO (*v/v*). A 15 µM solution of **1-tris** in 20% H_2O–DMSO (2.00 mL) was titrated with a 16.1 mM solution of tetrabutylammonium dihydrogenphosphate in 20% H_2O–DMSO at 24 °C (Table S12). Non-linear curve fitting of the titration data affords K = 1.5 x 10^4 M^{-1} and A_{max} = 0.465 (Figure S12).

Tris-thiourea 1 binding to OAc^- in 20% aqueous DMSO (*v/v*). A 15 µM solution of **1-tris** in 20% H_2O–DMSO (2.00 mL) was titrated with a 219 mM solution of tetrabutylammonium acetate in 20% H_2O–DMSO containing 15 µM of **1-tris** at 22 °C (Table S13). The wavelength of the maximum change in the concentration-corrected absorption of the thiourea shifted from λ = 406 nm to 384 nm and the titration data could not be fit to a 1:1 binding curve.

Table S12. Data for the titration of **1-tris** with $H_2PO_4^-$ in 20% H_2O–DMSO at 397 nm.

Entry	µL $H_2PO_4^-$ added	$[thiourea]_0$, µM	$[H_2PO_4^-]_0$, µM	Observed absorption	Calculated absorption*
0	0	15.00	0	0.2468	0.2468
1	1	14.99	7.73	0.2712	0.2662
2	2	14.99	15.5	0.2874	0.2829
3	3.5	14.97	27.0	0.3080	0.3036
4	5	14.96	38.6	0.3216	0.3204
5	7.5	14.94	57.8	0.3412	0.3419
6	10	14.93	77.0	0.3559	0.3578
7	12.5	14.91	96.1	0.3676	0.3700
8	15	14.89	115	0.3755	0.3795
9	20	14.85	153	0.3923	0.3932
10	25	14.82	191	0.4019	0.4024
11	30	14.78	229	0.4096	0.4090
12	40	14.71	303	0.4176	0.4172
13	50	14.63	377	0.4228	0.4218
14	70	14.49	523	0.4269	0.4258
15	90	14.35	666	0.4273	0.4265

* From the non-linear curve fit.

Figure S12. Non-linear least squares fitting of the titration data in Table S12.

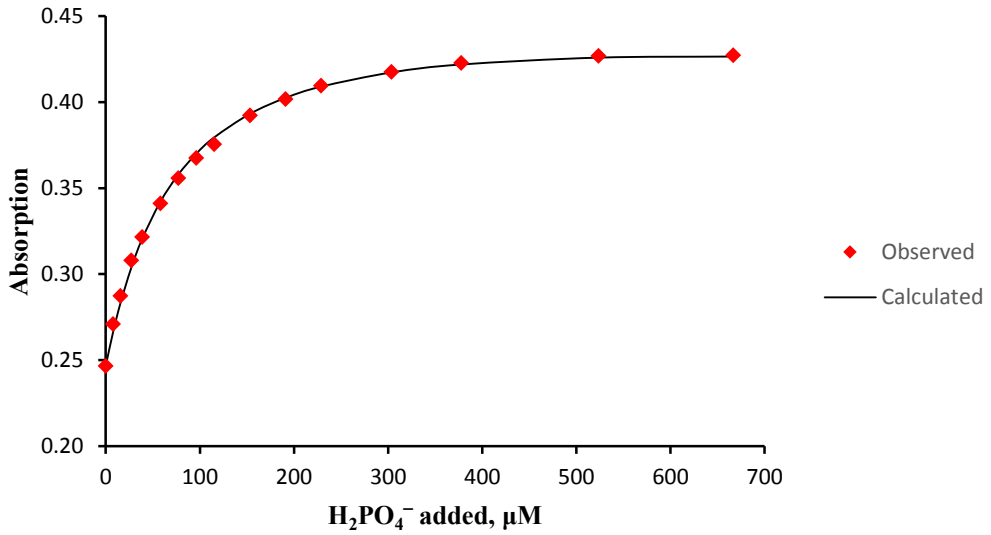

Table S13. Data for the titration of **1-tris** with OAc^- in 20% H_2O–DMSO at 384 nm.

Entry	μL OAc^- added	$[thiourea]_0$, mM	$[OAc^-]_0$, mM	Observed absorption
0	0	0.0150	0	0.4171
1	1	0.0150	0.11	0.4269
2	2	0.0150	0.22	0.4284
3	3	0.0150	0.33	0.4293
4	5	0.0150	0.55	0.4302
5	10	0.0149	1.09	0.4340
6	20	0.0149	2.17	0.4443
7	40	0.0147	4.29	0.4517
8	60	0.0146	6.37	0.4579
9	100	0.0143	10.41	0.4663
10	150	0.0140	15.26	0.4731
11	200	0.0136	19.88	0.4806
12	300	0.0130	28.53	0.4903
13	400	0.0125	36.45	0.4959
14	600	0.0115	50.48	0.5072
15	760	0.0109	60.24	0.5119

Tris-thiourea 1 binding to $H_2PO_4^-$ in 25% aqueous DMSO (*v/v*). A 15 μM solution of **1-tris** in 25% H_2O–DMSO (2.00 mL) was titrated with a 40.0 mM solution of tetrabutylammonium dihydrogenphosphate in 25% H_2O–DMSO at 24 °C (Table S14). Non-linear curve fitting of the titration data affords $K = 4000\ M^{-1}$ and $A_{max} = 0.477$ (Figure S13).

Tris-thiourea 1 binding to OAc^- in 25% aqueous DMSO (*v/v*). A 15 μM solution of **1-tris** in 25% H_2O–DMSO (2.00 mL) was titrated with a 0.513 M solution of tetrabutylammonium acetate in 25% H_2O–DMSO at 24 °C (Table S15). A linear least squares fit in the single-reciprocal plot affords $K = 35\ M^{-1}$ and $\Delta A_{max} = 0.120$ (Figure S14, entries 1–14, 8-62% bound (i.e., $\Delta A/\Delta A_{max}$); deviation was observed thereafter presumably due to sequential 1:2 binding).

Table S14. Data for the titration of **1-tris** with $H_2PO_4^-$ in 25% H_2O–DMSO at 395 nm.

Entry	µL $H_2PO_4^-$ added	$[thiourea]_0$, µM	$[H_2PO_4^-]_0$, µM	Observed absorption	Calculated absorption*
0	0	15	0	0.2398	0.2398
1	2.5	14.98	49.8	0.2807	0.2774
2	5	14.96	99.6	0.3056	0.3048
3	7.5	14.94	149	0.3244	0.3254
4	10	14.92	199	0.3408	0.3414
5	12.5	14.91	248	0.3528	0.3542
6	15	14.89	297	0.3647	0.3646
7	20	14.85	395	0.3804	0.3802
8	25	14.82	493	0.3919	0.3914
9	30	14.78	590	0.3993	0.3997
10	40	14.71	783	0.4110	0.4109
11	50	14.63	974	0.4182	0.4177

* From the non-linear curve fit.

Figure S13. Non-linear least squares fitting of the titration data in Table S14.

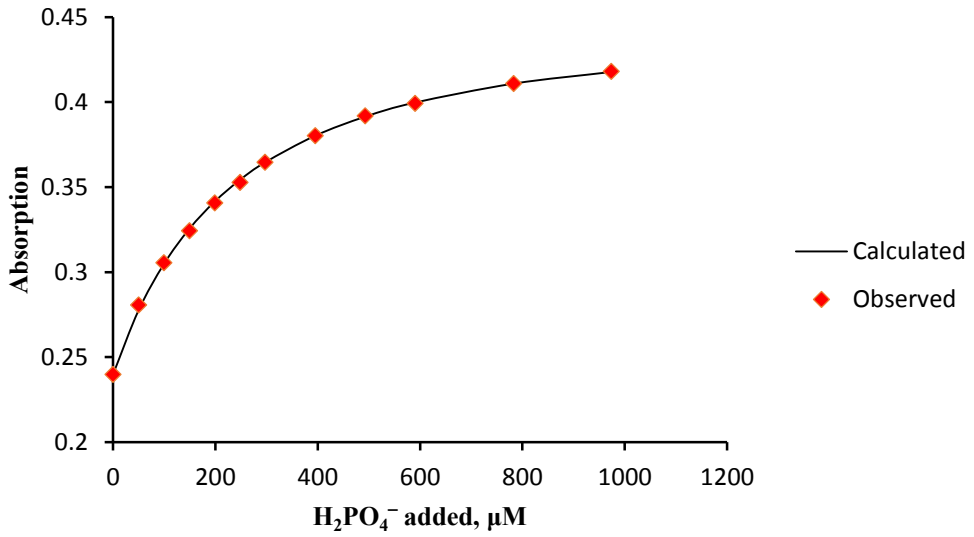

Table S15. Data for the titration of **1-tris** with OAc^- in 25% H_2O–DMSO at 379 nm.

Entry	μL OAc^- added	$[OAc^-]_0$, M	Observed absorption	ΔA_{cor}	$\Delta A_{cor}/[OAc^-]_0$
0	0	0	0.4075	–	–
1	10	0.00255	0.4153	0.0099	3.873
2	15	0.00381	0.4182	0.0139	3.641
3	20	0.00507	0.4213	0.0180	3.542
4	25	0.00632	0.4236	0.0213	3.376
5	30	0.00757	0.4264	0.0253	3.343
6	35	0.00881	0.4283	0.0283	3.213
7	40	0.01004	0.4299	0.0310	3.083
8	50	0.01249	0.4341	0.0375	2.999
9	60	0.01492	0.4349	0.0404	2.708
10	80	0.01970	0.4394	0.0495	2.511
11	100	0.02439	0.4408	0.0553	2.267
12	125	0.03013	0.4412	0.0612	2.031
13	150	0.03574	0.4401	0.0656	1.835
14	200	0.04657	0.4381	0.0744	1.597
15	300	0.06683	0.4315	0.0887	1.327
16	400	0.08539	0.4207	0.0972	1.138

Figure S14. Linear least squares fitting of the titration data in Table S15.

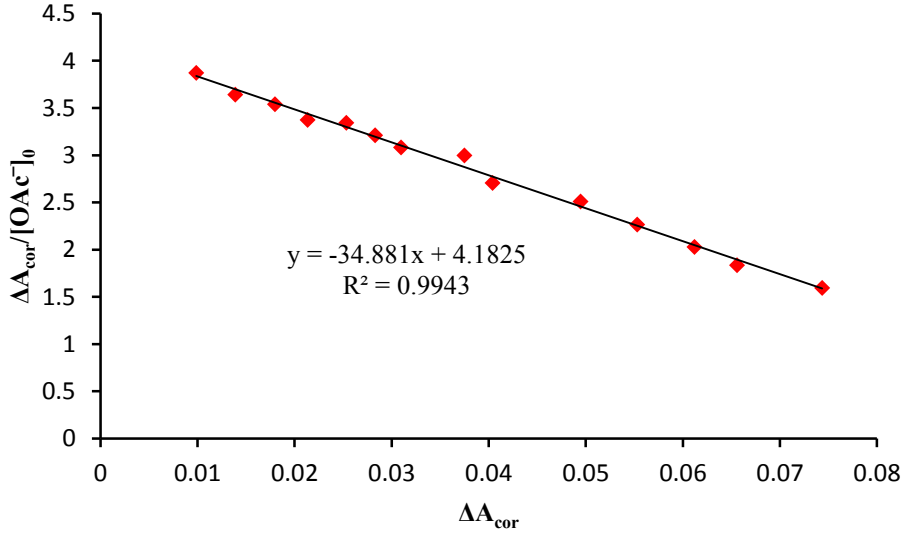

Tris-thiourea 1 binding to Cl^- in 25% aqueous DMSO (*v/v*). A 15 μM solution of **1-tris** in 25% H_2O–DMSO (2.00 mL) was titrated with solid tetrabutylammonium chloride at 24 °C (Table S16). The volume change was calculated based on the density of TBACl (i.e., 0.98 g/mL). A linear least squares fit in the single-reciprocal plot affords K = 1.5 M^{-1} and ΔA_{max} = 0.298 (Figure S15, 12-66% bound (i.e., $\Delta A/\Delta A_{max}$)).

Table S16. Data for the titration of **1-tris** with Cl^- in 25% H_2O–DMSO at 363 nm.

Entry	mg TBACl added	$[Cl^-]_0$, M	Observed absorption	ΔA_{cor}	$\Delta A_{cor}/[Cl^-]_0$
0	0	0	0.5324	–	–
1	50.7	0.0888	0.5550	0.0369	0.4153
2	103.7	0.1770	0.5662	0.0637	0.3598
3	193.7	0.3167	0.5706	0.0945	0.2985
4	362.7	0.5500	0.5629	0.1345	0.2445
5	632.4	0.8593	0.5311	0.1698	0.1976
6	966.4	1.163	0.4879	0.1956	0.1681

Figure S15. Linear least squares fitting of the titration data in Table S16.

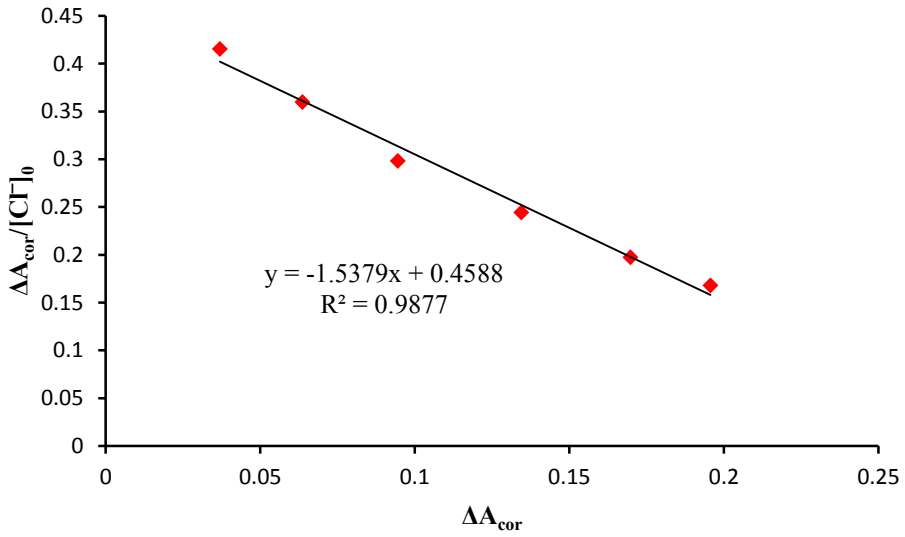

Bis-thiourea 1 binding to $H_2PO_4^-$ in 25% aqueous DMSO (*v/v*). A 22.5 μM solution of **1-bis** in 25% H_2O–DMSO (2.00 mL) was titrated with a 0.377 M solution of tetrabutylammonium dihydrogenphosphate in 25% H_2O–DMSO at 24 °C (Table S17). Non-linear curve fitting of the titration data affords K = 28 M^{-1} and A_{max} = 0.169 (Figure S16, 13-58% bound (i.e., $\Delta A/\Delta A_{max}$)).

Table S17. Data for the titration of **1-bis** with $H_2PO_4^-$ in 25% H_2O–DMSO at 389 nm.

Entry	μL $H_2PO_4^-$ added	$[thiourea]_0$, μM	$[H_2PO_4^-]_0$, mM	Observed absorption	Calculated absorption*
0		22.5	0	0.3151	0.3151
1	30	22.4	5.56	0.3349	0.3327
2	45	22.4	8.28	0.3400	0.3391
3	60	22.4	11.0	0.3446	0.3442
4	80	22.2	14.5	0.3493	0.3496
5	100	22.1	17.9	0.3515	0.3536
6	150	22.0	26.3	0.3582	0.3594
7	200	21.8	34.2	0.3622	0.3613
8	300	21.6	49.1	0.3594	0.3588

* From the non-linear curve fit.

Figure S16. Non-linear least squares fitting of the titration data in Table S17.

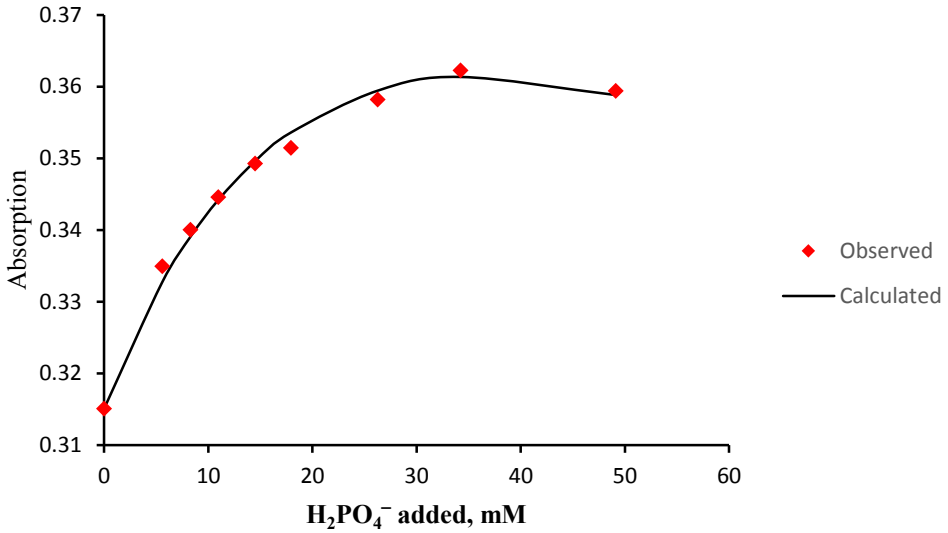

Mono-thiourea 1 binding to $H_2PO_4^-$ in 25% aqueous DMSO (*v/v*). A 45 μM solution of **1-mono** in 25% H_2O–DMSO (2.00 mL) was titrated with a 0.367 M solution of tetrabutylammonium dihydrogenphosphate in 25% H_2O–DMSO at 23 °C (Table S18). A linear least squares fit in the single-reciprocal plot affords K = 12 M^{-1} and ΔA_{max} = 0.315 (Figure S17, 4-54% bound (i.e., $\Delta A/\Delta A_{max}$)).

Mono-thiourea 1 binding to OAc^- in 25% aqueous DMSO (*v/v*). A 60 μM solution of **1-mono** in 25% H_2O–DMSO (1.00 mL) was titrated with a 0.367 M solution of tetrabutylammonium acetate in 25% H_2O–DMSO at 23 °C (Table S19). A linear least squares fit in the single-reciprocal plot affords K = 12 M^{-1} and ΔA_{max} = 0.436 (Figure S18, 9-68% bound (i.e., $\Delta A/\Delta A_{max}$)).

Table S18. Data for the titration of **1-mono** with $H_2PO_4^-$ in 25% H_2O–DMSO at 388 nm.

Entry	μL $H_2PO_4^-$ added	$[H_2PO_4^-]_0$, M	Observed absorption	ΔA_{cor}	$\Delta A_{cor}/[H_2PO_4^-]_0$
0	0	0	0.3935	–	–
1	30	0.00542	0.4069	0.0194	3.582
2	60	0.01067	0.4173	0.0363	3.401
3	90	0.01578	0.4212	0.0465	2.949
4	140	0.02398	0.4307	0.0672	2.804
5	200	0.03332	0.4369	0.0870	2.612
6	300	0.04781	0.4393	0.1116	2.334
7	400	0.06109	0.4360	0.1295	2.119
8	500	0.07331	0.4315	0.1457	1.988
9	700	0.09504	0.4180	0.1706	1.795

Figure S17. Linear least squares fitting of the titration data in Table S18.

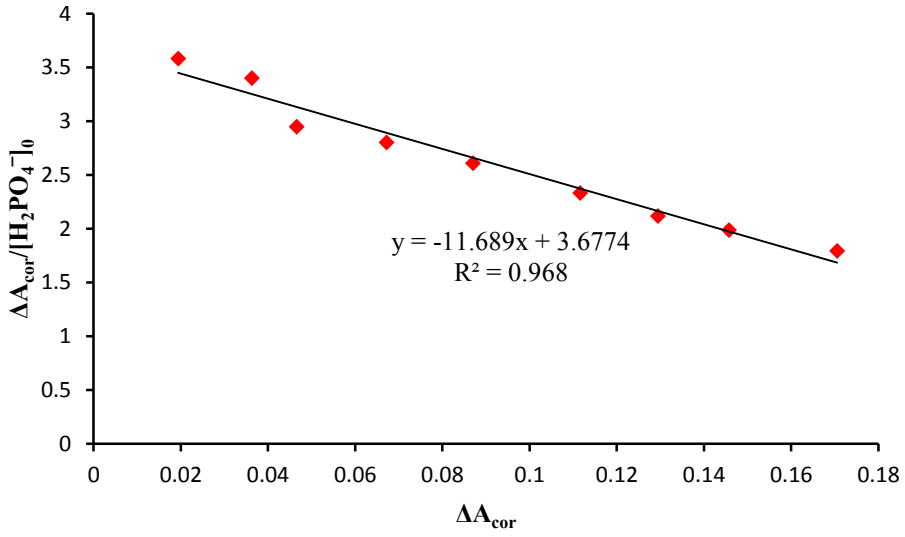

Table S19. Data for the titration of **1-mono** with OAc^- in 25% H_2O–DMSO at 387 nm.

Entry	µL OAc^- added	$[OAc^-]_0$, M	Observed absorption	ΔA_{cor}	$\Delta A_{cor}/[OAc^-]_0$
0	0	0	0.5513	–	–
1	15	0.00777	0.5829	0.0403	5.182
2	30	0.01532	0.6014	0.0681	4.443
3	50	0.02505	0.6207	0.1003	4.005
4	75	0.03670	0.6387	0.1352	3.684
5	100	0.04782	0.6454	0.1585	3.315
6	125	0.05845	0.6499	0.1796	3.073
7	150	0.06862	0.6597	0.2072	3.019
8	200	0.08769	0.6472	0.2250	2.566
9	250	0.1052	0.6357	0.2429	2.309
10	300	0.1214	0.6211	0.2558	2.106
11	400	0.1504	0.6010	0.2897	1.927
12	450	0.1633	0.5856	0.2973	1.820

Figure S18. Linear least squares fitting of the titration data in Table S19.

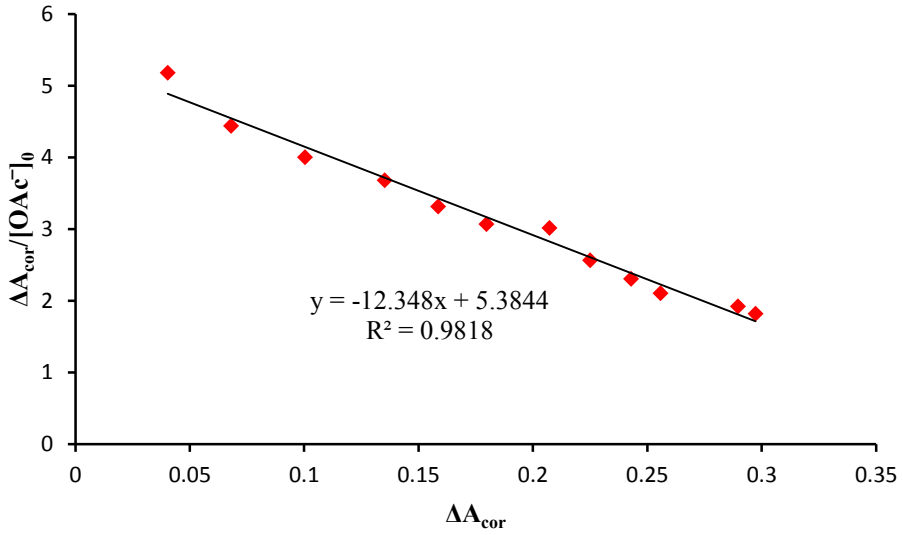

Tris-urea 2 binding to $H_2PO_4^-$ in 25% aqueous DMSO (*v/v*). A 15 µM solution of **2-tris** in 25% H_2O–DMSO (2.00 mL) was titrated with a 40.3 mM solution of

tetrabutylammonium dihydrogenphosphate in 25% H_2O–DMSO at 24 °C (Table S20). Non-linear curve fitting of the titration data affords K = 2300 M^{-1} and A_{max} = 0.526 (Figure S19).

Tris-urea 2 binding to OAc^- in 25% aqueous DMSO (*v/v*). A 15 μM solution of **2-tris** in 25% H_2O–DMSO (2.00 mL) was titrated with a 0.565 M solution of tetrabutylammonium acetate in 25% H_2O–DMSO at 24 °C (Table S21). A linear least squares fit in the single-reciprocal plot affords K = 154 M^{-1} and ΔA_{max} = 0.123 (Figure S20, 19-89% bound (i.e., $\Delta A/\Delta A_{max}$)).

Table S20. Data for the titration of **2-tris** with $H_2PO_4^-$ in 25% H_2O–DMSO at 382 nm.

Entry	μL $H_2PO_4^-$ added	$[urea]_0$, μM	$[H_2PO_4^-]_0$, μM	Observed absorption	Calculated absorption*
0	0	15	0	0.3472	0.3472
1	2.5	14.98	50.2	0.3638	0.3646
2	5	14.96	100	0.3777	0.3787
3	7.5	14.94	150	0.3909	0.3904
4	10	14.93	200	0.3995	0.4002
5	15	14.89	299	0.4149	0.4156
6	20	14.85	398	0.4283	0.4271
7	25	14.82	497	0.4387	0.4358
8	30	14.78	594	0.4434	0.4426
9	40	14.71	789	0.4501	0.4524
10	55	14.60	1076	0.4593	0.4610
11	80	14.42	1547	0.4669	0.4674
12	105	14.25	2006	0.4685	0.4690
13	130	14.09	2455	0.4709	0.4682
14	180	13.76	3321	0.4627	0.4633

* From the non-linear curve fit.

Figure S19. Non-linear least squares fitting of the titration data in Table S20.

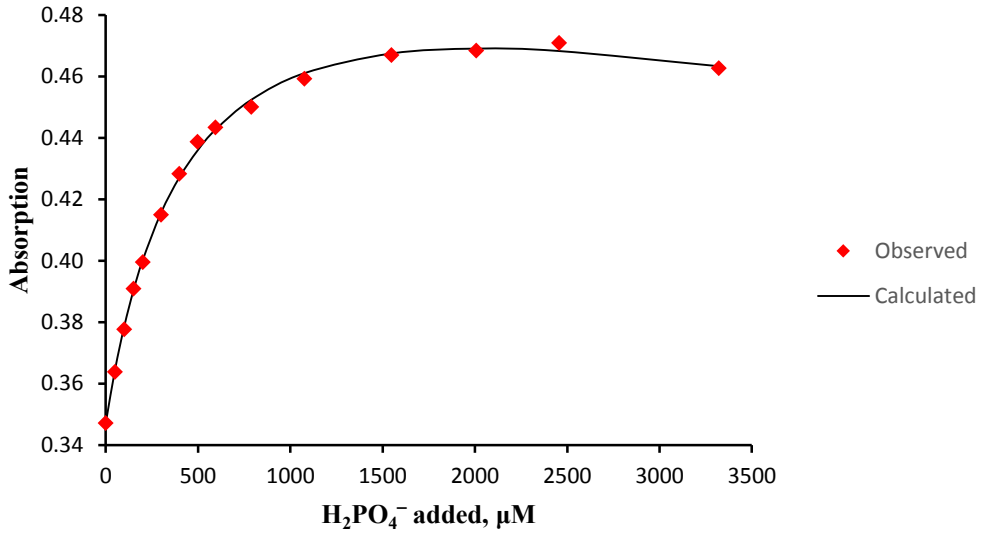

Table S21. Data for the titration of **2-tris** with OAc^- in 25% H_2O–DMSO at 375 nm.

Entry	µL OAc^- added	$[OAc^-]_0$, M	Observed absorption	ΔA_{cor}	$\Delta A_{cor}/[OAc^-]_0$
0	0	0	0.4496	–	–
1	5	0.00141	0.4715	0.0231	16.41
2	7.5	0.00211	0.4770	0.0292	13.85
3	10	0.00281	0.4848	0.0376	13.39
4	15	0.00420	0.4925	0.0466	11.09
5	20	0.00559	0.5018	0.0572	10.25
6	30	0.00834	0.5101	0.0682	8.178
7	45	0.01241	0.5203	0.0824	6.636
8	60	0.01643	0.5235	0.0896	5.455
9	80	0.02170	0.5213	0.0926	4.265
10	110	0.02941	0.5210	0.1001	3.402
11	150	0.03936	0.5185	0.1077	2.737
12	200	0.05129	0.5092	0.1105	2.154

Figure S20. Linear least squares fitting of the titration data in Table S21.

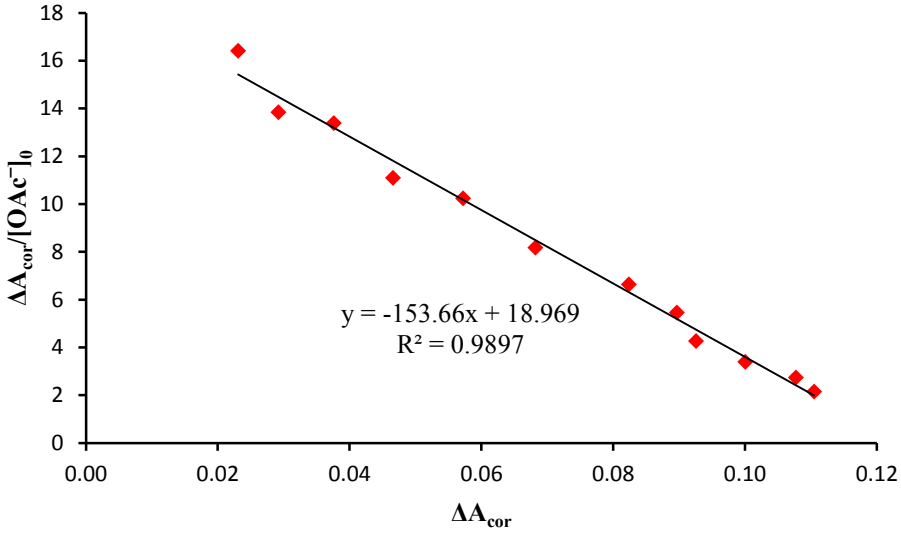

Tris-thiourea 1 binding to $H_2PO_4^-$ in 30% aqueous DMSO (*v/v*). A 15 μM solution of **1-tris** in 30% H_2O–DMSO (2.00 mL) was titrated with a 51.8 mM solution of tetrabutylammonium dihydrogenphosphate in 30% H_2O–DMSO at 23 °C (Table S22). Non-linear curve fitting of the titration data affords K = 1400 M^{-1} and A_{max} = 0.462 (Figure S21).

Tris-thiourea 1 binding to OAc^- in 30% aqueous DMSO (*v/v*). A 15 μM solution of **1-tris** in 30% H_2O–DMSO (2.00 mL) was titrated with a 0.462 M solution of tetrabutylammonium acetate in 30% H_2O–DMSO containing 15 μM of **1-tris** at 23 °C (Table S23). Non-linear curve fitting of the titration data with a fixed ΔA_{max} = 0.120 (i.e., as for the 25% H_2O–DMSO) affords K = 13 M^{-1} (entries 1–7, 1-40% bound (i.e., $\Delta A/\Delta A_{max}$); deviation was observed thereafter presumably due to sequential 1:2 binding, Figure S22).

Table S22. Data for the titration of **1-tris** with $H_2PO_4^-$ in 30% H_2O–DMSO at 395 nm.

Entry	µL $H_2PO_4^-$ added	$[thiourea]_0$, µM	$[H_2PO_4^-]_0$, µM	Observed absorption	Calculated absorption*
0	0	15.00	0	0.2271	0.2271
1	2	14.99	52	0.2494	0.2425
2	4	14.97	103	0.2616	0.2559
3	6	14.96	155	0.2710	0.2678
4	9	14.93	232	0.2865	0.2830
5	12	14.91	308	0.2980	0.2958
6	16	14.88	411	0.3088	0.3101
7	22	14.84	563	0.3249	0.3269
8	30	14.78	764	0.3388	0.3434
9	40	14.71	1014	0.3548	0.3579
10	50	14.63	1262	0.3658	0.3681
11	70	14.49	1749	0.3798	0.3809
12	90	14.35	2227	0.3877	0.3879
13	115	14.19	2813	0.3942	0.3923
14	140	14.02	3384	0.3978	0.3940

* From the non-linear curve fit.

Figure S21. Non-linear least squares fitting of the titration data in Table S22.

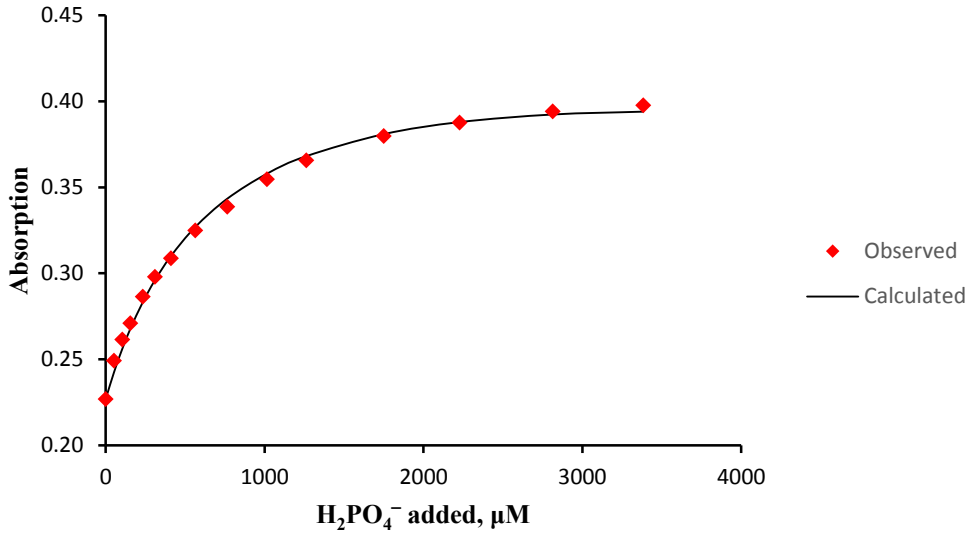

Table S23. Data for the titration of **1-tris** with OAc^- in 30% H_2O–DMSO at 379 nm.

Entry	μL OAc^- added	$[thiourea]_0$, mM	$[OAc^-]_0$, mM	Observed absorption	Calculated absorption*
0	0	0.015	0.00	0.3736	0.3736
1	5	0.015	1.15	0.3742	0.3754
2	10	0.015	2.30	0.3749	0.3771
3	50	0.015	11.25	0.3868	0.3890
4	100	0.015	21.97	0.3975	0.4004
5	150	0.015	32.19	0.4088	0.4091
6	200	0.015	41.94	0.4167	0.4161
7	250	0.015	51.26	0.4249	0.4218
8	300	0.015	60.18	0.4372	0.4265
9	400	0.015	76.90	0.4532	0.4338
10	500	0.015	92.29	0.4678	0.4393
11	600	0.015	106.49	0.4751	0.4435
12	775	0.015	128.89	0.4904	0.4490

* From the non-linear curve fit.

Figure S22. Non-linear least squares fitting of the titration data in Table S23.

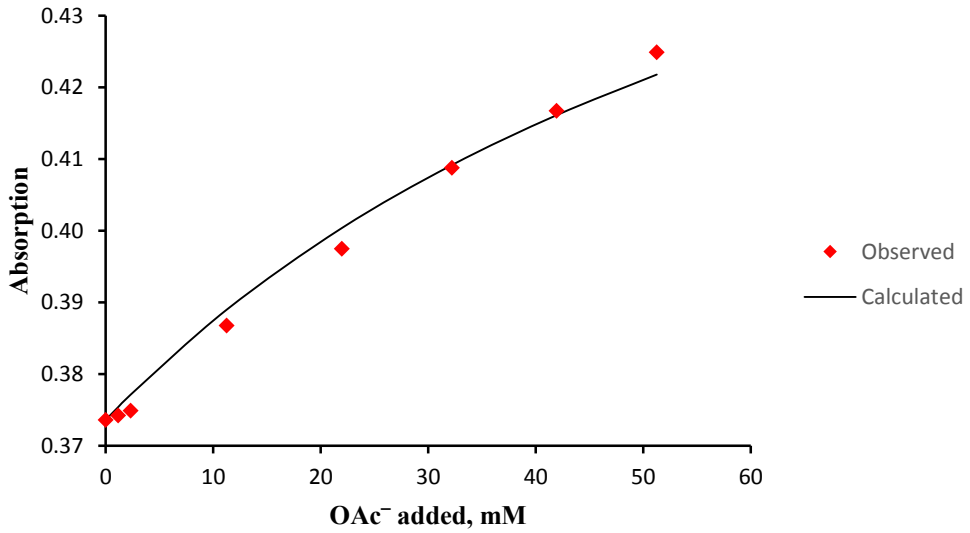

Tris-thiourea 1 binding to $H_2PO_4^-$ in 25% aqueous acetone (*v/v*). A 15 μM solution of **1-tris** in 25% H_2O–acetone (2.00 mL) was titrated with a 16.1 mM solution of tetrabutylammonium dihydrogenphosphate in 25% H_2O–acetone containing 15 μM of the thiourea at 24 °C (Table S24). Curve fitting for entries 1–8 (thereafter deviation was observed and the data could not be fit with a 1:1 binding curve) affords K = 5000 M^{-1} and A_{max} = 0.318 (Figure S23).

Tris-thiourea 1 binding to OAc^- in 25% aqueous acetone (*v/v*). A 15 μM solution of **1-tris** in 25% H_2O–acetone (2.00 mL) was titrated with a 0.513 M solution of tetrabutylammonium acetate in 25% H_2O–acetone containing 15 μM of the thiourea at

Table S24. Data for the titration of **1-tris** with $H_2PO_4^-$ in 25% H_2O–acetone at 383 nm.

Entry	μL $H_2PO_4^-$ added	$[thiourea]_0$, μM	$[H_2PO_4^-]_0$, μM	Observed absorption	Calculated absorption*
0	0	15	0.0	0.2398	0.2398
1	1	15	29.2	0.2499	0.2491
2	2	15	58.5	0.2565	0.2565
3	3	15	87.6	0.2632	0.2625
4	5	15	146	0.2723	0.2716
5	7.5	15	219	0.2784	0.2795
6	10	15	291	0.2844	0.2851
7	15	15	436	0.2921	0.2925
8	20	15	579	0.2982	0.2972
9	30	15	865	0.3068	0.3027
10	40	15	1147	0.3140	0.3058
11	60	15	1704	0.3241	0.3092
12	80	15	2251	0.3343	0.3111
13	110	15	3051	0.3443	0.3127
14	150	15	4083	0.3575	0.3138
15	200	15	5320	0.3739	0.3147
16	300	15	7634	0.3861	0.3155
17	0	15	146	0.2398	0.2398

* From the non-linear curve fit.

Figure S23. Non-linear least squares fitting of the titration data in Table S24 (entries 1-8).

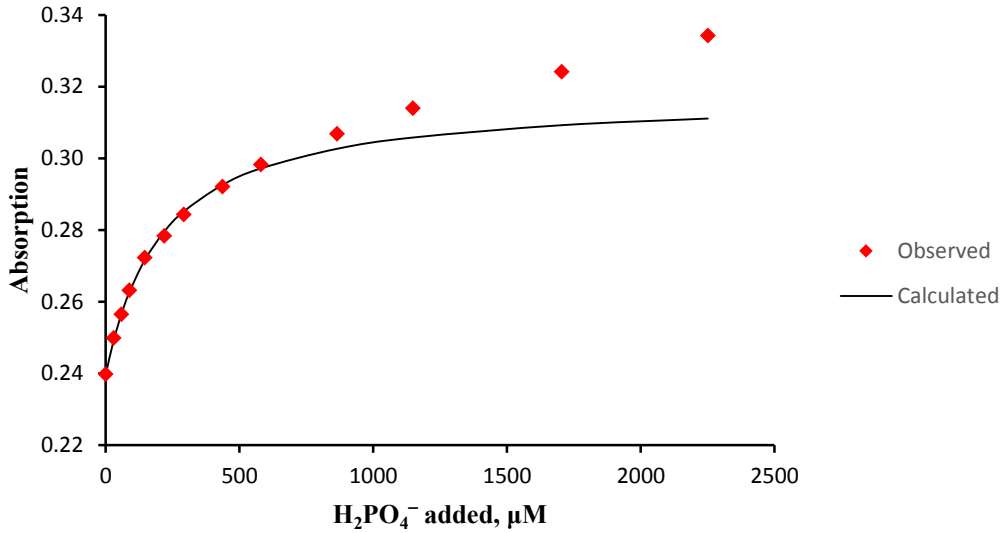

24 °C (Table S25). A linear least squares fit in the single-reciprocal plot affords K = 83 M^{-1} and ΔA_{max} = 0.210 (18-67% bound (i.e., $\Delta A/\Delta A_{max}$), Figure S24).

Table S25. Data for the titration of **1-tris** with OAc^- in 25% H_2O–acetone at 369 nm.

Entry	µL OAc^- added	$[OAc^-]_0$, M	Observed absorption	ΔA	$\Delta A/[OAc^-]_0$
0	0	0	0.4075	–	–
1	10	0.00243	0.4121	0.0348	14.29
2	15	0.00364	0.4259	0.0485	13.32
3	20	0.00484	0.4378	0.0605	12.48
4	25	0.00604	0.4487	0.0713	11.81
5	30	0.00723	0.4574	0.0801	11.07
6	40	0.00959	0.4729	0.0955	9.96
7	50	0.01193	0.4838	0.1064	8.92
8	65	0.01540	0.4932	0.1158	7.52
9	80	0.01882	0.5028	0.1254	6.67
10	100	0.02330	0.5158	0.1384	5.94

Figure S24. Linear least squares fitting of the titration data in Table S25.

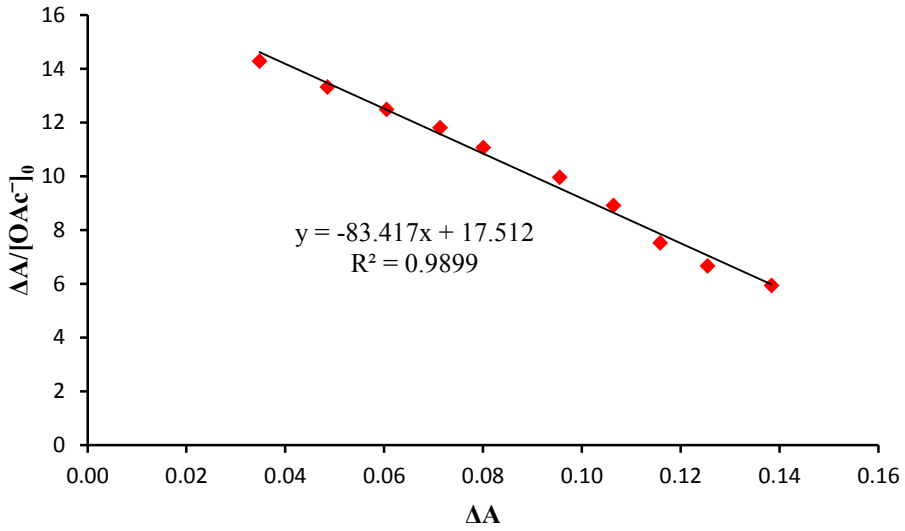

Tris-thiourea 5 binding to $H_2PO_4^-$ in 0.5 wt % aqueous DMSO. A 4.76 μM solution of **5-tris** in 0.5% H_2O–DMSO (2.10 mL) was titrated with a 1.00 mM solution of tetrabutylammonium dihydrogenphosphate in 0.5% H_2O–DMSO at 22 °C (Table S26). Non-linear curve fitting affords K = 7.7 x 10^5 M^{-1} and A_{max} = 0.312 (Figure S25).

Tris-thiourea 5 binding to Cl^- in 0.5 wt % aqueous DMSO-*d*$_6$. A 0.25 mM solution of **5-tris** in 0.5% H_2O–DMSO-*d*$_6$ (0.70 mL) was titrated with a 70.0 mM solution of tetrabutylammonium chloride in 0.5% H_2O–DMSO-*d*$_6$ at 23 °C (Table S27). Non-linear curve fitting affords K = 360 M^{-1} and δ_{max} = 10.740 ppm (Figure S26).

Tris-thiourea 5 binding to $H_2PO_4^-$ in 25% aqueous DMSO (v/v). A 25.0 μM solution of **5-tris** in 25% H_2O–DMSO (2.00 mL) was titrated with a 42.7 mM solution of

Table S26. Data for the titration of **5-tris** with $H_2PO_4^-$ in 0.5% H_2O–DMSO at 290 nm.

Entry	µL $H_2PO_4^-$ added	$[thiourea]_0$, µM	$[H_2PO_4^-]_0$, µM	Observed absorption	Calculated absorption*
0	0	4.76	0	0.2580	0.2580
1	4	4.75	1.90	0.2767	0.2730
2	5	4.75	2.38	0.2787	0.2763
3	6	4.75	2.85	0.2809	0.2793
4	7	4.74	3.32	0.2829	0.2820
5	8	4.74	3.80	0.2852	0.2845
6	9	4.74	4.27	0.2860	0.2867
7	10	4.74	4.74	0.2869	0.2887
8	11	4.74	5.21	0.2884	0.2905
9	12	4.73	5.68	0.2910	0.2920
10	14	4.73	6.62	0.2945	0.2945
11	16	4.72	7.56	0.2955	0.2964
12	18	4.72	8.50	0.2982	0.2978
13	20	4.72	9.43	0.2993	0.2989
14	30	4.69	14.1	0.3014	0.3014
15	40	4.67	18.7	0.3021	0.3017
16	50	4.65	23.3	0.3011	0.3013

* From the non-linear curve fit.

Figure S25. Non-linear least squares fitting of the titration data in Table S26.

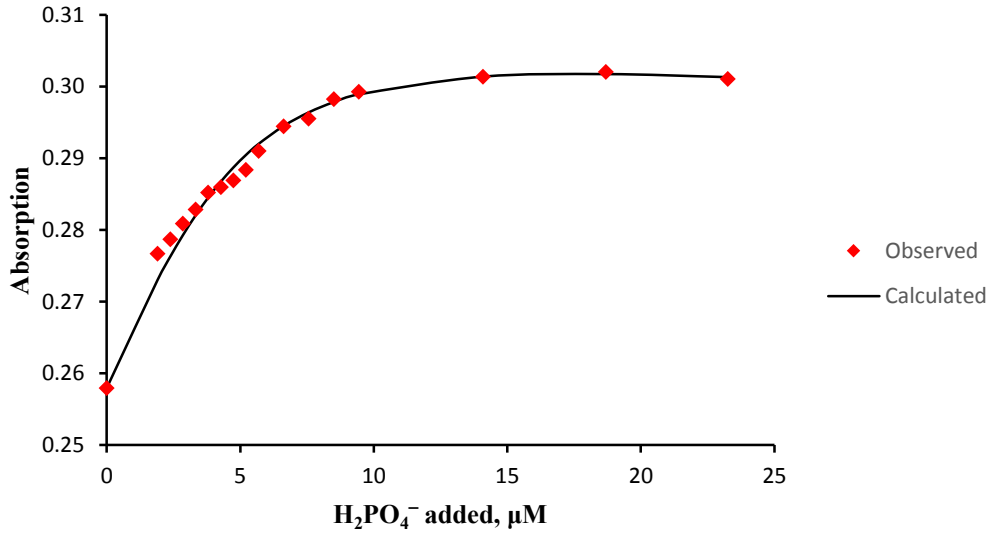

Table S27. Data for the ^{1}H NMR titration of **5-tris** with Cl^- in 0.5% H_2O–DMSO-d_6.

Entry	µL Cl^- added	[thiourea]$_0$, mM	[Cl^-]$_0$, mM	Observed δ	Calculated δ*
0	0	0.25	0	10.051	10.051
1	10	0.25	0.99	10.228	10.224
2	20	0.24	1.94	10.334	10.327
3	30	0.24	2.88	10.396	10.395
4	50	0.23	4.67	10.469	10.479
5	80	0.22	7.18	10.540	10.546
6	110	0.22	9.51	10.580	10.583
7	150	0.21	12.3	10.624	10.613

* From the non-linear curve fit.

Figure S26. Non-linear least squares fitting of the titration data in Table S27.

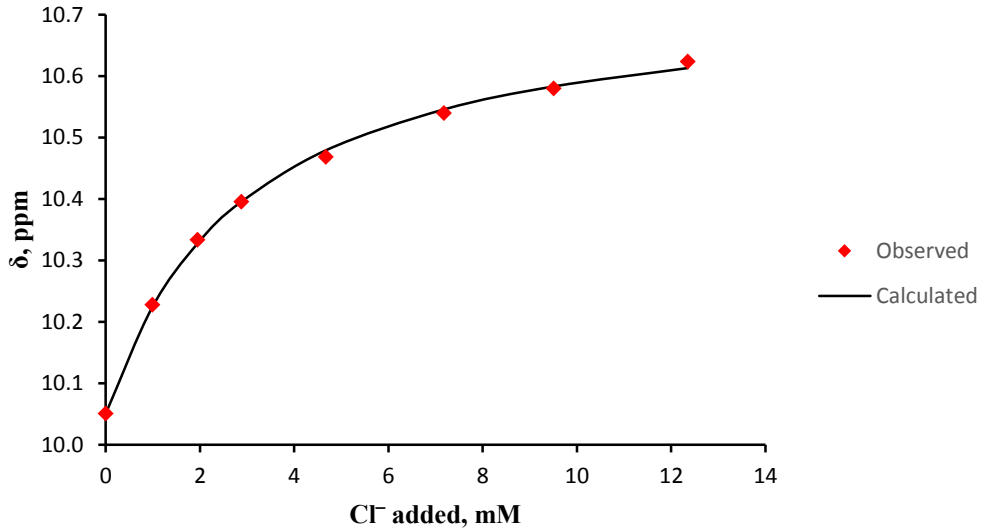

tetrabutylammonium dihydrogenphosphate in 25% H_2O–DMSO containing of **5-tris** 25.0 µM at 24 °C (Table S28). Non-linear curve fitting affords K = 1.0 x 10^4 M^{-1} and A_{max} = 1.332 (Figure S27).

Table S28. Data for the titration of **5-tris** with $H_2PO_4^-$ in 25% H_2O–DMSO at 289 nm.

Entry	µL $H_2PO_4^-$ added	$[thiourea]_0$, µM	$[H_2PO_4^-]_0$, µM	Observed absorption	Calculated absorption*
0	0	25	0.0	1.0623	1.1036
1	1	25	21.3	1.1057	1.1353
2	2	25	42.6	1.1386	1.1600
3	3	25	63.8	1.1600	1.1796
4	4	25	85.0	1.1793	1.1954
5	5	25	106	1.1891	1.2192
6	7	25	149	1.2191	1.2362
7	9	25	191	1.2356	1.2540
8	12	25	254	1.2553	1.2663
9	15	25	317	1.2723	1.2800
10	30	25	629	1.2907	1.3037
11	40	25	835	1.3049	1.1036

* From the non-linear curve fit.

Figure S27. Non-linear least squares fitting of the titration data in Table S28.

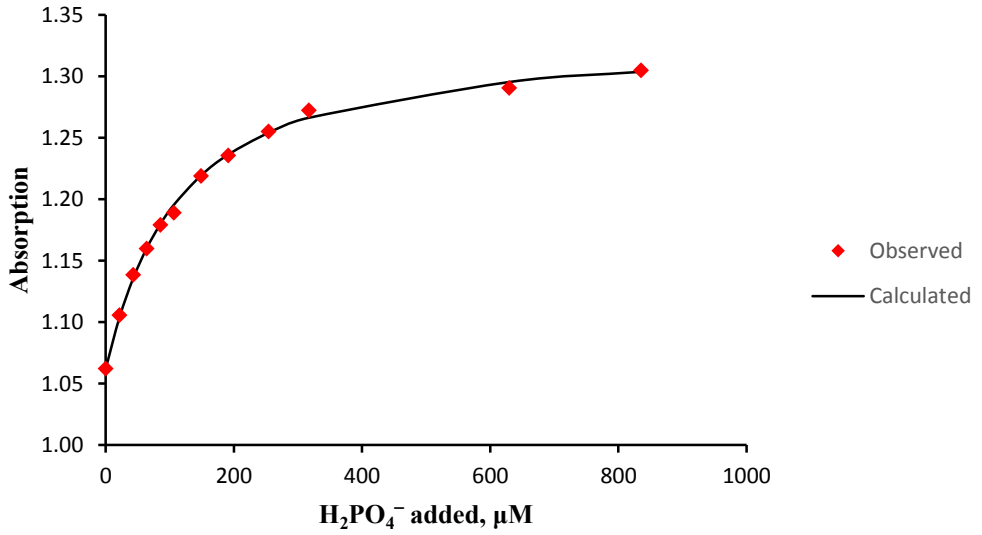

Tris-thiourea 6 binding to $H_2PO_4^-$ in 0.5 wt % aqueous DMSO. A 4.76 µM solution of **6-tris** in 0.5% H_2O–DMSO (2.10 mL) was titrated with a 1.00 mM solution of

tetrabutylammonium dihydrogenphosphate in 0.5% H_2O–DMSO at 22 °C (Table S29). Non-linear curve fitting affords K = 3.9 x 10^5 M^{-1} and A_{max} = 0.262 (Figure S28).

Table S29. Data for the titration of **6-tris** with $H_2PO_4^-$ in 0.5% H_2O–DMSO at 290 nm.

Entry	µL $H_2PO_4^-$ added	[thiourea]$_0$, µM	[$H_2PO_4^-$]$_0$, µM	Observed absorption	Calculated absorption*
0	0	4.76	0.00	0.2899	0.2899
1	4	4.75	1.90	0.2807	0.2828
2	6	4.75	2.85	0.2779	0.2798
3	8	4.74	3.80	0.2767	0.2772
4	10	4.74	4.74	0.2747	0.2750
5	15	4.73	7.09	0.2723	0.2707
6	17.5	4.72	8.26	0.2707	0.2690
7	20	4.72	9.43	0.2679	0.2677
8	25	4.70	11.8	0.2652	0.2655
9	30	4.69	14.1	0.2645	0.2638
10	40	4.67	18.7	0.2598	0.2611

* From the non-linear curve fit.

Figure S28. Non-linear least squares fitting of the titration data in Table S29.

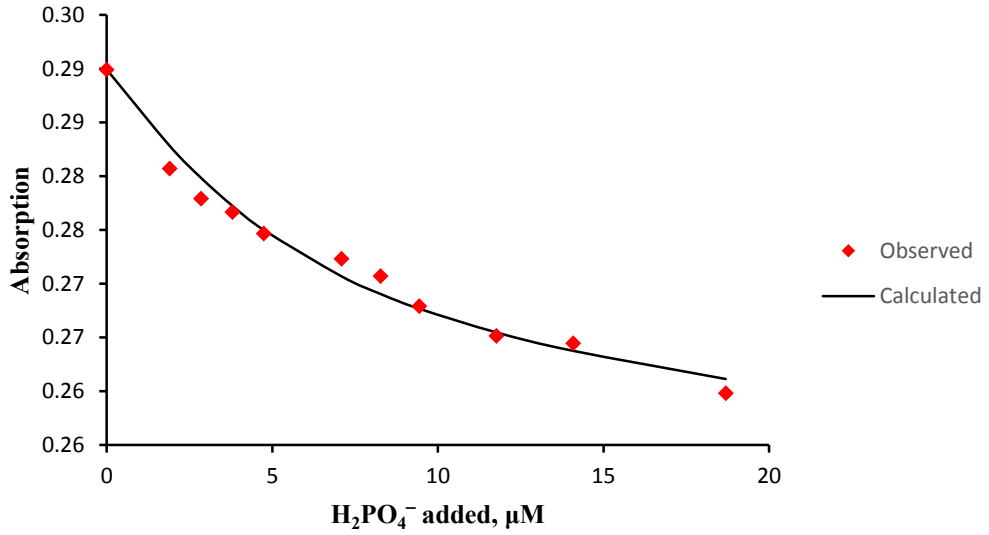

Tris-oxalamide 7 binding to $H_2PO_4^-$ in 0.5% aqueous DMSO (v/v). A 12.5 μM solution of **7** in 0.5% H_2O–DMSO (2.00 mL) was titrated with a 38.9 mM solution of tetrabutylammonium dihydrogenphosphate in 0.5% H_2O–DMSO containing 12.5 μM of **7** at 24 °C (Table S30). Non-linear curve fitting affords $K = 900\ M^{-1}$ and $A_{max} = 0.545$ (entries 1-13 were used for the analysis, deviations were observed thereafter presumably due to sequential 1:2 binding, Figure S29).

Table S30. Data for the titration of **7** with $H_2PO_4^-$ in 0.5% H_2O–DMSO at 432 nm.

Entry	μL $H_2PO_4^-$ added	$[amide]_0$, mM	$[H_2PO_4^-]_0$, mM	Observed absorption	Calculated absorption*
0	0	0.0125	0	0.0133	0.0133
1	2.6	0.0125	0.050	0.0412	0.0362
2	5	0.0125	0.097	0.0621	0.0556
3	7.5	0.0125	0.145	0.0770	0.0743
4	10	0.0125	0.193	0.0948	0.0916
5	15	0.0125	0.289	0.1242	0.1225
6	20	0.0125	0.384	0.1516	0.1493
7	30	0.0125	0.573	0.1941	0.1937
8	40	0.0125	0.761	0.2299	0.2288
9	55	0.0125	1.04	0.2627	0.2697
10	70	0.0125	1.31	0.2954	0.3008
11	85	0.0125	1.58	0.3208	0.3253
12	105	0.0125	1.94	0.3520	0.3508
13	150	0.0125	2.71	0.3974	0.3901
14	200	0.0125	3.53	0.4349	0.4175
15	300	0.0125	5.06	0.4869	0.4491
16	400	0.0125	6.47	0.5206	0.4669
17	500	0.0125	7.76	0.5426	0.4782

* From the non-linear curve fit.

Figure S29. Non-linear least squares fitting of the titration data in Table S30.

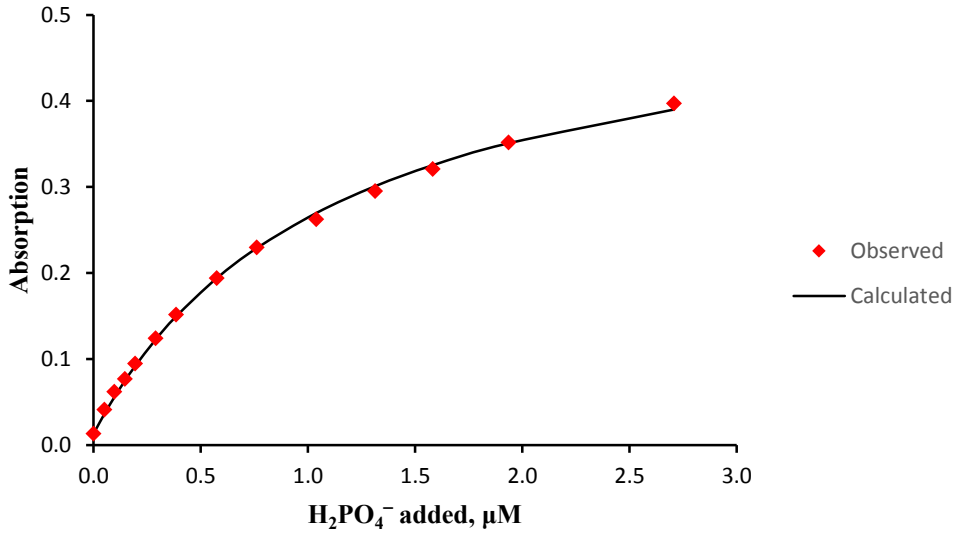

Tris-oxalamide 7 binding to OAc^- in 0.5% aqueous DMSO (v/v). A 12.5 µM solution of **7** in 0.5% H_2O–DMSO (2.00 mL) was titrated with a 49.7 mM solution of tetrabutylammonium acetate in 0.5% H_2O–DMSO containing 12.5 µM of **7** at 24 °C (Table S31). Non-linear curve fitting affords $K = 4.6 \times 10^4\ M^{-1}$ and $A_{max} = 0.264$ (entries 1-5 were used for the analysis; deviations were observed thereafter presumably due to sequential 1:2 binding, Figure S30).

Table S31. Data for the titration of **7** with OAc^- in 0.5% H_2O–DMSO at 432 nm.

Entry	µL OAc^- added	$[amide]_0$, mM	$[OAc^-]_0$, mM	Observed absorption	Calculated absorption*
0	0	0.0125	0	0.0250	0.0250
1	1	0.0125	0.025	0.1354	0.1365
2	2	0.0125	0.050	0.1850	0.1817
3	3	0.0125	0.074	0.1998	0.2041
4	4	0.0125	0.099	0.2194	0.2170
5	5	0.0125	0.124	0.2250	0.2254
6	7.5	0.0125	0.185	0.2524	0.2374
7	10	0.0125	0.247	0.2677	0.2436
8	15	0.0125	0.369	0.2906	0.2501
9	20	0.0125	0.491	0.3070	0.2534
10	30	0.0125	0.733	0.3280	0.2568
11	40	0.0125	0.972	0.3372	0.2584
12	60	0.0125	1.44	0.3554	0.2602
13	80	0.0125	1.91	0.3708	0.2610
14	120	0.0125	2.81	0.3969	0.2619

* From the non-linear curve fit.

Figure S30. Non-linear least squares fitting of the titration data in Table S31.

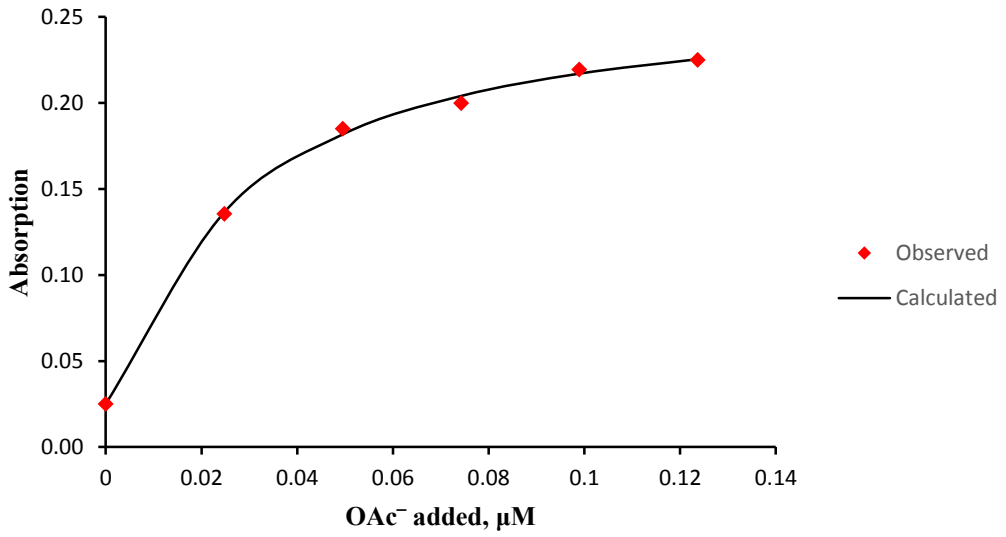

Kinetics of the Friedel-Crafts reaction of β-nitrostyrene with *N*-methylindole. A stock solution of β-nitrostyrene (89.4 mg, 0.600 mmol, 0.25 M) and *N*-methylindole (236 mg, 1.80 mmol, 0.75 M) in CD_2Cl_2 (2.10 mL) was prepared. Portions of this solution (1.00 mL) were added to **5-tris** (11.7 mg, 10.0 μmol) and **5-bis** (8.0 mg, 10.0 μmol), and the resulting mixtures were transferred into NMR tubes. The reactions were followed by ^{1}H NMR (Table S32) at 23 ± 1 °C (i.e., ambient temperature) as described earlier in Chapter 5. Second-order rate constants were obtained from linear least squares fits of the plots of $\ln([A][B]_0/[A]_0[B])/([A]_0 - [B]_0) = \ln((300\text{-}y)/(100\text{-}y)*3)/0.5$ versus time (Figure S31) where the slope is k and [A] = [β-nitrostyrene], [B] = [*N*-methylindole] and y is the yield. The resulting rate constants are $k_{tris} = 1.1 \times 10^{-2}$ M^{-1} h^{-1} and $k_{bis} = 6.1 \times 10^{-3}$ M^{-1} h^{-1}. This leads to $k_{tris}/k_{bis} = 1.8$. An estimate of the background rate ($k_0 = 3.5 \times 10^{-5}$) was obtained from a single point where y = 0.70% at 266 h.

Table S32. Kinetic data for the Friedel-Crafts reaction.

Catalyst	Time (h)	Yield, %	$\ln([A][B]_0/[A]_0[B])/([A]_0 - [B]_0)$
5-tris	1.05	1.01	0.0136
	2.33	2.09	0.0283
	5.63	4.73	0.0651
5-bis	2.45	1.24	0.0167
	5.68	2.68	0.0364

Figure S31. Linear least squares fits of the kinetic data in Table S32.

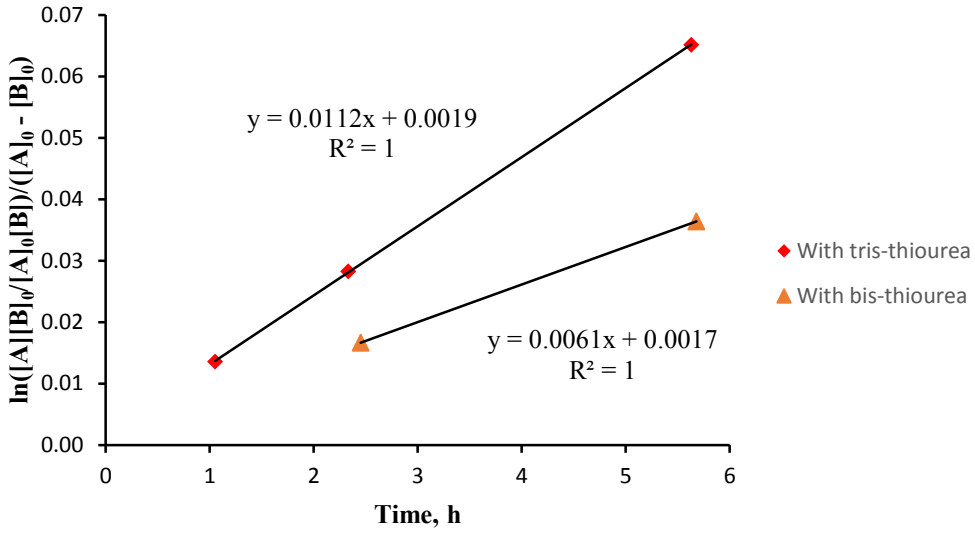

Kinetics of the ring opening reaction of styrene oxide with thiophenol. A stock solution of styrene oxide (180 mg, 1.50 mmol, 0.50 M) and thiophenol (154 µL, 1.50 mmol, 0.50 M) in toluene-d_6 (2.67 mL) was prepared. Portions of this solution (1.00 mL) were added to **5-tris** (11.7 mg, 10.0 µmol) and **5-bis** (8.0 mg, 10.0 µmol). Di-*iso*-propylethylamine (22 µl, 0.125 mmol. 0.125 M) was added to each of the solutions and they were transferred into NMR tubes. The reactions were followed by ^{1}H NMR (Table S33) at 23 ± 1 °C (i.e., ambient temperature) as described earlier in Chapter 5. Second-order rate constants were obtained from linear least squares fits of the plots of [P]/[SM] versus time (Figures S32 and S33) where the slope is $k/[SM]_0$ and [SM] = styrene oxide], and [P] = [product]. The resulting rate constants are $k_{tris}(CH_2)$ = 7.2 x 10^{-2} M^{-1} h^{-1} and $k_{bis}(CH_2)$ = 4.5 x 10^{-2} M^{-1} h^{-1} with the relative rate of k_{tris}/k_{bis} (CH_2) = 1.6 for the attack at

the primary position, and k_{tris}(CH) = 6.9 x 10^{-2} M^{-1} h^{-1} and k_{bis}(CH) = 3.4 x 10^{-2} M^{-1} h^{-1} with the relative rate of k_{tris}/k_{bis} (CH) = 2.0 for the attack at the CH of the epoxide.

Table S33. Kinetic data for the epoxide ring-opening reaction.

With **5-tris**			With **5-bis**		
Time	[P-CH_2]/[SM]	[P-CH]/[SM]	Time	[P-CH_2]/[SM]	[P-CH]/[SM]
0.943	0.108	0.0939	0.953	0.0756	0.0563
1.89	0.235	0.207	1.93	0.158	0.119
2.92	0.394	0.358	2.95	0.254	0.193

Figure S32. Linear least square fits for the P-CH_2 data in Table S33.

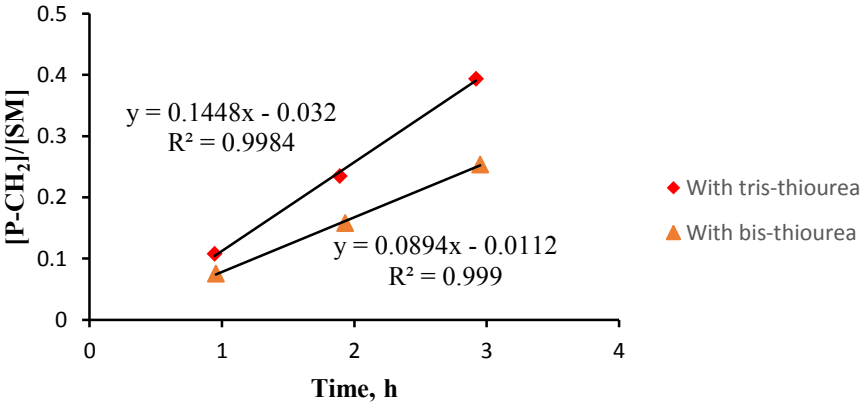

Photoelectron spectroscopy. These spectra were recorded for clusters of thioureas **1-tris**, **1-bis** and **1-mono** with Cl^-, OAc^- and $H_2PO_4^-$ (Figure S34) as reported in the experimental section of Chapter 4. Adiabatic detachment energies were obtained from the rapidly rising onset energies and have an estimated uncertainty of ± 0.1 eV.

Figure S33. Linear least square fits for the P-CH data in Table S33.

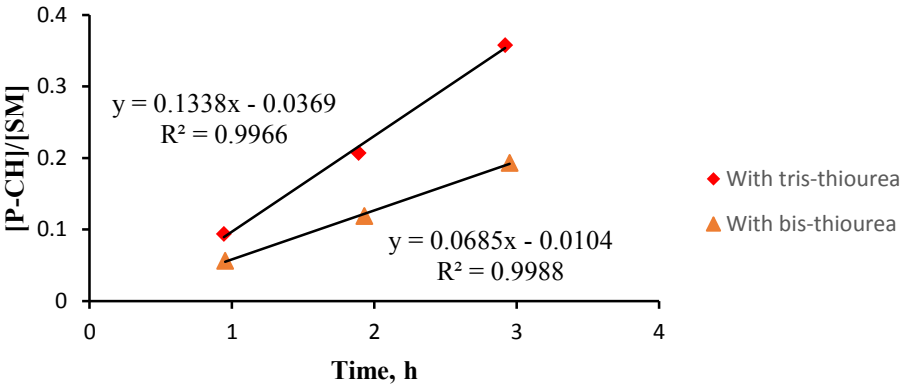

Figure S34. Low-temperature (20 K) photoelectron spectra of thioureas anion clusters **1** • X^- at 157 nm (7.867 eV).

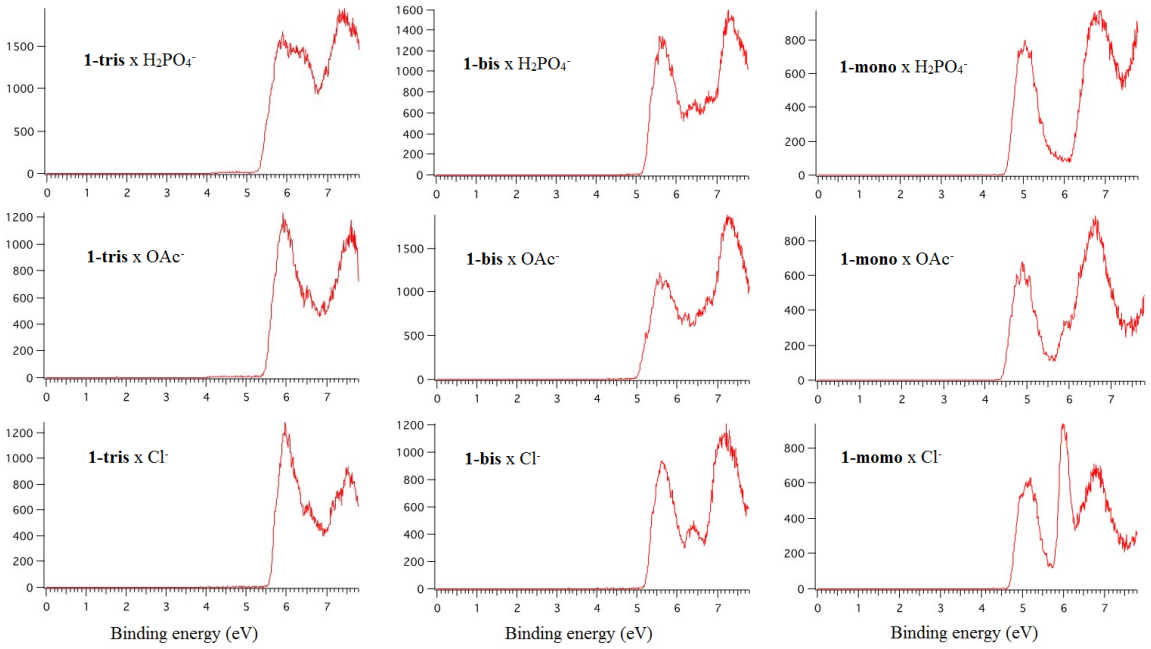

Chapter 8: Rigid 1,3,5-triarylbenzene receptors

Anion binding studies of functionalized 1,3,5-triarylbenzenes were discussed in Chapters 4 and 7. To establish the influence of the rigidity (i.e., rotation about the Ar–Ar bond) on the binding properties, rigid tris-phenol (*syn*-**1**, Chapter 4) and its freely rotating analog (**1a**, Chapter 5) were compared (i.e., R = Me and H, respectively, in Table 1). Large differences were observed between these two compounds in binding to Br^-. This suggests that the freely rotating compound, unlike its rigid analog, is not as twisted and is stabilized by conjugation of the aryl rings by at least 2.7 kcal/mol (i.e., –RTln(4300/46) at 23 °C).

Table 1. Binding affinities to Br^- of rigid and freely rotating tris-phenols in CD_3CN.

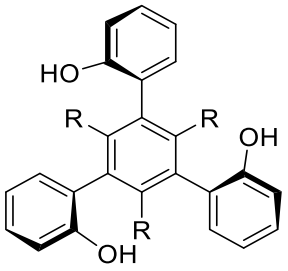

R	K_{11}, M^{-1}
H	46
Me	4300

To measure the effect of the rigidity on the binding affinities of 1,3,5-tris(2-aminophenyl)benzene-based (i.e., **4-tris**, Chapter 7) receptors, the analogous tris-amine bearing three methyl groups on the central benzene ring was synthesized (**1**, Scheme 1). The rotation of the 2-aminophenyl substituent about the Ar–Ar bond in this compound is slow and occurs only at temperatures above 180 °C. This allows the separation of the two isomers (i.e., *syn* and *anti*) at room temperature. The key step in the synthesis is a sterically

Scheme 1. Synthesis of the rigid tris-amine ***syn*-9**.

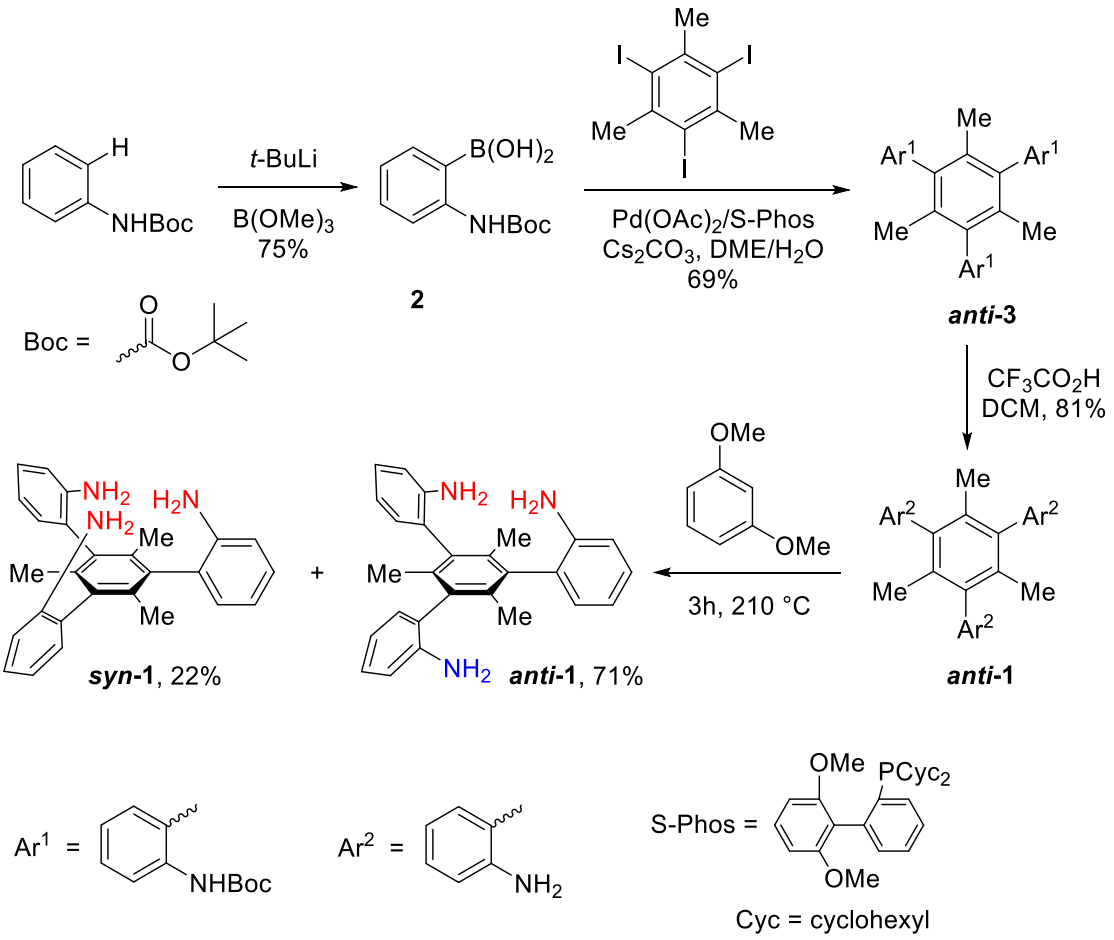

challenging Suzuki cross-coupling reaction of the protected 2-aminophenylboronic acid (**2**) with triiodomesitylene. No reaction was achieved with the trimethylacetyl amide (i.e., the pivaloyl group) of the boronic acid, but a good yield was obtained with the more electron rich and less sterically hindered Boc-protected derivative when S-Phos, a ligand designed by Buchwald for bulky substrates,[1] was used. Only the *anti*-isomer of **3** was isolated from this reaction, but upon deprotection of the *anti*-rotamer its tris-amine could be isomerized at 210 °C to a 1 : 3.2 *syn*-**1** : *anti*-**1** mixture. 1,3-Dimethoxybenzene was

found to be a much better solvent than xylene for this thermolysis reaction as it led to a much cleaner product mixture.

Tris-amide **4** and tris-thiourea **5** were synthesized from the amine *syn*-**1** (Scheme 2). The binding affinities of these rigid receptors were compared to their analogs without

Scheme 2. Synthesis of the rigid amide and thiourea based receptors.

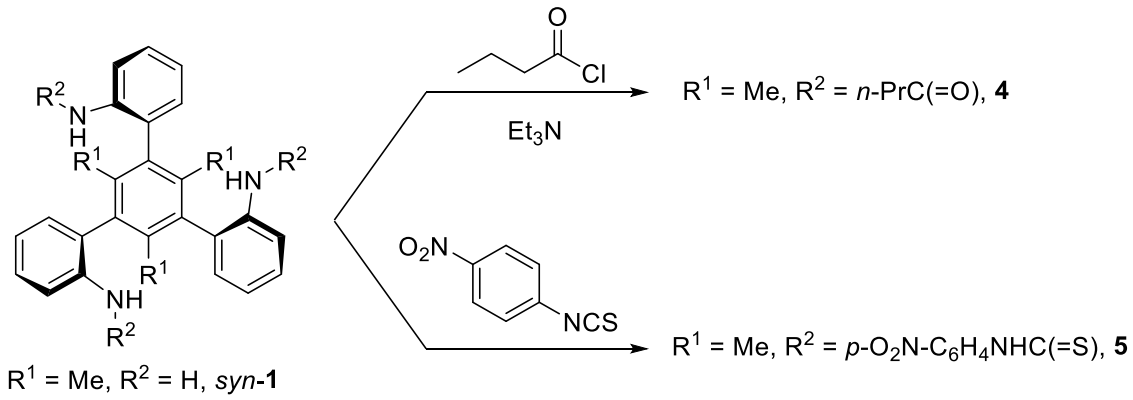

methyl groups on the central ring. That is, amide **4** was compared with the previously reported freely rotating compound,[2] and thiourea **5** with its analog described in Chapter 7 (**1-tris**). Rigid receptors are expected to bind more strongly since they are locked in the preferred conformation, however, binding studies (Table 2) showed that the observed differences for both amide and thiourea compounds were small. This suggests that the freely rotating amides and thioureas (i.e., R^1 = H) exist as a mixture of conformers, but there is a significant amount of the *syn*-rotamer unlike their tris-phenol derivatives. This difference can be attributed to the larger size of the NHR^2 substituent compared to the hydroxyl group and thus the destabilization of the in-plane rotamer of the amide and

thiourea receptors. The N–H bonds must also point in towards the central aryl ring whereas the OH substituents can point away from it.

Table 2. Comparison of binding affinities of rigid and freely rotating receptors.

Anion	Compound			K_{11}, M^{-1}
Cl^- [a]	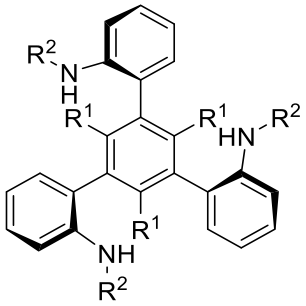	$R^1 = H$	$R^2 = n$-PrCO	1540
		$R^1 = Me$		9200
$H_2PO_4^-$ [b]		$R^1 = H$	$R^2 = p$-O_2N–$C_6H_4NHC(=S)$	4000
		$R^1 = Me$		8400

[a] In CH_3CN. [b] In 25% H_2O–DMSO (v/v).

In summary, the binding affinities of freely rotating and rigid receptors were compared. Tris-phenols had a large difference (i.e., *ca.* 100 fold) indicative of a strong stabilization of the in-plane conformation of the freely rotating compound. In contrast, the amide and thiourea N–H receptors showed only small differences, suggesting destabilization of the planar conformation and the presence of a significant rotation barrier about the Ar–Ar bond in the "freely" rotating species.

Experimental

***anti*-1,3,5-tris(2-*t*-Butyloxycarbonylaminophenyl)-2,4,6-trimethylbenzene (3).** A round-bottomed flask equipped with a reflux condenser was charged with 2-*t*-Boc-

aminophenylboronic acid (**2**)[3] (22.0 g, 93 mmol), triiodomesitylene[4] (6.04 g, 12.1 mmol), cesium carbonate (39.0 g, 120 mmol), palladium (II) acetate (138 mg, 0.61 mmol) and 2-dicyclohexylphsphino-2',6'-dimethoxybiphenyl (SPhos, 503 mg, 1.23 mmol). The system was purged with nitrogen and 120 mL of a 1:1 1,2-dimethoxyethane–water mixture that had been deoxygenated by bubbling nitrogen in it for 15 min was added via syringe. The resulting bilayer solution was refluxed with vigorous stirring for 16 h under nitrogen. Ethyl acetate (50 mL) was added and both layers were separated and the organic layer was dried over Na_2SO_4 and concentrated under reduced pressure. Medium pressure liquid chromatography (MPLC) on silica gel of the residue with ethyl acetate : hexanes (2 : 98 to 20 : 80) afforded 5.90 g (69%) of **3** as a white solid (R_f = 0.23 (EtOAc : hexanes, 10 : 90)). ^{1}H NMR (500 MHz, $CDCl_3$) δ 8.07 (br d, *J* = 8.0 Hz, 3H), 7.38 (dt, *J* = 1.5 and 8.0 Hz, 3H), 7.15 (t, *J* = 7.5 Hz, 3H), 7.10 (dd, *J* = 1.5 and 7.0 Hz, 2H), 7.07 (d, *J* = 7.5 Hz, 1H), 6.07 (s, 1H), 6.05 (s, 2H), 1.71 (s, 3H), 1.68 (s, 6H), 1.49 (s, 9H), 1.47 (s, 18H). ^{13}C NMR (75 MHz, $CDCl_3$) δ 152.9, 136.4, 135.9, 135.7, 135.6, 129.8, 129.7, 129.6, 129.6, 128.4, 128.4, 123.4, 123.2, 120.0, 119.9, 80.8, 80.6, 28.2, 18.5, 18.2 (four signals are not resolved, but presumably are at 152.9, 136.4, 135.9 and 28.2). HRMS-ESI: calcd for $C_{42}H_{51}N_3O_6Na$ $(M + Na)^+$ 716.3670, found 716.3664.

***anti*-1,3,5-tris(2-Aminophenyl)-2,4,6-trimethylbenzene (*anti*-1).** To a solution of tris-Boc-amine **3** (4.85 g, 7.0 mmol) in DCM (100 mL) was added trifluoroacetic acid (10 mL, 130 mmol) at 0 °C under nitrogen. The reaction mixture was stirred for 16 h at ambient temperature and quenched with saturated aqueous $NaHCO_3$ solution (300 mL). The organic layer was washed with water (300 mL), dried over Na_2SO_4 and concentrated under reduced

pressure to afford 2.24 g (81%) of *anti*-**1** as a pale yellow powder (R_f = 0.72 (EtOAc : hexanes, 50 : 50)). ^{1}H NMR (500 MHz, $CDCl_3$) δ 7.17 (app tt, *J* = 1.5 and 8.0 Hz, 3H), 6.99 (dd, *J* = 1.5 and 7.5 Hz, 2H), 6.97 (dd, *J* = 1.5 and 7.5 Hz, 1H), 6.84 (dt, *J* = 1.0 and 7.5 Hz, 3H), 6.79 (dd, *J* = 1.0 and 8.0 Hz, 3H), 3.52 (s, 2H), 3.47 (s, 4H), 1.79 (s, 6H), 1.78 (s, 3H). ^{13}C NMR (75 MHz, $CDCl_3$) δ 143.6, 143.4, 136.6, 136.5, 135.5, 135.5, 130.0, 128.0, 127.1, 127.0, 118.7, 118.5, 115.1, 17.9, 17.7 (three signals are not resolved, but presumably are at 130.0, 128.0 and 115.1). HRMS-ESI: calcd for $C_{27}H_{27}N_3Na$ $(M + Na)^+$ 416.2097, found 416.2103.

***syn*-1,3,5-tris(2-Aminophenyl)-2,4,6-trimethylbenzene (*syn*-1).** Tris-amine ***anti*-1** (2.21 g, 5.62 mmol) was dissolved in 1,3-dimethoxybenzene (30 mL) by gentle heating in a round bottomed flask under nitrogen. Nitrogen was bubbled through the solution with stirring over 30 min to remove oxygen from the system. The reaction mixture was heated at 210 °C with stirring for 3 h and concentrated under reduced pressure. Medium pressure liquid chromatography (MPLC) on silica gel of the residue with methanol : ethyl acetate : hexanes (0 : 12 : 88 to 20 : 80 : 0) afforded 1.57 g (71%) of *anti*-**1**, and 495 mg (22%) of *syn*-**1** as a pale yellow powder (R_f = 0.27 (MeOH : EtOAc, 5 : 95)). ^{1}H NMR (500 MHz, $CDCl_3$) δ 7.17 (dt, *J* = 1.5 and 7.5 Hz, 3H), 7.02 (dd, *J* = 1.5 and 7.5 Hz, 3H), 6.86 (dt, *J* = 1.5 and 7.5 Hz, 3H), 6.80 (dd, *J* = 1.0 and 8.0 Hz, 3H), 3.41 (s, 6H), 1.79 (s, 9H). ^{13}C NMR (75 MHz, $CDCl_3$) δ 143.2, 136.6, 135.7, 130.0, 128.1, 127.2, 118.9, 115.2, 18.0. HRMS-ESI: calcd for $C_{27}H_{27}N_3Na$ $(M + Na)^+$ 416.2097, found 416.2098.

***syn*-1,3,5-tris(2-*n*-Butyrylaminophenyl)-2,4,6-trimethylbenzene (4).** To a solution of tris-amine *syn*-**1** (36.5 mg, 0.0929 mmol) and triethylamine (65 μL, 0.47 mmol) in dry

DCM (2.0 mL) was added butyryl chloride (39 μL, 0.38 mmol) at 0 °C under nitrogen. The reaction mixture was stirred at ambient temperature for 24 h and then ethyl acetate (10 mL) was added. The resulting solution was washed with water (2 x 5 mL) and brine (5 mL), dried over Na_2SO_4, and concentrated under reduced pressure. Medium pressure liquid chromatography (MPLC) on silica gel of the residue with ethyl acetate : dichloromethane (2 : 98 to 30 :70) afforded 48 mg (86%) of **4** as a white powder (R_f = 0.24 (EtOAc : DCM, 10 : 90)). ^{1}H NMR (500 MHz, acetone-d_6) δ 8.08 (app br s, 3H), 7.75 (br s, 3H), 7.36 (dt, J = 1.5 and 8.0 Hz, 3H), 7.23 (dt, J = 1.0 and 7.5 Hz, 3H), 7.13 (dd, J = 1.5 and 7.5 Hz, 3H), 2.28 (t, J = 7.5 Hz, 6H), 1.71 (s, 9H), 1.65 (sext, J = 7.5 Hz, 6H), 0.92 (t, J = 7.5 Hz, 9H). ^{13}C NMR (75 MHz, acetone-d_6) δ 172.0, 137.8, 137.5, 136.4, 134.2, 131.7, 129.2, 126.0, 123.9, 40.0, 20.2, 19.5, 14.5. HRMS-ESI: calcd for $C_{39}H_{45}N_3O_3Na$ $(M + Na)^+$ 626.3353, found 626.3363.

***syn*-1,3,5-tris[2-(3-(4-Nitrophenyl)thioureido)phenyl]-2,4,6-trimethylbenzene (5).** To a mixture of tris-aniline ***syn*-2** (26.3 mg, 66.9 μmol) and 4-nitrophenylisothiocyanate (55.2 mg, 307 μmol) was added dry THF (0.5 mL) under nitrogen. The solution was stirred for 16 h and concentrated under reduced pressure. Medium pressure liquid chromatography (MPLC) on silica gel of the residue with ethyl acetate : hexanes (16 : 84 to 100 : 0, with 2% methanol additive) afforded 33 mg (53%) of **5** as a yellow powder (R_f = 0.22 (MeOH : EtOAc, 10 : 90)). ^{1}H NMR (500 MHz, DMSO-d_6) δ 9.78 (br s, 3H), 8.64 (br s, 3H), 7.83 – 7.79 (m, 9H), 7.59 (t, J = 9.0 Hz, 6H), 7.42 (t, J = 7.0 Hz, 3H), 7.35 (t, J = 7.5 Hz, 3H), 7.21 (d, J = 7.0 Hz, 3H), 1.75 (s, 9H). ^{13}C NMR (75 MHz, DMSO-d_6) δ 179.4, 145.6, 142.3, 136.2, 135.9, 135.8, 134.3, 130.7, 127.6, 126.6, 123.4, 122.5, 19.3

(one signal is not resolved, but presumably is at 127.6). HRMS-ESI: calcd for $C_{48}H_{39}N_9O_6S_3Na$ $(M + Na)^+$ 956.2078, found 956.2060.

Binding constant determinations. Measurements of binding affinities to anions were carried out as described in the experimental sections of Chapter 4 (for ^1H NMR measurements) and 7 (for UV-VIS determinations).

Triol binding to Br^- in CD_3CN. A 250 μM solution of the triol (**1a**, Chapter 5) in CD_3CN (0.70 mL) was titrated with a 70.0 mM solution of tetrabutylammonium bromide in CD_3CN at 23 °C (Table S1). The chemical shift of the hydroxyl proton was followed by ^1H NMR. A single-reciprocal plot (i.e., $\Delta\delta/[Br^-]_0$ against $\Delta\delta$) of the data is linear initially (Figure S1) which is consistent with 1:1 binding (see Chapter 4 for details), and then deviates from the line as expected for a competitive 1:2 binding process. The 1:1 association constant was estimated from the slope of the linear portion (i.e., entries 1-5) to give $K = 46\ M^{-1}$ and $\Delta\delta_{max} = 1.29$.

Tris-amide binding to Cl^- in CH_3CN. A 25 μM solution of amide **4** in CH_3CN (2.00 mL) was titrated with a 20.0 mM solution of tetrabutylammonium chloride in CH_3CN containing 25 μM of the amide at 24 °C (Table S2). Curve fitting yielded $K = 9200\ M^{-1}$ and $A_{max} = 1.083$ (Figure S2).

Tris-thiourea binding to $H_2PO_4^-$ in 25% aqueous DMSO (v/v). A 15 μM solution of thiourea **5** in 25% H_2O–DMSO (2.00 mL) was titrated with a 10.0 mM solution of tetrabutylammonium dihydrogenphosphate in 25% H_2O–DMSO at 24 °C (Table S3). Non-linear curve fitting yielded $K = 8400\ M^{-1}$ and $A_{max} = 0.528$ (Figure S3).

Table S1. Data for the titration of the freely rotating tris-phenol **1a** with Br^-.

Entry	µL Br^- added	$[Br^-]_0$, mM	δ, ppm	Δδ, ppm	$\Delta\delta/[Br^-]_0$
0	0	0.00	6.902	0	–
1	5	0.50	6.931	0.029	0.0584
2	15	1.47	6.986	0.084	0.0572
3	45	4.23	7.109	0.207	0.0490
4	75	6.77	7.207	0.305	0.0450
5	125	10.6	7.334	0.432	0.0407
6	225	17.0	7.514	0.612	0.0359
7	475	28.3	7.768	0.866	0.0306
8	775	36.8	7.926	1.024	0.0278

Figure S1. Linear least squares fit of the titration data in Table S1 (entries 1-5).

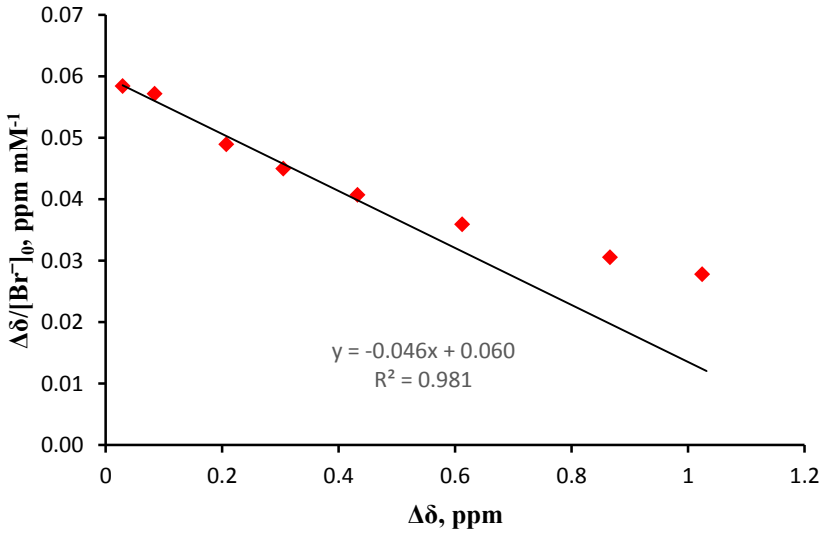

Table S2. Data for the titration of **4** with Cl^- in CH_3CN at 251 nm.

Entry	µL Cl^- added	[amide]$_0$, µM	[Cl^-]$_0$, µM	Observed absorption	Calculated absorption*
0	0	25	0.0	0.7622	0.7622
1	1	25	10.0	0.7821	0.7848
2	2	25	19.9	0.7995	0.8049
3	3	25	29.9	0.8186	0.8227
4	4	25	39.8	0.8326	0.8386
5	5	25	49.8	0.8495	0.8529
6	7	25	69.6	0.8801	0.8773
7	9	25	89.4	0.8979	0.8974
8	14	25	138	0.9352	0.9342
9	20	25	197	0.9648	0.9632
10	30	25	294	0.9985	0.9927
11	40	25	391	1.0151	1.0105
12	60	25	581	1.0332	1.0309
13	100	25	950	1.0449	1.0493
14	150	25	1392	1.0546	1.0593

* From the non-linear curve fit.

Figure S2. Non-linear least squares fitting of the titration data in Table S2.

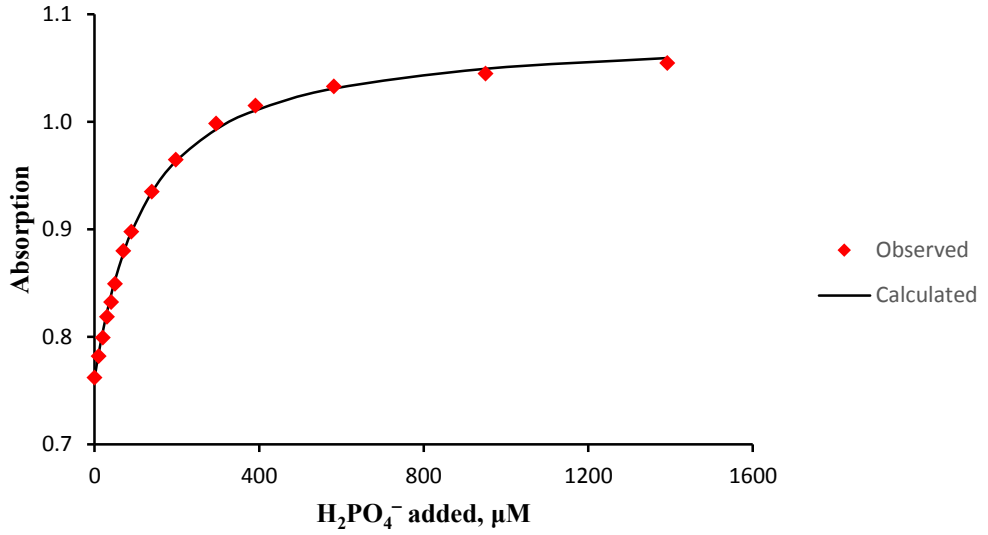

Table S3. Data for the titration of **5** with $H_2PO_4^-$ in 25 % H_2O–DMSO at 374 nm.

Entry	µL $H_2PO_4^-$ added	[thiourea]$_0$, µM	[$H_2PO_4^-$]$_0$, µM	Observed absorption	Calculated absorption*
0	0	15.0	0	0.4156	0.4156
1	2.5	15.0	12.5	0.4255	0.4246
2	5	14.9	24.9	0.4329	0.4323
3	7.5	14.9	37.3	0.4408	0.4387
4	10	14.9	49.7	0.4441	0.4443
5	15	14.9	74.3	0.4534	0.4531
6	20	14.8	98.9	0.4595	0.4598
7	30	14.8	147.6	0.4682	0.4689
8	40	14.7	195.8	0.4726	0.4744
9	70	14.5	337.7	0.4804	0.4807
10	95	14.3	452.8	0.4809	0.4809
11	120	14.1	565.2	0.4803	0.4789

* From the non-linear curve fit.

Figure S3. Non-linear least squares fitting of the titration data in Table S3.

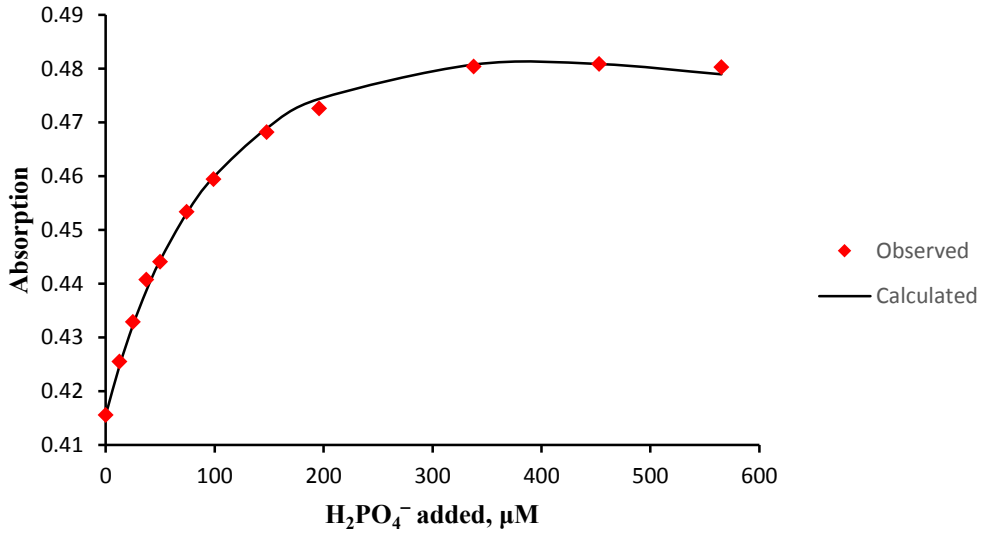

Chapter 9: Development of a fluorescent receptor

Due to the importance of dihydrogen phosphate detection (see Chapter 7), construction of a new fluorescent receptor for its selective recognition is a need.[1] Since most samples of interest are aqueous solutions (i.e., blood or waste/natural water samples), it is particularly important to develop receptors that would strongly and selectively bind in a competitive aqueous environment. The binding studies of the tris-thiourea functionalized 1,3,5-triphenylbenzene (**1-tris**, Chapter 7) in 25% aqueous DMSO solution showed over a 100-fold $H_2PO_4^-/OAc^-$ selectivity. Studies with model compounds indicated that $H_2PO_4^-$ binds to all three arms of this receptor whereas OAc^- binds to just one. This provides an opportunity to further improve the $H_2PO_4^-/OAc^-$ detection selectivity (Scheme 1).

Scheme 1. Proposed enhancement of the detection selectivity by the tris-thiourea receptor.

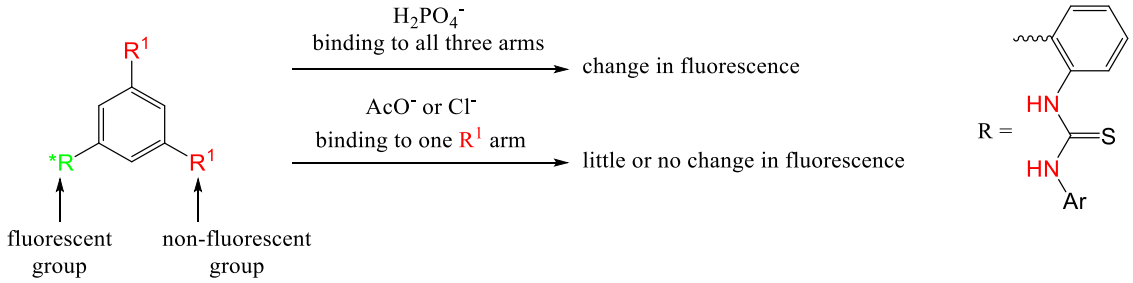

Substitution of one thiuorea arm with another that binds anions less tightly and has a fluorescent substituent presumably will not change the binding mode of $H_2PO_4^-$ or OAc^-, but the latter ion should bind with just the non-fluorescent thiourea arm. In this case binding

of $H_2PO_4^-$ is expected to change the fluorescence spectra whereas OAc^- will not. As a result, the detection selectivity would be higher than the binding selectivity.

Receptor **1** with three fluorescent pyrene-substituted thiourea-arms, as well as receptor **2** with only one fluorescent arm and two bis-CF_3-phenyl-substituted arms (as in **5-tris** in Chapter 7) were synthesized (Scheme 2). Compound **1** was obtained from 1-isothiocyanatopyrene and tris-amine **3** (**4-tris** in Chapter 7). Although no reaction was observed in THF at ambient temperature presumably due to the steric hindrance of the substrates, heating provided a low conversion and partial decomposition whereas the reaction was much faster in DMSO. After 2 h at 40 °C the reaction was complete and

Scheme 2. Synthesis of the fluorescent tris-thiourea receptors.

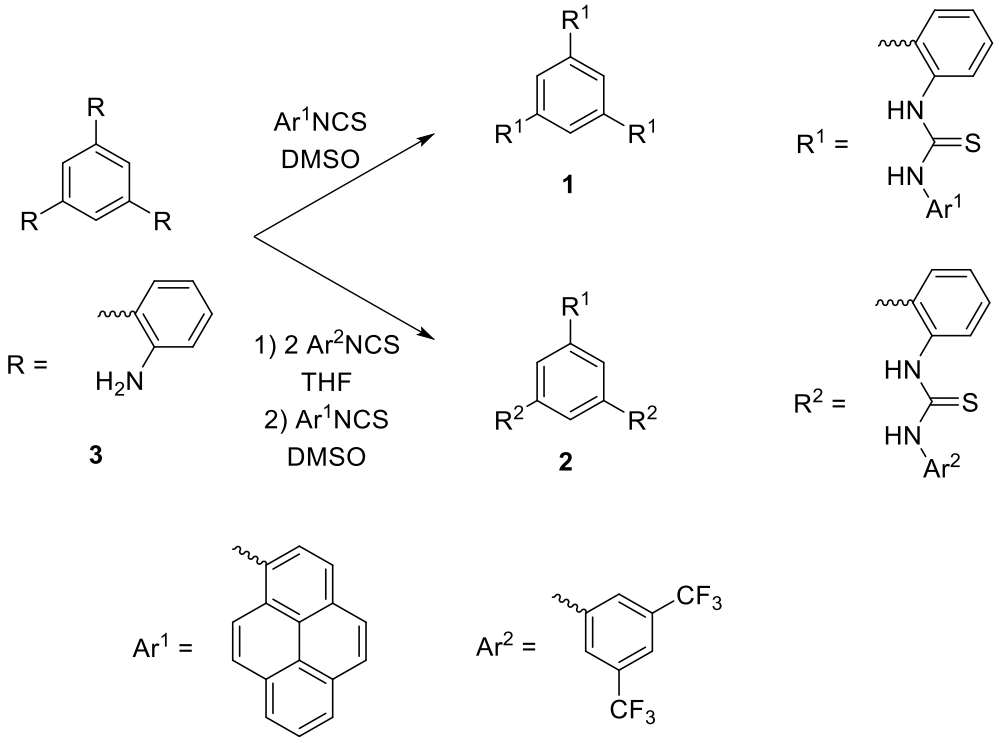

afforded almost pure **1**. To synthesize **2**, two equivalents of the bis-CF_3-phenyl isocyanate were added to **3** in THF to afford a mixture consisting of the mono, bis and tris thioureas. The bis-thiourea was isolated by column chromatography, recrystallized, and reacted with 1-isothiocyanatopyrene in DMSO to afford **2**.

Measurements in 25% aqueous DMSO revealed that the binding affinity of the symmetrical receptor **1** to $H_2PO_4^-$ is very weak (i.e., K = 71 M^{-1}) which precluded its use as a fluororeceptor. The mixed tris-thiourea **2** interacts with this anion much more strongly (i.e., K = 1600 M^{-1}) due to the presence of the two CF_3-substituted thiourea arms (K = 1.0 x 10^4 M^{-1} when all three arms have the CF_3 substituents (i.e., **5-tris** in Chapter 7)). We studied the fluorescence spectra of **2** in the presence of different anions in 25% aqueous DMSO. Free **2** showed a maximum at λ = 436 nm in the emission spectrum (Figure 1). Addition of $H_2PO_4^-$ (1 mM) to a 15 μM solution of **2** caused a new band in the subtraction

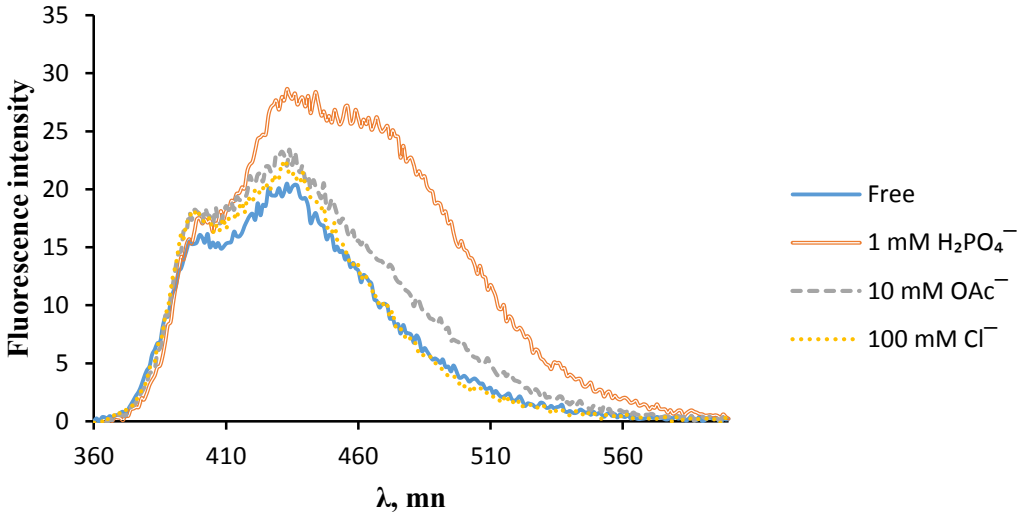

Figure 1. Fluorescent emission spectra of **2** alone and upon the addition of Bu_4N^+ salts of $H_2PO_4^-$, OAc^- and Cl^- in 25% aqueous DMSO (excitation λ_{ex} = 350 nm).

spectrum (i.e., **2** • $H_2PO_4^-$ – **2**) at λ = 474 nm, whereas acetate caused only slight spectral changes at higher concentration (i.e., 10 mM), and chloride did not produce any changes even at 100 mM.

In summary, we have constructed a selective fluororeceptor for dihydrogen phosphate in a 25% aqueous DMSO mixture. To make the receptor more useful for analytical applications, further research needs to be done in order to increase the response to $H_2PO_4^-$ and the detection limit which is *ca.* 0.1 mM for **2**.

Experimental

1,3,5-tris[2-(3-(Pyren-1-yl)thioureido)phenyl]benzene (1). To a mixture of tris-aniline **3** (70.2 mg, 0.20 mmol) and 1-isothiocyanatopyrene[2] (175 mg, 0.68 mmol) was added 5 mL of DMSO and the reaction mixture was stirred at 40 °C under nitrogen for 1 h. The solution was diluted with ethyl acetate (150 mL), washed with water (3 x 50 mL) and brine (50 mL), and dried over Na_2SO_4. Concentration under reduced pressure to *ca.* 50 mL and filtration of the precipitate afforded 166 mg (74%) of **1** as a light yellow powder (R_f = 0.36 (EtOAc : hexanes, 67 : 33)). ^{1}H NMR (500 MHz, DMSO-d_6) δ 10.22 (br s, 3H), 9.82 (br s, 3H), 8.25 (d, J = 7.5 Hz, 3H), 8.17 (d, J = 7.5 Hz, 3H), 8.13–7.99 (m, 15H), 7.86–7.78 (m, 15H), 7.53 (t, J = 7.5 Hz, 3H), 7.36 (t, J = 7.5 Hz, 3H). ^{13}C NMR (75 MHz, DMSO-d_6) δ 182.6, 139.2, 137.8, 136.6, 133.1, 130.6, 130.4, 129.7, 129.13, 129.05, 127.9, 127.23, 127.10, 126.94, 126.81, 126.47, 126.32, 125.3, 125.0, 124.5, 124.3, 123.7, 122.4

(two signals are not resolved, but possibly are at 127.2 and 126.3 ppm). HRMS-ESI: calcd for $C_{75}H_{48}N_6S_3Na$ $(M + Na)^+$ 1151.2995, found 1151.2990.

1,3-bis[2-(3-(3,5-Trifluoromethylphenyl)thioureido)phenyl]-5-[2-(3-(pyren-1-yl)thioureido)-phenyl]benzene (2). To a solution of tris-aniline **3** (105.3 mg, 0.30 mmol) in dry THF (3.0 mL) was added 3,5-trifluoromethylphenylisothiocyanate (110 μL, 0.60 mmol) dropwise at 0 °C under nitrogen. The reaction mixture was stirred at 0 °C for 1 h and at ambient temperature for 2 h. The solution was concentrated under reduced pressure and medium pressure liquid chromatography (MPLC) on silica gel of the residue with ethyl acetate : hexanes (30 : 70 to 100 : 0) followed by recrystallization from diethyl ether – hexanes (1 : 1) afforded 120 mg (45%) of the corresponding bis-thiourea as a white powder (R_f = 0.21 (EtOAc : hexanes, 50 : 50)). ^{1}H NMR (500 MHz, $CDCl_3$) δ 8.96 (br s, 2H), 7.90 (br s, 2H), 7.77 (s, 4H), 7.59 (app br s, 4H), 7.52–7.44 (m, 9H), 7.12 (t, *J* = 7.5 Hz, 1H), 6.98 (d, *J* = 7.0 Hz, 1H), 6.73 (t, *J* = 7.5 Hz, 1H), 6.67 (d, *J* = 8.0 Hz, 1H), 3.79 (s, 2H).

A solution of the bis-thiourea (36 mg, 40 μmol) and 1-isothiocyanatopyrene (16 mg, 60 μmol) in DMSO-d_6 (0.4 mL) was heated at 40 °C and monitored by ^{1}H NMR. Ethyl acetate (15 mL) was added after 2 h (complete conversion) and this solution was washed with water (3 x 50 mL) and brine (50 mL), dried over Na_2SO_4 and concentrated under reduced pressure. Medium pressure liquid chromatography (MPLC) on silica gel of the residue with ethyl acetate : hexanes (12 : 78 to 65 : 35) followed by recrystallization from chloroform – hexanes (1:1) afforded 16.2 mg (35%) of **2** as a white powder (R_f = 0.46 (EtOAc : hexanes, 50 : 50)). ^{1}H NMR (500 MHz, acetone-d_6) δ 9.89 (s, 1H), 9.46 (s, 4H), 9.21 (s, 1H), 8.12

(d, J = 7.0 Hz, 1H), 7.99 (d, J = 7.5 Hz, 1H), 7.93 (t, J = 7.0 Hz, 2H), 7.86–7.83 (m, 3H), 7.75–7.69 (m, 8H), 7.56–7.53 (m, 3H), 7.50–7.47 (m, 6H), 7.40–7.36 (m, 6H). ^{13}C NMR (75 MHz, acetone-d_6) δ 181.86, 181.79, 142.8, 141.5, 140.29, 140.18, 140.06, 136.9, 133.8, 132.6, 132.16, 132.09, 131.9, 131.65, 131.50 (q, $J_{C–F}$ = 34 Hz), 130.74, 130.63, 130.49 (br), 130.3 (br), 130.1, 129.9, 129.4, 129.3, 128.7 (br), 128.10, 128.01, 127.5, 126.68, 126.54, 125.9, 125.2, 124.5 (q, $J_{C–F}$ = 272 Hz), 123.52 (br), 123.38, 123.1, 117.8 (br) (three signals are not resolved, but presumably are at 130.49, 130.30 and 128.7 ppm). HRMS-ESI: calcd for $C_{59}H_{37}N_6S_3F_{12}$ $(M + H)^+$ 1153.2045, found 1153.2031.

Binding constant determinations. Binding affinities of the thioureas to $H_2PO_4^-$ were determined as described in the experimental section of Chapter 7.

Tris-thiourea 1 binding to $H_2PO_4^-$ in 25% aqueous DMSO (v/v). A 15.0 μM solution of **1** in 25% H_2O–DMSO (2.00 mL) was titrated with 40.0 mM (10 μL was added and no change in the spectrum was observed) and 209 mM (entries 1-14) solutions of tetrabutylammonium dihydrogenphosphate in 25% H_2O–DMSO at 24 °C (Table S1). Non-linear curve fitting of the titration data affords K = 71 M^{-1} and A_{max} = 0.826 (Figure S1).

Tris-thiourea 2 binding to $H_2PO_4^-$ in 25% aqueous DMSO (v/v). A 25.0 μM solution of **2** in 25% H_2O–DMSO (2.00 mL) was titrated with a 37.7 mM solution of tetrabutylammonium dihydrogenphosphate in 25% H_2O–DMSO at 24 °C (Table S2). Non-linear curve fitting of the titration data affords K = 1600 M^{-1} and A_{max} = 0.424 (Figure S2).

Table S1. Data for the titration of **1** with $H_2PO_4^-$ in 25% H_2O–DMSO at 362 nm.

Entry	µL $H_2PO_4^-$ added	$[thiourea]_0$, mM	$[H_2PO_4^-]_0$, mM	Observed absorption	Calculated absorption*
0	0	0.0150	0	0.6541	0.6541
1	5	0.0149	0.72	0.6572	0.6575
2	10	0.0149	1.23	0.6600	0.6614
3	20	0.0148	2.25	0.6673	0.6679
4	30	0.0147	3.26	0.6717	0.6731
5	45	0.0146	4.76	0.6779	0.6791
6	60	0.0145	6.24	0.6819	0.6832
7	85	0.0143	8.66	0.6909	0.6872
8	110	0.0142	11.0	0.6913	0.6886
9	160	0.0138	15.6	0.6857	0.6864
10	210	0.0135	19.9	0.6787	0.6804

* From the non-linear curve fit.

Figure S1. Non-linear least squares fitting of the titration data in Table S1.

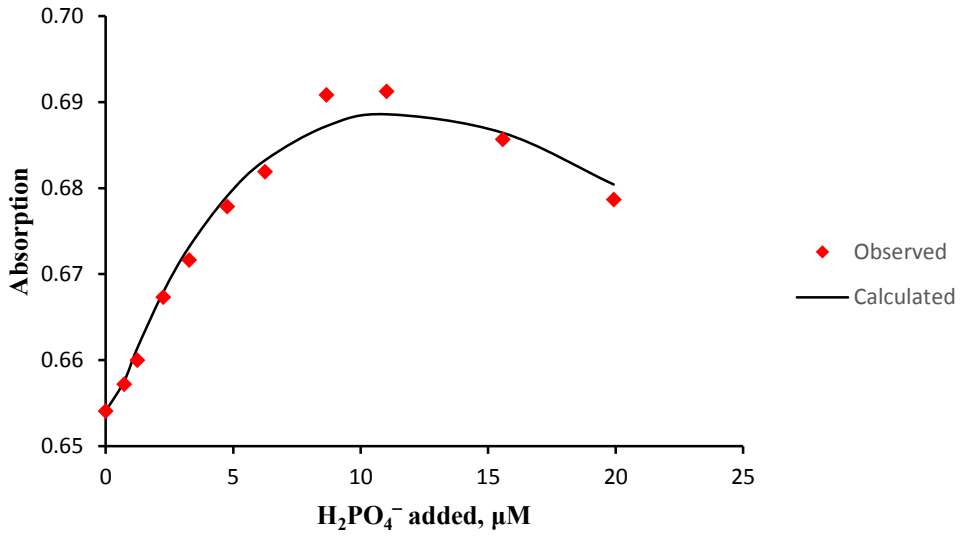

Table S2. Data for the titration of **2** with $H_2PO_4^-$ in 25% H_2O–DMSO at 363 nm.

Entry	µL $H_2PO_4^-$ added	$[thiourea]_0$, µM	$[H_2PO_4^-]_0$, µM	Observed absorption	Calculated absorption*
0	0	25.00	0	0.2557	0.2557
1	2	24.98	38	0.2667	0.2644
2	4	24.95	75	0.2736	0.2723
3	10	24.88	187	0.2916	0.2915
4	15	24.81	280	0.3038	0.3037
5	20	24.75	372	0.3131	0.3136
6	30	24.63	556	0.3282	0.3282
7	40	24.51	737	0.3376	0.3384
8	60	24.27	1095	0.3512	0.3509
9	80	24.04	1447	0.3570	0.3578
10	110	23.70	1961	0.3634	0.3625

* From the non-linear curve fit.

Figure S2. Non-linear least squares fitting of the titration data in Table S2.

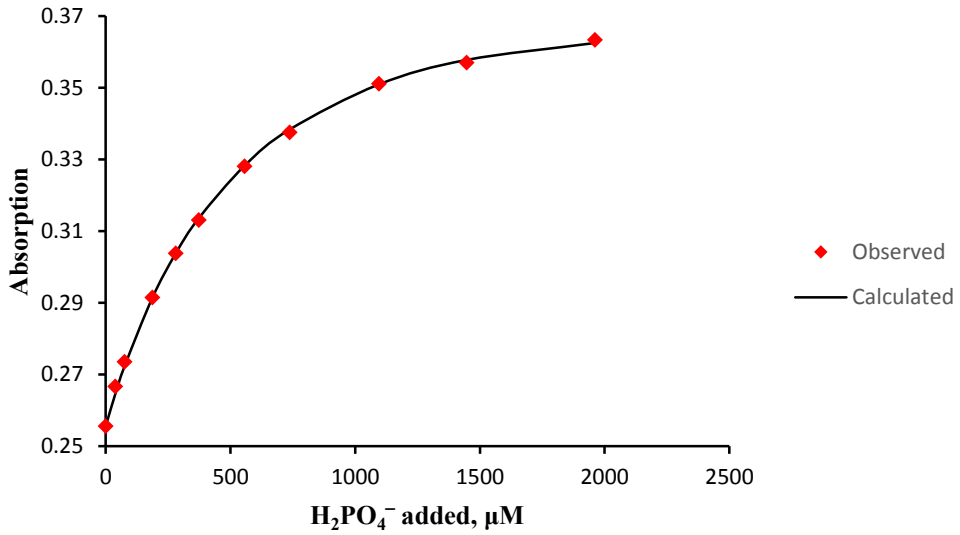

Tris-thiourea 2 fluorescence upon addition of anions in 25% aqueous DMSO (v/v). Fluorescence spectra (360-600 nm, λ_{ex} = 350 nm) of 15.0 μM solutions of **2** were recorded in 25% H_2O–DMSO (2.00 mL) alone and in the presence of tetrabutylammonium dihydrogenphosphate (1 mM), acetate (10 mM) and chloride (100 mM) using a Varian Cary Eclipse fluorescence spectrophotometer. Background corrected spectra (i.e., that of the solvent) were obtained in each case.

Chapter 10: Bifunctional receptors based on a 1,3,5-triphenylbenzene core

In order to further improve the selectivity of the thiourea receptor **1-tris** for $H_2PO_4^-$ over OAc^-, we decided to incorporate a basic site into each arm to take advantage of the acidic O–H's in dihydrogen phosphate (Scheme 1). This approach has been used by Kondo *et al.* to increase the $H_2PO_4^-/OAc^-$ selectivity for a tetraamide receptor in Scheme 1.[1] The compound with no basic groups (i.e., X = CH) has similar binding affinities to $H_2PO_4^-$ and OAc^- in a 0.5% DMSO-acetonitrile solution. In contrast, changing the phenyl groups in the amide linkages to 2-pyridyls rings had little impact on the binding of OAc^-, but

Scheme 1. Proposed selectivity enhancement of **1-tris** based on a literature precedent.

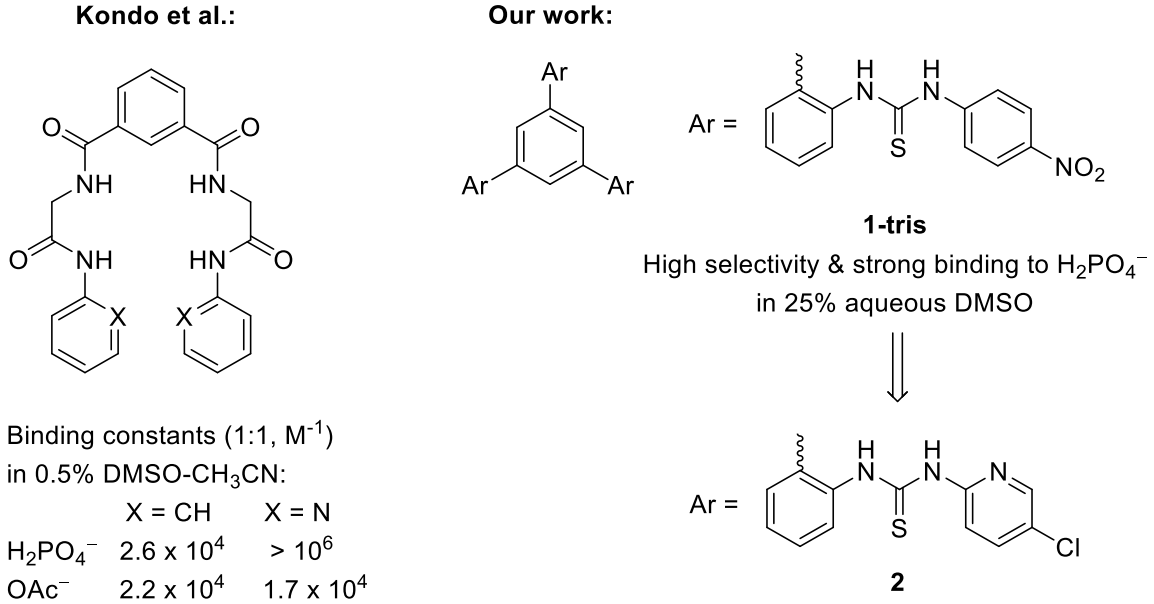

Binding constants (1:1, M^{-1}) in 0.5% DMSO-CH_3CN:

	X = CH	X = N
$H_2PO_4^-$	2.6×10^4	$> 10^6$
OAc^-	2.2×10^4	1.7×10^4

significantly increased the association constant to $H_2PO_4^-$, thereby improving the $H_2PO_4^-/OAc^-$ selectivity by over 60 fold. Since **1-tris** already possesses over a 100 fold selectivity, this approach could lead to a highly selective dihydrogen phosphate receptor in an aqueous solution by introducing a basic group into the thiourea arms of **1-tris**.

Compound **2** was synthesized in an analogous fashion to **1-tris** by adding the previously reported 5-chloro-2-isocyanatopyridine to tris-amine **4-tris** (Scheme 2). Unfortunately, a dramatic decrease in both binding affinity and selectivity for $H_2PO_4^-$ was observed compared to the parent compound (**1-tris**): little or no change in the UV spectra were observed upon titration in 25% aqueous DMSO indicating low binding, and in 0.5% H_2O–DMSO binding constants of 920 M^{-1} for $H_2PO_4^-$ and 4.0 x 10^4 M^{-1} for OAc^- were obtained. Evidence for an intramolecular hydrogen bond in **2** was obtained by ^1H NMR as the chemical shifts of the thiourea hydrogens are unusually high in DMSO-d_6 (i.e., 10.9 and 12.9 ppm for **2** compared to 10.3 and 10.4 ppm for **1-tris**). Tris-thiourea **1-tris** binds to OAc^- with only one thiourea arm (see Chapter 7) but uses all three with $H_2PO_4^-$. If this is also the case for **2**, then three intramolecular hydrogen bonds must be broken to bind with

Scheme 2. Synthesis of bifunctional receptors **2** and **3**.

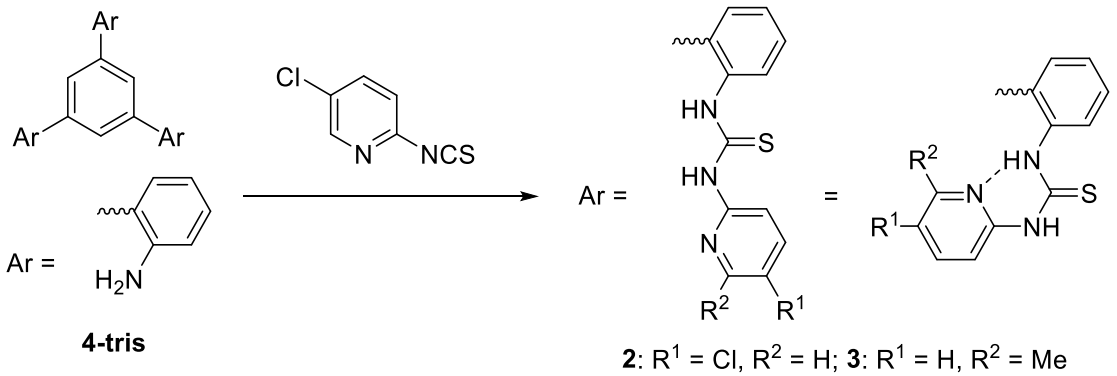

$H_2PO_4^-$ whereas only one needs to break to associate with OAc^-. This difference accounts for the decrease in the binding affinity and selectivity of **2** compared to **1-tris**. To overcome this issue and eliminate the intramolecular hydrogen bonding in **2**, a methyl group was introduced on to the pyridine ring ortho to the nitrogen atom. This stericaly more encumbered substrate (**3**) still forms intramolecular hydrogen bonds as indicated by the ^1H NMR shifts of the NH groups at 10.8 and 13.7 ppm. As a result, it is not surprising that the binding of $H_2PO_4^-$ is even smaller (i.e., K = 230 M^{-1} in 0.5% H_2O-DMSO).

Tris-semicarbazide **5**, a hydrazine analog of the tris-thiourea **1-tris**, was synthesized to try and produce a bifunctional thiourea that does not form intramolecular hydrogen bonds. This was accomplished in this case as the N–H chemical shifts are typical of a thiourea (9.1 and 9.5 ppm in DMSO-d_6). Unfortunately, **5** is still a poor receptor and has a low binding affinity for $H_2PO_4^-$ even in acetonitrile (i.e., K = 540 M^{-1}).

Scheme 3. Synthesis of tris-semicarbazide **5**.

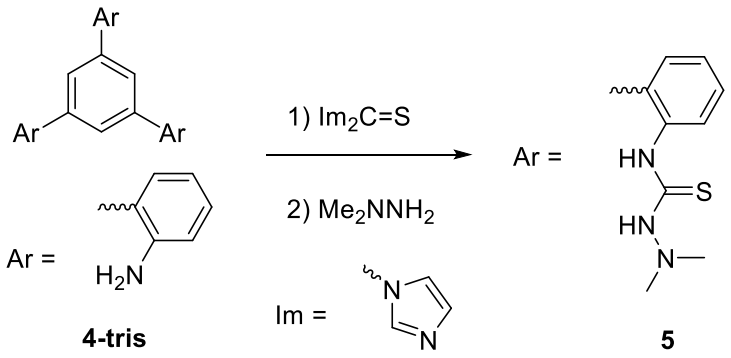

Since the thiourea-derived bifunctional receptors that were synthesized were unsuccessful, a 2-aminoquinoline-based three hydrogen bond donor (**6**) was prepared

(Scheme 4). Due to its rigidity and the distance between the aminoquinoline arms, the formation of intramolecular hydrogen bonds are not expected. In accord with this assumption, **6** was found to strongly bind $H_2PO_4^-$ in acetonitrile and while the $H_2PO_4^-/OAc^-$ selectivity is only *ca.* 1 : 1, this represents a 20-fold improvement over the analogous tris-amide receptor.[2]

Scheme 4. Synthesis of a bifunctional aminoquinoline-derived receptor **6** and comparison of its binding affinities with an analogous amide receptor.

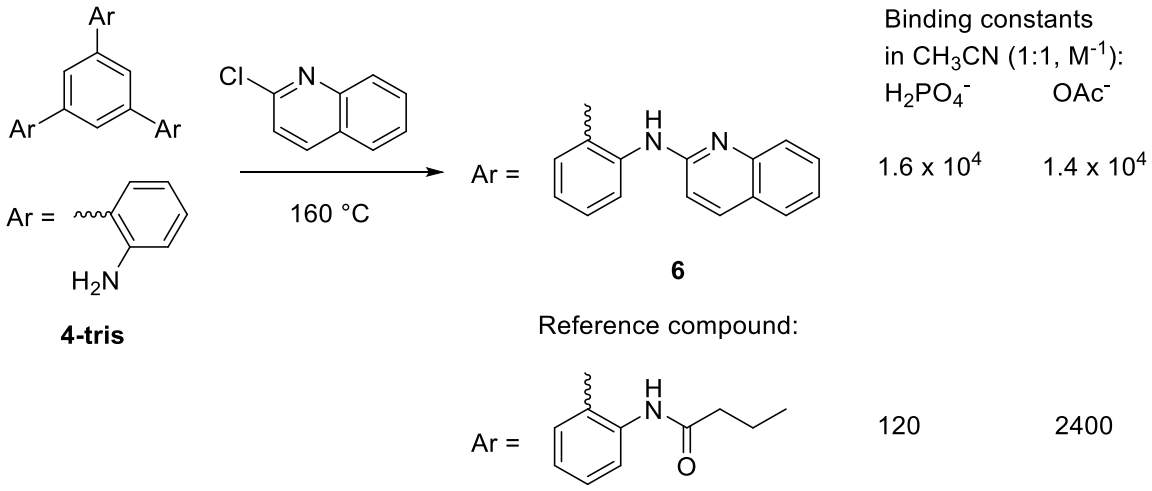

Experimental

1,3,5-tris[2-(3-(5-Chloro-2-pyridyl)thioureido)phenyl]benzene (2). To a mixture of tris-aniline **4-tris** (35.1 mg, 0.10 mmol) and 5-chloro-2-isothiocyanatopyridine[3] (68.2 mg, 0.40 mmol) was added dry THF (0.5 mL) under nitrogen. Thick precipitation occurred

within 10 min and more THF (10 mL) was added after 3 h to dissolve all of the solid material. The resulting solution was concentrated under reduced pressure onto a small amount of silica gel. Medium pressure liquid chromatography (MPLC) on silica gel of the residue with ethyl acetate : hexanes (16 : 84 to 100 : 0) afforded 40.3 mg (47%) of **2** as a white powder (R_f = 0.39 (EtOAc : hexanes, 66 : 33)). ^{1}H NMR (500 MHz, DMSO-d_6) δ 12.89 (s, 3H), 10.87 (s, 3H), 7.82 (d, *J* = 8.0 Hz, 3H), 7.79 (dd, *J* = 3.0, 8.5 Hz, 3H), 7.50 (d, *J* = 2.5 Hz, 3H), 7.43 (s, 3H), 7.40 (dt, *J* = 1.5, 8.0 Hz, 3H), 7.18 (dt, *J* = 1.0, 7.5 Hz, 3H), 7.09 (d, *J* = 9.0 Hz, 3H), 6.93 (dd, *J* = 1.5, 7.5 Hz, 3H). ^{13}C NMR (75 MHz, DMSO-d_6) δ 179.0, 151.4, 143.3, 138.9, 138.3, 136.4, 136.1, 129.3, 129.0, 128.4, 127.7, 126.5, 123.9, 113.9. HRMS-ESI: calcd for $C_{42}H_{30}Cl_9N_9S_3Na$ $(M + Na)^+$ 884.0744, found 884.0742.

2-Isothiocyanato-6-methylpyridine. To a solution of 2-amino-6-methylpyridine (540 mg, 5.0 mmol) and triethylamine (1.50 mL, 10.5 mmol) in dry THF (10 mL) was added thiophosgene (0.40 mL, 5.25 mmol) in dry THF (10 mL) at 0 °C over 10 min. The reaction mixture was stirred at 0 °C for an additional 2 h and then celite was added and the mixture was concentrated under reduced pressure. Medium pressure liquid chromatography (MPLC) on silica gel of the residue with ethyl acetate : hexanes (2 : 98 to 10 : 90) afforded 218 mg (29%) of the thiocyanate as a yellow oil (R_f = 0.29 (EtOAc : hexanes, 10 : 90)). ^{1}H NMR (300 MHz, $CDCl_3$) δ 7.60 (t, *J* =7.8 Hz, 1H), 7.07 (d, *J* =7.8 Hz, 1H), 6.95 (d, *J* =7.8 Hz, 1H), 2.52 (s, 3H). ^{13}C NMR (75 MHz, $CDCl_3$) δ 159.3, 145.1, 139.4, 138.7, 122.0, 117.1, 24.1. HRMS-ESI: calcd for $C_7H_7N_2S$ $(M + H)^+$ 151.0324, found 151.0324.

1,3,5-tris[2-(3-(6-Methyl-2-pyridyl)thioureido)phenyl]benzene (3). To a mixture of tris-aniline **4-tris** (35.1 mg, 0.10 mmol) and 6-methyl-2-isothiocyanatopyridine (60.0 mg, 0.40 mmol) was added dry THF (0.5 mL) under nitrogen. Thick precipitation occurred within 10 min and more THF (10 mL) was added after 3 h to dissolve all of the solid material. The resulting solution was concentrated under reduced pressure onto a small amount of silica gel. Medium pressure liquid chromatography (MPLC) on silica gel of the residue with methanol : ethyl acetate : hexanes (0 : 16 : 84 to 20 : 80 : 0), concentration of the fractions containing **3** to *ca.* 10 mL and filtration afforded 21.4 mg (27%) of pure **3** as a white powder (R_f = 0.22 (EtOAc : hexanes, 67 : 33)). ^{1}H NMR (500 MHz, DMSO-d_6) δ 13.69 (s, 3H), 10.84 (s, 3H), 7.72 (d, J = 8.0 Hz, 3H), 7.64 (t, J = 8.0 Hz, 3H), 7.41 (s, 3H), 7.36 (t, J = 7.5 Hz, 3H), 7.06 (t, J = 7.5 Hz, 3H), 7.01 (d, J = 8.0 Hz, 3H), 6.70 (d, J = 7.5 Hz, 3H), 6.66 (d, J = 7.5 Hz, 3H), 1.70 (s, 9H). ^{13}C NMR (75 MHz, DMSO-d_6) δ 179.7, 154.4, 152.9, 139.5, 138.6, 136.2, 136.0, 129.7, 129.2, 128.8, 127.5, 126.4, 117.1, 109.5, 22.7. HRMS-ESI: calcd for $C_{45}H_{39}N_9S_3Na$ $(M + Na)^+$ 824.2383, found 824.2389.

1,3,5-tris[2-Isothiocyanatophenyl]benzene. To a solution of thiocarbonyldiimidazole (89 mg, 0.50 mmol) in dry THF (0.7 mL) was added tris-aniline **4-tris** (46 mg, 0.13 mmol) in dry THF (0.8 mL) at 0 °C. The solution was stirred at ambient temperature for 18 h and was concentrated under reduced pressure. Medium pressure liquid chromatography (MPLC) on silica gel of the residue with ethyl acetate : hexanes (5 : 95 to 40 : 60) afforded 36.8 mg (59%) of pure tris-isocyanate as a white powder (R_f = 0.32 (EtOAc : hexanes, 20 : 80)). ^{1}H NMR (500 MHz, $CDCl_3$) δ 7.65–7.63 (m, 3H), 7.58 (s, 3H), 7.40–7.35 (m, 9H).

^{13}C NMR (75 MHz, $CDCl_3$) δ 138.4, 137.9, 135.5, 130.9, 129.4, 129.2, 128.8, 127.6, 126.8. HRMS-ESI: calcd for $C_{27}H_{15}N_3S_3Na$ $(M + Na)^+$ 500.0326, found 500.0320.

1,3,5-tris[2-(2,2-Dimethylhydrazine-1-carbothioamido)phenyl]benzene (5). To a solution of the tris-isothiocyanate (36.8 mg, 0.077 mmol) in dry THF (1.0 mL) was added N,N-dimethylhydrazine (18.2 μL, 0.24 mmol) under nitrogen. The solution was stirred for 1 h and concentrated under reduced pressure to *ca.* 0.2 mL. Diethyl ether (2 mL) was added and filtration afforded 27.2 mg (47%) of **5** as a white powder (R_f = 0.28 (EtOAc : hexanes, 67 : 33)). ^{1}H NMR (500 MHz, DMSO-d_6) δ 9.49 (s, 3H), 9.11 (s, 3H), 7.88 (d, J = 8.0 Hz, 3H), 7.54 (s, 3H), 7.41 (dd, J = 1.0, 7.0 Hz, 3H), 7.37 (dt, J = 1.5, 8.0 Hz, 3H), 7.29 (t, J = 7.5 Hz, 3H), 2.20 (s, 18H). ^{13}C NMR (75 MHz, DMSO-d_6) δ 177.9, 138.8, 136.4, 136.1, 129.9, 128.6, 127.8, 127.5, 125.9, 46.0. HRMS-ESI: calcd for $C_{33}H_{39}N_9S_3Na$ $(M + Na)^+$ 680.2383, found 680.2388.

1,3,5-tris[2-(Quinolin-2-ylamino)phenyl]benzene (6). A mixture of tris-aniline **4-tris** (70.2 mg, 0.20 mmol) and 2-chloroquinoline (327 mg, 2.0 mmol) was sealed in a nitrogen flushed screw-cap 1 dram vial and heated to 160 °C. The resulting solution was heated at this temperature for 2 h. Medium pressure liquid chromatography (MPLC) on silica gel with acetone : hexanes (12 : 88 to 65 : 35) followed by crystallization from diethyl ether (2 mL) afforded 77 mg (53%) of **6** as a white powder (R_f = 0.52 (acetone : hexanes, 50 : 50)). ^{1}H NMR (500 MHz, $CDCl_3$) δ 7.93 (d, J = 8.0 Hz, 3H), 7.73 (d, J = 8.5 Hz, 3H), 7.70 (d, J = 9.0 Hz, 3H), 7.57–7.55 (m, 6H), 7.49 (br s, 3H), 7.39 (s, 3H), 7.34 (d, J = 7.5 Hz, 3H), 7.26 (t, J = 7.5 Hz, 3H), 7.17 (d, J = 7.5 Hz, 3H), 7.06 (t, J = 7.5 Hz, 3H), 6.80 (d, J = 9.0 Hz, 3H). ^{13}C NMR (75 MHz, $CDCl_3$) δ 155.3, 147.5, 139.6, 137.7, 137.3, 134.2, 130.7,

129.7, 129.4, 128.5, 127.4, 126.4, 124.3, 124.0, 123.4, 122.9, 111.5. HRMS-ESI: calcd for $C_{51}H_{37}N_6$ $(M + H)^+$ 733.3074, found 733.3075.

Binding constant determinations. Binding affinities of the thioureas to anions were determined as described in the experimental section of Chapter 7.

Tris-thiourea 2 binding to $H_2PO_4^-$ in 0.5% aqueous DMSO (v/v). A 15.0 μM solution of **2** in 0.5% H_2O–DMSO (2.00 mL) was titrated with a 34.2 mM solution of tetrabutylammonium dihydrogenphosphate in 0.5% H_2O–DMSO containing 15.0 μM of **2** at 24 °C (Table S1). Non-linear curve fitting of the titration data affords K = 920 M^{-1} and A_{max} = 0.290 (Figure S1).

Tris-thiourea 2 binding to OAc^- in 0.5% aqueous DMSO (v/v). A 15.0 μM solution of **2** in 0.5% H_2O–DMSO (2.00 mL) was titrated with a 40.8 mM solution of tetrabutylammonium acetate in 0.5% H_2O–DMSO containing 15.0 μM of **2** at 24 °C (Table S2). Non-linear curve fitting of the titration data affords K = 4.0 x 10^4 M^{-1} and A_{max} = 0.204 (Figure S2, entries 1-5 were used for analysis, as deviation was observed thereafter presumably due to consecutive 1:2 binding).

Tris-thiourea 3 binding to $H_2PO_4^-$ in 0.5% aqueous DMSO (v/v). A 15.0 μM solution of **3** in 0.5% H_2O–DMSO (2.00 mL) was titrated with a 277 mM solution of tetrabutylammonium dihydrogenphosphate in 0.5% H_2O–DMSO containing 15.0 μM of **3** at 24 °C (Table S3). Non-linear curve fitting of the titration data affords K = 230 M^{-1} and A_{max} = 0.209 (Figure S3).

Tris-thiosemicarbazide 5 binding to $H_2PO_4^-$ in CH_3CN. A 15.0 μM solution of **14** in CH_3CN (2.00 mL) was titrated with a 277 mM solution of tetrabutylammonium dihydrogenphosphate in CH_3CN containing 15.0 μM of **5** at 24 °C (Table S4). Non-linear curve fitting of the titration data affords K = 540 M^{-1} and A_{max} = 0.329 (Figure S4).

tris-Quinolinylamine 6 binding to $H_2PO_4^-$ in CH_3CN. A 20.0 μM solution of **6** in CH_3CN (2.00 mL) was titrated with a 3.77 mM solution of tetrabutylammonium dihydrogenphosphate in CH_3CN containing 20.0 μM of **6** at 24 °C (Table S5). Non-linear curve fitting of the titration data affords K = 1.6 x 10^4 M^{-1} and A_{max} = 0.337 (Figure S5).

tris-Quinolinylamine 6 binding to OAc^- in CH_3CN. A 20.0 μM solution of **6** in CH_3CN (2.00 mL) was titrated with a 92.9 mM solution of tetrabutylammonium acetate in CH_3CN containing 20.0 μM of **6** at 24 °C (Table S6). Non-linear curve fitting of the titration data affords K = 1.4 x 10^4 M^{-1} and A_{max} = 0.509 (Figure S6).

Table S1. Data for the titration of **2** with $H_2PO_4^-$ in 0.5% H_2O–DMSO at 338 nm.

Entry	μL $H_2PO_4^-$ added	$[thiourea]_0$, mM	$[H_2PO_4^-]_0$, mM	Observed absorption	Calculated absorption*
0	0	0.015	0.000	0.1259	0.1259
1	5	0.015	0.085	0.1397	0.1377
2	10	0.015	0.170	0.1504	0.1478
3	15	0.015	0.254	0.1579	0.1567
4	20	0.015	0.338	0.1656	0.1645
5	30	0.015	0.505	0.1754	0.1775
6	40	0.015	0.670	0.1876	0.1880
7	55	0.015	0.914	0.1971	0.2004
8	60	0.015	0.995	0.2069	0.2039
9	80	0.015	1.31	0.2167	0.2153
10	110	0.015	1.78	0.2263	0.2275
11	150	0.015	2.38	0.2369	0.2383
12	200	0.015	3.10	0.2458	0.2472
13	300	0.015	4.45	0.2577	0.2576
14	400	0.015	5.69	0.2657	0.2635

* From the non-linear curve fit.

Figure S1. Non-linear least squares fitting of the titration data in Table S1.

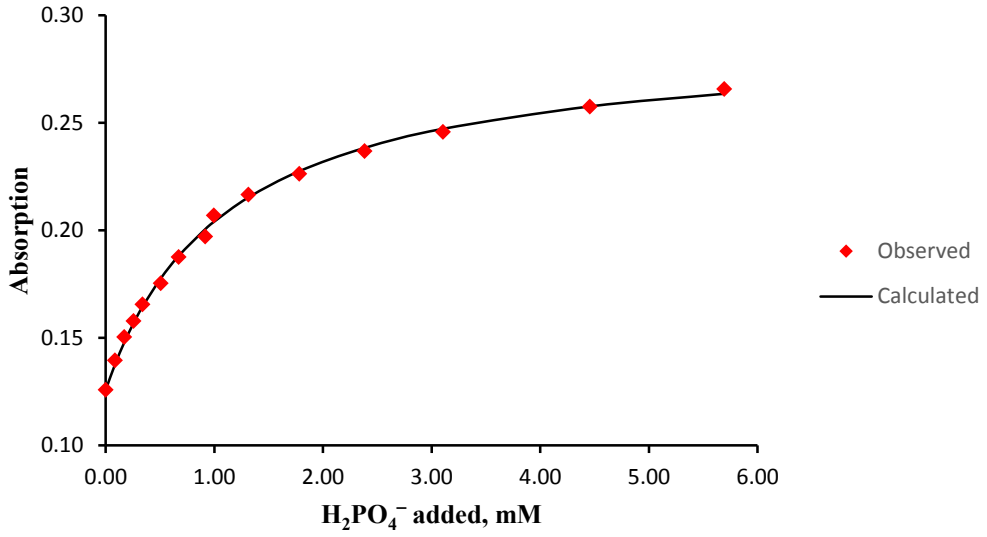

Table S2. Data for the titration of **2** with OAc^- in 0.5% H_2O–DMSO at 338 nm.

Entry	μL OAc^- added	$[thiourea]_0$, mM	$[OAc^-]_0$, mM	Observed absorption	Calculated absorption*
0	0	0.015	0.000	0.1253	0.1253
1	1	0.015	0.020	0.1565	0.1546
2	2	0.015	0.041	0.1699	0.1697
3	3	0.015	0.061	0.1758	0.1781
4	5	0.015	0.102	0.1865	0.1869
5	7.5	0.015	0.152	0.1935	0.1921
6	10	0.015	0.203	0.1996	0.1949
7	15	0.015	0.303	0.2062	0.1978
8	20	0.015	0.403	0.2114	0.1993
9	30	0.015	0.602	0.2190	0.2009
10	40	0.015	0.799	0.2224	0.2017

* From the non-linear curve fit.

Figure S2. Non-linear least squares fitting of the titration data in Table S2 (entries 1-5).

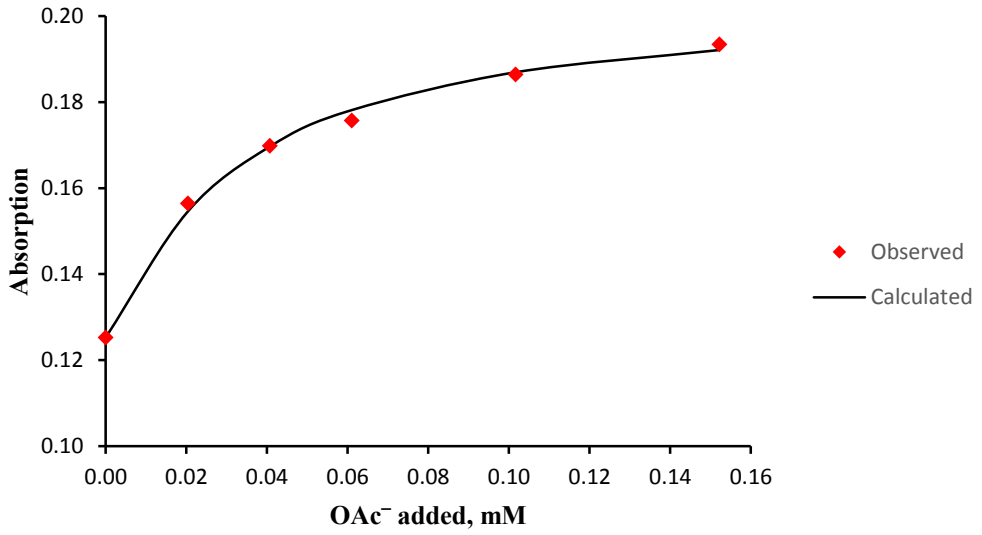

Table S3. Data for the titration of **3** with $H_2PO_4^-$ in 0.5% H_2O–DMSO at 331 nm.

Entry	μL $H_2PO_4^-$ added	$[thiourea]_0$, mM	$[H_2PO_4^-]_0$, mM	Observed absorption	Calculated absorption*
0	0	0.015	0	0.1341	0.1341
1	5	0.015	0.69	0.1449	0.1443
2	10	0.015	1.38	0.1533	0.1521
3	15	0.015	2.06	0.1606	0.1581
4	20	0.015	2.74	0.1618	0.1630
5	30	0.015	4.09	0.1674	0.1703
6	50	0.015	6.75	0.1791	0.1795
7	70	0.015	9.35	0.1890	0.1850
8	100	0.015	13.2	0.1851	0.1902
9	150	0.015	19.3	0.1965	0.1949
10	200	0.015	25.1	0.1985	0.1976

* From the non-linear curve fit.

Figure S3. Non-linear least squares fitting of the titration data in Table S3.

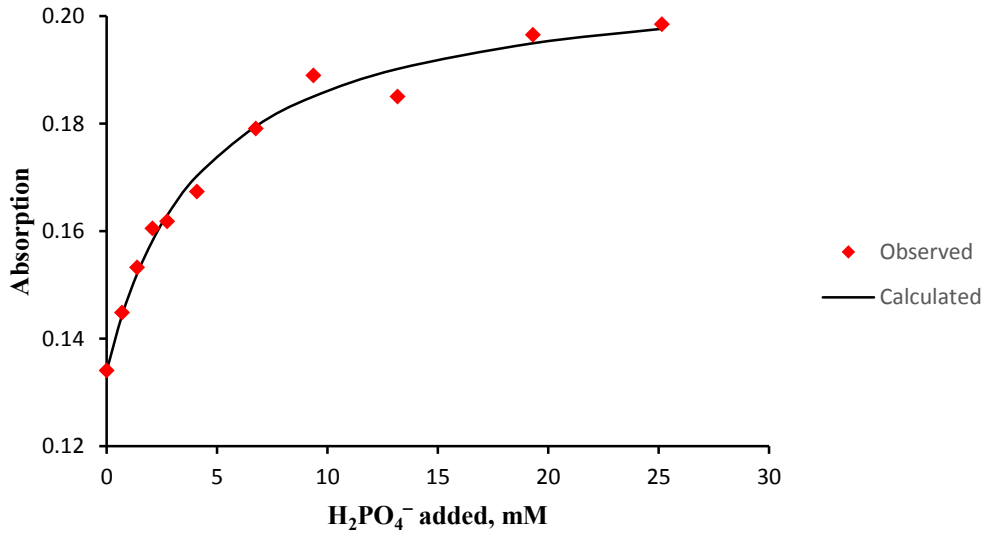

Table S4. Data for the titration of **5** with $H_2PO_4^-$ in CH_3CN at 283 nm.

Entry	μL $H_2PO_4^-$ added	$[receptor]_0$, mM	$[H_2PO_4^-]_0$, mM	Observed absorption	Calculated absorption*
0	0	0.015	0	0.3752	0.3752
1	1	0.015	0.18	0.3725	0.3712
2	2.5	0.015	0.44	0.3673	0.3664
3	5	0.015	0.87	0.3597	0.3604
4	7.5	0.015	1.31	0.3562	0.3560
5	10	0.015	1.74	0.3530	0.3527
6	12.5	0.015	2.18	0.3505	0.3501
7	15	0.015	2.61	0.3476	0.3481
8	20	0.015	3.47	0.3447	0.3449
9	30	0.015	5.18	0.3418	0.3409
10	40	0.015	6.87	0.3383	0.3385
11	50	0.015	8.55	0.3366	0.3369

* From the non-linear curve fit.

Figure S4. Non-linear least squares fitting of the titration data in Table S4.

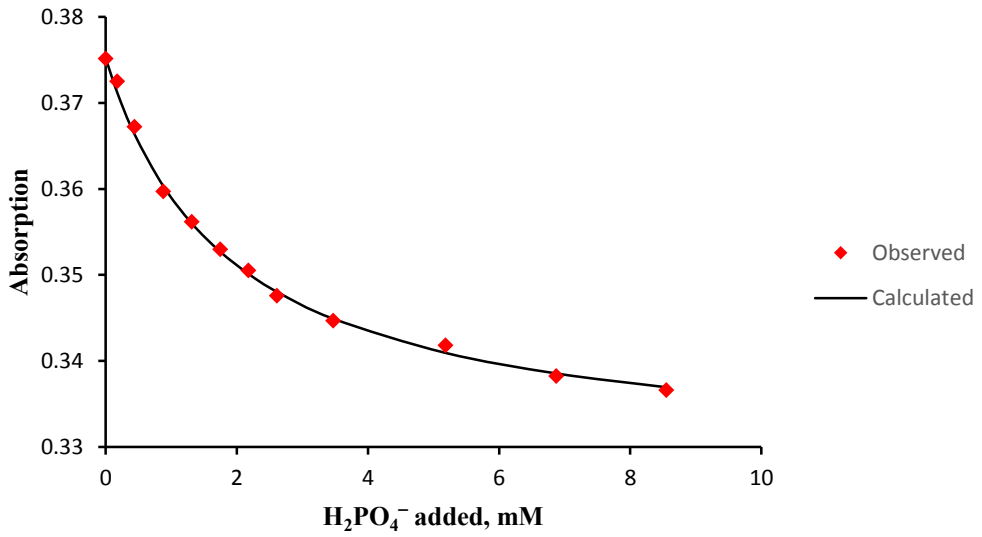

Table S5. Data for the titration of **6** with $H_2PO_4^-$ in CH_3CN at 374 nm.

Entry	μL $H_2PO_4^-$ added	$[receptor]_0$, mM	$[H_2PO_4^-]_0$, mM	Observed absorption	Calculated absorption*
0	0	0.020	0	0.1378	0.1378
1	2.5	0.020	0.0047	0.1531	0.1487
2	5	0.020	0.0094	0.1531	0.1586
3	7.5	0.020	0.0141	0.1634	0.1678
4	10	0.020	0.0187	0.1729	0.1761
5	12.5	0.020	0.0234	0.1806	0.1838
6	15	0.020	0.0280	0.1889	0.1909
7	20	0.020	0.0373	0.2043	0.2034
8	25	0.020	0.0465	0.2156	0.2141
9	30	0.020	0.0556	0.2230	0.2234
10	40	0.020	0.0738	0.2439	0.2384
11	50	0.020	0.0918	0.2540	0.2500
12	65	0.020	0.118	0.2628	0.2631
13	80	0.020	0.145	0.2728	0.2727
14	100	0.020	0.179	0.2810	0.2822
15	120	0.020	0.213	0.2866	0.2891

* From the non-linear curve fit.

Figure S5. Non-linear least squares fitting of the titration data in Table S5.

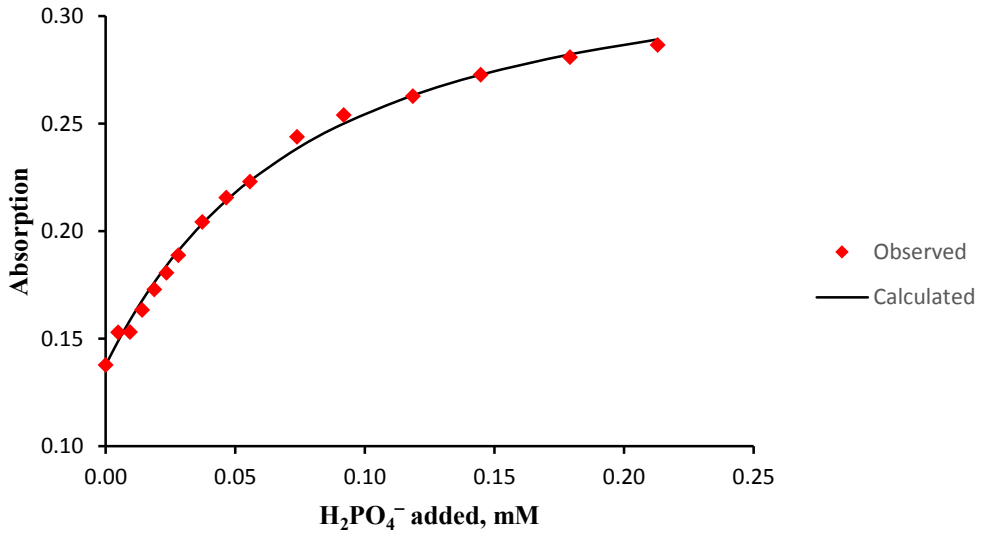

Table S6. Data for the titration of **6** with OAc^- in CH_3CN at 373 nm.

Entry	μL OAc^- added	$[receptor]_0$, mM	$[OAc^-]_0$, mM	Observed absorption	Calculated absorption*
0	0	0.020	0	0.1770	0.1770
1	1	0.020	0.046	0.2938	0.2933
2	2	0.020	0.093	0.3522	0.3527
3	3	0.020	0.139	0.3870	0.3873
4	4	0.020	0.185	0.4097	0.4097
5	5	0.020	0.231	0.4265	0.4252
6	7.5	0.020	0.346	0.4481	0.4488
7	10	0.020	0.461	0.4613	0.4620
8	15	0.020	0.690	0.4770	0.4764

* From the non-linear curve fit.

Figure S6. Non-linear least squares fitting of the titration data in Table S6.

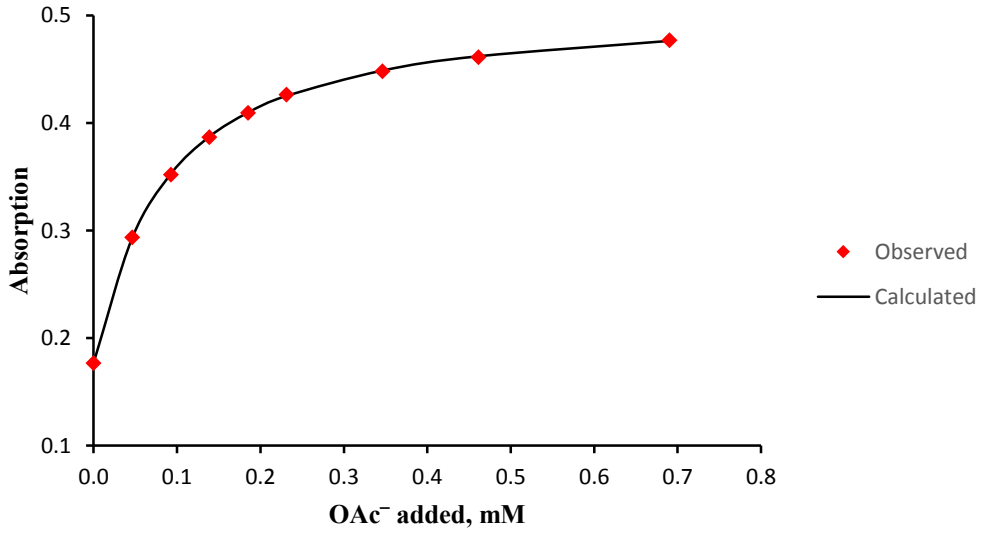

References

Chapter 1:

1. Kakiuchi, F.; Kochi, T. "Transition-Metal-Catalyzed Carbon–Carbon Bond Formation via Carbon–Hydrogen Bond Cleavage" *Synthesis* **2008**, 3013-3039.

2. Tsuji, J.; Ohno, K. "Organic syntheses by means of noble metal compounds. XXIX. Decarbonylation of acid halides and carbonylation of alkyl halides catalyzed by rhodium complex" *Tetrahedron Lett.* **1966, *7*,** 4713-4716.

3. Sakai, K.; Ide, J.; Oda, O.; Nakamura, N. "Synthetic studies on prostanoids 1 syntheses of methyl 9-oxoprostenoate" *Tetrahedron Lett.* **1972**, 13, 1287-1290.

4. Lochow, C. F.; Miller, R. G. "Transition-metal-promoted aldehyde-alkene addition reactions" *J. Am. Chem. Soc*. **1976**, *98*, 1281-1283.

5. Suggs, J. W. "Isolation of a stable acylrhodium(III) hydride intermediate formed during aldehyde decarbonylation. Hydroacylation" *J. Am. Chem. Soc*. **1978**, *100*, 640-641.

6. Larock, R. C.; Oertle, K.; Potter, G. "A convenient synthesis of cyclopentanones via rhodium(I)-catalyzed intramolecular hydroacylation of unsaturated aldehydes" *J. Am. Chem.* Soc. **1980**, *102*, 190-197.

7. Campbell Jr, R. E.; Lochow, C. F.; Vora, K. P.; Miller, R. G. "A Mechanistic Study of the Rhodium-Catalyzed Cyclization of 4-Hexenals. Reactions of Deuterio-4-hexenals" *J.Am. Chem. Soc*. **1980**, *102*, 5824-5830.

8. Milstein, D. "Isolation and Direct Observation of Intramolecular hydroacylation of a cis-Hydridopent-4-enoylrhodium(III) Complex" *J. Chem. Soc., Chem. Commun.* **1982**, 1357-1358.

9. Fairlie, D. P.; Bosnich, B. "Homogeneous catalysis. Conversion of 4-pentenals to cyclopentanones by efficient rhodium-catalyzed hydroacylation" *Organometallics* **1988**, *7*, 936-945.

10. Bosnich, B. "Asymmetric Catalysis. A Comparative Study of the Mechanisms of Intramolecular Hydroacylation and Hydrosilation" *Acc. Chem. Res.* **1998**, *31*, 667-674.

11. Fairlie, D. P.; Bosnich, B. "Homogeneous Catalysis. Mechanism of Catalytic Hydroacylation: The Conversion of 4-Pentenals to Cyclopentanones" *Organometallics* **1988**, *7*, 946-954.

12. James, B. R.; Young, C. G. "Catalytic dacarbonylation, hydroacylation, and resolution of racemic pent-4-enals using charal bis(ditertiaryphosphine) complexes of rhodium(I)" *J. Organomet. Chem.* **1985**, *285*, 321-332.

13. Taura, Y.; Tanaka, M.; Wu, X.-M.; Funakoshi, K.; Sakai, K. "Asymetric cyclization reactions. Cyclization of substituted 4-pentenals into cyclopentanone derivatives using rhodium(I) with chiral ligands" *Tetrahedron* **1991**, *47*, 4879-4888.

14. Barnhart, R. W.; Wang, X.; Noheda, P.; Bergens, S. H.; Whelan, J.; Bosnich, B. "Asymmetric Catalysis. Asymmetric Catalytic Intramolecular Hydroacylation of 4-Pentenals Using Chiral Rhodium Diphosphine Catalysts" *J. Am. Chem. Soc*. **1994**, *116*, 1821-1830.

15. Barnhart, R. W.; McMorran, D. A.; Bosnich, B. "Asymmetric catalytic intramolecular hydroacylation of 4-substituted pent-4-enals to b-substituted cyclopentanones" *Chem. Commun.* **1997**, 589-590.

16. Oonishi, Y.; Mori, M.; Sato, Y. "Rhodium(I)-Catalyzed Intramolecular Hydroacylation of 4,6-Dienals: Novel Synthesis of Cycloheptenones" *Synthesis* **2007**, *15*, 2323-2336.

17. Jun, C.-H.; Lee, H.; Hong, J.-B. "Chelation-Assisted Intermolecular Hydroacylation: Direct Synthesis of Ketone from Aldehyde and 1-Alkene" *J. Org. Chem.* **1997**, *62*, 1200-1201.

18. C.-H. Jun, D.-Y. Lee, H. Lee, J.-B. Hong, "A highly active catalyst system for intermolecular hydroacylation" *Angew.Chem. Int. Ed.* **2000**, *39*, 3070–3072.

19. C.-H. Jun, H. Lee, J.-B. Hong, B.-I. Kwon, "Efficient and Selective Hydroacylation of 1-Alkynes with Aldehydes by a Chelation-Assisted Catalytic System" *Angew. Chem. Int. Ed.* **2002**, *41*, 2146–2147.

20. Kokubo, K.; Matsumasa, K.; Miura, M.; Nomura, M. "Rhodium-Catalyzed Coupling Reaction of Salicyl Aldehydes with Alkynes via Cleavage of the Aldehyde C-H Bond" *J. Org. Chem.* **1997**, *62*, 4564-4565.

21. Tanaka, M.; Imai, M.; Yamamoto, Y.; Tanaka, K.; Shimowatari, M.; Nagumo, S.; Kawahara, N.; Suemune, H. "Double-Chelation-Assisted Rh-Catalyzed Intermolecular Hydroacylation" *Org. Lett.* **2003**, *5*, 1365-1367.

22. Tanaka, K.; Tanaka, M.; Suemune, H. "Rh-catalyzed π-facial selective intermolecular hydroacylation of norbornenes" *Tetrahedron Lett.* **2005**, *46*, 6053-6056.

23. Imai, M.; Tanaka, M.; Tanaka, K.; Yamamoto, Y.; Imai, N.; Shimowatari, M.; Nagumo, S.; Kawahara, N.; Suemune, H. "Double-Chelation-Assisted Rh-Catalyzed Intermolecular Hydroacylation between Salicylaldehydes and 1,4-Penta- or 1,5-Hexadienes" *J. Org. Chem.* **2004**, *69*, 1144-1150.

24. Imai, M.; Tanaka, M.; Nagumo, S.; Kawahara, N.; Suemune, H. "Nitrile-Promoted Rh-Catalyzed Intermolecular Hydroacylation of Olefins with Salicylaldehyde" *J. Org. Chem.* **2007**, *72*, 2543-2546.

25. Bendorf, H. D.; Colella, C. M.; Dixon, E. C.; Marchetti, M.; Matukonis, A. N.; Musselman, J. D.; Tiley, T. A. "Chelation-assisted intramolecular hydroacylation: synthesis of medium ring sulfur heterocycles" *Tetrahedron Lett.* **2002**, *43*, 7031 – 7034.

26. Willis, M. C.; McNally, S. J.; Beswick, P. J. "Chelation-Controlled Intermolecular Hydroacylation: Direct Addition of Alkyl Aldehydes to Functionalized Alkenes" *Angew. Chem., Int. Ed.* **2004**, *43*, 340-343.

27. Moxham, G. L.; Randell-Sly, H. E.; Brayshaw, S. K.; Woodward, R. L.; Weller, A. S.; Willis, M. C. "A Second-Generation Catalyst for Intermolecular Hydroacylation of Alkenes and Alkynes Using β-S-Substituted Aldehydes: The Role of a Hemilabile P-O-P Ligand" *Angew. Chem., Int. Ed.* **2006**, *45*, 7618-7622.

28. Moxham, G. L.; Randell-Sly, H.; Brayshaw, S. K.; Weller, A. S.; and Willis, M. C. "Intermolecular Alkene and Alkyne Hydroacylation with β-S-Substituted Aldehydes: Mechanistic Insight into the Role of a Hemilabile P–O–P Ligand" *Chem. Eur. J.* **2008**, *14*, 8383-8397.

29. Osborne, J. D.; Randell-Sly, H. E.; Currie, G. S.; Cowley, A. R.; Willis, M. C. "Catalytic Enantioselective Intermolecular Hydroacylation: Rhodium-Catalyzed Combination of *β-S*-Aldehydes and 1,3-Disubstituted Allenes" *J. Am. Chem. Soc.* **2008**, *130*, 17232-17233.

30. Tanaka, K.; Shibata, Y.; Suda, T.; Hagiwara, Y.; Hirano, M. "Direct Intermolecular Hydroacylation of N,N-Dialkylacrylamides with Aldehydes Catalyzed by a Cationic Rhodium(I)/dppb Complex" *Org. Lett.* **2007**, *9*, 1215-1218.

31. Shibata, Y.; Tanaka, K.; "Rhodium-Catalyzed Highly Enantioselective Direct Intermolecular Hydroacylation of 1,1-Disubstituted Alkenes with Unfunctionalized Aldehydes" *J. Am. Chem. Soc.* **2009**, *131*, 12552-12553.

32. Lenges, C. P.; White, P. S.; Brookhart, M. "Mechanistic and Synthetic Studies of the Addition of Alkyl Aldehydes to Vinylsilanes Catalyzed by Co(I) Complexes" *J. Am. Chem. Soc.* **1998**, *120*, 6965-6979.

33. Roy, A. H.; Lenges, C. P.; Brookhart, M. "Scope and Mechanism of the Intermolecular Addition of Aromatic Aldehydes to Olefins Catalyzed by Rh(I) Olefin Complexes" *J. Am. Chem. Soc.* **2007**, *129*, 2082-2093.

34. Fukuyama, T.; Doi, T.; Minamino, S.; Omura, S.; Ryu, I. "Ruthenium Hydride Catalyzed Regioselective Addition of Aldehydes to Enones To Give 1,3-Diketones" *Angew. Chem., Int. Ed.* **2007**, *46*, 5559-5561.

35. Omura, S.; Fukuyama, T.; Horiguchi, J.; Murakami, Y.; Ryu, I. "Ruthenium Hydride-Catalyzed Addition of Aldehydes to Dienes Leading to *β,γ*-Unsaturated Ketones" *J. Am. Chem. Soc.* **2008**, *130*, 14094-14095.

36. Kundu, K.; McCullagh, J. V.; Morehead, A. T. "Hydroacylation of 2-Vinyl Benzaldehyde Systems: An Efficient Method for theSynthesis of Chiral 3-Substituted Indanones" *J. Am. Chem. Soc.* **2005**, *127*, 16042–16043.

37. Tanaka, K.; Fu, G. C. "Rhodium-Catalyzed Synthesis of Cyclohexenones via a Novel [4 + 2] Annulation" *Org. Lett.* **2002**, *4*, 933-935.

38. Hojo, D.; Noguchi, K.; Hirano, M.; Tanaka, K. "Enantioselective Synthesis of Spirocyclic Benzopyranones by Rhodium-Catalyzed Intermolecular [4+2] Annulation" *Angew. Chem. Int. Ed.* **2008**, *47*, 5820.

39. Bedford, R. B.; Limmert, M. E. "Catalytic Intermolecular Ortho-Arylation of Phenols" *J. Org. Chem.*, **2003**, *68*, 8669-8682.

40. (a) Chen, D.-J.; Chen, Z.-C. "Hypervalent Iodine in Synthesis 59: Application of Polymeric Diaryliodonium Salts as Aryl Transfer Reagents in SPOS" *Synlett* **2000**, *8*, 1175-1177. (b) Xia, M.; Chen, Z.-C. "Hypervalent Iodine in Synthesis XXXIV: Palladium-Catalyzed Coupling Reaction of o-Hydroxyarylaldehydes with Hypervalent Iodonium Salts Via Cleavage of the Aldehyde C–H Bond" *Syn. Comm.* **2000**, *30*, 531-536.

41. Ko, S.; Kang, B.; Chang, S. "Cooperative Catalysis by Ru and Pd for the Direct Coupling of a Chelating Aldehyde with Iodoarenes or Organostannanes" *Angew. Chem., Int. Ed.* **2005**, *44*, 455-457.

Chapter 2:

1. For reviews on hydroacylation, see: (a) González-Rodríguez, C.; Willis, M. C. *Pure Appl. Chem.* **2011**, *83*, 577. (b) Willis, M. C. *Chem. Rev.* **2010**, *110*, 725. (b) Fu, G. C. In Modern Rhodium-Catalyzed Organic Reactions; Evans, P. A., Ed.; Wiley-VCH: New York, 2005; pp 79–91. (c) Tanaka, M.; Sakai, K.; Suemune, H. *Curr. Org. Chem.* **2003**, *7*, 353. (d) Bosnich, B. *Acc. Chem. Res.* **1998**, *31*, 667.

2. (a) Marcé, P.; Díaz, Y.; Matheu, M. I.; Castillón, S. *Org. Lett.* **2008**, *10*, 4735. (b) Kundu, K.; McCullagh, J. V.; Morehead, A. T. *J. Am. Chem. Soc.* **2005**, *127*, 16042. (c) Cyclobutanones also formed: Tanaka, K.; Fu, G. C. *J. Am. Chem. Soc.* **2003**, *125*, 8078. (d) Tanaka, M.; Imai, M.; Fujio, M.; Sakamoto, E.; Takahashi, M.; Eto-Kato, Y.; Wu, X.-M.; Funakoshi, K.; Sakai, K.; Suemune, H. *J. Org. Chem.* **2000**, *65*, 5806. (e) Barnhart, R. W.; McMorran, D. A.; Bosnich, B. *Chem. Commun.* **1997**, 589. (f) Barnhart, R. W.; Wang, X.; Noheda, P.; Bergens, S. H.; Whelan, J.; Bosnich, B. *J. Am. Chem. Soc.* **1994**, *116*, 1821. (g) Taura, Y.; Tanaka, M.; Wu, X.-M.; Funakoshi, K.; Sakai, K. *Tetrahedron* **1991**, *47*, 4879. (h) Larock, R. C.; Oertle, K.; Potter, G. F. *J. Am. Chem. Soc.* **1980**, *102*, 190. (i) Lochnow, C. F.; Miller, R. G. *J. Am. Chem. Soc.* **1976**, *98*, 1281. (j) Sakai, K.; Ide, J.; Oda, O.; Nakamura, N. *Tetrahedron Lett.* **1972**, 1287.

3. (a) Coulter, M. M.; Dornan, P. K.; Dong, V. M. *J. Am. Chem. Soc.* **2009**, *131*, 6932. (b) Shen, Z.; Dornan, P. K.; Khan, H. A.; Woo, T. K.; Dong, V. M. *J. Am. Chem. Soc.* **2009**, *131*, 1077. (c) Bendorf, H. D.; Colella, C. M.; Dixon, E. C.; Marchetti, M.; Matukonis, A. N.; Musselman, J. D, Tily, T. A. *Tetrahedron Lett.* **2002**, *43*, 7031.

4. The use of acrylamides as the alkene in intermolecular hydroacylation avoids this limitation: (a) Shibata, Y.; Tanaka, K. *J. Am. Chem. Soc.* **2009**, *131*, 12552. (b) Tanaka, K.; Shibata, Y.; Suda, T.; Hagiwara, Y.; Hirano, M. *Org. Lett.* **2007**, *9*, 1215.

5. For alternative hydrogenation or transfer hydrogenation approaches, see: Shibahara, F.; Bower, J. F.; Krische, M. J. *J. Am. Chem. Soc.* **2008**, *130*, 14120. (b) Hong, Y.-T.; Barchuk, A.; Krische, M. J. *Angew. Chem. Int. Ed.* **2006**, *45*, 6885.

6. Medium rings can be formed by hydroacylation of more elaborate substrates, wherein a proximal alkene can stabilize metal acyl intermediates: For an intramolecular hydroacylation with 1,3-dienes to form cycloheptenones: (a) Oonishi, Y.; Mori, M.; Sato, Y. *Synthesis* **2007**, 2323. (b) Sato, Y.; Oonishi, Y.; Mori, M. *Angew. Chem. Int. Ed.* **2002**, *41*, 1218. For ring-expanding intramolecular hydroacylation of vinyl cyclopropanes: (c) Aloise, A. D.; Layton, M. E.; Shair, M. D. *J. Am. Chem. Soc.* **2000**, *122*, 12610. For cascade-type cyclization reactions involving hydroacylation and multi-component insertions to form six-membered and larger rings: (d) Oonishi, Y.; Hosotani, A.; Sato, Y. *J. Am. Chem. Soc.* **2011**, *133*, 10386. (e) Tanaka, K.; Hojo, D.; Shoji, T.; Hagiwara, Y.; Hirano, M. *Org. Lett.* **2007**, *9*, 2059. (f) Tanaka, K. Hagiwara, Y.; Hirano, M. *Angew. Chem. Int. Ed.* **2006**, *45*, 2734. (g) Tanaka, K. Hagiwara, Y.; Noguchi, K. *Angew. Chem. Int. Ed.* **2005**, *44*, 7260. (h) Tanaka, K.; Fu, G. C. *Org. Lett.* **2002**, *4*, 933.

7. Salicylaldehyde derivatives: (a) Murphy, S. K.; Coulter, M. M.; Dong, V. M. *Chem. Sci.* **2012**, *3*, 355. (b) Murphy, S. K.; Petrone, D. A.; Coulter, M. M.; Dong, V. M. *Org. Lett.* **2011**, *13*, 6216. (c) Zhang, H.-J.; Bolm, C. *Org. Lett.* **2011**, *13*, 2900. (d) Coulter, M. M.; Kou, K. G. M.; Galligan, B.; Dong, V. M. *J. Am. Chem. Soc.* **2010**, *132*, 16330. (e) Phan, D. H. T.; Kou, K. G. M.; Dong V. M. *J. Am. Chem. Soc.* **2010**, *132*, 16354. (f) Stemmler, R. T.; Bolm, C. *Adv. Syn. Catal.* **2007**, *349*, 1185. (g) Imai, M.; Tanaka, M.; Nagumo, S.; Kawa-rara, N.; Suemune, H. *J. Org. Chem.* **2007**, *72*, 2543. (h) Imai, M.; Tanaka, M.; Tanaka, K.; Yamamoto, Y.; Imai-Ogata, N.; Shimowatari, M.; Najumo, S.; Kawahara, N.; Suemune, H. *J. Org. Chem.* **2004**, *69*, 1144. (g) Aldehydes containing a chelating sulfide: Osborne, J. D.; Randell-Sly, H. E.; Currie, G. S.; Cowley, A. R.; Willis, M. C. *J. Am. Chem. Soc.* **2008**, *130*, 17232.

8. Tsuji, J.; Ohno, K. *Tetrahedron Lett.* **1965**, *6*, 3969.

9. Suggs, J. W. *J. Am. Chem. Soc.* **1979**, *101*, 489.

10. Review: (a) Park, Y. J.; Par, J.-W.; Jun, C.-H. *Acc. Chem. Res.* **2008**, *41*, 222. Leading references: (b) Vautravers, N. R.; Regent, D. D.; Breit, B. *Chem. Commun.* **2011**, *47*, 6635. (c) Willis, M. C.; Sapmaz, S.; *Chem. Commun.* **2001**, 2558. (d) Jun, C.-H.; Lee, D.-Y.; Lee, H.; Hong, J.-B. *Angew. Chem. Int. Ed.* **2000**, *39*, 3070. (e) Jun, C.-H.; Hong, J.-B. *Org. Lett.* **1999**, *1*, 887. (f) Jun, C.-H.; Lee, H.; Hong, J.-B. *J. Org. Chem.* **1997**, *62*, 1200.

11. An alternative approaches for suppression of undesired pathways in hydroacylation: (a) Roy, A. H.; Lenges, C. P.; Brookhart, M. *J. Am. Chem. Soc.* **2007**, *129*, 2082. (b) Lenges, C. P.; White, P. S.; Brookhart, M. *J. Am. Chem. Soc.* **1998**, *120*, 6965.

12. Compound **2a** was characterized by ^{1}H, ^{13}C, COSY, HMQC, HMBC NMR spectroscopy experiments; IR spectroscopy; and mass spectrometry. See supporting information for details.

13. Ogawa, A.; Curran, D. P. *J. Org. Chem.* **1997**, *62*, 450.

14. Compound **2g** was reportedly prepared by an alternative synthesis, but our spectroscopic data did not match those provided in this preparation: Fillion, E.; Fishlock, D.; Wilsily, A.; Goll, J. M. *J. Org. Chem.* **2005**, *70*, 1316. We hypothesize that the compound prepared in this report was 3-phenethyl-2,3-dihydroinden-1-one.

15. We assigned **2g** as the benzosuberone system using ^{1}H, ^{13}C, COSY, HMQC, HMBC NMR spectroscopy experiments, selected frequency decoupled ^{1}H NMR, IR spectroscopy (carbonyl at 1667 cm-1); and mass spectrometry. Prof. Fillion concurs with our assignment of **2g**.[16]

16. Personal Communication with Prof. Fillion, April 11th, 2011 and May 26th, 2011.

17. Piel, I.; Steinmetz, M.; Hirano, K. Frölich, R.; Grimme, S.; Glorius, F. *Angew. Chem. Int. Ed.* **2011**, *50*, 4983.

18. Kinetics of six- versus seven-membered ring forming reactions: (a) Norman, R. O. C.; Coxon, J. M. in *Principles of Organic Synthesis, 3rd Ed*. CRC Press, 1993, pg 67. From a synthesis standpoint, seven-membered rings are often prepared by ring expansion of six-membered rings. For a review, see: (b) Kantorowski, E. J.; Kurth, M. J. *Tetrahedron* **2000**, *56*, 4317.

19. Hyatt, I. F. D.; Anderson, H. K.; Morehead, A. T.; Sargent, A. L. *Organometallics* **2008**, *27*, 135 and references therein.

20. For related approaches to asymmetric catalysis using cooperative catalysis, i.e. chiral scaffolding ligands, see (a) Joe, C. L.; Tan, K. L. *J. Org. Chem.* **2011**, *76*, 7590. (b) Worthy, A. D.; Joe, C. L.; Lightburn, T. E.; Tan, K. L. *J. Am. Chem. Soc.* **2010**, *132*, 14757.

21. Van der Ent, A.; Onderdelinden, A. L. *Inorg. Synth.* **1990**, 90.

22. Dreis, A. M.; Douglas, C. J. *J. Am. Chem. Soc.* **2009**, *131*, 412.

23. Watson, I. D. G.; Ritter, S.; Toste, F. D. *J. Am. Chem. Soc.* **2009**, *131*, 2056.

24. Conditions for these alkylations were adapted from the following: Bailey, W. F.; Wachter-Jurcsak, N. M.; Pineau, M. R.; Ovaska, T. V.; Warren, R. R.; Lewis, C. E.; *J. Org. Chem.* **1996**, *61*, 8216.

25. Prepared by allylic bromination of 2-phenylpropene according to Miyamura, H.; Akiyama, R.; Ishida, T.; Matsubara, R.; Takeuchi, M.; Kobayashi, S. *Tetrahedron* **2005**, *61*, 12177. Residual 2-phenylpropene was removed by column chromatography on silica (hexanes as eluent) prior to use.

26. Levine, S. R.; Krout, M. R.; Stolz, B. M. *Org. Lett.* **2009**, *11*, 289.

27. Bonnaventure, I.; Charette, A. B. *J. Org. Chem.* **2008**, *73*, 6330.

28. Previous preparation: Kirmse, W.; Höberger, G. *J. Am. Chem. Soc.* **1991**, *113*, 3925.

29. See supporting information for an assignment diagram summarizing key data.

30. Roy, H. N.; Rahman, A. F. M. M.; Islam, M. A. *J. Chem. Res., Synop.* **2003**, 594.

31. Zhang, T.; Huang, X.; Xue, J.; Sun, S. *Tetrahedron Lett.* **2009**, *50*, 1290.

32. Adamczyk, M.; Watt, D.; Netzel, D. *J. Org. Chem.* **1984**, *49*, 4226.

33. Gram-scale iodination of 2-aminopicoline (**3**) is previously described: Tao, L.; McLaughlin, L. W. *J. Am. Chem. Soc.* **2000**, *122*, 6512.

34. Procedure adapted from Zhang, H.; Cai, Q; Ma, D. *J. Org. Chem.* **2005**, *70*, 5164.

Chapter 3:

1. For reviews on hydrogen bonding catalysis see: (a) Taylor, M. S.; Jacobsen, E. N. *Angew. Chem. Int. Ed.* **2006**, *45*, 1520–1543; (b) Doyle, A. G.; Jacobsen, E. N. *Chem. Rev.* **2007**, *107*, 5713–5743; (c) Akiyama, T. *Chem. Rev.* **2007**, *107*, 5744–5758; (d) MacMillan, D. W. C. *Nature* **2008**, *455*, 304–308; (e) Zhang, Z.; Schreiner, P. R. *Chem. Soc. Rev.* **2009**, *38*, 1187–1198; (f) Knowles, R. R.; Jacobsen, E. N. *Proc. Natl. Acad. Sci. USA* **2010**, *107*, 20678–20685; (g) Wende, R. C.; Schreiner, P. R. *Green Chem.* **2012**, *14*, 1821–1849.

2. Wassermann, A. *J. Chem. Soc.* **1942**, 618–621.

3. Yates, P.; Eaton, P. *J. Am. Chem. Soc.* **1960**, *82*, 4436–4437.

4. For a review on asymmetric Lewis catalyzed Diels-Alder reaction see: Kagan, H. B.; Riant, O. *Chem. Rev.* **1992**, *92*, 1007–1019.

5. Sigman, M. S.; Jacobsen, E. N. *J. Am. Chem. Soc.* **1998**, *120*, 4901–4902.

6. Sigman, M. S.; Vachal, P.; Jacobsen, E. N. *Angew. Chem. Int. Ed.* **2000**, *39*, 1279–1281.

7. Vachal, P.; Jacobsen, E. N. *Org. Lett.* **2000**, *2*, 867–870.

8. Wenzel, A. G.; Jacobsen, E. N. *J. Am. Chem. Soc.* **2002**, *124*, 12964–12965.

9. Joly, G. D.; Jacobsen, E. N. *J. Am. Chem. Soc.* **2004**, *126*, 4102–4103.

10. Raheem, I. T.; Jacobsen, E. N. *Adv. Synth. Catal.* **2005**, *347*, 1701–1708.

11. Yoon, T. P.; Jacobsen, E. N. *Angew. Chem. Int. Ed.* **2005**, *44*, 466–468.

12. Zuend, S. J.; Coughlin, M. P.; Lalonde, M. P.; Jacobsen, E. N. *Nature* **2009**, *461*, 668–670.

13. Zuend, S. J.; Jacobsen, E. N. *J. Am. Chem. Soc.* **2009**, *131*, 15358–15374.

14. Okino, T.; Hoashi, Y.; Furukawa, T.; Xu, X.; Takemoto, Y. *J. Am. Chem. Soc.* **2005**, *127*, 119–125.

15. For a review see: Takemoto, Y. *Chem. Pharm. Bull.* **2010**, *58*, 593–601.

16. Hamza, A.; Schubert, G.; Soos, T.; Papai, I. *J. Am. Chem. Soc.* **2006**, *128*, 13151–13160.

17. Vakulya, B.; Varga, S.; Csampai, A.; Soos, T. *Org. Lett.* **2005**, *7*, 1967–1969.

18. Hammar, P.; Marcelli, T.; Hiemstra, H.; Himo, F. *Adv. Synth. Catal.* **2007**, *349*, 2537–2548.

19. Marcelli, T.; van der Haas, R. N. S.; van Maarseveen, J. H.; Hiemstra, H. *Synlett* **2005**, *18*, 2817–2819.

20. Marcelli, T.; van der Haas, R. N. S.; van Maarseveen, J. H.; Hiemstra, H. *Angew. Chem. Int. Ed.* **2006**, *45*, 929–931.

21. Zhu, J.-L., Zhang, Y.; Liu, C.; Zheng, A.-M.; Wang, W. *J. Org. Chem.* **2012**, *77*, 9813–9825 and references therein.

22. For a review on ion-pairing catalysis see: Brak, K.; Jacobsen, E. N. *Angew. Chem. Int. Ed.* **2013**, *52*, 534–561.

23. Taylor, M. S.; Jacobsen, E. N. *J. Am. Chem. Soc.* **2004**, *126*, 10558–10559.

24. Raheem, I. T.; Thiara, P. S.; Peterson, E. A; Jacobsen, E. N. *J. Am. Chem. Soc.* **2007**, *129*, 13404–13405.

25. Reisman, S. E.; Doyle, A. G., Jacobsen, E. N. *J. Am. Chem. Soc.* **2008**, *130*, 7198–7199.

26. Yamaoka, Y.; Miyabe, H.; Takemoto, Y. *J. Am. Chem. Soc.* **2007**, *129*, 6686–6687.

27. Klausen, R. S.; Jacobsen, E. N. *Org. Lett.* **2009**, *11*, 887–890.

28. Weil, T.; Kotke, M.; Kleiner, C. M.; Schreiner, P. R. *Org. Lett.* **2008**, *10*, 1513–1516.

29. Yamada, Y. M. A.; Ikegami, S. *Tetrahedron Lett.* **2000**, *41*, 2165–2169.

30. McDougal, N. T.; Schaus, S. E. *J. Am. Chem. Soc.* **2003**, *125*, 12094–12095.

31. Huang, Y.; Unni, A. K.; Thadani, A. N.; Rawal, V. H. *Nature* **2003**, *424*, 146–146.

32. Hadani, A. N.; Stankovic, A. R.; Rawal, V. H. *Proc. Natl. Acad. Sci. USA* **2004**, *101*, 5846–5850.

33. Carrasco, N.; Hiller, D. A.; Strobel, S. A. *Biochemistry* **2011**, *50*, 10491–10498.

34. Kraut, J. *Ann. Rev. Biochem.* **1977**, *46*, 331–358.

35. Robertus, J. D.; Kraut, J.; Alden, R. A.; Birktoft, J. J. *Biochemistry* **1972**, *11*, 4293–4303.

36. Quinn, D. N. *Chem. Rev.* **1987**, *87*, 955–979.

37. Harel, M.; Quinn, D. M.; Nair, H. K.; Selman, I.; Sussman, J. L. *J. Am. Chem. Soc*. **1996**, *118*, 2340–2346.

38. Zhou, Y.; Wang, S.; Zhang, Y. *J. Phys. Chem. B*. **2010**, *114*, 8817–8825.

39. Simon, L.; Muniz, F. M.; Saez, S.; Raposo, C.; Moran, J. R. *ARKIVOC* **2007**, 47–64.

40. Schreiner, P. R.; Wittkopp, A. *Org. Lett.* **2002**, *4*, 217–220.

41. Rodriguez, A. A.; Yoo, H.; Ziller, J. W.; Shea, K. J. **2009**, *50*, 6830–6833.

Chapter 4:

1. (a) Childs, W.; Boxer, S. G. *Biochemistry* **2010**, *49*, 2725–2731. (b) Sigala, P. A.; Kraut, D. A.; Caaveiro, J. M. M.; Pybus, B.; Rubin, E. A.; Ringe, D.; Petsko, G. A.; Herschlag, D. *J. Am. Chem. Soc*. **2008**, *130,* 13696–13708. (c) Zhang, Y.; Kua, J.; McCammon, J. A. *J. Am. Chem. Soc.* **2002**, *124,* 10572–10577. (d) Whiting, A. K.; Peticolas, W. L. *Biochemistry* **1994**, *33*, 552–561.

2. Simon, L.; Goodman, J. M. *J. Org. Chem*. **2010**, *75*, 1831–1840.

3. (a) Schreiner, P. R.; Wittkopp, A. *Org. Lett.* **2002**, *4*, 217–220. (b) Schreiner, P. R. *Chem. Soc. Rev*. **2003**, *32*, 289–296. (c) Takemoto, Y. *Org. Biomol. Chem*. **2005**, *3*, 4299–4306. (d) Taylor, M. S.; Jacobsen, E. N. *Angew. Chem. Int. Ed.* **2006**, *45*, 1520–1543. (d) Stephen, J. C. *Chem. Eur. J.* **2006**, *12*, 5418–5427. (e) Kotke, M.; Schreiner, P. R. *Synthesis* **2007**, 779–790. (f) Doyle, A. G.; Jacobsen, E. N. *Chem. Rev.* **2007**, *107*, 5713–5743. (g) Rawal, V. H.; Thadani, A. N. *Asymmetric Synthesis – The Essentials*, 2nd Edition; Christmann, M., Brase, S., Eds., Wiley–VCH: Weinheim, 2008, pp 144–148. (h) Pihko, P. M. Ed., *Hydrogen Bonding in Organic Synthesis*, Wiley–VCH: Weinheim, 2009, pp 1–395. (i) Zhang, Z.; Schreiner, P. R. *Chem. Soc. Rev.* **2009**, *38*, 1187–1198. (j) Knowles, R. R.; Jacobsen, E. N. *Proc. Natl. Acad. Sci. USA* **2010**, *107*, 20678–20685.

4. Reisman, S. E.; Doyle, A. G.; Jacobsen, E. N. *J. Am. Chem. Soc.* **2008**, *130*, 7198–7199.

5. For related work, see: (a) Schafer, A. G.; Wilting, J. M.; Mattson, A. E. *Org. Lett.* **2011**, *13*, 5228–5231. (b) Liu, M.; Tran, N. T.; Franz, A. K.; Lee, J. K. *J. Org. Chem.* **2011**, *76*, 7186–7194. (c) Rodriguez, A. A.; Yoo, H.; Ziller, J. W.; Shea, K. J. *Tetrahedron Lett.* **2009**, *50*, 6830–6833. (d) Kondo, S. I.; Harada, T.; Tanaka, R.; Unno, M. *Org. Lett.* **2006**, *8*, 4621–4624.

6. Negative charge centers develop in the transition state of hydrogen bond catalyzed nucleophilic reactions, and thus a hydrogen bond donor–anion complex can be viewed as a transition state analog or mimic. Such structures do not always closely resemble the transition state. For example, see: Schramm, V. L. et al., *Biochemistry* **2012**, *51*, 6892–6894.

7. Jakab, G.; Tancon, C.; Zhang, Z.; Lipper, K. M.; Schreiner, P. R. *Org. Lett*. **2012**, *14*, 1724–1727.

8. (a) Martinez, C.; Nicolas, A.; van Tilbeurgh, H.; Egloff, M. P.; Cudrey, C.; Verger, R.; Camilla, C. *Biochemistry* **1994**, *33*, 83–89. (b) Harel, M.; Quinn, D. M.; Nair, H. K.; Selman, I.; Sussman, J. L. *J. Am. Chem. Soc*. **1996**, *118*, 2340–2346. (c) Machajewski, T. D.; Wong, C. H. *Angew. Chem. Int. Ed*. **2000**, *39*, 1352–1374. (d) Zhang, Y.; Kua, J.; McCammon, J. A. *J. Am. Chem. Soc*. **2002**, *124*, 10572–10577. (e) Zhu, X.; Larsen, N. A.; Basra, A.; Bruce, N. C.; Wilson, I. A. *J. Biol. Chem.* **2003**, *278*, 2008–2014. (f) Lo, Y. C.; Lin, S. C.; Shaw, J. F.; Law, Y. C. *J. Mol. Biol*. **2003**, *330*, 539–551. (g) Nachon, F.; Adobo, O. A.; Borgstahl, G. E. O.; Masson, P.; Lockridge, O. *Biochemistry* **2005**, *44,* 1154–1162. (h) Simon, L.; Muñiza, F. M.; Sáeza, S.; Rap sob, C.; Moran, J. R. *ARKIVOC* **2007**, 47–64. (i) Chen, X.; Fang, L.; Liu, J.; Zhan, C. G. *Biochemistry* **2012**, *51*, 1297−1305.

9. Abe, H.; Aoyagi, Y.; Inouye, M. *Org. Lett.* **2005**, *7*, 59–61.

10. Other compounds have been reported to bind Cl^- upon ESI. See: (a) Jiang, Y.; Cole, R. B. *J. Am. Soc. Mass Spectrum.* **2005**, *16*, 60–70. (b) Cai, Y.; Cole, R. B. *Anal. Chem.* **2002**, *74*, 985–991. (c) Cai, Y.; Concho, M. C.; Murray, J. S.; Cole, R. B. *J. Am. Soc. Mass Spectrum.* **2002**, *13*, 1360–1369. (d) Zhu, J.; Cole, R. B. *J. Am. Soc. Mass Spectrum.* **2000**, *11*, 932–941.

11. Schmidt, J.; Meyer, M. M.; Spector, I.; Kass, S. R. *J. Phys. Chem. A* **2011**, *115*, 7625–7632.

12. (a) Zhao, Y.; Truhlar, D. G. *J. Phys. Chem. A* **2008**, *112*, 1095–1099. (b) Zhao, Y.; Truhlar, D. G. *Theor. Chem. Acc.* **2008**, *120*, 215–241. (c) Zhao, Y.; Truhlar, D. G. *Acc. Chem. Res.* **2008**, *41*, 157–167.

13. Dunning, Jr., T. H. *J. Chem. Phys.* **1989**, *90*, 1007–1023.

14. Papaya, E.; Truhlar, D. G. *J. Chem. Theory Compute.* **2010**, *6*, 597–601.

15. The corresponding free energies are 32.2 and 37.8 kcal mol^{-1}.

16. Wang, X. B.; Wang, L. S. *Rev. Sci. Instrum*. **2008**, *79*, 073108–1–073108–8.

17. Berlins, U.; Gustafsson, M.; Hamster, D.; Klinkmuller, A.; Ljungblad, U.; Martensson–Pendrill, A. M. *Phys. Rev*. *A* **1995**, *51*, 231–238.

18. The neutral phenol cluster is the only one that undergoes a hydrogen atom shift to the chlorine atom upon optimizing its structure starting from the anion geometry. The PES spectrum, consequently, maybe an example of transition state spectroscopy.

19. Bartmess, J. E. *NIST Chemistry WebBook, NIST Standard Reference Database Number 6;* Mallard, W. G., Lustrum, P. J., Eds.; National Institute of Standards and Technology: Gaithersburg, MD 20899 (http://webbook.nist.gov).

20. French, M. A.; Ikuta, S.; Earle, P. *Can. J. Chem*. **1982**, *60*, 1907–1918.

21. (a) Raghavan, A.; Sheik, T.; Graham, B. H.; Craigen, W. J. *Biochim. Biophys. Act, Biomembranes* **2012**, *1818*, 1477–1485. (b) Haynes, C. J. E.; Gale, P. A. *Chem. Commun*. **2011**, *47,* 8203–8209. (c) Gale, P. A. *Acc. Chem. Res*. **2011**, *44*, 216–226. (d) Brotherhood, P. R.; Davis, A. P. *Chem. Soc. Rev.* **2010**, *39*, 3633–3647. (e) Davis, J. T.; Okunola, O.; Quesada, R. *Chem. Soc. Rev.* **2010**, *39*, 3843–3862. (f) Gale, P. A. *Coord. Chem. Rev.* **2006**, *250*, 2939–2951.

22. (a) Jentsch, T. J.; Poet, M.; Fuhrmann, J. C.; Zdebik, A. A. *Annu. Rev. Physiol*. **2005**, *67*, 779–807. (b) Kornak, U.; Kasper, D.; Bosl, M. R.; Kaiser, E.; Schweizer, M.; Schulz, A.; Friedrich, W.; Delling, G.; Jentsch, T. J. *Cell* **2001**, *104*, 205–215. (c) Kaplan, R. S. *J. Membr. Biol*. **2001**, *179*, 165–183.

23. Smith, D. K. *Org. Biomol. Chem*. **2003**, *1*, 3874–3877.

24. Buhlmann, P.; Chen, L. D. *Supramolecular Chemistry: From Molecules to Nan materials*, Steed, A. W., Gale, P. A., Eds., Wiley: New York, 2012, Vol. 5, pp 2539–2580.

25. Herrera, R. P.; Sgarzani, V.; Bernard, L.; Ricci, A. *Angew. Chem. Int. Ed.* **2005**, *44*, 6576–6579.

Chapter 5:

1. Manabe, K.; Okamura, K.; Date, T.; Koga, K. *J. Org. Chem.* **1993**, *58*, 6692–6700.

2. Bovey, F.A., "Nuclear Magnetic Resonance Spectroscopy," Academic Press, New York, 1988, Chapter 5.

3. Hine, J.; Linden, S.-M.; Kanagasabapathy, V. M. *J. Org. Chem.* **1985**, *50*, 5096–5099.

4. Su, W.; Chen, J.; Wu, H.; Jin, C. *J. Org. Chem.* **2007**, *72*, 4524–4527.

5. (a) Bordwell, F. G.; Hughes, D. L. *J. Org. Chem.* **1982**, *47*, 3224–3232. (b) Bordwell, F. G.; McCallum, R. J.; Olmstead, W. N. *J. Org. Chem.* **1984**, *49*, 1424–1427. (c) Tabatskaya, A. A.; Sutula, V. D.; Vlasov, V. M. *Zhurnal Organicheskoi Khimii* **1987**, *23*, 2202–2207.

6. Marcelli, T.; van der Haas, R. N. S.; van Maarseveen, J. H.; Hiemstra, H. *Angew. Chem. Int. Ed.* **2006**, *45*, 929–931.

7. Fielding, L. *Tetrahedron* **200**, *56*, 6151–6170.

8. Vakulya, B.; Varga, S.; Csampai, A.; Soos, T. *Org. Lett.* **2005**, *7*, 1967–1969.

9. Yang, H.-M.; Li, L.; Li, F.; Jiang, K.-Z., Shang, J.-Y., Lai G.-Q., Xu, L.-W. *Org. Lett.* **2011**, *13*, 6508–6511.

10. Rabalakos, C.; Wulff, W. D. *J. Am. Chem. Soc.* **2008**, *130*, 13524–13525.

11. Herrera, R. P.; Sgarzani, V.; Bernard, L.; Ricci, A. *Angew. Chem. Int. Ed.* **2005**, *44*, 6576–6579.

12. Synthesized according to: Borredon, E.; Clavellinas, F.; Delmas, M.; Gaset A.; Sinisterra, J. V. *J. Org. Chem.* **1990**, *55*, 501–504.

13. NMR data for alchohols **4a** and **5a** was previously reported in $CDCl_3$: Su, W.; Chen J.; Wu H.; Jin C. *J. Org. Chem.* **2007**, *72*, 4524-4527. **4a**: 4.66 ppm (dd, J = 3.6, 9.2 Hz, 1H), **5a**: 4.27 ppm (t, J = 6.8 Hz, 1H).

14. NMR data for 2-nitro-1-phenylethanol was previously reported in $CDCl_3$: 5.44 (dd, J = 3.0, 9.6 Hz, 1H), 4.60 (dd, J = 9.6, 13.3 Hz, 1H), 4.50 (dd, J = 3.0, 13.3 Hz, 1H). MacDonald, F. K.; Carneiro, K. M. M.; Pottie, I. R. *Tetrahedron Letters* **2011**, *52*, 891–893.

15. NMR data for 2-nitro-1-(4-methoxypheny)lethanol was previously reported in $CDCl_3$: 5.43 (dd, J = 2.8, 9.6 Hz, 1H), 4.62 (dd, J = 9.6 ,13.2 Hz, 1H), 4.50 (dd, J = 2.8, 13.2, 1H) (ref. 14).

16. NMR data for 1-nitro-2-propanol was previously reported in $CDCl_3$: Sorgedrager, M. J.; Malpique, R.; van Rantwijk, F.; Sheldon, R. A. *Tetrahedron: Asymmetry* **2004**, *15*, 1295–1299.

17. Review on binding constant determination by NMR: Fielding, L. *Tetrahedron* **200**, *56*, 6151–6170.

18. NMR data for 5-pentan-2-one was previously reported in $CDCl_3$: 4.44 (t, J = 6.6 Hz, 2H). Janowitz, A.; Vavrecka, M.; Hesse, M. *Helv. Chim. Acta* **1991**, *74*, 1352–1361.

19. NMR data for 5-nitrononan-2,8-dione was previously reported in $CDCl_3$: 4.62–4.44 (quint like m, 1H) (*Ref.* 7).

20. NMR data for 2-nitrobutanal was previously reported in $CDCl_3$: Blidi, L. E.; Crstia, D.; Gallienne, E.; Demuynck, C.; Bolte, J.; Lemaire, M *Tetrahedron: Asymmetry* **2004**, *15*, 2951–2954.

21. NMR data for 5-nitropentan-2-one was previously reported in $CDCl_3$: Bapat, J. B.; Durie, A. *Aust. J. Chem.* **1984**, *37*, 211–219.

22. NMR data for 2-(*N*-methylindolyl)-2-phenyl-1-nitroethane was previously reported in $CDCl_3$: 5.06 (dd, J = 8.72, 7.92 Hz, 1H), 4.83 (dd, J = 12.32, 7.92 Hz, 1H), 4.76 (dd, J = 12.32, 8.72 1H). Lu, S.-F.; Du, D.-M.; Xu, J. *Org. Lett.* **2006**, *8*, 2115–2118.

Chapter 6:

1. Shriver, D. F.; Biallas, M. J. *J. Am. Chem. Soc.* **1967**, *89*, 1078–1081.

2. Park, C. H.; Simmons, H. E. *J. Am. Chem. Soc.* **1968**, *90*, 2431–2432.

3. Gale, P. A. *Chem. Commun.* **2011**, *47*, 82–86.

4. Duke, R. M.; Veale, E. B.; Pfeffer, F. M.; Kruger, P. E.; Gunnlaugsson, T. *Chem. Soc. Rev.* **2010**, *39*, 3936–3953.

5. Ojida, A.; Takashima, I.; Kohira, T.; Nonaka, H.; Hamachi, I. *J. Am. Chem. Soc.* **2008**, *130*, 12095–12101.

6. Weitz, E. A.; Chang, J. Y.; Rosenfield, A. H.; Pierre, V. C. *J. Am. Chem. Soc.* **2012**, *134*, 16099–16102.

7. Bondy, C. R.; Loeb, S. J. *Coord. Chem. Rev.* **2003**, *240*, 77–99.

8. Nguyen, B. T.; Anslyn, E. V. *Coord. Chem. Rev.* **2006**, *250*, 3118–3127.

9. Han, M. S.; Kim, D. H. *Angew. Chem. Int. Ed.* **2002**, *41*, 3809–3811.

10. Wright, A. T.; Anslyn, E. V. *Chem. Soc. Rev.* **2006**, *35*, 14–28.

11. For a review on ISE see; *Supramolecular Chemistry: From Molecules to Nanomaterials*; Steed, A. W., Ed, Gale P. A., Ed; John Wiley & Sons, Ltd: New York, 2012; Vol. 5, p 2539–2579.

12. Liu, W.; Li, X.; Song, M.; Wu, Y. *Sens. Actuator B: Chem.* **2007**, *126*, 609–615.

13. Sliwka-Kaszynska, M. *Crit. Rev. Anal. Chem.* **2007**, *37*, 211–224.

14. Sessler, J. L.; Gale, P. A.; Genge, J. W. *Chem. Eur. J.* **1998**, *4*, 1095–1099.

15. Jentsch, T. J.; Stein, V.; Weinrich, F.; Zdebik, A. A. *Phys. Rev.* **2002**, *82*, 503–568.

16. Gadsby, D. C. *Nat. Rev. Mol. Cell Biol.* **2009**, *10*, 344–352.

17. Gadsby, D. C.; Vergani, P.; Csanady, L. *Nature* **2006**, *440*, 477–483.

18. Tsui, L.-C. *Am. J. Respir. Crit. Care Med.* **1995**, *151*, S47–S53.

19. F. M. Ashcroft, *Ion Channels and Disease Channelopathies*, Academic Press, San Diego, CA, 2000.

20. For a reviews on anion transporters as prospective drugs see: (a) Alfonso, I.; Quesada, R. *Chem. Sci.* **2013**, *4*, 3009–3019; (b) Busschaert, N.; Gale, P. A. *Angew. Chem. Int. Ed.* **2013**, *52*, 1374–1382.

21. Jiang, C.; Lee, E. R.; Lane, M. B.; Xiao, Y.-F.; Harris, D. J.; Cheng, S. H. *Am. J. Physiol.* **2001**, *281*, L1164–L1172.

22. Moore, K. S.; Wehrli, S.; Roder, H.; Rogers, M.; Forrest Jr., J. N.; McCrimmon, D.; Zasloff, M. *Proc.Natl. Acad. Sci. U.S.A.* **1993**, *90*, 1354–1358.

23. Merritt, M.; Lanier, M.; Deng, G.; Regen, S. L. *J. Am. Chem. Soc.* **1998**, *120*, 8494–8501.

24. (a) Chen, W.-H.; Shao, X.-B.; Moellering, R.; Wennersten, C.; Regen, S. L. *Bioconjugate Chem.* **2006**, *17*, 1582–1591. (b) Chen, W.-H.; Wennersten, C.; Moellering, R. C; Regen, S. L. *Chem. Biodiversity* **2013**, *10*, 385–393.

25. Furstner, A. *Angew. Chem. Int. Ed.* **2003**, *42*, 3582–3603.

26. (a) Nguyen, M.; Marcellus, R. C.; Roulston, A.; Watson, M.; Serfass, L.; Madiraju, S. R. M.; Goulet, D.; Viallet, J.; Belec, L.; Billot, X.; Acoca, S.; Purisima, E.; Wiegmans, A.; Cluse, L.; Johnstone, R. W.; Beauparlant, P, Shore, G. C. *Proc. Natl. Acad. Sci. U.S.A.* **2007**, *104*, 19512–19517.

27. For a mini-review on the possible mechanisms of action of prodiogiosins see: Perez-Tomas, R.; Vinas, M. *Curr. Med. Chem.* **2010**, *17*, 2222–2231.

28. (a) Ref. 25. (b) Hosseini, A.; Espona-Fiedler, M.; Soto-Cerrato, V.; Quesada, R.; Perez-Tomas, R.; Guallar, V. *PLOS One* **2013**, *8*, e57562.

29. Rastogi, S.; Marchal, E.; Uddin, I.; Groves, B.; Colppitts, J.; McFarland, S. A.; Davis, J. T.; Thompson, A. *Org. Biomol. Chem.* **2013**, *11*, 3834–3845.

30. Yamamoto, D.; Uemura, Y.; Tanaka, K.; Nakai, K.; Yamamoto, C.; Takemoto, H.; Kamata, K.; Hirata, H.; Hioki, K. *Int. J. Cancer* **2000**, *88*, 121–128.

31. Sessler, J. L.; Eller, L. R.; Cho, W.-S.; Nicolaou, S.; Aguilar, A.; Lee, J. T.; Lynch, V. M.; Magda, D. J. *Angew. Chem. Int. Ed.* **2005**, *44*, 5989–5992.

32. De Grenu, B. D.; Hernandez, P. I.; Espona, M.; Quinonero, D.; Light, M. E.; Torroba, T.; Perz-Tomas, R.; Quesada, R. *Chem. Eur. J.* **2011**, *17*, 14074–14083.

33. Lagadic-Gossmann, D.; Huc, L.; Lecureur, V. *Cell Death Differ.* **2004**, *11*, 953–961.

34. Kojiri, K.; Nakajima, S.; Suzuki, H. *J. Antibiot.* **1993**, *46*, 1894–1896.

35. Melvin, M. S.; Ferguson, D. C.; Lindquist, N.; Manderville, R. A. *J. Org. Chem.* **1999**, *64*, 6861–6869.

36. Hernandez, P. I.; Moreno, D.; Javier, A. A.; Torroba, T.; Perez-Tomas, R.; Quesada, R. *Chem. Commun.* **2012**, *48*, 1556–1558.

37. Saggiomo, V.; Otto, S.; Marques, I.; Felix, V.; Torroba, T.; Quesada, R. *Chem. Commun.* **2012**, *48*, 5274–5276.

38. Gale, P. A. *Acc. Chem. Res.* **2011**, *44*, 216–226.

39. Busschaert, N.; Wenzel, M.; Light, M. E.; Iglesias-Hernandez, P.; Perez-Tomas, R.; Gale, P. A. *J. Am. Chem. Soc.* **2011**, *133*, 14136–14148.

40. Lipinski, C. A.; Lombardo, F.; Dominy, B. W.; Feeney, P. J. *Adv. Drug Delivery Rev.* **1997**, *23*, 3–25.

41. Moore, S. J.; Wenzel, M.; Light, M. E.; Morley, R.; Bradberry, S. J.; Gomez-Iglesias, P.; Soto-Cerrato, V.; Perez-Tomas, R.; Gale, P. A. *Chem. Sci.* **2012**, *3*, 2501–2509.

42. McNally, B. A.; O'Neil, E. J.; Nguyen, A.; Smith, B. D. *J. Am. Chem. Soc.* **2008**, *130*, 17274–17275.

43. Davis, J. T., Okunola, O.; Quesada, R. *Chem. Soc. Rev.* **2010**, *39*, 3843–3862.

44. (a) Pedersen, B. P.; Kumar, H.; Waight, A. B.; Risenmay, A. J.; Zurz, Z. R.; Chau, B. H.; Schlessinger, A.; Bonomi, M.; Harries, W.; Sali, A.; Johri, A. K.; Stroud, R. M. *Nature* **2013**, *496*, 533–536. (b) Kamat, S. S.; Williams, H. J.; Raushel, F. M. *Nature* **2011**, *480*, 570–573. (c) Ubersax, J. A.; Ferrell, J. E. *Nature Rev. Mol. Cell Biol.* **2007**, *8*, 530–541. (d) Berridge, M. J.; Irvine, R. F. *Nature* **1989**, *341*, 197–205. (e) Westheimer, F. H. *Science* **1987**, *235*, 1173–1178.

45. (a) Ref. 43a. (b) Biber, J.; Hernando, N.; Forster, I. *Annu. Rev. Physiol.* **2013**, *75*, 535–550. (c) Forster, I.; Hernando, N.; Sorribas, V.; Wener, A. *Adv. Chronic Kidney Dis.* **2011**, *18*, 63–76. (d) Luecke, H.; Quiocho, F. A. *Nature* **1990**, *347*, 402–406.

46. Sabbagh, Y.; Giral, H.; Caldas, Y.; Levi, M.; Schiavi, S. C. *Adv. Chronic Kidney Dis.* **2011**, *18*, 85–90.

47. Prie, D.; Friedlander, G. *N. Engl. J. Med.* **2010**, *362*, 2399–2409.

48. Friedman, E. A. *Kidney Int.* **2005**, *67*, S1–S7.

49. Pohlmeier, R.; Vienken, J.; *Kidney Int.* **2001**, *59*, S190–S194.

50. (a) Jordheim, L. P.; Durantel, D.; Zoulim, F.; Dumontet, C. *Nature Rev.* **2013**, *12*, 447–464. (b) Jung, Y.-G.; Yeo, W.-S.; Lee, S.-B.; Hong, J.-I. *Chem. Commun.* **1997**, 1061–1062.

51. Sessler, J. N.; Kral, V.; Shishkanova, T. V.; Gale, P. A. *Proc. Natl. Acad. Sci. U.S.A.* **2002**, *99*, 4848–4853.

52. Kohira, T.; Honda, K.; Ojida, A.; Hamachi, I. *ChemBioChem* **2008**, *9*, 698–701.

53. Boon, J. M.; Lambert, T. N.; Sisson, A. L.; Davis, A. P.; Smith, B. D. *J. Am. Chem. Soc.* **2003**, *125*, 8195–8201.

54. DiVittorio, K. M.; Leevy, W. M.; O'Neil, E. J.; Johnson, J. R.; Vakulenko, S.; Morris, J. D.; Rosek, K. D.; Serazin, N.; Hilkert, S.; Hurley, S.; Marquez, M.; Smith, B. D. *ChemBioChem* **2008**, *9*, 286–293.

55. Leevy, W. M.; Gammon, S. T.; Jiang, H.; Johnson, J. R.; Maxwell, D. J.; Jackson, E. N.; Marquez, M.; Piwnica-Worms, D.; Smith, B. D. *J. Am. Chem. Soc.* **2006**, *128*, 16476–16477.

56. Smith, B. A.; Akers, W. J.; Leevy, W. M.; Lampkins, A. J.; Xiao, S.; Wolter, W.; Suckow, M. A.; Acjilefu, S.; Smith, B. D. *J. Am. Chem. Soc.* **2010**, *132*, 67–69.

57. Wang, Z.; Lecane, P. S.; Thiemann, P.; Fan, Q.; Cortez, C.; Ma, X.; Tonev, D.; Miles, D.; Naumovski, L.; Miller, R. A.; Magda, D.; Cho, D.-G.; Sessler, J. L.; Pike, B. L.; Yeligar, S. M.; Karaman, M. W.; Hacia, J. G. *Mol. Cancer* **2007**, *6*, 9–20.

58. Sessler, J. L.; Davis, J. M. *Acc. Chem. Res.* **2001**, *34*, 989–997.

59. Albelda, M. T.; Frias, J. C.; Garcia-Espana, E.; Schneider, H.-J. *Chem. Soc. Rev.* **2012**, *41*, 3859–3877.

60. (a) Huang, X.; Wu, B.; Jia, C.; Hay, B. P.; Li, M.; Yang, X.-J. *Chem. Eur. J.* **2013**, *19*, 9034–9041. (b) Rambo, B. M.; Sessler, J. L. *Chem. Eur. J.* **2011**, *17*, 4946–4959. (c) Eller, L. R.; Stepien, M.; Fowler, C. J.; Lee, J. T.; Sessler, J. L.; Moyer, B. A. *J. Am. Chem. Soc.* **2007**, *129*, 11020–11021. (d) Katayev, E. A.; Ustynyuk, Y. A.; Sessler, J. L. *Coord. Chem. Rev.* **2006**, *250*, 3004–3037.

61. Pavikumar, I.; Ghosh, P. *Chem. Soc. Rev.* **2012**, *41*, 3077–3098.

62. Fowler, C. J.; Haverlock, T. J.; Moyer, B. A.; Shriver, J. A.; Gross, D. E.; Marquez, M.; Sessler, J. L.; Hossain, M. A.; Bowman-James, K. *J. Am. Chem. Soc.* **2008**, *130*, 14386–14387.

63. Katayev, E. A.; Kolesnikov, G. V.; Sessler, J. L. *Chem. Soc. Rev.* **2009**, *38*, 1572–1586.

64. Beer, P. D.; Hopkins, P. K.; McKinney, J. D. *Chem. Commun.* **1999**, 1253–1254.

65. Alberto, R.; Bergamaschi, G.; Braband, H.; Fox, T.; Amendola, V. *Angew. Chem. Int. Ed.* **2012**, *51*, 9772–9776.

66. McConnell, A. J.; Beer, P. D. *Angew. Chem. Int. Ed.* **2012**, *51*, 5052–5061.

67. Aydogan, A.; Coady, D. J.; Kim, S. K.; Akar, A.; Bielawski, C. W.; Marquez, M.; Sessler, J. L. *Angew. Chem. Int. Ed.* **2008**, *47*, 9648–9652.

68. Tozawa, T.; Misawa, Y.; Tokita, S.; Kubo, Y. *Tetrahedron Lett.* **2000**, *41*, 5219–5223.

69. Choi, J. K.; No, K.; Lee, E.-H.; Kwon, S.-G.; Kim, K.-W.; Kim, J. S. *Supramol. Chem.* **2007**, *19*, 283–286.

Chapter 7:

1. (a) Pedersen, B. P.; Kumar, H.; Waight, A. B.; Risenmay, A. J.; Zurz, Z. R.; Chau, B. H.; Schlessinger, A.; Bonomi, M.; Harries, W.; Sali, A.; Johri, A. K.; Stroud, R. M. *Nature* **2013**, *496*, 533–536. (b) Kamat, S. S.; Williams, H. J.; Raushel, F. M. *Nature* **2011**, *480*, 570–573. (c) Ubersax, J. A.; Ferrell, J. E. *Nature Rev. Mol. Cell Biol.* **2007**, *8*, 530–541. (d) Berridge, M. J.; Irvine, R. F. *Nature* **1989**, *341*, 197–205. (e) Westheimer, F. H. *Science* **1987**, *235*, 1173–1178.

2. Bansal, V. K. *Serum Inorganic Phosphorus.* In: Walker, H. K.; Hall, W. D.; Hurst, J. W., Ed; *Clinical Methods: The History, Physical, and Laboratory Examinations. 3rd edition.* Butterworths: Boston, **1990**; Chapter 198, 895–899. Available from: http://www.ncbi.nlm.nih.gov/books/NBK310/.

3. (a) http://kidney.niddk.nih.gov/kudiseases/pubs/kustats/

(b) http://endocrine.niddk.nih.gov/pubs/hyper/.

4. Daly, J.A.; Ertingshausen, G. *Clin. Chem.* **1972**, *18*: 263–265.

5. Hargrove, A. E.; Nieto, S.; Zhang, T.; Sessler, J. L.; Anslyn, E. V. *Chem. Rev.* **2011**, *111*, 6603–6782.

6. http://water.epa.gov/type/rsl/monitoring/vms56.cfm/.

7. Bühlmann, P.; Pretsch, E.; Bakker, E.,*Chem. Rev.* **1998**, *98,* 1593–1687.

8. Sabbagh, Y.; Giral, H.; Caldas, Y.; Levi, M.; Schiavi, S. C. *Adv. Chronic Kidney Dis.* **2011**, *18*, 85–90.

9. Prie, D.; Friedlander, G. *N. Engl. J. Med.* **2010**, *362*, 2399–2409.

10. Friedman, E. A. *Kidney Int.* **2005**, *67*, S1–S7.

11. Pohlmeier, R.; Vienken, J.; *Kidney Int.* **2001**, *59*, S190–S194.

12. (a) Malberti, F. *Drugs* **2013**, *73*, 673–688. (b) Petkewich, R. *C & EN* **2008**, *43*, 9.

13. Qunibi, W. Y.; Nolan, C. R. *Kidney Int.* **2004**, *66*, S33–S38.

14. Spaia, S. *Hippokratia* **2011**, *15*, 22–26.

15. Wrong, O. M. *Lancet* **1973**, *3*, 493.

16. For an extensive review on phosphate receptors see: Hargrove, A. E.; Nieto, S.; Zhang, T.; Sessler, J. L.; Anslyn, E. V. *Chem. Rev.* **2011**, *111*, 6603–6782.

17. Hisaki, I.; Sasaki, S.-I.; Hirose, K.; Tobe, Y. *Eur. J. Org. Chem.* **2007**, *4*, 607–615.

18. *NIST Chemistry WebBook, NIST Standard Reference Database Number 69,* Linstrom, P.J., Ed; Mallard, W.G., Ed; National Institute of Standards and Technology, Gaithersburg MD, 20899, http://webbook.nist.gov.

19. Gale, P. A.; Hiscock, J. R.; Moore, S. J.; Caltagirone, C.; Hursthouse, M. B.; Light, M. E. *Chem. Asian J.* **2010**, *5*, 555–561.

20. Bordwell, F. G.; Algrim, D. J. *J. Am. Chem. Soc.* **1988**, *110*, 2964–2968.

21. Jacab, G.; Tancon, C.; Zhang, Z.; Lippert, K. M.; Schreiner, P. R. *Org. Lett.* **2012**, *14*, 1724–1727.

22. Christ, P.; Lindsay, A. G.; Vormittag, S. S.; Neudorfl, J.-M.; Berkessel, A.; O'Donoghue, A. C. *Chem. Eur. J.* **2011**, *17*, 8524–8528.

23. Busschaert, N.; Wenzel, M.; Light, M. E.; Iglesias-Hernandez, P.; Perez-Tomas, R.; Gale, P. A. *J. Am. Chem. Soc.* **2011**, *133*, 14136–14148.

24. Lozanova, C.; Galabov, B.; Ililva, M.; Vassilev, G. *J. Mol. Structure* **1984**, *115*, 427–430.

25. Prepared according to: Youn, S. W.; Bihn, J. H.; Kim, B. S. *Org. Lett.* **2011**, *13*, 3738–3741.

26. Piatek, P.; Slomiany, N. *Synlett* **2006**, *13*, 2027–2030.

27. Roice, M.; Christensen, S. F.; Meldal, M. *Chem. Eur. J.* **2004**, *10*, 4407–4415.

28. Prepared according to: Yamada, Y.; Ochiai, C.; Yoshimura, K.; Tanaka, T.; Ohashi, N.; Narumi, T.; Nomura, W.; Harada, S.; Matsushita, S.; Tamamura, H. *Bioorg. & Med. Chem. Lett.* **2010**, *20*, 354–358.

29. Connors, K. A. *Binding Constants*; John Wiley & Sons: New York, 1987.

30. Olson, E. J.; Buhlmann, P. *J. Org. Chem.* **2011**, *76*, 8406–8412.

Chapter 8:

1. Walker, S. D.; Barder, T. E.; Martinelli, J. R.; Buchwald, S. L. *Angew. Chem.* **2004**, *116*, 1907–1912.

2. Piatek, P. *Tetrahedron Letters* **2007**, *48*, 4427–4430.

3. Prepared according to: Guillier, F.; Nivoliers, F.; Godard, A.; Marsais, F.; Quenguiner, G.; Siddiqui, M. A.; Snieckus, V. *J. Org. Chem.* **1985**, *60*, 292–296.

4. Prepared according to: Abe, H.; Aoyagi, Y.; Inouye, M. *Org. Lett.* **2005**, *7*, 59-61.

Chapter 9:

1. Kondo, S.; Takai, R. *Org. Lett.* **2013**, *15*, 538–541, and references therein.

2. Prepared according to: Sasaki, S.; Citterio, D.; Ozawa, S.; Susuki, K. *J. Chem. Soc., Perkin Trans. 2* **2001**, *12*, 2309–2313.

Chapter 10:

1. Kondo, S.; Hiraoka, Y.; Kurumatani, N.; Yano, Y. *Chem. Commun.* **2005**, *13*, 1720–1722.

2. Piatek, P. *Tetrahedron Letters* **2007**, *48*, 4427–4430.

3. Prepared according to: Ganesh, M.; Seidel, D. *J. Am. Chem. Soc.* **2008**, *130*, 16464–16465.